# Agronomy Research

Established in 2003 by the Faculty of Agronomy, Estonian Agricultural University

**Aims and Scope:**
*Agronomy Research* is a peer-reviewed international Journal intended for publication of broad-spectrum original articles, reviews and short communications on actual problems of modern biosystems engineering incl. crop and animal science, genetics, economics, farm- and production engineering, environmental aspects, agro-ecology, renewable energy and bioenergy etc. in the temperate regions of the world.



***Agronomy Research* online:**
*Agronomy Research* is available online at: http://agronomy.emu.ee/

**Acknowledgement to Referees:**
The Editors of *Agronomy Research* would like to thank the many scientists who gave so generously of their time and expertise to referee papers submitted to the Journal.

**Abstracted and indexed:**
SCOPUS, CABI Full Paper and Thompson Scientific database: (Zoological Records, Biological Abstracts and Biosis Previews, AGRIS, ISPI, CAB Abstracts, AGRICOLA (NAL; USA), VINITI, INIST-PASCAL.)

**Subscription information:**
Estonian Grassland Society
St. Teaduse 4, 75501 Saku, ESTONIA
E-mail: heli.meripold@eria.ee

**Journal Policies:**
Estonian University of Life Sciences, Estonian Research Institute of Agriculture, Latvia University of Agriculture, Aleksandras Stulginskis University, Lithuanian Institute of Agriculture and Lithuanian Institute of Horticulture and Editors of *Agronomy Research* assume no responsibility for views, statements and opinions expressed by contributors. Any reference to a pesticide, fertiliser, cultivar or other commercial or proprietary product does not constitute a recommendation or an endorsement of its use by the author(s), their institution or any person connected with preparation, publication or distribution of this Journal.

**ISSN 1406-894X**

# CONTENTS

# I AGRICULTURAL MACHINERY

*Agronomy Research* **13**(1), 7–16, 2015

# Effects of the divers olive harvesting systems on oil quality

L.M. Abenavoli* and A.R. Proto

Department of AGRARIA, *Mediterranean* University of Reggio Calabria, Italy; *Correspondence: laben@unirc.it

**Abstract.** Three olives harvesting systems from the tree have been compared (manual, facilitated and mechanical) through experimental trials carried out respectively in three plots of a Calabrian olive orchard in the Province of Crotone. The grove is traditional and monovarietal, composed of *Carolea* cultivar with a planting density of about 150 plants $ha^{-1}$. In this study, work productivity in three divers sites where harvesting was achieved according to different systems has been examined, as well as their effects on produced oil quality. Olives have been harvested by mean of sticks and nets in the manual harvesting (system I), by mechanical aids and nets in the facilitated harvesting (system II), and finally, by mean of trunk shaker and nets in mechanical harvesting (system III).The different work sites have been examined in terms of work productivity, as well as in terms of impact on final product quality, through the withdrawal of a series of oil samples extracted separately and analyzed in laboratory. From the effectuated trials, it has emerged that the site operating with mechanical harvesting has achieved the best results, both from quantitative and qualitative points of view. Indeed, olives harvested mechanically, certainly more intact than those harvested with other systems, produced oil with the best organoleptic parameters.

**Key words:** olives, mechanical harvesting, oil quality.

## INTRODUCTION

With about 3,300,000 tones, Italian production of olives is situated at the second place in the world after Spain, and it is concentrated for almost 80% in three southern regions: Apulia, Calabria and Sicily (FAOSTAT, 2009 & ISTAT, 2002–2008).

The high economical value assumed by such cultivation in the territories where it is spread justifies the numerous researches aimed to solve problems related to the production. The main one is represented by olives harvesting and its economical and management aspects. For example, in traditional groves, the cost of manual harvesting only at times exceeds 60% of the entire production cost (Zimbalatti, 2004). To promote more suitable harvesting systems with use of trunk shakers or other modern machinery, it is necessary therefore, to encourage new intensive plants, able to be fully mechanized, utilizing new trunk shakers that through a correct use improve olive harvesting and subsequently oil quality.

Currently in Calabria mechanical harvesting is quite diffused, especially in some areas. Indeed, date the exceptional rusticity of the plant, the orographic conditions of the area where traditionally it has developed the olive (with the exception of the '*Piana di GioiaTauro*') are characterized by sloping or very slope lands, and frequently inaccessible to machines of great sizes (as are the shakers). Are widespread, according to the size of the trees, other forms of mechanization: the rods shakers portable and/or the mechanical pick up from ground. (Abenavoli & Marcianò, 2013)

Despite the persistence of the economic crisis, there is a consolidated part of consumers that prefers to acquire high quality oil. This purchase tendency would certainly be reinforced in the future if accompanied by lower prices, therefore lower production costs. This is possible only through a larger spread of modern machinery such as trunk shakers that preserve furthermore product quality. (Giametta & Pipitone, 2004)

In this context, Mechanics Section of the Department of Agriculture of Reggio Calabria carried out a number of harvesting trials in a Calabrian olive farm situated in the Province of Crotone. In this study, work productivity in three divers sites where harvesting was achieved according to different systems has been examined, as well as their effects on produced oil quality.

## MATERIALS AND METHODS

The research was conducted in the harvesting period during the years 2012 and 2013. In particular, the harvesting tests were performed during the last week of November in which were analyzed three different systems of harvesting of olives and for each yard was picked an oil sample for analysis in a specific laboratory analysis to determine the quality organoleptic properties.

The olive farm, subject of this study, is located in the Calabria territory of *Cotronei* at 500 meters above sea level, in the province of Crotone (in *Alto Marchesato*), and in addition to having a surface with about 200 ha of olive trees, has its own oil mill for the processing of olives.

Based on the data collected for half a century in 'Hydrological Yearbooks of the Hydrographic Service of the State' and made available by ARPACAL on its website (ARPACAL, 2009), is apparent that the station weather-hydrological of Cotronei is interested by average annual rainfall including between 800 and 1,200 mm, distributed on average on 73 rainy days. In particular in the 2011 (1,746 mm) and in the 2012 (1,647 mm) there has been an increase of mean annual precipitation, distributed an average of about 100 rainy days per year. The average annual temperatures vary between 16 °C and 18 °C, with absolute minimum temperatures that does not descend below zero and those maxims that reach the 42 °C.

By virtue of this brief analysis, for the station of Cotronei, can be attributed the climate to the type Mediterranean, with a period of aridity variable from 4 to 5 months (May to September) and precipitation of stormy character generally confined to the autumn and winter.

In the corresponding olive campaign, the total production of olives in the farm concerned by the trials was equivalent to 1,300,000 kg, with about 240,000 kg of extra-virgin oil obtained with an average yield of 18.46%.

The farm, the subject of this work, consists of a traditional monovarietal grove of *Carolea* cv, and is composed of three plots (indicated in the following as: a, b and c), not homogeneous in ground topography and planting distance. In each of these plots, it has been adopted a harvesting system retained more suitable for the specific features (Table 1 and 2).

**Table 1.** Studied plots with respective ground topography and utilized harvesting system

| Plot | Ground topography | Harvesting system |
|---|---|---|
| a | plane | mechanical |
| b | declivous | facilitated |
| c | high slope | manual |

**Table 2.** The three harvesting organizations

| Workers for activities | Plot 'a' | Plot 'b' | Plot 'c' |
|---|---|---|---|
| Mechanical shaker | 1 | 0 | 0 |
| Vibrating rod | 0 | 2 | 0 |
| Wood sticks | 0 | 2 | 3 |
| Harvesting nets | 8 | 4 | 2 |
| Moving boxes | 2 | 2 | 2 |

The three harvesting organizations utilized in the three plots are described in the following:

**Mechanical harvesting in plot 'a'** (plane ground):

The site of the first trial is made up of a level ground and the olive trees are the cultivar *Carolea* with groves are planted of 10 x 10 m and an average age of about 100 years (Fig. 1). The trees are grown vase-shaped and have a framework composed of three or four main branches. The latter have the characteristic trend assurgent (typical of this cultivar) while the height of the trunk average of 1–1.20 m. Accordingly, the trees are even considering the heavy weight (3÷5 g) of the fruit, particularly suitable for mechanical harvesting with the employment of the trunk shaker.

The harvest was performed using self-propelled vibratory shaker (SICMA F3) wheel drive on three wheels(the singleis posterior and steering axle) hydraulic transmission. The warhead-carrying arm is telescopic and the commands for the handling of machine and the vibrations are carried out by a joystick; the vibrating head is at very high frequencies and self-braking. The engine is a supercharged 4-cylinder IVECO that packs a punch of 93 kW at 2,300 g min-motor$^{-1}$ (Fig. 2).

**Figure 1.** Plane ground (plot 'a').


**Figure 2.** Mechanical harvesting.

The collection began with the drawing up of the networks under the foliage of the olive trees and along the between rows and after the shaker proceeded along the line directing the head of the vibrator to the trunk of each tree (usually about 10 cm below the point of insertion of the main branches). In the meantime in which the machine shaking trees already provided with networks, some workers continue to drawing up the other networks under the olive trees yet to shake, in order to ensure a certain continuity of the work, while the fallen olives in networks were unloaded into the cassettes by other workers. The free networks were then dragged under the following trees, while the olives, after clearing them from leaves and twigs, were initiated at the oil mill.

The main critical issues were reported by this phase mainly concerned the difficulties of combining the action of the shaker with the movement of networks by the workers for the burden of managing them (due to the weight and size), plus some downtime of the vibrator during the maneuvers of approach and departure from the trunk of the trees.

**Facilitated harvesting in plot 'b'** (declivous ground):

The site of the second test he was in a declivous ground, with an average slope at around 22% and the majority of olive trees were arranged in terracing. The trees were of cultivars *Carolea*, with groves are planted of 10 x 10 m and an average age of about 100 years (Fig. 3). The trees are grown polyconic vase-shaped and had an average height of the trunk of about 1 m. The orographic conditions of the terrain does not have allowed to execute the harvest with the vibrators self-propelled (given the dimensions that have the machines) and so this was made with portable mechanical devices fitted with hooks shakers of boughs.

The machine used is the Cifarelli SC800 which is provided with a motor of 52 $cm^3$, single-cylinder two-stroke air-cooled. The rod is of the telescopic type with variable length (from 3 to 5 cm), and is provided with terminal hook. The whole device weighs about 15 kg and can produce more than 2,000 oscillations $min^{-1}$ (Fig. 4).

**Figure 3.** Declivous ground (plot 'b').

**Figure 4.** Facilitated harvesting.

In this second yard after you have spread networks manually under the trees, two workers with facilitators devices were starting to shake up the single fruit bearing boughs of each tree. The operations of shaking are completed with the manual down hearting by two workers fitted with wooden rods for dropping the remaining drupes. Finally, the fallen olives were being transferred from the nets in crates and after clearing them from leaves and twigs, promptly sent to the oil mill.

During the tests of harvest were observed some dead times determined both by fatigue of workers in the use of the shaking portable because of the vibrations transmitted in the arms, and the difficulties encountered in networks drafting along the rows because of the slope of the ground and of the irregular terracing.

**Manual harvesting in plot 'c'** (ground with high slope):

In the third test site the ground was strongly declivous, with an average gradient of 32% and the majority of the plants were disposed in terraces. The trees were reared free-form and they had an average height of the trunk of about 1.00 m (Fig. 5). In this case the orographic conditions of the ground and the difficulty of displacement of workers had not allowed to perform the harvest with no mechanical device also of portable type. Harvesting was therefore carried out only manually utilizing the wooden poles (Fig. 6).

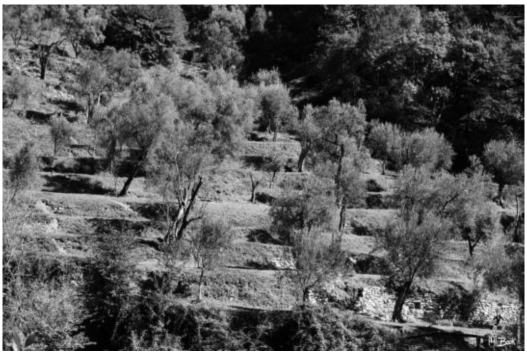

**Figure 5.** Groundwith a high slope (plot 'c').

**Figure 6.** Manual harvesting (beating).

In this yard, once the networks were drawn under the foliage of the olive trees, three workers equipped with wooden poles started to beat the fruiting boughs. The olives have fallen into the nets were collected in crates and, after clearing them from leaves and twigs, sent directly to the oil mill.

The high slope of the ground and the irregular terracing, made it difficult the working conditions especially in the movements of the workers when they spread forth their nets along the rows. The olives for more were falling away from them for the action rather vigorous of the wooden poles on fruiting boughs.

After having examined productivity in the three different work sites, the study focused on the characterization of oil quality influenced by harvesting system. Indeed, olives harvesting techniques and delivery time to the extraction unit may affect organoleptic properties of the transformed product. Therefore, olive oil samples have been extracted for each harvesting systems adopted according to the following parameters:

- 3 samples of olive oil pressed after 8 hours from harvesting, identified with the letter ‘A’.
- 3 samples of olive oil pressed after 24 hours from harvesting, identified with the letter ‘B’.
- 3 samples of olive oil pressed after 48 hours from harvesting, identified with the letter ‘C’.


**Figure 7.** Some of the oil samples used for the analysis.

Each oil sample of 250 ml has been labelled according to the corresponding harvesting system and extraction time (Fig. 7) and it has been sent to an appropriated laboratory to be analyzed. The laboratory analyses are aimed at determine acidity percentage and peroxide quantity present in each sample of oil. Acidity represents a fundamental indicator for olive oil quality because it defines commodity classification. Peroxide quantity; however, indicate oxidation level of unsaturated fatty acids that provide a characteristic rancid smell to the oil, especially, if it is subject to high temperatures, light and oxygen. Less is the number of peroxide, better is olive oil quality and its shelf-life. The oxidative processes may be revealed through measurement of spectrophotometric constants:

- K232 (value of specific extinction at 232 nm, the wavelength corresponding to the maximum absorption of conjugated dienes);
- K270 (value of specific extinction 270 nm, the wavelength corresponding to the maximum absorption of conjugated trienes).
- DK (trend of the absorption curve in the range of 264–272 nm; sheds light on the presence of the compounds of secondary oxidation).

## RESULTS AND DISCUSSION

Work analysis in the three harvest sites has shown that plot ‘**a**’ (mechanical harvesting) has a higher yield, with a work capacity equal to 80 plants a day (during an 8 hours working day. Plot ‘**b’** (facilitated harvesting) has instead presented a work capacity of 36 plants a day with about 4,000 kg day$^{-1}$ of harvested olives. Such capacity resulted two times higher than in plot ‘**c**’ (manual harvest) that reached a productivity of 2,000 kg day$^{-1}$.

Finally, elaborated data show how the use of mechanical aids and shaker machines during harvesting guarantees an important increasing of productivity, compared to the site where harvesting was effectuated manually (Table 3) (Giametta & Zimbalatti, 1997).

**Table 3.** Summarized scheme of obtained yields with the three harvesting systems

| Harvesting system | Utilized machine | Lab./site | Site capacity | | Work productivity | | Variation with manual harvest (%) |
|---|---|---|---|---|---|---|---|
| | | | Plant day$^{-1}$ | kg day$^{-1}$ | plant ay-lab.$^{-1}$ | kg day-lab.$^{-1}$ | |
| Mechanical (Plot 'a') | shaker *Sicma F3* | 11 | 80 | 7,000 | 7.3 | 636 | 143 |
| Facilitated (Plot 'b') | mechanical aids *Cifarelli* | 10 | 36 | 4,000 | 3.6 | 400 | 20 |
| Manual (Plot 'c') | – | 7 | 20 | 2,000 | 3.0 | 300 | 0 |

Moreover, there is another aspect to consider that concerns damages undergone by olives with the employment of divers harvesting systems. Particularly, olives from plot '**a**', obtained by mechanical harvesting, are visibly intact; however, olives obtained by mean of facilitated harvesting appear partially damaged because of beating. Thus, in order to avoid that oxidative and fermentative processes affect qualitative features of oil, a fast transport to the extraction unit is necessary for an immediate transformation. Effectuated analyses in a renowned regional laboratory demonstrated that samples have different characteristics between them, although, they fulfil all requirements of UE Regulation about extra virgin olive oil quality.Acidity, peroxide number and UV spectrophotometric (K232, K270 and Delta-K) are parameters determined in the laboratory. The measure of acidity is the oldest parameter used to assess the quality of olive oil and its product classification. As it can be noted in Table 4, obtained oil from olives harvested mechanically, has the best parameters in the three analyzed samples. The following figure (Fig. 8) shows acidity and peroxides tendency in the three extracted samples for each harvesting system.

**Table 4.** Results of the analyses on olive oil samples (UE Reg. n° 1531/2001)

| Sample | Harvesting system | Acidity (%) | Peroxides (meq $O^2$/ kg$^{-1}$) | UE Reg. n° 1531/2001 | | |
|---|---|---|---|---|---|---|
| | | | | Acidity (%) | Peroxides (meq $O^2$ kg$^{-1}$) | Classification |
| 1 A | *mechanical* | 0.42 | 9.2 | < 0.8 | < 20 | Extra virgin olive oil |
| 2 A | *facilitated* | 0.49 | 10.4 | < 0.8 | < 20 | ' |
| 3 A | *Manual* | 0.56 | 13.0 | < 0.8 | < 20 | ' |
| 1 B | *mechanical* | 0.49 | 9.4 | < 0.8 | < 20 | ' |
| 2 B | *facilitated* | 0.56 | 11.8 | < 0.8 | < 20 | ' |
| 3 B | *Manual* | 0.63 | 13.9 | < 0.8 | < 20 | ' |
| 1 C | *mechanical* | 0.59 | 10.4 | < 0.8 | < 20 | ' |
| 2 C | *facilitated* | 0.64 | 13.8 | < 0.8 | < 20 | ' |
| 3 C | *Manual* | 0.77 | 14.3 | < 0.8 | < 20 | ' |

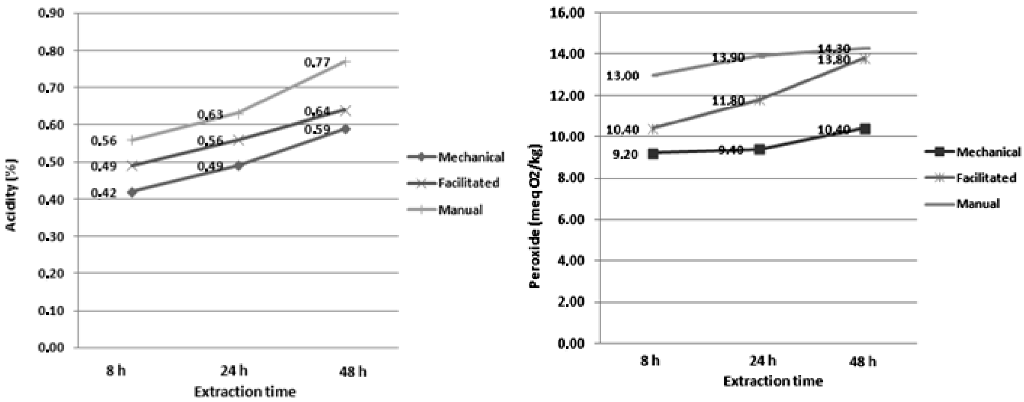


**Figure 8.**Acidity and peroxides tendency in analyzed samples.

Always according to the forward regulation (UE Reg. n° 1531/2001), the results of UV-spectrophotometric analyses effectuated on the same samples are reported in Table 5. In this case also the analyses complete and confirm the previous results about the best quality of oil obtained from olives harvested mechanically.

**Table 5.** Results of spectrophotometric analyses on extracted samples

| Sample | Harvesting system | Acidity (%) | Peroxides (meq $O^2$ $kg^{-1}$) | UE Reg. n° 1531/2001 | | |
|---|---|---|---|---|---|---|
| | | | | Acidity (%) | Peroxides (meq $O^2$ $kg^{-1}$) | Classification |
| 1 A | Mechanical | 0.42 | 9.2 | < 0.8 | < 20 | Extra virgin olive oil |
| 1 B | (plot ‘a’) | 0.49 | 9.4 | < 0.8 | < 20 | ‘ |
| 1 C | | 0.59 | 10.4 | < 0.8 | < 20 | ‘ |
| 2 A | Facilitated | 0.49 | 10.4 | < 0.8 | < 20 | ‘ |
| 2 B | (plot ‘b’) | 0.56 | 11.8 | < 0.8 | < 20 | ‘ |
| 2 C | | 0.64 | 13.8 | < 0.8 | < 20 | ‘ |
| 3 A | Manual | 0.56 | 13.0 | < 0.8 | < 20 | ‘ |
| 3 B | (plot ‘c’) | 0.63 | 13.9 | < 0.8 | < 20 | ‘ |
| 3 C | | 0.77 | 14.3 | < 0.8 | < 20 | ‘ |

The analyzes carried out on the chemical quality of olive oil, have shown that the collection system can influence the composition of olive oil (Giuffrè, 2013; Giuffrè & Louadj, 2013).

## CONCLUSIONS

From the effectuated trials, it has emerged that the site operatingwith mechanical harvesting has achieved the best results, both from quantitative and qualitative points of view. Indeed, olives harvested mechanically, certainly more intact than those harvested with other systems, produced oil with the best organoleptic parameters (Giametta & Zimbalatti, 1994).

Despite this, olive harvesting in Calabria is still effectuated almost exclusively with manual systems or facilitated ones, from the tree when possible or worst from the ground. All these problems engender unfortunately a product mostly characterized by a scarce quality. Consequently, Calabria although being the second region in Italy for olive oil production, as well as particularly devoted to such cultivation, occupies the last places for high quality olive oil production (Giametta & Zimbalatti, 1991).

The studied case demonstrates that also in Calabria, as in other Italian region, there are excellent farms which adopt harvesting and extraction techniques that guarantee a product of high quality, obtaining recognition at National and International levels. Such farms found however difficulties to emerge in extra regional markets because of the reputation of the local sector (Zimbalatti et al., 2009).Innovative mechanized harvesting operations represent a real watershed in the process of modernization of world olive growing. The use of mechanized system of harvesting, which responds to issues linked to chronic shortage of labor and to the need to contain production costs, is likely to revamp that portion of obsolete and non-cost-effective practices which are no longer competitive in the olive growing sector.

The Calabrian oliviculture, except sporadic innovative examples, remains substantially related to traditional systems of production characterized by high costs, low unitary productivity, and a low index of mechanization.

For more competitiveness, it is necessary to have in the entire region a further spread of more modern and dynamic orchards, easier to mechanize and therefore more productive. Such innovations would certainly allow to lower production costs, particularly those of harvesting which remain very high. (Giametta & Morabito, 2006)

Quality, transparency and orchards accurate management through an appropriate and rational use of innovative machines as trunk shaker, that permit a deep restructuration of the orchards are important goals to consider for olive farms competitiveness.

## REFERENCES


Abenavoli, L.M. & Marcianò, C., 2013. Technical and economic analysis of alternative pruning systems in high dimensions olive trees in Calabria. *Agronomy Research* **11**(1), 7–12.

Arpacal. 2009. Centro Funzionale Multirischi della Calabria. Sito internet *http://www.cfc.alabria.it/*.

Giametta, G. & Zimbalatti, G. 1991. *Meccanizzazione dell'olivicoltura calabrese situazione attuale e prospettive future*, Convegno di studio: 'Quale futuro per l'olivicoltura calabrese?', 4–12.

Giametta, G. & Zimbalatti, G. 1994. *The influence of harvesting methods and periods on the quality of olive oil*. Abstracts del 'XXIV International Horticultural Congress'. Kyoto, Giapp, G. & Zimbalatti, G. 1997. *Developments in mechanized olive harvesting in southern* *italy*, Proceedings of ‘3rd International Symposium on Olive Growing’. Chania, Creta, Grecia, 22–26.

Giametta, G. & Pipitone, F., 2004. *La raccolta delle olive: innovazioni tecnologiche.* Atti del Convegno UNACOMA e Accademia Nazionale di Agricoltura: ‘Innovazione tecnologica e ricerca per lo sviluppo di una moderna meccanizzazione agricola’, Bologna, 17 giugno, 79–93.

Giametta, G. & Morabito, S., 2006. *Innovazione tecnologica in olivicoltura tra esigenze di qualità e di tutela dell’ambiente*, Estratto da: ‘Seminario Internazionale sull’olivicoltura’.

Giuffrè, A.M. 2013. Influence of cultivar and harvest year on triglyceride composition of olive oils produced in Calabria (Southern Italy). *Eur. J. Lipid Sci. Technol.* **115**, 928–934. DOI: 10.1002/ejlt.201200390.

Giuffrè, A.M., Louadj, L. 2013. *Influence of crop season and cultivar on sterol composition of monovarietal olive oils in Reggio Calabria (Italy)*. Czech J.Food Sci. 31, 256–263.

Zimbalatti, G. 2004. *Macchine e impianti per la raccolta e la trasformazione delle olive da olio*. Il Perito Agrario, settembre-ottobre, **5**, 20–28.

Zimbalatti, G., Bernardi, B., Morabito, S. 2009. *Using a self-propelled radio-controlled shaker: mechanized harvesting tests and economic evaluation*, Olive bioteq, Third International Seminar ‘For a renovated profitable and competitive Mediterranean olive growing sector’.

*The authors each contributed equally to this work.*

*Agronomy Research* **13**(1), 17–24, 2015

# Maintenance interval optimization based on fuel consumption data via GPS monitoring

Z. Aleš, J. Pavlů* and V. Jurča

Faculty of Engineering, CULS-Czech University of Life Sciences Prague, Kamycka 129, 16521 Prague 6, Czech Republic;
*Correspondence: jindrichpavlu@seznam.cz

**Abstract.** Properly performed preventive maintenance is one of the basic conditions for ensuring the operability of the mobile machines. There are basically two types of preventive maintenance: scheduled maintenance with pre-determined intervals and maintenance by the technical state. Common practice shows that maintenance intervals are often determined only by a qualified estimate of the machine manufacturer or maintenance manager, which results in costs increase. The authors proposed new method of using the modern technology of Global Positioning System, in order to reduce costs of preventive maintenance. Mentioned technologies allow users to monitor a number of operational parameters of mobile machinery in real time. Collected data obtained from the operation can be used for decision-making of maintenance activities. For ensuring the availability of mobile machinery it is important to determine the optimal maintenance interval. The authors proposed method for using data from satellite monitoring using the criterial function in order to determine the optimal interval for performing preventive maintenance. Proposed method is demonstrated on the example of accurate determination of preventive maintenance intervals for several mobile machines. Using data from satellite monitoring and subsequent data processing contribute to better maintenance planning and consequently to economical operation.

**Key words:** maintenance interval, preventive maintenance, maintenance costs, satellite monitoring.

## INTRODUCTION

There are two basic maintenance systems for ensuring preventive maintenance (CSN EN 13306, 2002) of vehicles and mobile machines - maintenance by the technical state (condition-based maintenance – on-board diagnostic) (Honig et.al., 2014) or maintenance according predetermined operating time intervals (general unit w; examples: travelled distance (km), operated hours (hrs) measured by hour meter, etc.) (Drozyner & Mikolajczak, 2007). Amount of the specific fuel consumption is possible indicator used as an overall diagnostic signal in the maintenance system according to technical state of mobile machines (Lan & Kuo, 2003; Jin et al., 2009). Monitoring of specific fuel consumption faces several problems – a relatively accurate measurement of the roller bed test is very expensive, and furthermore, there are problems with the measurement of combustion engines with high power and engines of some construction machinery. Significantly cheaper acceleration methods are not without problems too, especially when measuring the nowadays conventional turbocharged engines, where delay of turbocharger during engine acceleration must be eliminated by various correction methods. For these reasons, second system (i.e. maintenance according predetermined operating time intervals) is mostly applied for group of construction machinery and machines with high power engines (Pexa & Marik, 2014).

Maintenance intervals are often determined only by a qualified estimate of the machine manufacturer or maintenance manager, which results in costs increase of operating machines – if the intervals are too short, it leads to unnecessary increase in maintenance costs, on the other hand, if the intervals are too long it also leads to increase of costs resulting from the poor technical condition of machines (Wiest, 1998). In addition, predetermined intervals do not precisely reflect operational utilization of a particular machine; the interval is set for the entire group of machines of the same type. Attempts to use known methods of mathematical optimization of preventive maintenance is problematic (Kucera et al., 2013). Known stochastic models are based on knowledge of the probability of failure in different periods of durability of technical object. This way of determination of optimal preventive maintenance interval requires usage of statistical methods and monitoring of a number of other machine operational indicators (dependability characteristics). The required stochastic model of renewal could be described and formulated after analysis of the history of machine operation (Eti et al., 2006; Jardine & Tsang, 2006; Jurca & Ales, 2007).

One of the other options how to determine the optimal preventive maintenance interval is the application of renewal theory using data from satellite monitoring equipment (Darnopykh, 2010). Satellite monitoring of mobile machinery is now relatively common, but companies use it in a very limited way – practically only for monitoring of machines (operational state, position, etc.). Transmitted data recorded via satellite monitoring can be utilized in more sophisticated way. In order to achieve such a goal, authors propose to set up and apply proper algorithm for data processing. Based on data of fuel consumption it is possible to determine the optimal preventive maintenance interval of a particular machine and determine the losses which result from not complying with optimal maintenance interval.

Algorithm of determination of optimal preventive maintenance interval is based on the known value of preventive maintenance costs and slope of linear trend of specific fuel consumption, which is obtained by processing data from a satellite monitoring of machinery. Calculated optimal preventive maintenance interval is corrected according to increasing operating time. In addition, it is possible to verify if previous maintenance interval was chosen correctly and how effectively operator of machinery contributes to production efficiency and effect of change in operating conditions, etc (Jurca et al., 2008).

## MATERIALS AND METHODS

Principle of operational monitoring using GPS (Global Positioning System) of machinery is widely known (Geske, 2007; Cai et al., 2011; Grieshop et al., 2012), therefore there are only briefly described issues related to this paper. After turning on the ignition system of vehicle, control unit starts up from sleep mode and starts to track and store data into its memory and connects to the server (Kans, 2008). After connecting the control unit quickly sends the recorded data and subsequently data sends at specified intervals, for instance in 120 second intervals. Data is processed in the device according to the configuration file. Obtained data is in a various form: immediate values, maximum or minimum for the recorded period, the average, statistical parameters and it is also possible to apply various filters, and all data is conveniently available from user web application.

In order to use the theory of renewal to determine the optimal maintenance interval of machinery it is important to measure fuel consumption with sufficient precision. Use of the CAN-BUS information is not suitable because the accuracy is determined by the fuel float up to 10% according to CAN-BUS standard. For this reason, capacitance probe CAP04 (Partner mb.) were mounted into fuel tank.

Capacitive probe CAP04 consists of two tubes of different diameter, which are the electrodes of capacitor. The dielectric is composed of electrically non-conductive material, specifically with a fuel and air. The relative permittivity of air is $\varepsilon r = 1$, during re-fuelling the air is replaced with diesel which has relative permittivity $\varepsilon r = 2$ and due to this fact the capacity of the capacitor increases. The capacitive sensor measures the position of the boundary between air and diesel fuel.

The probe is also equipped with thermometers to sense temperature of fuel and the surface temperature of the fuel tank. The processor evaluates data according to the actual capacity of the probe to match the measured volume of diesel at a reference temperature 15 °C. This method ensures that the reported amounts of fuel are not distorted by thermal expansion of diesel. Furthermore, the probe measures the tilt of the tank in two axes. While driving terrain when the level of diesel fluctuates rapidly and strongly, the probe indicates stable signal by means of appropriate filters of the signal.

General criterial function of renewal (replacement) seeks the minimum of mean unit costs of renewal and operation – the minimum of the function marks the optimum time for renewal (see Equation 1). It is obvious, that the costs of maintenance itself act in the way of prolonging the standard preventive maintenance period. Conversely, the costs of operation, which rise due to worsening technical condition when extending the maintenance period, make the preventive maintenance period as short as possible. The sum curve $u(\bar{t})$ must have a local minimum, which needs to be found in order to determine the optimum period of preventive maintenance. Specific fuel consumption is a comprehensive diagnostic signal indicating instantaneous extent of wear of machine. (Legat et al. 1996)

$$u(\bar{t}) = \frac{N_O + N_P(\bar{t})}{\bar{t}} \rightarrow \min \qquad (1)$$

where: $NO$ – Costs of renewal (CZK); $N_P(\bar{t})$ – Costs of operation (CZK); $\bar{t}$ – mean time of operation (w); $u(\bar{t})$ – mean unit costs of renewal and operation (CZK $w^{-1}$).

Author's proposed method for optimizing maintenance intervals of machinery uses information about fuel consumption that is assessed for each day of machine's operation in unit l,100 $km^{-1}$ or l $hrs^{-1}$.

For the calculation of the local minimum of a function of mean unit costs, its first derivative set equal to 0, thus:

$$\frac{\partial u(\bar{t})}{\partial \bar{t}} = \frac{\frac{\partial N_P(\bar{t})}{\partial \bar{t}} \cdot \bar{t} - \left[N_O + N_P(\bar{t})\right]}{\bar{t}^2} \tag{2}$$

$$\frac{\partial N_P(\overline{t_O})}{\partial \overline{t_O}} \cdot \bar{t}_O - \left[N_O + N_P(\overline{t_O})\right] = 0 \tag{3}$$

$$\frac{\partial N_P(\overline{t_O})}{\partial \overline{t_O}} = \frac{N_O + N_P(\overline{t_O})}{\overline{t_O}} \tag{4}$$

The right side of equation (4) equals to the intermediate mean unit costs $u(\bar{t}_O)$ at optimum of operating time for renewal. The left side of the equation (4) equals to the intermediate immediate operation unit costs $v_P(\bar{t}_O)$ at optimum of operating time for renewal. The equation describes that the optimal moment of renewal, i.e. a local minimum of the criterial function when immediate operation unit costs equal to the mean unit costs of operation and renewal.

Consequently, in order to find the minimum of sum function $u(\bar{t})$ it is necessary to know two basic values – renewal costs $N_O$ (the costs of performed maintenance) and mean unit costs of operation $u_P(\bar{t})$, which are based on the tracking of specific fuel consumption (therefore, it is necessary to determine the equation of growth trend of specific fuel consumption).

## RESULTS AND DISCUSSION

Proposed algorithm for determining the optimum of maintenance interval is using MS Excel spreadsheet. Imported data on specific fuel consumption of the machine are listed in the table by date and time of their recording and from these data it is necessary to select only the data which characterize the utilization of machinery. The algorithms for data filtering are different according to different groups of machines and their utilization. For example, when filtering data on fuel consumption of truck the algorithm filters out data on fuel consumption at idle mode of engine – the engine consumes fuel, but the distance travelled is zero – the value of specific fuel consumption (litres 100 $km^{-1}$) is reaching the infinity. Specific fuel consumption of construction equipment is evaluated in litres per operating hours – changing position of the machine cannot be used for filtering data, on the contrary for some machines (e.g. excavators) change of position has to be excluded from data processing because machinery does not perform intended work. A properly designed algorithm for filtering data affects the entire primary data processing and results of optimal maintenance interval of a particular machine.

After selection, the mean specific fuel consumption is calculated for each day and linear trend is constructed.

Specific fuel consumption is a comprehensive diagnostic signal and depends on many operational factors and therefore there is large variance in monitored specific fuel consumptions.

The unit costs of operation $u_P(\bar{t})$ are determined by a linear trend, which is set by slope of specific fuel consumption trend and the average price of diesel fuel (1.2 EUR $l^{-1}$ – November 2014) during vehicle operation. Slope of specific fuel consumption trend is calculated from the cumulative fuel consumption (polynomial function of second degree, Fig. 1) divided by operational time.

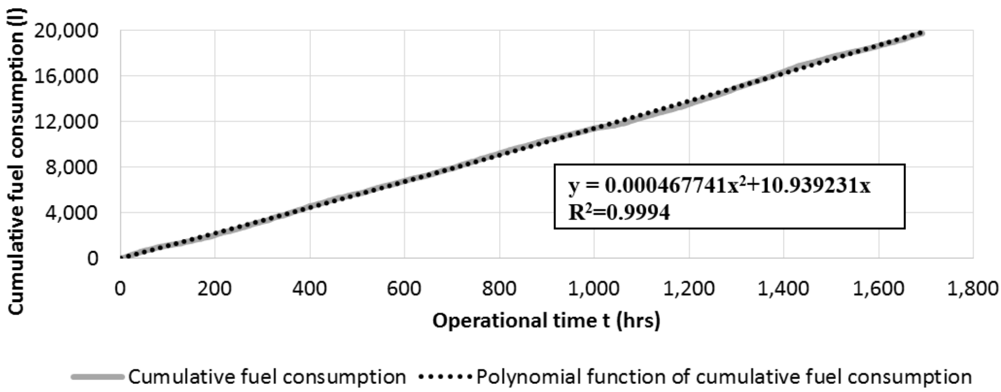


**Figure 1.** Cumulative fuel consumption with polynomial function of second degree.

The function of the mean unit costs is determined by the sum of two functions – unit operational costs function and unit costs of replacement function. The optimal maintenance interval is determined by a local minimum of the mean unit costs function. In this case, the function $u_P(\bar{t})$ is linear, the local minimum of the function $u(\bar{t})$ located at the same spot as intersection of both forming curves $u_O(\bar{t})$ and $u_P(\bar{t})$. The specific examples of the graphic solution are shown in Fig. 2.

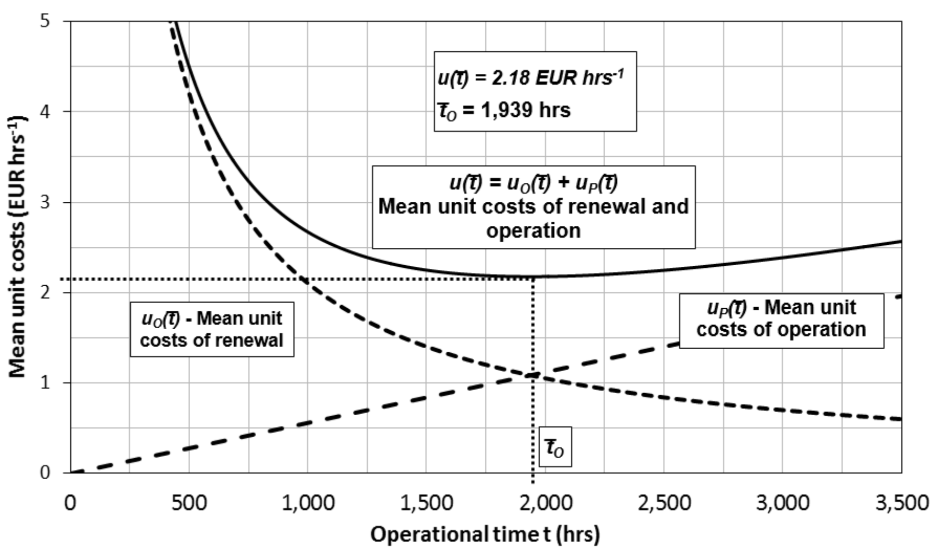


**Figure 2.** Determination of maintenance intervals of TATRA 815 – graphic interpretation.

Proposed method is applied for truck TATRA 815 operated in construction site. The costs of renewal (maintenance) for this truck are estimated at 2,110.14 EUR. In this particular case, the amount of 2,110.14 EUR represents costs of diagnostic maintenance of motor vehicle TATRA 815. Maintenance is performed within one working day and during this day the maintenance costs are calculated as follows:

1) The driver generates a financial loss during the day when the maintenance is carried out because transport of vehicle to the service shop and back does not generates any profit, but the driver has to be paid anyway. The financial loss can be calculated as follows: 1,000 EUR month$^{-1}$ (driver's salary) × 1.35 (deductions from wages) / 20 (working days) = 67.50 EUR.

2) The financial loss due to downtime of the vehicle is calculated: 1.25 EUR km$^{-1}$ (the price of material transported by vehicle) × 220 km day$^{-1}$ (the average distance travelled per day) = 275 EUR.

3) The financial loss occurred due to fuel consumed on a journey into and back: 42 l 100 km$^{-1}$ (average specific consumption of the vehicle) × 35 km (average distance to the maintenance service and back) × 1.2 EUR l$^{-1}$ = 17.64 EUR.

4) Costs of diagnostic maintenance = 750 EUR

5) The price of labour after diagnostic maintenance and the average price of spare parts (e.g., fuel, air and oil filter, injector, pump alignment, oil change, etc.) = 1,000 EUR.

This practical example shows that the optimal preventive maintenance interval is 1,939 hrs for vehicle TATRA 815 (Fig. 1). After rounding to the nearest hundred hours the maintenance interval is set to 2,000 hrs.

For the calculated procedure, it is clear that the maintenance interval is variable and can be influenced by:

- Maintenance costs,
- Function of mean unit operational costs (influenced by fuel costs).

Specific fuel consumption is influenced by the conditions of operation of the machine and therefore determined maintenance interval has to be continually updated. Data analysis of plenty same types of vehicles will help determine the intervals for maintenance for a particular type of machine and use it for simple long-term maintenance planning of mobile machines in the enterprise (see examples below in Table 1).

**Table 1.** Determination of the mean maintenance interval for TATRA 815 and Renault Kerax

| Vehicle | Operational time (hrs) | Polynomial function | Trend of slope of specific fuel consumption | Determined maintenance interval $t_O$ |
|---|---|---|---|---|
| 01 TATRA 815 | 1,692 | $0.00046x^2 + 10.9x$ | 0.0005612894 | 1,939 hrs |
| 02 TATRA 815 | 1,856 | $0.00042x^2 + 9.6x$ | 0.0005108268 | 2,032 hrs |
| 03 TATRA 815 | 1,848 | $0.00051x^2 + 9.8x$ | 0.0006150768 | 1,852 hrs |
| 01 Renault Kerax | 1,765 | $0.00026x^2 + 9.1x$ | 0.000322144 | 2,559 hrs |
| 02 Renault Kerax | 1,986 | $0.00031x^2 + 8,8x$ | 0.000375100 | 2,372 hrs |
| 03 Renault Kerax | 1,848 | $0.00028x^2 + 8,9x$ | 0.0003414192 | 2,486 hrs |

Table 1 provides data on vehicle type, monitored time of operation (hrs), polynomial function, slope of linear trend of specific fuel consumption and data of specified maintenance intervals $\tau_O$ (hrs). Slope of linear trend of specific fuel consumption is different for each particular vehicle. Such a fact is due to different operational conditions of certain vehicles and also due to different style of driving of drivers. For example, slope of trend for vehicles Renault Kerax range from 0.000322144 to 0.0003751. Determined optimal intervals were calculated with $N_O$ = 2,110.14 EUR and average fuel costs 1.2 EUR per litre. Mean maintenance interval for vehicles Renault Kerax was 2,500 hrs and for TATRA 815 was 2,000 hrs.

The same algorithm can be used for any type of machinery (transportation, construction, mining, railroad, agricultural, etc.), but with the difference of operational time unit (kilometres, tones, hectares, volumes, etc.).

## CONCLUSIONS

The paper presents proposed methodology for optimization of planned preventive maintenance, which is based on the use of data from satellite monitoring - data collection, their final selection and algorithmic processing and therefore finding optimal preventive maintenance interval for a particular machine or group of machines. Algorithm of determination of optimal preventive maintenance interval is based on renewal theory and its modification for solving particular problem. Principle of this algorithm is based on minimization of operational and renewal costs.

The proposed methodology for determining the optimal maintenance interval is particularly suitable for companies that already use satellite monitoring, but mostly in its elementary form for the current position of the vehicle, construction equipment downtime monitoring, etc. It is obvious that the observed specific fuel consumption relatively largely varies, which is influenced by variability of operating conditions, load weight, driver's driving style, nature of extracted material within construction machinery, etc. This variance is eliminated by large quantities of raw data and therefore processing of raw data allows for a precise determination of the optimal preventive maintenance interval for a specific machine, its current operational conditions and the changes of their technical state during deterioration.

Algorithm of data processing from satellite monitoring provides timely reports on individual machine maintenance requirements and enables continuous refinement of maintenance intervals during operational time. Suspiciously different maintenance interval of particular machine (calculated optimal maintenance interval deviates from the average) might be followed by detailed diagnostics in order to determine the causes of short maintenance interval. Proposed algorithm may contribute to better maintenance planning and consequently to economical operation of machinery.

ACKNOWLEDGEMENTS. Paper was created with the grant support – CZU 2014: 31190 / 1312 / 3128 – Utilization of satellite monitoring for detection of operational parameters of machines.

## REFERENCES


Cai, S., Becherif, M., Henni, A., Wack, M, & Aboubou, A. 2011. Processing of information gathered from hybrid or electrical vehicle for reduction of fuel consumption and gas emission. *Mediterranean Journal of Measurement and Control* **7**(2), 236–242.

CSN EN 13306 (2002): Maintenance terminology. Prague: The Czech Office for Standards, Metrology and Testing. (In Czech)

Drożyner, P. & Mikołajczak, P. 2007. Maintenance of vehicles, machines and equipment in view of the ISO 9001 requirements. *Eksploatacja i Niezawodność - Maintenance and Reliability* **4**, 55–58.

Darnopykh, V.V. 2010. Application of unified methodical approach to online planning of target operation of satellite monitoring and communication systems. *Journal of Computer and Systems Sciences International* **49**(1), 115–134.

Eti, M.C., Ogaji, S.O. & Probert, S.D. 2006. Reducing the cost of preventive maintenance (PM) through adopting a proactive reliability-focused culture, *Applied Energy* **83**, 1235–1248.

Geske, D.M. 2007. Mapping a cleaner route. *Diesel Progress North American Edition* **73**(6), 108–109.

Grieshop, A.P., Boland, D., Reynolds, C.C., Gouge, B., Apte, J.S., Rogak, S.N. & Kandlikar, M. 2012. Modelling air pollutant emissions from Indian auto-rickshaws: Model development and implications for fleet emission rate estimates. *Atmospheric Environment* **50**, 148–156.

Hönig, V., Horníčková, Š. & Orsák, M. 2014. Monitoring of wear particles during running-in diesel engines of tractors. *2nd International Conference on Materials, Transportation and Environmental Engineering, CMTEE 2014.* Kunming; China, Volume 1030–1032, 1206–1209.

Jardine, A. & Tsang, A. 2006 Maintenance, replacement, and reliability: theory and applications. *Mechanical engineering, Boca Raton: CRC/Taylor*, 322. ISBN 08-493-3966-9.

Jin, G., Xiang, Z. & Lv, F. 2009 Semantic Integrated Condition Monitoring and Maintenance of Complex System. *In: IEEE 16th International Conference on Industrial Engineering and Engineering Management*. Beijing, PRC, pp. 670–674.

Jurca, V. & Ales, Z. 2007. Maintenance Management Efficiency Evaluation. *Eksploatacja i Niezawodnosc – Maintenance and Reliability* **1**, 13–19.

Jurca, V., Hladik, T. & Ales, Z. 2008. Optimization of Preventive Maintenance Intervals. *Eksploatacja i Niezawodność - Maintenance and Reliability* **3**, 41–44.

Kans, M. 2008. An approach for determining the requirements of computerised maintenance management systems. *Compunters in industry* **59**, 32–40.

Kučera, M., Aleš, Z., Ivandić, Z. & Hujo, L. 2013. Possibility of hydraulic fluids with a low environmental impact application in agriculture and transport machinery. *Journal of Central European Agriculture* **14(4)**, 1575–1584.

Lan, L. W. & Kuo, A.Y. 2003. Modelling bus drivers' aberrant behaviours and the influences on fuel and maintenance costs. *Journal of Advanced Transportation* **38 (1)**, 93–113.

Legat, V., Zaludova A.H., Cervenka, V. & Jurca, V. 1996. Contribution to optimization of preventive replacement. *Reliability Engineering and System Safety* **51**, Elsevier Science Limited, ISSN 0951-8320. 259–266.

Pexa, M. & Mařík, J. 2014. The impact of biofuels and technical engine condition to its smoke - Zetor 8641 Forterra. *Agronomy Research* **12**(2), 367–372.

Wiest, W. 1998 Improvement of the availability through quality control and preventive maintenance of self-propelled vehicles. *In: Conference on Agricultural Engineering, VDI BERICHTE* **1449**, Germany, pp. 351–356.

*Agronomy Research* **13**(1), 25–32, 2015

# Determination of power loss of combine harvester travel gear

L. Beneš*, P. Heřmánek and P. Novák

Czech University of Life Sciences Prague, Faculty of Engineering, Department of Agricultural Machines, Kamýcká 129, 165 21 Prague 6, Czech Republic;
*Correspondence: benesl@tf.czu.cz

**Abstract.** This contribution aims at determining the power loss in hydraulic circuits of the John Deere S680i combine harvester travel gear. The individual elements of the circuit were measured, followed by an energy intensity analysis. The analysis includes the calculation of pressure losses in direct piping, local resistance, as well as pressure losses in the individual elements of the circuit. Subsequently, power loss was calculated based on pressure losses. In the case of the John Deere S680i combine harvester, the power loss equals 16.95 kW.

**Key words:** combine harvester, hydrostatic travel, pressure loss, power loss.

## INTRODUCTION

Combine harvesters are machines in which we require, in terms of the content of their work, sensitive control and continuous travelling speed variation. Consequently, hydrostatic transmission is the most frequently used in combine harvester travel gear (Kutzbach, 2000).

Hydrostatic transmission is a transmission mechanism with a pump and hydraulic motor as its basic elements. The principle of mechanical energy transfer through the hydrostatic transmission rests in the transformation of mechanical energy into pressure energy of the fluid in the pump and, vice versa, pressure energy of the fluid into mechanical energy in the hydraulic motor (Kučík & Strážovec, 2000). The transmission consists of a closed hydraulic circuit and an auxiliary open hydraulic circuit (Lou Xi-Yin, 2014). The auxiliary hydraulic circuit fulfils the following tasks:

- it cleans the fluid;
- it refills the fluid in a closed circuit;
- it maintains the required pressure of the fluid in a low-pressure branch of the closed circuit;
- it cools the fluid down;
- it is a source of required energy when controlling regulation piston converters (Roh, 1992).

The diagram of hydraulic circuits of the hydrostatic transmission of the John Deere S680i combine harvester is shown in Fig. 1.

The auxiliary circuit includes a gear pump (P16), which draws in the fluid from the tank (R1). The fluid runs both into the servo-valves (Y119 and Y126) and the servo-cylinders (C40 and C41), when adjusting the position of the swing plate of the pump and of the hydraulic motor, and into the closed circuit through non-return valves (V160) or (V161), depending on which branch of the closed circuit currently has low fluid pressure. The auxiliary circuit is protected against overload by a pressure valve (V198).

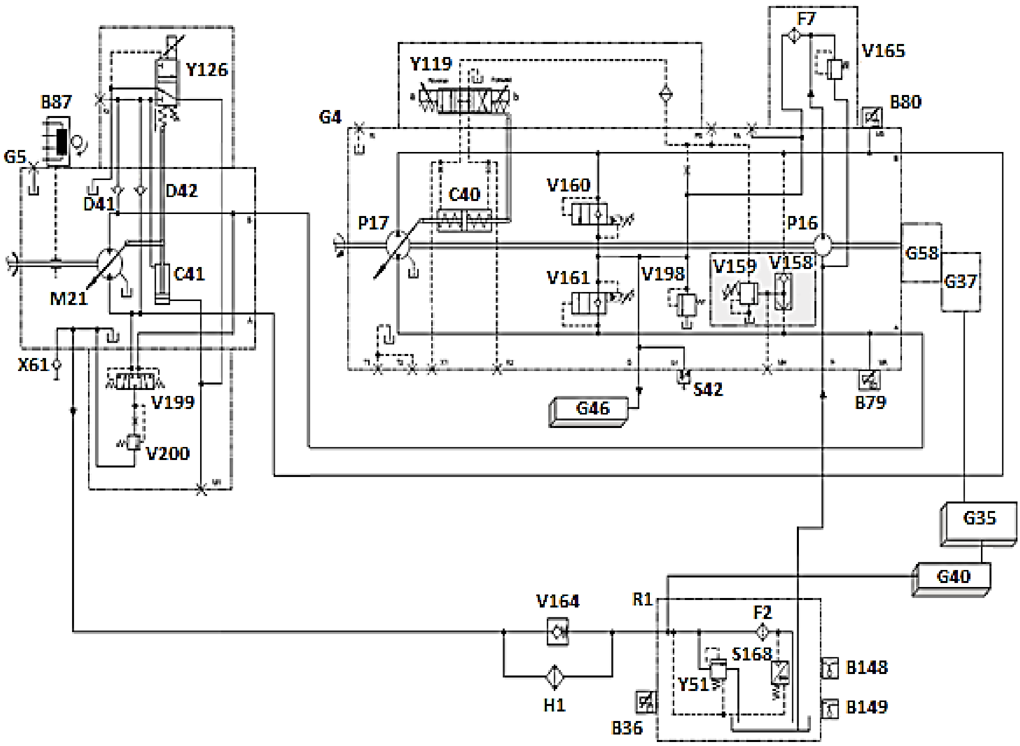


**Figure 1.** Diagram of hydraulic circuits of the hydrostatic transmission of the JD S680i combine harvester.

The valve block of the hydraulic motor is equipped with a hydraulically controlled distributor (V199), which connects the low-pressure branch of the closed circuit with the discharge pipe. The fluid, however, must pass through the bypass valve (V200) maintaining the required charging pressure in the closed circuit. The fluid passes from the filling pump (P16) through the axial piston pump (P17) and axial piston hydraulic motor (M21) and it exists the hydraulic converters through the hydraulic elements (V199 and V200). The cooler (H1), through which the fluid flows back to the tank, is placed separately. If the fluid is cool, it runs through the bypass valve (V164) which puts up lesser resistance than the cooler. The discharge fluid is joined by waste, so-called leakage, fluid, leaking around the moving parts of the pump and the hydraulic motor. The pressure-relief filling valve of the circuit (V198) is usually adjusted to a pressure of 4.2 MPa, the bypass valve (V200) is usually adjusted to a pressure of 2.8 MPa and the high-pressure valves (V160 and V161) are usually adjusted to a pressure of 49 MPa.

The presented complex hydraulic circuits clearly indicate the occurrence of pressure losses and, consequently, power loss. We classify pressure losses occurring in hydraulic circuits into three types:

- losses in direct piping;
- losses in local resistances;
- losses in the individual elements of the circuit (Roh, 1989).

Calculations performed in this article provide a better understanding of hydraulic losses of combine harvester travel gear. At the same time, these values will be used in future for comparison with the real measured values. And for comparison of the energy intensity of travel gear of combine harvesters with wheeled and tracked chassis.

## MATERIALS AND METHODS

Measurements were carried out on the John Deere S680i combine harvester owned by the Agricultural Business Co-operative Zálabí with its registered office in Ovčáry.

Materials for measurement were prepared based on the obtained diagram of hydraulic circuits of the combine harvester hydrostatic transmission. We measured all the necessary external dimensions of the hydraulic circuit (piping length, diameter), ascertained the number of elbow pipes, tees, etc. The internal dimensions of these elements have been ascertained from the catalogues of manufacturers based on the external dimensions measured. The parameters of the pumps and hydraulic motor, such as geometric volume, working pressures, speeds and efficiencies, have been ascertained from the machine's technical manual. The pump capacities have subsequently been calculated based on these parameters. For subsequent calculations in the high-pressure circuit, we assume a maximum flow rate at which the combine harvester reaches the maximum travelling speed. The technical manual also provided the set pressures of pressure-relief valves, pressure losses of some elements (cooler, filter). It was also necessary to ascertain the specifications of the working fluid (kinematic viscosity, density) which were obtained from the materials of the fluid manufacturer.

Each element is registered under a 'code' determining its parameters. In the direct piping, the hoses are designated as **H** and steel pipes are designated as **R**. A number of items can also be indicated before the letter. The letter is followed by a number indicating the internal diameter of the element in millimetres; the number after the slash indicates the length of the element in millimetres. For example, **3xR30/200** means that the circuit contains **3** steel pipes with an internal diameter of **30 mm** and a length of **200 mm**. In local resistances, the number of items is designated similarly, before the name of the element. The name of the element is followed by a number indicating the internal diameter of the element in millimetres and the figure after the slash represents the bending of the element in degrees. For example, **elbow pipe 25/100°** means an elbow pipe element with an internal diameter of **25 mm** and a bending of **100°**.

To calculate the power loss $P_Z$, we use the equation (1), where we multiply each element of the pressure loss at the given point of the circuit by the flow rate at the given point of the circuit.

$$P_Z = p_Z \cdot Q \tag{1}$$

where: $P_Z$ – power loss (W); $Q$ – working fluid flow rate ($m^3$ $s^{-1}$); $p_Z$ – pressure loss (Pa).

The flow rate at the given point of the circuit was calculated using the parameters of the pump indicated by the manufacturer using the equation (2).

$$Q = \frac{V_g \cdot n \cdot \eta_Q}{1{,}000} \tag{2}$$

where: $Q$ – working fluid flow rate ($m^3\ s^{-1}$); $V_g$ – geometric volume of the pump($m^3$); $n$ – pump speed ($s^{-1}$); $\eta_Q$ – flow efficiency of the pump (-).

Losses in the direct piping, i.e. losses in hydraulic hoses and steel pipes, represent the first component of the pressure loss. They are calculated from the equation (3) and related formulas.

$$p_Z = \lambda \cdot \frac{l}{d} \cdot \frac{v^2}{2} \cdot \rho \tag{3}$$

where: $p_Z$ – pressure loss (Pa); $\lambda$ – coefficient of linear losses (-); $l$ – hydraulic piping length (m); $d$ – hydraulic piping internal diameter (m); $v$ – fluid flow velocity through piping ($m\ s^{-1}$); $\rho$ – working fluid density ($kg\ m^{-3}$).

First, it is necessary to calculate the flow velocity of the fluid through piping (4) using the formula for calculation of the cross-section of hydraulic piping (5).

$$v = \frac{Q}{S} \tag{4}$$

where: $Q$ – working fluid flow rate ($m^3\ s^{-1}$); $S$ – hydraulic piping cross-section ($m^2$); $v$ – fluid flow velocity through piping ($m\ s^{-1}$).

$$S = \frac{\pi \cdot d^2}{4} \tag{5}$$

where: $S$ – hydraulic piping cross-section ($m^2$); $d$ – hydraulic piping internal diameter (m).

For the coefficient of linear losses (7, 8, 9, 10), it is necessary to first calculate the so-called Reynolds number and classify it into the correct group for the given flow situation.

$$\mathrm{Re} = \frac{v \cdot d}{\upsilon} \tag{6}$$

where: $Re$ – Reynolds number (-); $v$ – fluid flow velocity through piping ($m\ s^{-1}$); $\upsilon$ – kinematic viscosity ($m^2\ s^{-1}$).

$Re$ < 2,300 - laminar flow range
2,300 < $Re$ < 5,000 - transition range
5,000 < $Re$ - turbulent flow range
For laminar flow in hoses:

$$\lambda = \frac{80}{\mathrm{Re}} \tag{7}$$

For laminar flow in pipes:

$$\lambda = \frac{64}{\mathrm{Re}} \tag{8}$$

For transition flow range:

$$\lambda = \frac{0.316}{\sqrt[4]{\mathrm{Re}}} \tag{9}$$

For turbulent flow range:

$$\lambda = \left(\frac{200}{\mathrm{Re}}\right)^2 \tag{10}$$

Losses in local resistances, the so-called local losses, represent the second component of pressure losses. The calculation (11) is similar to that in the case of pressure losses in direct piping; only the coefficient of linear losses $\lambda$ and the ratio of direct piping length l to its internal diameter d is replaced by the coefficient of local resistance $\xi$ which is determined empirically for each element of the circuit.

$$p_Z = \xi \cdot \frac{v^2}{2} \cdot \rho \tag{11}$$

where: $p_Z$ – pressure loss (Pa); $\xi$ – coefficient of local resistance (-); $v$ – fluid flow velocity through piping (m s$^{-1}$); $\rho$ – working fluid density (kg m$^{-3}$).

The third component is represented by pressure losses in the individual elements (12). They are determined based on efficiencies of the elements stipulated by the manufacturer where the calculation requires primarily the pressure efficiency $\eta_p$. For other elements, we directly indicate the pressure loss stipulated by the manufacturers of the particular hydraulic elements.

$$p_Z = (1 - \eta_p) \cdot p \tag{12}$$

where: $p_Z$ – pressure loss (Pa); $\eta_p$ – pressure efficiency (-); $p$ – pressure in piping (Pa).

To obtain the resulting value of power loss, we add up the power losses of the individual components.

## RESULTS AND DISCUSSION

After the substitution in the previous formulas, using MS Excel software, we calculated the values for pressure losses and power losses in the elements of the direct piping circuits, local resistances and the individual elements of the circuit (tables 1, 2, 3).

**Table 1.** Pressure loss and power losses in direct piping

| Element Code | $p_Z$ (kPa) | $P_Z$ (W) |
|---|---|---|
| H30/4250 | 1.78 | 8.13 |
| H30/3855 | 1.61 | 7.38 |
| H25/5555 | 13.89 | 12.22 |
| H25/3500 | 8.75 | 7.70 |
| H25/1700 | 4.25 | 3.74 |
| H25/550 | 1.38 | 1.21 |
| H25/450 | 1.13 | 0.99 |
| 3xR30/200 | 0.08 | 1.15 |
| 2xR30/100 | 0.04 | 0.38 |
| R30/400 | 0.17 | 0.77 |
| R30/660 | 0.28 | 1.26 |
| 2xR25/300 | 0.75 | 1.32 |
| R25/900 | 2.25 | 1.98 |
| R25/500 | 1.25 | 1.10 |
| R25/200 | 0.50 | 0.44 |
| R25/100 | 0.25 | 0.22 |
| Total | 39.31 | 50.00 |

**Table 2.** Pressure loss and power losses in local resistances

| Element Code | $p_Z$ (kPa) | $P_Z$ (W) |
|---|---|---|
| 3x elbow pipe 30/90° | 26.51 | 364.21 |
| elbow pipe 30/135° | 30.04 | 137.59 |
| 6x elbow pipe 25/90° | 2.03 | 10.71 |
| elbow pipe 25/100° | 2.30 | 2.02 |
| elbow pipe 25/135° | 2.10 | 1.85 |
| 4x tee-piece 25 | 2.03 | 7.14 |
| inlet into tank 25 | 1.35 | 1.19 |
| outlet from tank 25 | 1.35 | 1.19 |
| Total | 136.96 | 525.91 |

**Table 3.** Pressure loss and power losses in individual elements

| Element Code | $p_Z$ (kPa) | $P_Z$ (W) |
|---|---|---|
| gear pump | 76.09 | 66.96 |
| axial pump | 1,616.49 | 7,403.55 |
| axial hydraulic motor | 1,616.49 | 7,403.55 |
| cooler | 800.00 | 704.00 |
| filter | 900.00 | 792.00 |
| Total | 5009.08 | 16370.05 |

The resulting tables indicate that the lowest losses occur in the direct piping. By contrast, the highest losses are in the individual elements of the circuits which is 96.6% of the total losses in the circuits of the travel gear hydrostatic transmission.

We can find out the total power losses by adding up the power losses of all components of the circuits specified in Tables 1, 2, 3. This indicates the power that is taken from the combustion engine of the combine harvester to overcome the losses in the circuits of the travel gear hydrostatic transmission at its maximum travelling speed.

$$\boldsymbol{P_Z} = 50.00 + 525.91 + 16370.05 = 16945.96 \text{ W} = \mathbf{16.95\ kW}$$

Taking into account the fact that the combustion engine of the combine harvester has a rated power (according to ECE R120) $P$ = 353 kW, the percentage representation of hydrostatic transmission according to the formula (13) equals **4.8%**. This is reflected in the energy performance and the fuel consumption (Jokiniemi et al., 2012).

$$\frac{P_Z}{P} = \frac{16.95}{353} = 0.048 \Rightarrow 4.8\% \tag{13}$$

From the results it is clear that the proposal to improve the direct piping and the local resistances of the hydraulic system is unnecessary. The losses are negligible. The biggest losses occur in the individual elements which have given construction, thus given losses.

## CONCLUSIONS

After measuring all elements in the circuits and their calculation, we have determined the pressure losses and power losses in the direct piping, in local resistances and in the individual elements of the circuit. Losses in the individual elements of the circuits, i.e. 16.37 kW (96.6%), constitute the greatest fraction of the total losses. The total losses in the circuits of the travel gear hydrostatic transmission of the combine harvester equal 16.95 kW. This value applies to the maximum flow rate in the high-pressure circuit at the maximum travelling speed of the combine harvester. With declining travelling speed and, consequently, also the flow rate in the high-pressure circuit, the losses in this circuit would also decline.

Calculations presented in this article will be used for comparison with the real values which will be measured in the future.

ACKNOWLEDGEMENTS. This contribution has been drawn up on the basis of the solution of project 2014: 31160/1312/3118 financed by the Internal Grant Agency of the Faculty of Engineering of the Czech University of Life Sciences Prague.

## REFERENCES


Jokiniemi, T., Rossner, H., Ahokas, J. 2012. Simple and cost effective method for fuel consumption measurements of agricultural machinery. *Agronomy Research* **10**(1), 97–107.

Kutzbach, H.D. 2000. Trends in power and machinery. *Journal of Agricultural Engeneering Research* **76**, 237–247.

Kučík, P., Strážovec, I. 2000. *Hydraulic Transfer of Energy*. University of Žilina, Žilina. 384 pp. (in Slovak).

Lou Xi-Yin, 2014. Application of Tracked Combine Harvester Step-less Speed Regulated System. *Advanced Materials Research* **940**, 128–131.

Roh, J. 1989. *Hydraulic Mechanisms of Agricultural Machines*. Státní zemědělské nakladatelství. Prague, 344 pp. (in Czech).

Roh, J. 1992. *Management and operation of combine harvesters*. University of life sciences Prague. Prague, 245 pp. (in Czech).

*Agronomy Research* **13**(1), 33–45, 2015

# Use of Euler equations in research into three-dimensional oscillations of sugar beet root during its vibration-assisted lifting

V. Bulgakov[1], V. Adamchuk[2], J. Olt[3,*] and D. Orszaghova[4]

[1]National University of Life and Environmental Sciences of Ukraine, 15, Heroyiv Oborony Str., 03041 Kyiv, Ukraine
[2]National Scientific Centre 'Institute for Agricultural Engineering and Electrification', 11, Vokzalna Str., Glevaкha-1, Vasylkiv District, 08631 Kiev Region, Ukraine
[3]Estonian University of Life Sciences, Institute of Technology, Kreutzwaldi 56, EE51014 Tartu, Estonia; [*]Correspondence: jyri.olt@emu.ee
[4]Slovak University of Agriculture in Nitra, 2, Trieda Andreja Hlinku, 949 76 Nitra, Slovakia

**Abstract.** Following the results of the research into the physical process of the vibratory interaction between the digging tool and the beet root, it has been found that the latter, while standing in soil, i.e. amid an elastic medium, has strong attachment to the soil in its lower (the densest and driest) part, which virtually implies one conventional fixed point. This finding provides the basis for examination of the three-dimensional motion of the beet root's body during its lifting from the ground in case of its asymmetric interaction with one of the shares of the vibrating digging tool. We have studied the gyration of the beet root's body about a point initiated by its interaction with the inclined face of the vibrating digging tool share that makes oscillatory movements in the longitudinal vertical plane. The aim of the study is to establish the values of the angular displacements of the root's body at the moment of its getting in asymmetric contact with the vibrating digging tool followed by the breaking of its bonds with the surrounding elastic medium, i.e. to develop a new mathematical model of the vibration-assisted digging of a beet root out of the soil. Basing on the use of the original equations of Euler, a new differential equation system has been obtained, which facilitates the analytical treatment of the mentioned work process. That system of differential equations for the three-dimensional oscillations of the root caused by the action of a perturbing force comprises three dynamic and three kinematic equations. It is a determined system, which makes possible its solution, i.e. the numerical modelling of the process of root lifting from the ground under different digging conditions, because it includes all necessary parameters of the vibrating digging tool, the sugar beet root and the soil surrounding it.

**Key words:** sugar beet root, vibrating digging tool, three-dimensional motion, lifting, modelling.

## INTRODUCTION

The theoretical and field research into the work processes and the use of its results for the development of improved tools for digging sugar beet roots out of the ground are critically important tasks for the sugar beet growing industry, because just this final operation is the most complex and energy-intensive work process in the cultivation of sugar beet (Bulgakov & Ivanovs, 2010; Lammers, 2011; Lammers & Schmittmann, 2013; Gu et al., 2014). The extensive use of vibrating digging tools for the digging out of beet roots observed recently is stipulated by the lowest energy input for the break-up of the soil surrounding roots, the reduced loss and damage of roots in the harvesting process in this case. However, the described advantages are achieved under relatively favourable harvesting conditions, especially when the soil has low hardness indices and a sufficient moisture content. Under all other conditions vibrating digging tools do not display the said advantages.

Hence, that is exactly the work process that needs in-depth theoretical and field research followed by the development and implementation of improved vibrating digging tools.

Study (Dubrovski, 1968) should be regarded as the first analytical treatment of the vibration-assisted process of sugar beet root digging out of the soil. Still, the paper did not offer a mathematical model of the vibration-assisted lifting of the root from the ground. The oscillatory process of the interaction between the vibrating digging tool and the root's body was assumed to take place in the transverse vertical plane, which would not be implemented later in any digging tool employed in any commercially produced root crop harvester.

The further analytical study of the oscillations of the root's body fixed in soil was presented in publication (Vasilenko et al., 1970). As the paper itself states, the process of lifting sugar beet roots from the ground per se is analysed here with the use of the generated kinetostatic equations, which, in the authors' opinion, allow to find the conditions for the complete lifting of a sugar beet root from the soil. However, the detailed analysis of the mentioned equations has proved that they effectively do not characterise the work process of digging roots from soil.

Publication Pogorely et al. (2004) features the setting up of the Ostrogradsky-Hamilton functional that characterises the natural transverse oscillations of a sugar beet root's body modelled as a fixed low end bar. Meanwhile, it considers the case when the perturbing force is applied to the root crop in the transverse horizontal plane, which has also never been implemented in any real vibrating digging tool.

Paper (Pogorely et al., 1983), which is an essentially first published study on sugar beet harvesting machinery, adopts the main provisions and assumptions stated in the previous studies (Vasilenko et al., 1970). It should be pointed out that this work also does not furnish a model of the vibration-assisted lifting of a sugar beet root from the soil.

The further elaborations on the theory of the vibration-assisted sugar beet root digging out of the soil with application of the perturbing forces exactly in the longitudinal vertical plane were highlighted in studies (Bulgakov, 2005; Sarec et al., 2009; Bulgakov et al., 2014). Nevertheless, to advance further on it is necessary to consider separately and in more depth the dynamic system 'beet root – vibrating digging tool', in order to analyse both the process of oscillations of the beet root itself in the soil and the very process of lifting of the root as a solid body from the soil, the latter taking place under the effect of the vibrating digging tool that oscillates in the longitudinal vertical plane and also due to its translational motion.

The analysis of many literary sources (Vermeulen & Koolen, 2002; Lammers, 2011; Wang & Zhang, 2013; Wu et al., 2013; Gu et al., 2014) makes it evident that the research into new sugar beet harvesting technologies attracts substantial attention worldwide.

## MATERIALS AND METHODS

In order to explore the process of sugar beet root digging, let's start with one of the first stages in this work process, when the beet root is still sufficiently strongly attached to the soil. The vibrating digging tool, advancing linearly at a preset running depth in the soil and at the same time oscillating in the longitudinal vertical plane, approaches the beet root from one side and breaks the surrounding soil. The bonds between the beet root and the soil in the immediate zone of movement of the work faces of the vibrating digging tool (on that side, from which the tool linearly advances and on which it starts making contact with the root), can be considered almost broken, while the soil surrounding the root in its upper part (within the tool running depth in the soil) is already sufficiently loosened (longitudinal fissures are possible in the soil layers across the whole thickness of the upper part). Meanwhile, the actual lifting of the beet root from the ground has not yet begun, even if the vibrating digging tool work faces have already started making contact with the root's body. It is quite apparent that at this stage of the work process of root digging out of the soil the root has already started carrying out its motions in the ground as a solid body with one fixed attachment point or a solid body pivoting about a fixed axis. It is to be stressed in the first instance that the soil surrounding the beet root provides resistance to the latter's lifting positively all over the whole conic surface, because the root gets sufficiently strongly embedded in the soil in the process of its growth.

Thus, during the straining of top soil by the work faces of the vibrating digging tool that move at a certain running depth and the subsequent breaking of bonds between the beet root and the soil at the upper part, the lower part of the root continues to reside in the unstrained and very dense layer of soil. The said circumstances substantiate the assumption that this is exactly the part of the soil, where the point on the root's symmetry axis, which can be conventionally considered the fixing point of the root in the soil, is located. But, this stage of digging the root out of soil continues only for a short while and is succeeded by the second stage, where the vibrating digging tool actually starts imparting its forces to the root body. Therefore, the motions of the beet root at the second stage can be characterised with the use of kinematic and dynamic Euler equations considering it as a symmetrical solid body with one fixed attachment point or a solid body pivoting about a fixed axis in the longitudinal vertical plane. At the same time, the beet root begins oscillating in the soil as an elastic medium, because just at this stage of the lifting the soil surrounding the root (especially on the side opposed to the tool's travel direction) can be with good reasons considered an elastic medium.

To facilitate the analytical treatment of the process of digging the beet root out of the soil by the vibrating digging tool, we build first the equivalent schematic model, where the beet root is approximated by a regular cone, point O being its only (conventional) point of fixation in the ground. The vibrating digging tool comprises two digging shares, which can be represented by two conventional wedges $A_1B_1C_1$ and $A_2B_2C_2$, their wedged forward parts and lower parts moving in soil (Fig. 1). Each of the said wedges has angles of tilting in space designated $\alpha$, $\beta$ and $\gamma$, which are determined so that the share faces form an angled working passage, which necks in rearwards. Structurally, the vibrating digging tool is a usual share lifter, but kinematically it is connected to a drive (not shown in the schematic model), which induces its oscillations in the longitudinal vertical plane at preset frequency and amplitude. The digging tool as a whole advances linearly at a preset velocity $\overline{V}$ , down the direction shown by an arrow.

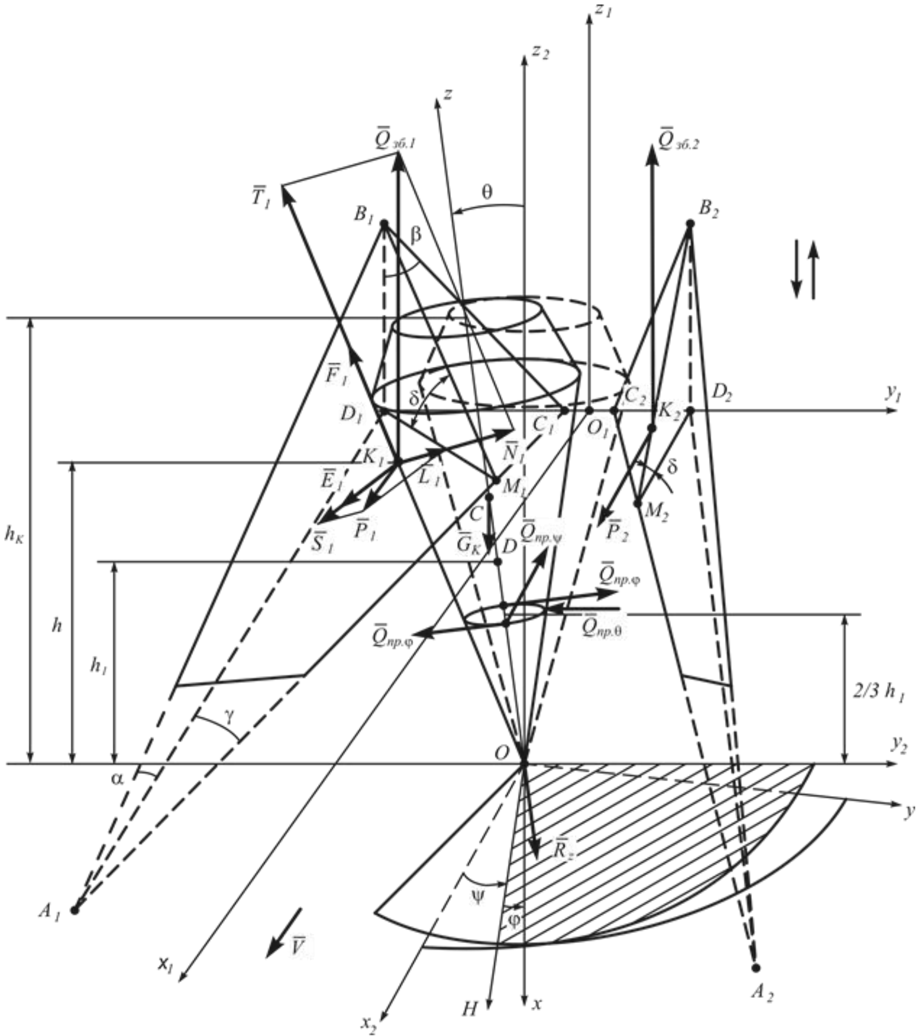

**Figure 1.** Equivalent schematic model of the force interaction between the vibrating digging tool and the beet root during the latter's gyration about the conventional point of fixation in the ground.

Further, we have to show in the equivalent schematic model the adopted coordinate systems. First, we relate to the vibrating digging tool the orthogonal Cartesian coordinate system $O_1x_1y_1z_1$ with the centre $O_1$ in the middle of its necked-in passage. In this system, the axis $O_1x_1$ is in line with the direction of the tool's translational motion, the axis $O_1z_1$ is vertically pointing up, and the axis $O_1y_1$ is pointing to the right (Fig. 1). The vibrating digging tool's oscillatory movements in the longitudinal vertical plane should be examined in reference to just that coordinate system $O_1x_1y_1z_1$.

We also introduce the moving coordinate system Oxyz rigidly connected with the beet root and having an origin at the point O, which is the point of fixation of the beet root in the ground, its axis Oz being aligned with the root's symmetry axis and pointing upwards, the axes Ox and Oy placed in the plane that is perpendicular to the axis Oz.

Besides, to characterise the gyration of the root about the fixation point O it is necessary to introduce one more orthogonal Cartesian coordinate system $O_2x_2y_2z_2$, which is shown in Fig. 1.

Since the vibrating digging tool at the moment of its getting in contact with the beet root advances linearly along the axis $O_1x_1$ ($O_1x_2$), the root deflects from its vertical position (effectively from the axis $Oz_2$) through some angle $\psi$ unidirectionally with the motion of the tool. In the most general case, the initial contact between the beet root and the tool is asymmetric meaning that one of the digging shares gets into direct contact with the root body, while the other one makes contact through some thickness of the broken soil. This results, following the deformation of the said thickness of soil, in the beet root's deflection from its vertical position transversely through some angle $\theta$. Moreover, the difference of the torques produced by the direct contact of the root with one of the shares and its contact with the other share through the thickness of soil can result in the rotation of the root through some angle $\varphi$ about the axis Oz. Overall, summing up the above-mentioned physical conditions, we have good reasons to believe that the beet root in its interaction with the vibrating digging tool immediately during its lifting performs simultaneously the rotation about some line OH (nodal line) through the angle $\theta$, the rotation about the axis $Oz_2$ through the angle $\psi$ and the rotation about the axis Oz through the angle $\varphi$. Hence, the introduced angular displacements in space of the root during its lifting from the ground are Euler angles, the angle $\theta$ having a name of nutation angle, the angle $\psi$ – precession angle, the angle $\varphi$ – intrinsic rotation angle.

We also have to take into account that, since the root body has a conical shape, the direct contact between the digging shares and the root body is lost in case of the vibrating digging tool going down. As a result, the perturbing force stops acting on the beet root, therefore, the root under the effect of the elasticity of the soil surrounding it on the front and the root body's own elastic properties tends to return to the vertical equilibrium position. With the following upward motion the digging shares resume their contact with the root body, take hold of the root, impart to it first of all the perturbing force and the mentioned process of root's rotations recurs.

Thus, the beet root performs oscillations about the line of nodes OH, about the axis $Oz_2$ and about the axis Oz. Actually, the root's oscillations at the first stage of its lifting from the ground comprise the longitudinal linear oscillations of the point of the root's fixation in the ground O and the angular oscillations of the root relative to the point O characterised by the variation of the Euler angles $\theta$, $\psi$ and $\varphi$.

## THEORY AND MODELLING

We have assumed that the beet root is in direct contact with only one of the work faces of vibrating digging tool, specifically $A_1B_1C_1$ at the point $K_1$, while the face $A_2B_2C_2$ acts on the root body surface via some thickness of the soil and this contact can occur at the point $K_2$ (Fig. 1). Certainly, the contact between the vibrating digging tool and the root body at the point $K_2$ is made throughout some area surrounding the point $K_2$, but in our further considerations we are going to assume that the point $K_2$ is the point of application of the forces imparted to the beet root.

Besides, the asymmetry of the contact with the beet root is also due to the fact that its symmetry axis (axis Oz) can be offset aside relative to the centre line of the sowing rows (due to the requirements of the agricultural sowing and plant handling technologies). We assume that prior to the commencement of the direct contact between the beet root and the digging tool, the axis Oz is parallel to the axis $O_1z_1$.

Also, we have to designate some representative points in the equivalent schematic model. Thus, the right lines drawn via the points $B_1$ and $B_2$ perpendicular to the wedge sides $A_1C_1$ and $A_2C_2$, respectively, generate at their intersections with the said wedge sides the respective points $M_1$ and $M_2$. Hence, $\delta$ is the dihedral angle ($\angle B_1M_1D_1$) between the first wedge's lower base $A_1D_1C_1$ and the work face $A_1B_1C_1$ and also the dihedral angle ($\angle B_2M_2D_2$) between the second wedge's lower base $A_2D_2C_2$ and the work face wedge $A_2D_2C_2$. Angle $2\gamma_k$ is the apical angle of the cone used as a model of the beet root. The meaning of other dimensions can be understood from the equivalent schematic model (Fig. 1).

Now, let's consider the forces originating from the interaction between the vibrating digging tool and the beet root.

Since the digging tool, as it has been stated, is a vibrational tool, it imparts the vertical perturbing force $\overline{Q}_{зб.}$, which varies under the following harmonic law:

$$Q_{зб.} = H \sin \omega t\,, \tag{1}$$

where: $H$ – amplitude of the perturbing force; $\omega$ – frequency of the perturbing force.

That force plays the primary role in the process of soil breaking in the zone of the digging tool's work passage and the direct lifting of the beet root out of the ground. The perturbing force $\overline{Q}_{зб.}$ is applied to the beet root or the soil surrounding it on two sides, therefore, it is represented in the equivalent schematic model by two components $\overline{Q}_{зб.1}$ and $\overline{Q}_{зб.2}$, which apparently have the following values:

$$Q_{зб.1} = Q_{зб.2} = \frac{1}{2} H \sin \omega t \tag{2}$$

Further considerations require careful analysis of the relation between the oscillations of the vibrating digging tool and the concurrent action of the perturbing force $\overline{Q}_{зб.}$ on the root. It is sufficient to carry out the analysis only for one oscillation period, from $\omega t = 0$ to $\omega t = 2\pi$. In all other oscillation periods the process is repeated. As we already mentioned above, the perturbing force $\overline{Q}_{зб.}$ acts on the beet root only when the digging shares of the tool move up from their lowermost position to their uppermost position, making in this process contact with the conical root body.

For this reason, during the movement of the digging shares of the tool up on the interval $(0, \pi)$, the perturbing force $\overline{Q}_{зб.}$ acts on the beet root following the sinusoidal law

(1). In this process, on the interval $\left[0,\ \frac{\pi}{2}\right]$ it increases from the zero value $Q_{зб.} = 0$ at the point $\omega t = 0$ to the maximum value $Q_{зб.} = H$ at the point $\omega t = \frac{\pi}{2}$.

On the interval $\left[\frac{\pi}{2},\ \pi\right]$ it decreases from its maximum value $Q_{зб.} = H$ to the minimum one $Q_{зб.} = 0$. On the interval $(\pi,\ 2\pi)$ the digging shares of the tool move down, therefore, the perturbing force $\overline{Q}_{зб.}$ does not act on the root on this leg. On the interval $(2\pi,\ 4\pi)$ everything recurs. Thus, in general on the intervals $(2k\pi,\ (2k + 1)\pi)$, $k = 0, 1, 2, \ldots$, the perturbing force $\overline{Q}_{зб.}$ acts on the beet root following the sinusoidal law (1), and on the intervals $((2k - 1)\pi,\ 2k\pi)$, $k = 0, 1, 2, \ldots$, it has no effect on the beet root, since it is equal to zero.

As the cutting edges $A_1C_1$ and $A_2C_2$ of the digging shares are located below the contact points $K_1$ and $K_2$, the soil in the area of the contact between the beet root and the vibrating digging tool is already sufficiently much broken, but the soil breaking occurs primarily in the front part of the tool's passage, while the direct contact between the beet root and the tool – in the middle and rear parts of the work passage. Therefore, in case of asymmetric contact with the beet root at the point $K_1$ the root is under the direct effect of the perturbing force $\overline{Q}_{зб.1}$, while at the contact point $K_2$ the perturbing force $\overline{Q}_{зб.2}$ acts only on the thickness of broken soil, which makes us assume that this latter force is virtually not imparted directly to the root body. Hence, at the first contact between the root body and the vibrating digging tool, the effect of perturbing force $\overline{Q}_{зб.2}$ on the beet root can be ignored and it can be assumed that the root is under the effect of only the perturbing force $\overline{Q}_{зб.1}$ acting from the side of the face $A_1B_1C_1$, i.e. only one digging share.

In addition, it is to be pointed out that the interesting aspect of the asymmetric contact with the beet root is that it makes possible the rotation of the root about its axis, promoting the intensive break-up of the bonds between the root and the soil (phenomenon of the root's spinning in the ground during its digging out). So, in case of asymmetric contact between the beet root and the vibrating digging tool we are going to take into the differential equations for the root's motion only the force action of the work face $A_1B_1C_1$ of one digging share. For this purpose we decompose the force $\overline{Q}_{зб.1}$ into two components: $\overline{N}_1$, normal to the face $A_1B_1C_1$, and $\overline{T}_1$, tangential to the same face, as shown in the equivalent schematic model in Fig. 1. This force is equal to:

$$\overline{Q}_{зб.1} = \overline{N}_1 + \overline{T}_1 \qquad (3)$$

Apparently, the $\overline{T}_1$ force vector is parallel to the right line $B_1M_1$.

As the vibrating digging tool advances linearly along the axis $O_1x_1$ relative to the beet root fixed in the ground, we have a driving force $\overline{P_1}$ that acts along the course of the translational movement (along the axis $O_1x_1$) and also acts on the root along that axis at the moment, when contact is made between the beet root and digging tool. Now, let's decompose the force $\overline{P_1}$ also into two components: $\overline{L_1}$, normal to the wedge face $A_1B_1C_1$ and $\overline{S_1}$, tangential to the same face, i.e.:

$$\overline{P}_1 = \overline{L}_1 + \overline{S}_1. \tag{4}$$

Thus, at the contact point $K_1$ the beet root is under the effect of the force applied by the wedge $A_1B_1C_1$, which is equal to:

$$\overline{N}_{K_1} = \overline{N}_1 + \overline{L}_1, \tag{5}$$

and points along the normal to the surface of the wedge $A_1B_1C_1$.

Apparently, the magnitude of this force is:

$$N_{K_1} = N_1 + L_1 \tag{6}$$

Also, at the contact point $K_1$ the force of friction $\overline{F}_{K_1}$ is applied, which counteracts the slipping of the beet root on the work face of the wedge $A_1B_1C_1$ during its contact with the vibrating digging tool. The vector of this force is in opposition to the vector of the relative velocity of the wedge's slipping on the surface of the beet root. The root weight force $\overline{G}_k$ is applied vertically at the centre of mass of the beet root. Also, during the contact between the beet root and the vibrating digging tool, when the latter's shares move upwards, the root is under the effect of the soil's elastic deformation force acting along axis Oz, designated as $\overline{R}_z$ in the equivalent schematic model.

The tangential component $\overline{T_1}$ of the perturbing force $\overline{Q}_{зб.1}$ and the tangential component $\overline{S_1}$ of the driving force $\overline{P_1}$ do not act directly on the beet root, they only cause the breaking of the soil around the beet root, therefore, they are not included in the differential equations of the movement of the root as a solid body. Then, it is possible to derive from the equivalent schematic model (Fig. 1) the expressions for determining the normal $\overline{N}_1$ and tangential $\overline{T_1}$ components of the perturbing force $\overline{Q}_{зб.1}$, as well as the expressions for determining the normal $\overline{L}_1$ and tangential $\overline{S}_1$ components of the driving force $\overline{P_1}$.

Meanwhile, the forces, generated by the straining of the soil as an elastic medium during the displacement of the beet root in it, need to be determined.

The moment of the elastic soil deformation force due to the angular displacement of the beet root through the angle $\varphi$ is equal to:

$$M_{np.\varphi} = -\int_0^{h_1}\int_0^{2\pi} \frac{c_1 z^2 dz\,\varphi \sin^2\gamma_k\, d\alpha}{2\pi\cos^3\gamma_k} = -\frac{c_1 h_1^3 \varphi \sin^2\gamma_k}{3\cos^3\gamma_k}, \tag{7}$$

where $c_1$ – elastic stiffness of the soil that determines the increase of the force acting on the contact surface in case of displacement of the contact surface for a contact area unit (N m$^{-2}$).

Similarly, it is possible to determine that the elastic forces in the soil resulting from the angular displacements of the beet root fixed in it about the axis $Oz_2$ through the angle $\psi$ – $\overline{Q}_{np.\psi}$ and about the line of nodes $OH$ through the angle $\theta$ – $\overline{Q}_{np.\theta}$ are equal to, respectively:

$$Q_{np.\psi} = \int_0^{h_1}\int_0^{\pi} \frac{c\sin\gamma_k \psi\, d\alpha\, z^2 dz}{\cos^3\gamma_k} = \frac{c\pi h_1^3 \sin\gamma_k\,\psi}{3\cos^3\gamma_k}, \tag{8}$$

$$Q_{np.\theta} = \int_0^{h_1}\int_0^{\pi} \frac{c\sin\gamma_k \theta\, d\alpha\, z^2 dz}{\cos^3\gamma_k} = \frac{c\pi h_1^3 \sin\gamma_k\,\theta}{3\cos^3\gamma_k}, \tag{9}$$

where $c$ – elastic stiffness of the soil (ratio of the first coefficient of Winkler to the contact area) (N m$^{-3}$).

Apparently, the vectors $\overline{Q}_{np.\psi}$ and $\overline{Q}_{np.\theta}$ point along the normal to the surface of the beet root. The forces determined by the expressions (7, 8, 9) act as the restoring forces in the oscillatory process under consideration.

The force $\overline{R}_z$ is the resultant of the load distributed over the beet root's surface with an unbroken thickness of soil and the intensity vectors of this load point downwards parallel to the axis Oz. Therefore, the force $\overline{R}_z$ acts along the axis Oz and points downwards.

The magnitude of the force $\overline{R}_z$ is determined with the use of the following formula:

$$R_z = \int_0^{h_1}\int_0^{2\pi} \frac{c_1 z\, tg\gamma_k\, d\alpha\, dz}{h_1\cos\gamma_k} z_k = \frac{c_1 \pi h_1 \sin\gamma_k\, z_k}{\cos^2\gamma_k}. \tag{10}$$

Further, we proceed to the generation of differential equations for the gyration about a point of the beet root as a solid body during its asymmetric contact with the vibrating digging tool. In this case, according to what was said earlier, the beet root moves as a solid body with one fixed point, the position of which is determined by the variation of the above-mentioned Euler angles $\varphi$, $\psi$ and $\theta$ under the effect of the described forces and moments of forces acting on the root and characterised with the use of dynamic and kinematic equations of Euler.

In this case, if the moving coordinate system Oxyz is chosen in such a way that the coordinate axes are the principal axes of inertia for the point O, then the dynamic equations of Euler will take the following form (Dreizler & Lüdde, 2010):

$$\left.\begin{aligned} I_x \frac{d\omega_x}{dt} + \left(I_z - I_y\right)\omega_y\omega_z = M_x^e, \\ I_y \frac{d\omega_y}{dt} + \left(I_x - I_z\right)\omega_x\omega_z = M_y^e, \\ I_z \frac{d\omega_z}{dt} + \left(I_y - I_x\right)\omega_x\omega_y = M_z^e, \end{aligned}\right\} \tag{11}$$

where: $\omega_x$, $\omega_y$ and $\omega_z$ – projections of the root's angular velocity during its angular displacement about the instantaneous axis of rotation on the axes of the moving coordinate system Oxyz; $I_x$, $I_y$ and $I_z$ – the moments of inertia of the beet root in reference to the coordinate axes Ox, Oy and Oz (principal axes of inertia of the root), respectively; $M_x^e$, $M_y^e$ and $M_z^e$ – principal moments of all external forces acting on the beet root in reference to the coordinate axes Ox, Oy and Oz, respectively.

As shown in the equivalent schematic model (Fig. 1), the axes of the moving coordinate system Oxyz are the principal axes of inertia of the beet root. Indeed, the axis Oz is the root's material symmetry axis. The axes Ox and Oy lie in the plane that is perpendicular to the axis Oz. According to (11), if a body has a material symmetry axis, it is a principal axis of inertia at all its points. The other two principal axes passing through any point of the symmetry axis (including the point O) lie in the planes that are perpendicular to that axis.

Further, to express the angular velocity projections $\omega_x$, $\omega_y$ and $\omega_z$ in terms of the Euler angles and their derivatives, we have to add to the dynamic equations of Euler the kinematic Euler equations (11), which are of the following form:

$$\left.\begin{aligned} \omega_x = \dot{\psi}\sin\theta\sin\varphi + \dot{\theta}\cos\varphi, \\ \omega_y = \dot{\psi}\sin\theta\cos\varphi + \dot{\theta}\sin\varphi, \\ \omega_z = \dot{\psi}\cos\theta + \dot{\varphi}. \end{aligned}\right\} \tag{12}$$

## RESULTS AND DISCUSSION

It is possible to derive from the equivalent schematic model (Fig. 1) the moments of the external forces acting on the beet root during its contact with the vibrating digging tool about the axes Ox, Oy and Oz. After the substitution of the necessary axial moments of inertia and the derived magnitudes of the principal moments of all external forces into the system of differential equations, we obtain the following system of differential equations for the three-dimensional oscillations of the beet root fixed in the ground in the form of dynamic and kinematic equations of Euler:

$$\left.\begin{aligned}
&\left(0,48+0,15tg^2\gamma_k\right)m_k h_k^2\frac{d\omega_x}{dt}+\left(0,15tg^2\gamma_k+0,52\right)m_k h_k^2\omega_x\omega_z=\\
&=\Big[-P_1\left(h\,tg\gamma_k-h\theta\right)-f\left(0,5H\cos\delta\sin\omega t+P_1\sin\gamma\right)\cos\left(\alpha_{K_1\max}\sin\omega t-\gamma\right)\times\\
&\times\left(h\,tg\gamma_k-h\theta\right)+\frac{c\pi h_1^4\sin\gamma_k\theta\psi\left[\cos\left(\gamma_k-\theta\right)+\cos\left(\gamma_k+\psi\right)\right]}{4\cos^3\gamma_k}\Big]\sin\theta\sin\varphi+\\
&+\Big[-0,5H\,h\,tg\gamma_k\sin\omega t+hP_1\sin\psi+f\left(0,5H\cos\delta\sin\omega t+P_1\sin\gamma\right)\times\\
&\times\cos\left(\alpha_{K_1\max}\sin\omega t-\gamma\right)\sin\psi h+\frac{2}{3}G_k h_k\theta-\frac{c\pi h_1^4\sin\gamma_k\theta\cos\psi}{4\cos^3\gamma_k}\Big]\cos\varphi,\\
&\left(0,48+0,15tg^2\gamma_k\right)m_k h_k^2\frac{d\omega_y}{dt}+\left(0,48-0,15tg^2\gamma_k\right)m_k h_k^2\omega_z\omega_x=\\
&=\Big[-P_1\left(h\,tg\gamma_k-h\theta\right)-f\left(0,5H\cos\delta\sin\omega t+P_1\sin\gamma\right)\cos\left(\alpha_{K_1\max}\sin\omega t-\gamma\right)\times\\
&\times\left(h\,tg\gamma_k-h\theta\right)+\frac{c\pi h_1^4\sin\gamma_k\theta\psi\left[\cos\left(\gamma_k-\theta\right)+\cos\left(\gamma_k+\psi\right)\right]}{4\cos^3\gamma_k}\Big]\sin\theta\sin\varphi-\\
&-\Big[-0,5H\,h\,tg\gamma_k\sin\omega t+hP_1\sin\psi+f\left(0,5H\cos\delta\sin\omega t+P_1\sin\gamma\right)\times\\
&\times\cos\left(\alpha_{K_1\max}\sin\omega t-\gamma\right)\sin\psi h+\frac{2}{3}G_k h_k\theta-\frac{c\pi h_1^4\sin\gamma_k\theta\cos\psi}{4\cos^3\gamma_k}\Big]\sin\varphi,\\
&0,3m_k h_k^2 tg^2\gamma_k\frac{d\omega_z}{dt}=hP_1\cos\theta tg\gamma_k+f\left(0,5H\cos\delta\sin\omega t+P_1\sin\gamma\right)\times\\
&\times\cos\left(\alpha_{K_1\max}\sin\omega t-\gamma\right)\cos\theta\,tg\gamma_k h-\frac{c_1h_1^3\varphi\sin^2\gamma_k}{3\cos^3\gamma_k}+\Big[P_1\left(h\,tg\gamma_k-h\theta\right)+\\
&+f\left(0,5H\cos\delta\sin\omega t+P_1\sin\gamma\right)\cos\left(\alpha_{K_1\max}\sin\omega t-\gamma\right)\left(h\,tg\gamma_k-h\theta\right)-\\
&-\frac{c\pi h_1^4\sin\gamma_k\theta\psi\left[\cos\left(\gamma_k-\theta\right)+\cos\left(\gamma_k+\psi\right)\right]}{4\cos^3\gamma_k}\Big]\cos\theta,\\
&\omega_x=-\dot\psi\sin\theta\sin\varphi-\dot\theta\cos\varphi,\\
&\omega_y=-\dot\psi\sin\theta\cos\varphi+\dot\theta\sin\varphi,\\
&\omega_z=\dot\psi\cos\theta+\dot\varphi.
\end{aligned}\right\}\quad(13)$$

We have obtained the system of differential equations (13) for the three-dimensional oscillations of the beet root caused by the perturbing force, which is a determined system that allows to carry out the multivariate modelling of the beet root digging process, because it contains the parameters of the vibrating digging tool, sugar beet root and the soil surrounding the root.

The solution of the differential equation system allows to determine first of all the law of the three-dimensional oscillations of the beet root about the conventional point of fixation in the ground, i.e. find the functions $\varphi = \varphi(t)$, $\psi = \psi(t)$ and $\theta = \theta(t)$. According to the results of calculations, if we assume the following averaged initial data: mass of root $m_k = 0.9$ kg; mass of soil surrounding root $m_{гр.} = 0.4$ kg; length of root $h_k = 0.25$ m; angles of trihedral wedges of vibrating digging tool $\gamma = 14°$, $\beta = 52°$; friction coefficient of steel on root body surface $f = 0.45$; amplitude of perturbing force $H = 500$ N; magnitude of lateral driving force $P_1 = 400$ N; maximum angle of deviation of friction force vector from the vector of this force at minimum magnitude $\alpha_{K_1 \max} = 30°$; frequency of oscillations of digging shares of vibrating digging tool $\nu = 10$ Hz; cone angle of the root $\gamma_k = 15°$; elastic stiffness of soil $c = 3 \cdot 10^5$ N m$^{-3}$, $c_1 = 2 \cdot 10^5$ N m$^{-2}$; current time $t = 0.025$ s, then the Euler angles obtain the following values: $\varphi = 10^o$, $\psi = 9^o$, $\theta = 7°$.

It is to be noted as well that the system of differential equations (13) characterises not only the three-dimensional oscillatory process, but also the angular displacement of the beet root about its own axis (spinning phenomenon), which has an especially notable effect on the process of breaking up the bonds between the root and the soil during the first stage of its lifting from the ground.

The results of the accomplished analytical treatment have been used in the design and engineering of new vibrating digging tools for state-of-the-art sugar beet harvesting machines.

## CONCLUSIONS

1. The physical process of a sugar beet root standing in soil as an elastic medium and its interaction with a vibrating digging tool at the first stage of its lifting from the ground has been investigated.

2. It has been established that, for the purposes of analytical treatment of the process of sugar beet root lifting from the ground, the root can be represented by an elastic conical body residing in elastic medium and having one fixed point at its bottom. All necessary conditions for the use of kinematic and dynamic equations of Euler in the research into the root lifting have been obtained.

3. The new mathematical model of the vibration-assisted beet root lifting from the ground with the use of the theory of the body motion about a fixed point has been developed.

4. Using the original kinematic and dynamic equations of Euler, the system of differential equations has been set up for the oscillations of the beet root during its vibration-assisted lifting in the case, when the root interacts only with one digging share at one its point, i.e. when an asymmetric contact with the root body occurs.

5. Following the solution of the system of Euler differential equations, particular values have been obtained for the angular displacements of the beet root about the

coordinate axes, at which its efficient lifting from the ground is achieved. Specifically, for the average values of the parameters of the vibrating digging tool, root body and the soil surrounding it included in the equations, the Euler angles have the following numeric values: $\varphi = 10°$, $\psi = 9°$, $\theta = 7°$.

6. The obtained mathematical model allows to carry out the multivariate modelling of the process of vibration-assisted root digging out of the soil under various conditions of harvesting.

## REFERENCES


Bulgakov, V.M., 2005. Theory of beet harvesting machines. Kiev: Publishing Centre of the National Agrarian University, 352 pp. (in Russian).

Bulgakov, V., Adamchuk, V., Kaletnik, G., Arak, M., Olt, J. 2014. Mathematical model of vibration digging up of root crops from soil. *Agronomy Research* **12**(1), 41–58.

Bulgakov, V., Golovats, I., Špokas, L. & Voitjuk, D. 2005. Theoretical investigation of a root crop cross oscillations at vibratinal digging up. *Research papers of IAg Eng LUA & LU of Ag*. **37**(1), 19–35. (in Russian).

Bulgakov, V., Ivanovs, S. 2010. Mathematical simulation of beet vibration extraction. In: Engineering for Rural Development. pp. 25–31.

Dobrovski, A.A. 1968. *Agricultural Machinery Vibration*. Mechanical Engineering, Moskow, 204 pp. (in Russian).

Dreizler, R.M., Lüdde, C.S. 2010. Theoretical Mechanics. Springer, 402 pp.

Gu, F., Hu, Z., Wu, H., Peng, B., Gao, X., Wang, S. 2014. Development and experiment of 4LT-A staggered-dig sugar beet combine. *Nongye Gongcheng Xuebao/Transactions of the Chinese Society of Agricultural Engineering* **30**(23), 1–9.

Lammers, P.S. 2011. Harvest and loading machines for sugar beet – new trends. *International Sugar Journal* **113(**1348), 253–256.

Lammers, P.S., Schmittmann, O., 2013. Testing of sugar beet harvesters in Germany 2012. *International Sugar Journal* **115**(1370): 100–106.

Pogorely, L.V., Tatyanko, N.V. & Bray, V.V. 1983. *Beet-harvesting machines (designing and calculation)*. Under general editorship of Pogorely, L. V. Tehnika, Kyiv, 232 pp.

Pogorely, L.V., Tatyanko, N.V. & Bray, V.V. 2004. *Beet-harvesting machines: History, Construction, Theory, Prognosis*, Feniks, Kyiv, 232 pp. (in Ukrainian).

Sarec, P., Sarec, O., Przybyl, J., & Srb, K. 2009. Comparison of sugar beet harvesters. *Listy cukrovarnicke a reparske* **125**(7–8), 212–216. (in Czech).

Vasilenko, P.M., Pogorely, L.V., & Brey, V.V. 1970. Vibrational Method of Harvesting Root Plants. *Mechanisation and Electrification of the Socialist Agriculture* **2**, 9–13 (in Russian).

Vermeulen, G.D., Koolen A.J. 2002. Soil dynamics of the origination of soil tare during sugar beet lifting. *Soil & Tillage Research* **65**, 169–184.

Wang, F., Zhang, D. 2013. Design and experiment of disc-dig sugar beet combine. *Nongye Gongcheng Xuebao/Transactions of the Chinese Society of Agricultural Engineering* **29**(13), 7–14.

Wu, H., Hu, Z., Peng, B., Wang, H., Wang, B. 2013. Development of auto-follow row system employed in pull-type beet combine harvester. *Nongye Gongcheng Xuebao/Transactions of the Chinese Society of Agricultural Engineering* **29**(12), 17–24.

*Agronomy Research* **13**(1), 46–52, 2015

# Mulcher energy intensity measurement in dependence on performance

J. Čedík[1,*], M. Pexa[1], R. Pražan[2], K. Kubín[2] and J. Vondřička[1]

[1]Czech University of Life Sciences, Faculty of Engineering, Department for Quality and Dependability of Machines, Kamycka 129, 16521, Prague 6, Czech Republic
[2]Research Institute of Agricultural Engineering, p.r.i., Drnovská 507, 16101, Prague 6, Czech Republic
[*]Correspondence: cedikj@tf.czu.cz

**Abstract.** Conventional impact grass cutting and chopping is energy intensive and therefore it is important to reduce energy demands of such a device. In the paper the energy demands of three-rotor mulcher with vertical axis of rotation was measured and analyzed in dependence on the mass performance of the mulcher. Different mass performance was achieved by different ground speed and yield of the grass cover. The measurement was performed on clover-grass meadow hay, from which the samples were taken and analyzed in order to determine the yield and moisture content of the vegetation. The results showed relatively high energy demands of the mulcher. In dependence on the mass performance of the mulcher it is necessary to deliver in average 10.4–22.6 kW m$^{-1}$ of the width of the machine. Specific energy consumption varied in average from 3.35 to 6.34 kWh t$^{-1}$ of the processed material and unit fuel consumption varied in average from 2.56 to 0.94 kg t$^{-1}$.

**Key words:** mulcher, energy consumption, grass cutting, meadow hay.

## INTRODUCTION

The power requirement of the rotary mower and the mulching machine is usually 2 to 4 times greater than in case of the finger mower with the same width range. Concrete values of the required power per one meter width cut differ in various scientific sources, e.g. the power requirement 5 kW m$^{-1}$ and the required power requirement for the mower with the conditioner 8 kW m$^{-1}$ (ASABE D497.7., 2011), the power requirement 11 to 16 kW m$^{-1}$ on the mower at speed 15 km h$^{-1}$ (Srivastava et al., 2006), the power requirement 10 to 12 kW m$^{-1}$ with a worn out blade (Tuck et al., 1991), the power requirement for mower conditioners 3.5 to 6.5 Kw m$^{-1}$ and the power requirement for mowing without the conditioner is 5 kW m$^{-1}$ (McRandal & McNulty, 1978b). Other scientific sources state that the average required power for mowing and treatment of grass is 8 kW m$^{-1}$, with the range 5.6–10.4 kW m$^{-1}$ (Srivastava et al., 2006) and when the patency is 120 t h$^{-1}$, the energy intensity of the rotary mower is approximately 6.67 kW m$^{-1}$ and when sharp knives are used, the energy intensity is 5.67 kW m$^{-1}$ (Syrový et al., 2008).

The typical cutting speed of the disc and rotary mowers ranges from 71–84 m $s^{-1}$ (O'Dogherty, 1982). Optimization of the cutting speed, the knife shape, the blade oblique angle and the blade rake angle can significantly reduce the energy consumption and increase the efficiency of mowing and crushing (Hosseini & Shamsi, 2012; Johnson et al., 2012; Kakahy et al., 2014). The power requirement depends not only on the cutting speed, knives, blades wear, the type of the mower and patency, but also on the kind of processed crop (Chen et al., 2004; Igathinathanea et al., 2010; Ghahraei et al., 2011; Johnson et al., 2012; Jasinskas et al., 2013; Kronbergs et al., 2013; Pecenka et al. 2014). The power requirement also depends on the moisture and stems inclination (Igathinathanea et al., 2010; Kakahy et al., 2013).

The identified energy losses in case of rotary mowers are caused by air flow (so called ventilation effect), pulling of the mower, friction in the drive mechanism and friction with the stubble under the knives (McRandal & McNulty, 1978b). The experiments with the mowers with the vertical rotation axis proved that 50% of the input energy is used for the transport of the plants, while only 3% of the input energy is used for cutting the plant stems (McRandal & McNulty, 1978a). The power requirement of the rotary mowers can be calculated according to the relation number 1 (Persson, 1987).

$$P_{mow} = \left(P_{LS} + E_{SC} \cdot v_f\right) \cdot B_f \tag{1}$$

where: $P_{mow}$ – total power requirement (kW); $P_{LS}$ – losses (air, stubble, gear loses) (kW $m^{-1}$); $E_{SC}$ – power of cut (kJ $m^{-2}$); $v_f$ – ground speed (m $s^{-1}$); $B_P$ – range width (m).

The goal was to determine the energy demands of the mulching machine with different patency of the material. Other goal was to evaluate impact of the material patency on the unit fuel consumption. It can be expected that the unit fuel consumption reach values between 7.5–9.5 l $ha^{-1}$ (Syrový et al., 2013).

## MATERIALS AND METHODS

The main goal of the measurement was to determine the input power taken from the PTO shaft of the tractor during mulching the clover-grass cover. The measurement was done on selected land, south of the town Žamberk (latitude 50.0565725°N, longitude 16.4375197°E). The working set consisted of the tractor John Deere 7930 and the mulching machine MULCHER MZ6000 (Table 1). The tested mulching machine with the range width 6 m is part of the current production programme of the company BEDNAR FMT, s.r.o.

**Table 1.** Basic parameters of the mulcher MZ6000

| | | |
|---|---|---|
| Total weight | kg | 3,300 |
| Rotor diameter | m | 2 |
| Number of rotors | pcs | 3 |
| Number of blades per rotor | pcs | 4 |
| Rotations per minute | $min^{-1}$ | 1,000 |
| Recomended tractor power | kW | 110–150 |

The torque sensor MANNER Mfi 2500 Nm_2000U/min (accuracy 0.25%) was installed on the PTO shaft of the tractor and the flowmeter AIC VERITAS 4004 (measurement error 1%, 2,000 pulse $l^{-1}$) was placed into the fuel system of the tractor. The flowmeter served for monitoring of the fuel consumption and determination of the energy intensity of the mulching machine. In order to determine the location of the working set and its speed, the GPS receiver was placed on the roof of the tractor. All sensors were connected with the measuring computer (netbook) by means of the analog digital converter LabJack U6. The netbook was placed to the tractor cab. Data were recorded with the frequency of 2 Hz.

Seven measuring sections were marked out on the chosen land, each approx. 100–180 m long (1–7). These sections were used to perform the measuring rides, using the working speed of 3 km $h^{-1}$, 6 km $h^{-1}$ and 9 km $h^{-1}$ to cover the range of working ground speed used in praxis. The mass performance of the mulching machine was calculated according to the relation (2).

$$W_t = 0.1 \cdot v_p \cdot B \cdot \omega \qquad (2)$$

where: $W_t$ – mass performance of the mulching machine (t $h^{-1}$); $v_p$ – working speed (km $h^{-1}$); $B$ – actual range width of the mulching machine (m); $\omega$ – yield per hectare of grassland (t $ha^{-1}$).

The actual range width of the mulching machine was 5.79 m, the average speed of PTO was 998.1 $min^{-1}$ with standard deviation 11 1 $min^{-1}$. This corresponds with the cutting speed approx. 105 m $s^{-1}$.

Altogether three samples of mown vegetation were taken from each test section in order to determine the yield of the grass mater and its moisture. The average moisture was 72.8% with standard deviation 4.5%.

The measured data from the individual measuring sections (01 to 07) were loaded into the programme MS Excel and further processed.

## RESULTS AND DISCUSSION

The evaluated results of the measurement within the individual sections are presented in the Table 2 and 3. From the Table 2 it can be seen that values of mean power reaches up to approx. 130 kW. Also it can be seen that at speed of approx. 3 km $h^{-1}$ the unit fuel consumption in l $ha^{-1}$ is up to 71% higher than it was expected. At speed of approx. 6 km $h^{-1}$ the unit fuel consumption in l $ha^{-1}$ is approx. 9% higher than it was expected and at speed of approx. 9 km $h^{-1}$ the unit fuel consumption equals to the expectations.

Fig. 1 shows the performance requirement for one meter of the machine range. It is obvious that this requirement increases with the increasing mass performance of the machine, as it might be expected, when the performance of the mulching machine is greater than 30 t $h^{-1}$ it is taken up to 22.6 kW $m^{-1}$.

**Table 2.** Measurement results summary – part 1

| Section | Speed kmh$^{-1}$ | Yield t ha$^{-1}$ | Performance t h$^{-1}$ | Mean torque Nm | Mean power kW |
|---|---|---|---|---|---|
| 1 | 3.4 | 11.2 | 22.06 | 890.3 | 92.55 |
| 2 | 9.34 | 6.2 | 33.52 | 1,272.05 | 130.96 |
| 3 | 6.66 | 9.2 | 35.46 | 1,194.79 | 125.9 |
| 4 | 6.47 | 6.7 | 25.12 | 870.35 | 89.9 |
| 5 | 6.42 | 7 | 26.37 | 841.7 | 89.32 |
| 6 | 9.28 | 5.5 | 29.56 | 948.78 | 98.89 |
| 7 | 3.49 | 4.7 | 9.58 | 576.68 | 60.8 |

**Table 3.**Measurement results summary – part 2

| Section | Power requirement | Specific energy consumption | Unit fuel consumption | | |
|---|---|---|---|---|---|
| | kW m$^{-1}$ | kWh t$^{-1}$ | l ha$^{-1}$ | kg ha$^{-1}$ | kg t$^{-1}$ |
| 1 | 15.99 | 4.2 | 16.27 | 13.5 | 1.21 |
| 2 | 22.62 | 3.91 | 7.94 | 6.59 | 1.06 |
| 3 | 21.74 | 3.55 | 10.37 | 8.61 | 0.94 |
| 4 | 15.53 | 3.58 | 10.05 | 8.34 | 1.24 |
| 5 | 15.43 | 3.39 | 10.33 | 8.58 | 1.23 |
| 6 | 17.08 | 3.35 | 8.47 | 7.03 | 1.28 |
| 7 | 10.39 | 6.34 | 14.48 | 12.02 | 2.56 |

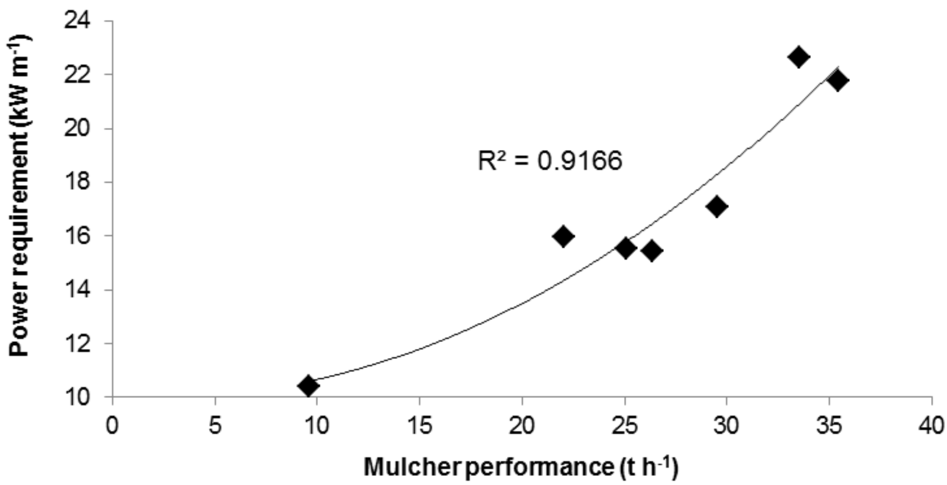


**Figure 1.** Mulcher power requirement.

Fig. 2 presents the specific energy consumption depending on the performance of the mulching machine. It is obvious that the specific energy consumption decreases along with the increasing mass performance of the mulching machine up to approximately 30 t $h^{-1}$ where the lowest value of the specific energy consumption was reached.

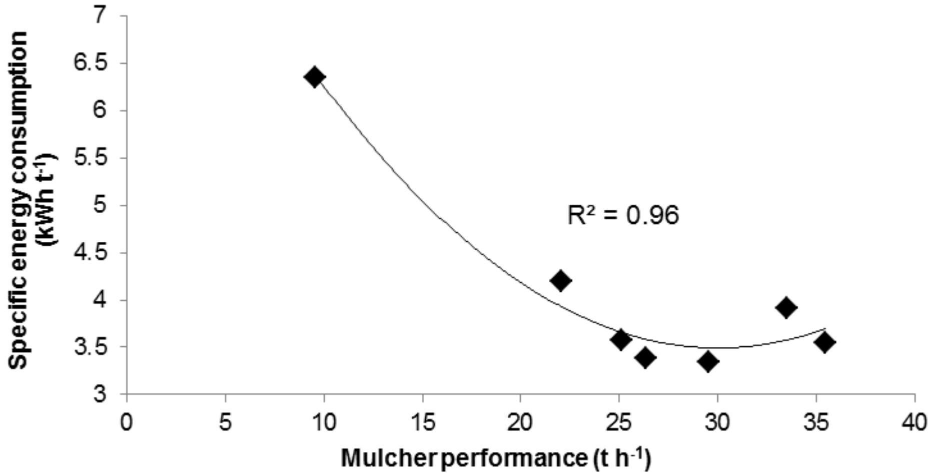


**Figure 2.** Specific energy consumption of the mulcher.

Fig. 3 shows the unit fuel consumption – kilograms per ton of processed material. As it might be expected the unit fuel consumption decreases along with the increasing mass performance of the mulching machine. However, contrary to the specific energy consumption of the mulching machine (Fig. 2), many other factors interferes in the fuel consumption, e.g. terrain inclination, tractor acceleration etc.

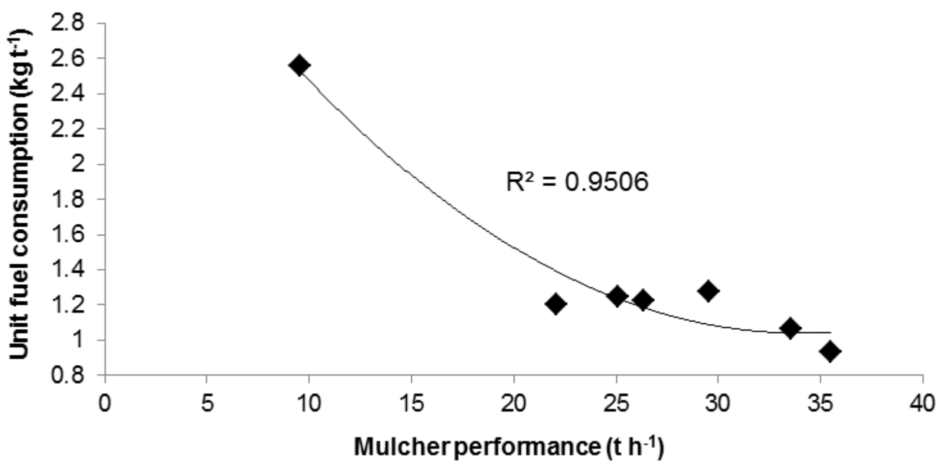


**Figure 3.** Unit fuel consumption.

## CONCLUSIONS

Impact cutting and crushing of the crop material by the rotary mowers requires very high energy consumption. This was confirmed by the measurement, during which the mulching machine needed in average up to 22.6 kW $m^{-1}$ while the patency was 33.5 t $h^{-1}$, which is much more in comparison with other published scientific work which states from 11 to 16 kW $m^{-1}$ (Srivastava et al., 2006). This could be caused mainly by the ventilation effect, which is required for mulching, and by high cutting speed (105 m $s^{-1}$). At the speed of 3–6 km $h^{-1}$ the unit fuel consumption in l $h^{-1}$ was also higher than it was expected from the other studies (Syrový et al., 2013). From the point of view of the lowest reached specific energy consumption, the optimal performance of the mulching machine is approximately 30 t $h^{-1}$ and is approximately equal to 3.4 kWh $t^{-1}$. From the point of view of usage of the fuel energy, the highest reached performance 35.5 t $h^{-1}$ appears to be optimal, because the unit fuel consumption was 0.94 kg $t^{-1}$. It is possible to reach the required performance by the appropriate working speed of the mulching machine based on the expected yield of the grass matter.

ACKNOWLEDGEMENTS. The paper was created with the grant support project CULS 2014:31190/1312/3127 – Utilization of biobutanol as a fuel for diesel engines and with institutional support for long-term conceptual development VÚZT, v.v.i. RO0614.

## REFERENCES

ASABE D497.7. 2011. *Agricultural Machinery Management Data*. The American Society of Agricultural and Biological Engineers. St. Joseph.

Ghahraei, O., Ahmad, D., Khalina, A., Suryanto, H. & Othman, J. 2011. Cutting tests of kenaf stems. *Transactions of the ASABE* **54**(1), 51–56.

Hosseini, S.S. & Shamsi, M. 2012. Performance optimization of a rotary mower using Taguchi method. *Agronomy Research* **10**(1), 49–54.

Chen, Y., Gratton, J.L. & Liu, J. 2004. Power Requirements of Hemp Cutting and Conditioning. *Biosystems Engineering* **87**(4), 417–424.

Igathinathane, C., Womac, A.R. & Sokhansanj, S. 2010. Corn stalk orientation effect on mechanical cutting. *Biosystems Engineering* **107**(2), 97–106.

Jasinskas, A., Simonavičiūtė, R., Šarauskis, E., Sakalauskas, A. & Čekanauskas, S. 2013. Assessment of unconventional bioenergy plant chopping, milling and pelleting quality indicators and physical-mechanical properties. *Agronomy Research* **11**(2), 307–318.

Johnson, P.C., Clementson, C.L., Mathanker, S.K., Grift, T.E. & Hansen, A.C. 2012. Cutting energy characteristics of Miscanthus x giganteus stems with varying oblique angle and cutting speed. *Biosystems Engineering* **112**(1), 42–48.

Kakahy, A.N.N., Ahmad, D., Akhir, M.D., Sulaiman, S. & Ishak, A. 2013. Effects of cutting speeds and moisture content on grass chopping (Pulverizing). *Advanced Science Letters* **19**(9), 2533–2535.

Kakahy, A.N.N., Ahmad, D., Akhir, M.D., Sulaiman, S. & Ishak, A. 2014.Effects of knife shapes and cutting speeds of a mower on the power consumption for pulverizing sweet potato vine. *Key Engineering Materials* **594**, 1126–1130.

Kronbergs, A., Kronbergs, E. & Repsa, E. 2013. Evaluation of reed canary grass shredding and compacting properties. *Agronomy research* **11**(1), 61–66.

McRandal, D.M. & McNulty, P.B. 1978a. Impact cutting behaviour of forage crops I. Mathematical models and laboratory tests. *Journal of Agricultural Engineering Research* **23**(3), 313–328.

McRandal, D.M. & McNulty, P.B. 1978b. Impact cutting behaviour of forage crops II. Field tests. *Journal of Agricultural Engineering Research* **23**(3), 329–338.
O'Dogherty, M.J. 1982. A review of research on forage chopping. *Journal of Agricultural Engineering Research*. **27**(4), 267–289.
Pecenka, R. Ehlert, D. & Lenz, H. 2014. Efficient harvest lines for Short Rotation Coppices (SRC) in agriculture and agroforestry. *Agronomy Research* **12**(1), 151–160.
Persson, S. 1987. *Mechanics of cutting plant mater*ial. American Society of Agricultural Engineers (ASAE), St. Joseph, 288pp.
Srivastava, A.K., Goering, C.E. & Rohrbach, R.P. 2006. *Engineering principles of agricultural machines.* American Society of Agricultural Engineers, St Joseph, 588 pp.
Syrový, O., Bauer, F., Gerndtová, I., Holubová, V., Hůla, J., Kovaříček, P., Krouhlík, M., Kumhála, F., Kvíz, Z., Mašek, J., Pastorek, Z., Podpěra, V., Rybka, A., Sedlák, V., Skalický, J. & Šmerda, T 2008. *Úspory energie v technologiích rostlinné výroby (Energy saving in crop production technologies)*. Research Institute of Agricultural Engineering p.r.i. Prague, 101 pp. (in Czech)
Syrový, O., Světlík, M., Pražan, R., Pastorek, Z., Kubín, K. & Gerndtová, I. 2013. *Mobilní energetické prostředky a orientační hodnoty jednotkových spotřeb paliv a energií (Mobile energy devices and the approximate values of unit fuel and energy consumption)*. Research Institute of Agricultural Engineering, p.r.i., Prague, pp. 56 (in Czech)
Tuck, C.R., O'Dogherty, M.J., Baker, D.E. & Gale, G.E. 1991. Field Experiments to Study the Performance of Toothed Disk Mowing Mechanisms. *Journal of Agricultural Engineering Research* **50**, 93–106.

*Agronomy Research* **13**(1), 53–62, 2015

# Comparison of tyres for self-propelled sprayers

J. Čedík* and R. Pražan

Research institute of Agriculture Engineering, Drnovská 507, 161 01, Prague 6, Czech Republic; *Correspondence: cedik@vuzt.cz

**Abstract.** This article deals with comparison of two types of tyres (MITAS VF and MITAS AC 85) for self-propelled sprayers in terms of their grip properties and effect on soil. The MITAS VF tyre has a new construction allowing it to work with lower inflation pressure and in higher speed than standard tyre. In order to compare the grip properties there was measured dependence of slippage on tractive force. In order to compare the effect on soil there will be measured footprint area of tyre, specific pressure on base (material), compaction of topsoil by means of wire profilograph and penetration resistance of soil by means of penetrometer. The measurement has been taken place on medium-heavy soil, on stubble after wheat cultivation. The MITAS AC tyres showed lesser tread pattern than the MITAS VF tyres. The VF tyres showed also better grip properties and lesser effect on the topsoil. The soil cone index showed statistically not significant difference in comparison with non-compacted soil and it was approximately the same in case of both variants.

**Key words:** tyres, sprayer, tractive force, slippage, soil compaction.

## INTRODUCTION

In agricultural practice there are increasingly implemented tyres with higher requirements for operation. To the important properties belong higher load at lower inflation pressure and higher maximum permitted speed. In case of standard tyres (MITAS AC 85) there are required inflation pressure of 400 kPa and max. operating speed of 20 km $h^{-1}$ for a given load on sprayer, new so-called VF (Very High Flexion) tyres requires the inflation pressure of 320 kPa and max. speed is increased up to 65 km $h^{-1}$ while carrying the same load. The advantages of use of these tyres are clear. By means of comparative tests we wanted to determine the effect of VF tyres on energy intensity and on soil in comparison with standard tyres.

The grip properties of tyres, especially dependence of tractive force or contact ratio coefficient on slippage of wheels, have an influence on traction efficiency and fuel consumption. The higher wheel slippage, the higher fuel consumption. The grip properties depend on load and soil conditions, it means moisture, type of soil or hardness of base material (Abrahám et al., 2014; Ahokas & Jokiniemi, 2014). Furthermore, the grip properties depend, of course, on parameters of tyres (Schreiber and Kutzbach, 2008), and especially on inflation pressure (Noréus & Trigell, 2008).

The soil compaction represents a negative consequence of interaction between a tyre and base material (soil). It reduces water infiltration, retention capacity of soil, accelerates erosion and increases soil cone index. It consists above all in changes in volume weight of soil, porosity and air and water capacity (Hůla et al., 2011; Chyba et al., 2013; Syrový et al., 2013; Głąb, 2014; Chyba et al., 2014;). High degree of compaction has an adverse effect on crop yields depending on kind of crop (Braunack et al., 2006; Kuth et al., 2012; Arvidsson & Håkansson, 2014). For the determination of soil compaction it can be used its dry bulk density. It should move approximately in the range of 1.2–1.5 g $cm^{-3}$ (Syrový et al., 2013). The density can be also determined by means of measured vertical soil stress (Eguchi & Muro, 2009). The soil compaction depends on many factors. To the main factors belong contact pressure between tyre and base material. This pressure increases with decreasing size of contact area between tyre and soil, with increasing pressure in a tyre with increasing stiffness of a tyre and higher normal static and dynamic load. The soil compaction increases also with decreasing travel speed and with higher number of passages. Furthermore, soil compaction depends on type of soil, moisture and density (Défossez et al., 2003; Lamandé & Schjønning, 2011a,b,c; Nugis & Kuth, 2012; Rodríguez et al., 2012; Głąb, 2014; Keller et al., 2014; Kviz et al., 2014; Taghavifar & Mardani, 2014; Varga et al., 2014). In order to determine contact area of tyre with soil it is possible to use, apart from measurement, also mathematical models based on commonly detectable parameters such as diameter and width of tyre, inflation pressure and various empirically determined coefficients (Prikner & Aleš, 2010; Palancar et al., 2001; McKyes, 1985). Max. pressure acting on soil can be more than twice greater, than specific pressure calculated from footprint area and a load of a tyre (Lamandé & Schjønning, 2011a,b,c). Lozano et al. (2013) says, that during the harvest of sugar cane with dry bulk density below 1.4 g $cm^{-3}$ and moisture over 16% there is a high risk of soil compaction. Braunack (2004) states, that better results can be achieved at use of one wide tyre (445/65R22.5) than when using double axle and narrow tyres (11R22.5).

The objective of measurement was to compare 2 MITAS tyres (MITAS VF and MITAS AC 85) for self-propelled sprayers in terms of grip properties and effect on soil. The VF tyre has new construction, which allow it to work in higher speeds with lower inflation pressure while carrying the same load, as mentioned above. For this purpose it was carried out measurement of dependance of tractor tractive force on slippage of wheels, measurement of topsoil compaction by means of profilograph and measurement of soil cone index by means of penetrometer.

## MATERIALS AND METHODS

Self-propelled sprayer Challenger RoGator (see Fig. 1) has the working width 30.2 m, two controlable axles, performance 167 kW and weight 17,420 kg. For the sprayer there were used tyres MITAS AC 85 with dimension 380/90 R 46, 159 A8, E8 and inflation pressure 400 kPa and tyres MITAS VF with dimension 380/90 R 46, 173 D, E8 with inflation pressure 320 kPa.

In order to determinate tyre loading the sprayer was weighed at first by means of portable weighing machine Haenni (precision ±20 kg). During the measurement the sprayer was filled by water. Then the tyre footprint area was measured and specific pressures on base calculated. This measurement was carried out on right rear wheel due to impossibility to lift the front axle at full sprayer.

Measurement of tyre grip properties was carried out at first without load of tractive force and then with unbraked tractor FENDT 415 VARIO with curb weight 5,740 kg.

Tractor wasn´t braked, because the sprayer isn´t destined for loading by tractive force and sole manner of load by longitudinal forces is the uphill driving. Another reason is hydrostatic drive of sprayer, which don´t permit high slippage of the wheels. For measurement of wheel revolutions there were used sensing elements SICK DKS 40 (360 pulses/revolution) and for measurement of revolutions of fifth wheel the speed indicator ZME ORS 120 (120 pulses/revolution). For measurement of tractive force there was used tensometer sensing element HBM U10M (rated load 125 kN). For the measurements there were determined 4 routes with length roughly 170 m. During the measurement there was recorded average speed about 13.5 km $h^{-1}$. In order to obtain the points for tensile characteristics there were used the average values from sections with stable parameters.

**Figure 1.** Self-propelled sprayer Challenger RoGator with tractor FENDT 415 VARIO during measurement.

For the measurement of effect on upper layer of soil there was used wire profilograph with wire pitch 25 mm. For every tyre there was determined unevenness of soil surface by means of profilograph in the direction perpendicular to the direction of driving. After cover of testing distance by right front and rear tyre of sprayer the measurements of unevenness of soil surface have been repeated in beforehand determined transversal directions. In this way there was measured the permanent deformation of upper layer of soil after driving by a given tyre. In order to measure of effect on soil there was used digital penetrometer. Measurement by means of penetrometer was carried out always both in track and out of track (as reference). For each measurement 6 repetitions were carried out. Results of measurement by means of penetrometer were evaluated using the analysis of variance (ANOVA). The penetrometer meets the standard of ASAE S313.3. The penetrometer has a cone angle of 30°, area of 130 $mm^2$, cone base diameter of 12.83 mm, driving shaft diameter of 9.53 mm. The penetrating speed was according to the standard approx. 30 mm $s^{-1}$.

During the measurements the data has been recorded on computer hard disc HP mini 5103 by means of analog digital converter LabJack U6 and I/O module for impulse sensor Papouch Quido 10/1 with frequency approximately 1 Hz. These data was processed by means of the MS Excel programme.

Measurements were carried out on field of AGROSS Klíčany company, near to Prague, on stubble after wheat with some places with emerged cereal shedding (latitude 50.1985325°N, longitude 14.4342406°E). For measurement conditions there was determined soil moisture depending on depth. At depth 0–50 mm the moisture was 22.27%, at the depth 50–100 mm the moisture was 18.31%, at the depth 100–150 mm the moisture was 18.79% and at the depth 150–200 mm it was 18.08%. Samples for determination of the soil moisture were taken at the time when measurement was carried out, and they were taken at eight places along the test route in approximate distance of 20 m between each other.

Furthermore, there were determined soil texture, soil type and average dry bulk density according to standard ČSN 46 5302 (Characterization of soils cultivated by implements). In soil there was prevailed the content of dust particles (average 0.002–0.05 mm) in range of 53.53 up to 73.39% over the share of sandy grains (average 0.05–2 mm) and clay. According to analysis of grains it is medium-heavy soil. It is fine loam with dusty texture. The average dry bulk density was determined to 1.57 g $cm^{-3}$.

## RESULTS AND DISCUSSION

In the Table 1 there are mentioned the loads falling on particular wheels. The sprayer was weighed in several combinations relating to setting of frame height and spraying arms for determination of maximum load. The maximum load was in transport position on left front wheel and makes 5,650 kg (55.4 kN) (Table 3). The MITAS AC 85 tyres was inflated to the pressure recommended by producer 400 kPa and MITAS VF tyres to 320 kPa. The total weight of full sprayer made roughly 18.3 t.

**Table 1.** Load on the individual wheels at transport position

| | Load (kg) | |
|---|---|---|
| | Left | Right |
| Front | 5,650 | 4,510 |
| Rear | 3,920 | 4,210 |
| Side total | 9,570 | 8,720 |
| Total | 18,290 | |

In the Fig. 2 and in the Table 2 we can see dependence of slippage of the left front and rear wheel on tractive force. It can be seen, that the MITAS VF tyres had with zero tractive force in average by 30.5% lower slippage, than MITAS AC 85. At tractive force around 11–13 kN (unbraked tractor) the MITAS VF tyres had in average by 35% lower slippage, than MITAS AC 85 tyres. This can be caused by lower inflation pressure which the VF tyres allow for the given load. Monteiro et al. (2013) also found that lower inflation pressure improves the fuel consumption and lowers the tyre slippage and thereby improves energetic efficiency of tractor tyres. Another reason may be the bigger fulness of tyre profile (Table 3, Fig. 3). From the Fig. 2 it is further obvious, that, the front wheel had always bigger slippage, than rear wheel. With regard to higher load of front wheel (see Table 1) this difference can be awaited.

**Table 2.** Measurement summary of results of dependence of slippage on tractive force

| Tyre | Average speed (km h$^{-1}$) | Section length (m) | Average tractive force (kN) | Average tyre slippage of left rear wheel (%) | Average tyre slippage of left front wheel (%) |
|---|---|---|---|---|---|
| MITAS | 13.67 | 106.94 | 0 | 5.771 | 4.183 |
| AC 85 | 11.77 | 96.07 | 12.63 | 7.456 | 5.711 |
| MITAS | 15.18 | 123.67 | 0 | 4.396 | 2.622 |
| VF | 13.52 | 110.73 | 10.85 | 5.156 | 3.475 |

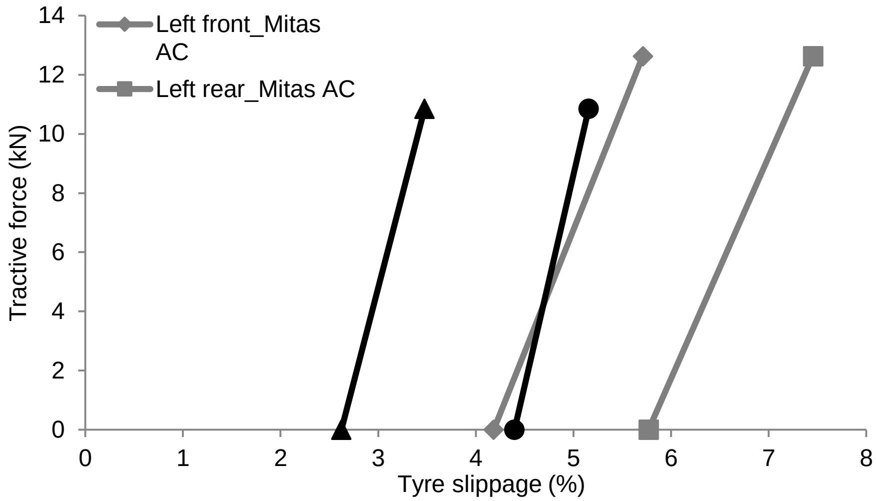


**Figure 2.** Dependence of tractive force on tyre slippage for both tested tyres.

In the Table 3 there are mentioned footprint areas of right front wheel (load 41.3 kN) and specific pressures acting on base material. Footprint area for MITAS AC 85 tyre was approx. by 13.7% bigger, than for MITAS VF tyre. However, from the depth of footprint measured by profilograph in Fig. 4 it is obvious, that the tyre moved along the field only on tyre profile area, which was in case of MITAS VF tyre by 21.5% bigger, it means by 45% bigger fulness of tyre profile and also corresponding lower pressure in tyre profile area. In these soil and moisture conditions it is more sound for soil use of VF tyres in comparison with standard ones.

**Table 3.** Footprint and mean pressure on the surface for both tested tyres

| Tyre | Load on right rear wheel | | Tyre footprint | Contact area of tyre profile | Fulness of footprint of tyre profile | Pressure in contact area of tyre | Pressure in footprint area of tyre |
|---|---|---|---|---|---|---|---|
| | M | $F_r$ | $S_o$ | $S_d$ | $\gamma$ | $p_s$ | $p_o$ |
| | (kg) | (kN) | (cm$^2$) | (cm$^2$) | (%) | (kPa) | (kPa) |
| MITAS AC 85 | 4,210 | 41.29 | 1,787 | 474 | 26.52 | 871.01 | 231.04 |
| MITAS VF | 4,210 | 41.29 | 1,572 | 604 | 38.42 | 683.54 | 262.63 |

In the Fig. 4 there is shown permanent compaction of topsoil measured by means of profilograph for the MITAS AC 85 and MITAS VF tyres. It can be seen, that the MITAS AC 85 tyre has in average by 9 mm deeper track and also by 50 mm wider. The cause is above all smaller area of footprint of tyre profile, which is smaller than in case of VF tyre. The footprint of the VF tyres is longer, therefore effect on soil is smaller. At the use of MITAS AC 85 tyres, the bigger area of topsoil is influenced into deeper layer of soil (almost 60 mm). Hamza et al. (2011) found that the ratio between the weight of the external load and the contact area between the load and the surface affects primarily the top layers of the soil, which was confirmed by our results (Fig. 4). The comparison of tyre footprints on hard base material is shown in the Fig. 3.

**Figure 3.** Tyre footprints – left MITAS AC 85, right – MITAS VF (load 4.29 kN).

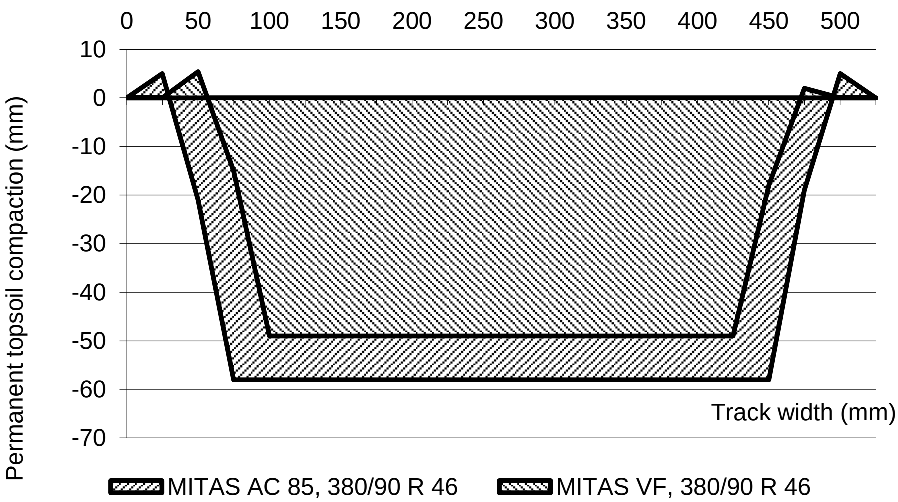


**Figure 4.** Profile of track in a perpendicular direction to the direction of travel for both tested tyres.

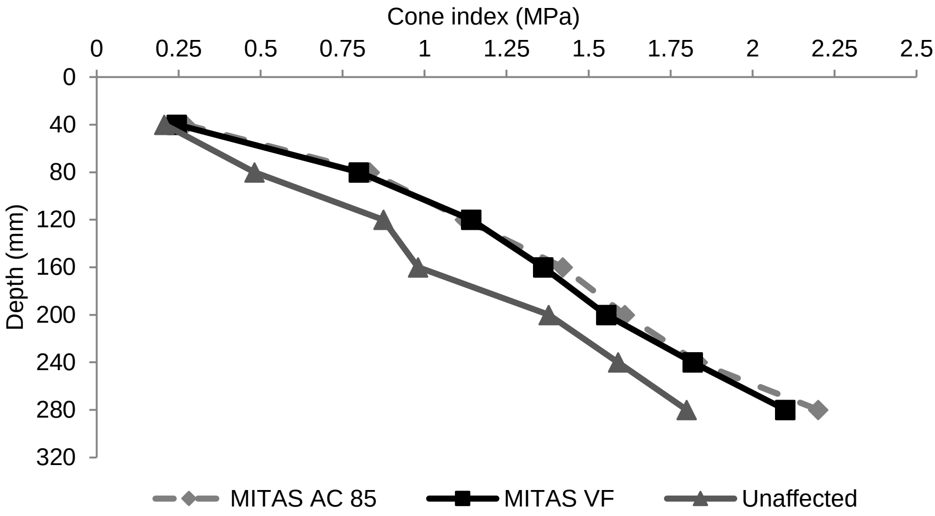


**Figure 5.** **S**oil cone index in dependence on depth for both tested tyres and unaffected soil as reference.

**Table 4.** Analysis of variance (ANOVA) for results of measurement using penetrometer ($F_{0,05(2,15)}$ = 3.68)

| Depth (mm) | Variability | Sum of Squares | Degree of Freedom | Mean Square | F-ratio | p-value |
|---|---|---|---|---|---|---|
| | Between groups | 0.012 | 2 | 0.006 | 0.357 | 0.706 |
| 40 | Within groups | 0.261 | 15 | 0.017 | | |
| | Total | 0.274 | 17 | | | |
| | Between groups | 0.454 | 2 | 0.227 | 2.865 | 0.088 |
| 80 | Within groups | 1.187 | 15 | 0.079 | | |
| | Total | 1.641 | 17 | | | |
| | Between groups | 0.268 | 2 | 0.134 | 0.417 | 0.667 |
| 120 | Within groups | 4.829 | 15 | 0.322 | | |
| | Total | 5.097 | 17 | | | |
| | Between groups | 0.688 | 2 | 0.344 | 1.386 | 0.28 |
| 160 | Within groups | 3.723 | 15 | 0.248 | | |
| | Total | 4.411 | 17 | | | |
| | Between groups | 0.175 | 2 | 0.088 | 0.286 | 0.756 |
| 200 | Within groups | 4.607 | 15 | 0.307 | | |
| | Total | 4.782 | 17 | | | |
| | Between groups | 0.223 | 2 | 0.111 | 0.465 | 0.637 |
| 240 | Within groups | 3.585 | 15 | 0.239 | | |
| | Total | 3.808 | 17 | | | |
| | Between groups | 0.523 | 2 | 0.261 | 0.666 | 0.528 |
| 280 | Within groups | 5.884 | 15 | 0.392 | | |
| | Total | 6.407 | 17 | | | |

In the Fig. 5 there are illustrated the average values of soil cone index in dependency on depth for MITAS VF and MITAS AC 85 tyres and for non-influenced soil. From the results it is evident, that there were no statistically significant differences between the soil cone index after passage with both of tyres and unaffected soil at any depth (Table 4) mainly because of large scattering of the measured values. However, from the graph it can be seen, that in comparison with non-compacted soil, in case of both tyres occurred slight increase of soil cone index in all depths apart from 0–40 mm. Between the tyres there are only small differences in favour of MITAS VF tyre, especially in the depths 120–160, 160–200 and 240–280 mm. Antille et al. (2013) found that decrease of inflation pressure by 30 and 60 kPa (at our case it was 80 kPa) results in statistically significant decrease in soil cone index which was not confirmed at this case.

## CONCLUSIONS

From the results it is obvious, that MITAS VF tyres have better grip properties than MITAS AC 85 tyres, because have lower slippage at the same load. Better traction contributes to lower fuel consumption and more economic operation. It can be caused by lower inflation pressure and bigger area of profile on MITAS VF tyres, which in combination with smaller footprint area create considerably higher fulness of tyre profile.

In relation to the effect on soil the MITAS VF tyre shows smaller permanent compaction of topsoil, than MITAS AC 85 tyre, because it has recognizable narrower and shallower track. In relation to soil penetration resistance we can say, that both tyres cause a slight but statistically not significant increase of soil cone index in comparison with non-compacted soil and this cone index is almost the same for both variants of tyres. It can be caused by the fact, that the MITAS AC 85 tyres have bigger area of tyre footprint, while the MITAS VF tyres have bigger area of tyre profile, which can produce different distribution of contact pressure on base material.

ACKNOWLEDGEMENT. The paper was created with institutional support for long-term conceptual development VÚZT, v.v.i. RO0614.

## REFERENCES

Abrahám, R., Majdan, R., Šima, T., Chrastina, J. & Tulík, J. 2014. Increase in tractor drawbar pull using special wheels. *Agronomy Research* **12**(1), 7–16.

Ahokas, J. & Jokiniemi, T. 2014. Light tractor simulator. *Agronomy Research* **12**(1), pp. 17–24

Antille, D.L., Ansorge, D., Dresser, M.L. & Godwin, R.J. 2013. Soil displacement and soil bulk density changes as affected by tire size. *Transactions of the ASABE* **56**(5), 1683–1693.

Arvidsson, J. & Håkansson, I. 2014. Response of different crops to soil compaction–Short-term effects in Swedish field experiments. *Soil and Tillage Research* **138**, 56–63.

ASAE S313.3 Soil Cone Penetrometer. 1999

Braunack, M.V. 2004. A tyre option for sugarcane haulout trucks to minimise soil compaction. *Journal of Terramechanics* **41**(4), 243–253.

Braunack, M.V., Arvidsson, J. & Håkansson, I. 2006. Effect of harvest traffic position on soil conditions and sugarcane (Saccharum officinarum) response to environmental conditions in Queensland, Australia. *Soil and Tillage Research* **89**(1), 103–121.

Défossez, P., Richard, G., Boizard, H. & O'Sullivan, M.F. 2003. Modeling change in soil compaction due to agricultural traffic as function of soil water content. *Geoderma* **116**(1–2), 89–105.
Eguchi, T. & Muro, T. 2009. Measurement of compacted soil density in a compaction of thick finishing layer. *Journal of Terramechanics* **44**(5), 347–353.
Głąb, T. 2014. Effect of soil compaction and N fertilization on soil pore characteristics and physical quality of sandy loam soil under red clover/grass sward. *Soil and Tillage Research* **144**, 8–19.
Hamza, M.A., Al-Adawi, S.S. & Al-Hinai, K.A. 2011. Effect of combined soil water and external load on soil compaction. *Soil Research* **49**(2), 135–142.
Hůla, J., Gutu, D., Kovaříček, P., Staněk, L. & Kroulík, M. 2011. Odolnost půdy vůči zhutňování při řízených přejezdech strojů. (Soil Resistance Against Compaction During the Machines Controlled Traffic). *Agritech Science* **5**(1), (online) http://www.agritech.cz/clanky/2011-1-3.pdf. Accessed 11.11.2014
Chyba, J., Kroulík, M., Krištof, K., Misiewicz, P.A. & Chaney, K. 2014. Influence of soil compaction by farm machinery and livestock on water infiltration rate on grassland. *Agronomy Research* **12**(1), 59–64.
Chyba, J., Kroulík, M., Lev, J. & Kumhála, F. 2013. Influence of soil cultivation and farm machinery passes on water preferential flow using brilliant blue dye tracer. *Agronomy Research* **11**(1), 25–30.
Keller, T., Berli, M., Ruiz, S., Lamandé, M., Arvidsson, J., Schjønning, P. & Selvadurai, A.P.S. 2014. Transmission of vertical soil stress under agricultural tyres: Comparing measurements with simulations. Soil and Tillage Research **140**, 106–117.
Kuht, J., Reintam, E., Edesi, L. & Nugis, E. 2012. Influence of subsoil compaction on soil physical properties and on growing conditions of barley. *Agronomy Research* **10**(1–2), 329–334.
Kviz, Z., Kroulik, M. & Chyba, J. 2014. Soil damage reduction and more environmental friendly agriculture by using advanced machinery traffic. *Agronomy Research* **12**(1), 121–128.
Lamandé, M. & Schjønning, P. 2011a. Transmission of vertical stress in a real soil profile. Part I: Site description, evaluation of the Söhne model, and the effect of topsoil tillage. *Soil and Tillage Research* **114**(2), 57–70.
Lamandé, M. & Schjønning, P. 2011b. Transmission of vertical stress in a real soil profile. Part II: Effect of tyre size, inflation pressure and wheel load. *Soil and Tillage Research* **114**(2), 71–77.
Lamandé, M. & Schjønning, P. 2011c. Transmission of vertical stress in a real soil profile. Part III: Effect of soil water content. *Soil and Tillage Research* **114**(2), 78–85.
Lozano, N., Rolim, M.M., Oliveira, V.S., Tavares, U.E. & Pedrosa, E.M.R. 2013. Evaluation of soil compaction by modeling field vehicle traffic with SoilFlex during sugarcane harvest. *Soil and Tillage Research* **129**, 61–68.
McKyes, E. 1985. *Soil cutting and tillage*. Elsevier Science Publishers Amsterdam.
Monteiro, L.D.A., Albiero, D., Lanças, K.P., Bueno, A.V. & Masiero, F.C. 2013. Energetic efficiency of an agricultural tractor in function of tire inflation pressure. *Engenharia Agricola* **33**(4), 758–763.
Noréus, O. & Trigell, A. 2008. Measurement of terrain values and drawbar pull for six wheeled vehicle on sand. In: *16th International Conference of the International Society for Terrain Vehicle Systems*. ISTVS, Turin, pp. 250–257 (in Italy)
Nugis, E. & Kuht, J. 2012. Outline of results concerning assessment of soil compaction in Estonia. *Agronomy Research* **10**(1), 175–180.
Palancar, T.C. & Terminiello, A.M., 2001. Determinación Expeditiva del Área de Contacto Rueda-Suelo en Máquinas Agrícolas (Determination of wheel-soil contact area in agricultural machines). *Universidad Nacional de La Plata* (In Spain).

Prikner, P. & Aleš, Z. 2010. Assessment of soil compaction risk by agricultural tyres. In: *4th International Conference on Trends in Agricultural Engineering 2010*, TAE 2010, Prague, pp 499–504.

Rodríguez, L.A., Valencia, J.J. & Urbano, J.A. 2012. Soil compaction and tires for harvesting and transporting sugarcane. *Journal of Terramechanics* **49**(3–4), 183–189.

Schreiber, M. & Kutzbach, H. 2008. Influence of soil and tire parameters on traction. *Research in Agricultural Engineering* **54**(2), 43–49.

Syrový, O., Světlík, M., Pražan, R., Pastorek, Z., Kubín, K. & Gerndtová, I. 2013. *Mobilní energetické prostředky a orientační hodnoty jednotkových spotřeb paliv a energií (Mobile energy devices and the approximate values of unit fuel and energy consumption)*. Research Institute of Agricultural Engineering, p.r.i., Prague, pp. 56 (in Czech).

Taghavifar, H. & Mardani, A. 2014. Effect of velocity, wheel load and multipass on soil compaction. *Journal of the Saudi Society of Agricultural Science* **13**(1), 57–66.

Varga, F., Tkáč, Z., Šima, T., Hujo, L., Kosiba, J. & Uhrinová, D. 2014. Measurement of soil resistance by using a horizontal penetrometer working with the two-argument comparative method. *Agronomy Research* **12**(1), 187–196.

*Agronomy Research* **13**(1), 63–72, 2015

# The influence of a system with permanent traffic lanes on physical properties of soil, soil tillage quality and surface water runoff

D. Gutu[1], J. Hůla[1], P. Kovaříček[2] and P. Novák[1,*]

[1]Czech University of Life Sciences Prague, Faculty of Engineering, Kamycka 129, 165 21 Prague 6 – Suchdol, Czech Republic; [*]Correspondence: novakpetr@tf.czu.cz
[2]Research Institute of Agricultural Engineering, p.r.i., Drnovska 507, 161 01 Prague 6 – Ruzyne, Czech Republic

**Abstract.** The system with permanent driving tracks at the module of machines working width 6 metres, practised in a 10-ha field, allowed to consistently separate the area designed for restricted traffic lanes of farm machines from the production area of the field. The aim of the study is to assess the selected indicators of the condition of topsoil, which is characterized by soil porosity, indicators of soil workability, soil ability to absorb water from rainfall and soil loss by wash after four years of controlled traffic system application in a field trial. Indicators of soil condition were evaluated in four variants with different wheel impacts of tractors and other machines on the soil. A field trial was established in the spring 2010; the measured values in the study are from 2013 and 2014. The results show an advantage, which represents concentration of passages into permanent tracks aimed at protection of most part of a plot from soil compaction. Hardness of clods after tillage in autumn 2013 was five times higher in places with random traffic (356.7 kPa) than outside traffic lanes in the system of controlled traffic (70 kPa). An important result is that the system with permanent traffic lanes made it possible to increase the soil capacity of taking up water under intensive rainfall – in comparison to a part of the land with random passes. The results of measurements with a rainfall simulator in April 2014 showed that cumulative surface runoff after sixty minutes was 7.6 l $m^{-2}$ on the land with random passes while 3.9 l $m^{-2}$ outside the traffic lanes (32% of the area of the field). The soil loss by wash during water surface runoff was also lower with controlled traffic compared to the variant with random passes. Therefore it is to assume that suitable application of the controlled traffic farming system may be a contribution to soil protection from water erosion.

**Key words:** soil compaction, controlled traffic farming, surface water runoff, water erosion.

## INTRODUCTION

The wheel traffic of tractors, conveyances, fertilizer and pesticide distributors, harvesters, implements and trucks causes soil compaction. The soil has different resistance to compression. Crucial factors are soil texture, instantaneous soil moisture, content of organic compounds in the soil and soil structure. One of the consequences of undesirable soil compaction is the increased energy requirement for its primary and secondary cultivation.

Technogenic soil compaction cannot be eliminated but it is possible to significantly contribute to a reduction in its intensity. One of the possibilities is to confine the necessary wheel traffic in fields to permanent tracks in order to ensure that a major part of the production area of fields will remain without the negative influence of wheel traffic (Chamen et al., 2003; Tullberg, 2010). A system with permanent tracks is called Controlled Traffic Farming (CTF). This system can be used in practical farming conditions due to the existence of precise navigation systems in combination with the automated steering of tractors and other machines passing in fields. A contribution of the CTF system is a reduction in the rolling resistance of wheels, and also lower energy requirement for soil tillage if the major part of the field area is without soil compression by wheels or tracks of machines (Kroulík et al., 2011; Tullberg et al., 2007).

In compacted soils there is a substantially lower rate of infiltration for water especially under intensive rainfall. Yuxia et al. (2001) reported for the uncompacted soil a four to five times higher rate of infiltration than in the soil compacted by wheel traffic. These authors also documented that soil compaction has a greater influence on the rate of water infiltration into the soil than soil tillage. According to Li et al. (2004) the losses of the area by wheel tracks can be compensated by higher yield.

The issues of controlled traffic are known. The aim of the field experiment was to clarify the differences in the state of topsoil after several years of use of the system with permanent traffic lanes and compare selected soil properties with parts of field with random traffic.

It turns out that not only physical soil properties and indicators of soil workability shall be evaluated, but it is relevant to evaluate as well the indicators of risk of water erosion. These include surface water runoff and soil loss by wash.

## MATERIALS AND METHODS

A field trial on a land of 10 ha in size was established in spring 2010. Soil conditions: loamy soil (content of particles smaller than 0.01 mm in the topsoil layer: 38.3% by weight). Content of carbon in topsoil: 3.8%.

After medium-deep soil tillage to a depth of 0.25 m (Horsch Tiger 4MT, October 15, 2009) the field remained without wheel traffic until spring 2010, when wheel traffic was organised within the CTF system using OutTrac (Chamen, 2006) – Fig. 1. On this field the soil properties were evaluated in four variants of wheel effect:

1. Traffic lanes of tractors during sowing, application of chemicals for plant protection, application of mineral fertilizers, lanes of tractors during soil tillage – repeated 10 times, working width 18 m.
2. Traffic lanes of wheels of a tractor during sowing, lanes of a combine harvester and lanes of a tractor during soil tillage (without lanes of tractors at chemicals for plant protection and mineral fertilizers application) – repeated 30 times, working width 6 m.
3. Outside the traffic lanes.
4. Part of the field with uncontrolled wheel traffic (area of 3 ha) – Random – repeated 12 times, the traffic lanes were moved every year.

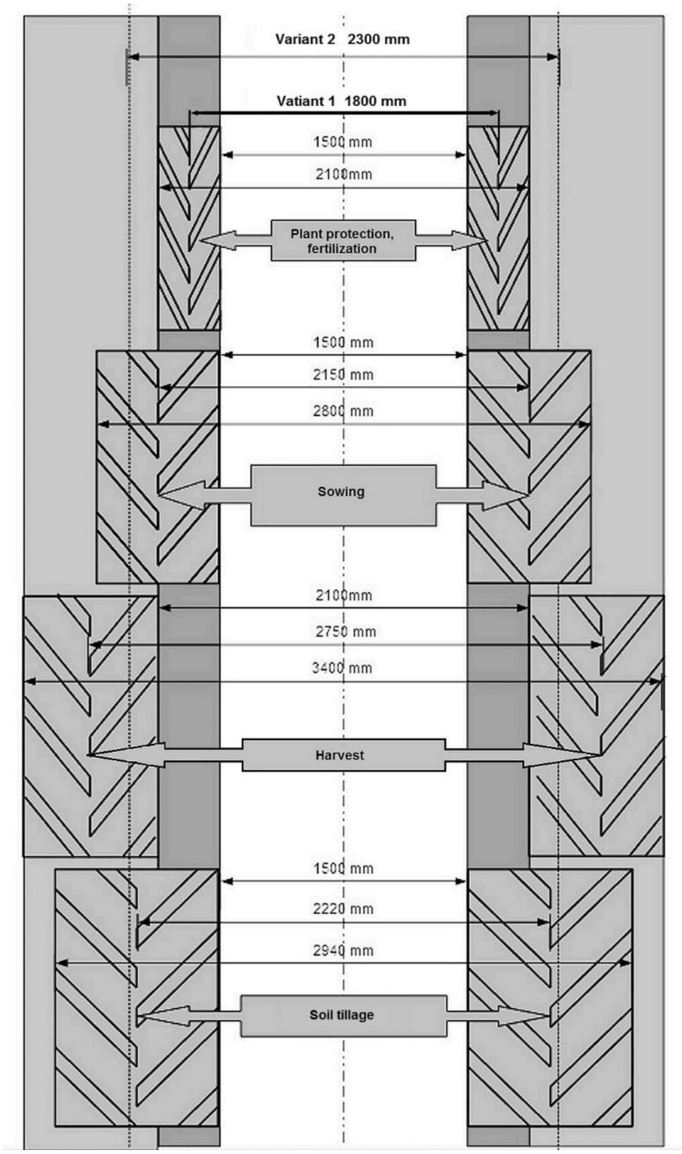


**Figure 1.** Wheel ruts of tractors and combine harvester after their concentration to permanent traffic lanes.

In the variants of the field trial measurements basic physical properties of soil were evaluated. Spatial distribution of soil particles was evaluated by means of undisturbed soil samples taken into Kopecky´s rings (100 cm$^3$). The samples were processed in the standard way and soil bulk density, total porosity and moisture content was determined (Valla et al., 2008). Undisturbed soil samples were taken from a depth of 0.05 to 0.10 m, 0.15 to 0.20 m, 0.25 to 0.30 m and 0.35 to 0.40 m. Samples were always in five replications.

After soil tillage process the topsoil from the area of 0.25 m$^2$ was collected from a depth of 0 to 0.10 m and sieved on sieves with square openings of 100 mm, 50 mm, 30 mm and 10 mm (three repetitions). Individual fractions were weighed and calculated the proportion of fractions in weight percent. For the measuring of penetration resistance of surface soil layer and penetration resistance of clods after soil tillage it was used the pocked penetrometer Ejkelkamp with cylindrical body (foot diameter 6.35 mm, depth of pushing the cylinder: 6.35 mm).

This paper contains the results of evaluation of wheel traffic impacts on the soil in a field trial in 2013 (the fourth year of the consistent application of controlled traffic farming in a field). Measurements by the rain simulator were held in April 2014.

Surface water runoff was measured under simulated sprinkling on a measurement area of 0.5 $m^2$ in size and at rainfall intensity of 87.8 mm $h^{-1}$, using three replications for each treatment. Infiltration rate is determined from the defined rainfall intensity that is constant for the time of measurement and from surface runoff of water from the measurement area (Kovaříček et al., 2008). Intercepted water from surface runoff is filtered, quantity of filtered soil is dried up and from the dry weight of washed soil the unit loss of soil (g $m^{-2}$ $h^{-1}$) caused by water erosion is determined (the average sample).

For basic data processing was used software MS Excel 2010. It was also used STATISTICA CZ software version 12 (StatSoft) for graphic processing of the resulting values and the statistical analysis ANOVA with Tukey HSD test –homogeneous groups test ($\alpha = 0.05$).

For the navigation of machines during soil tillage, sowing, application of chemicals for plant protection, application of mineral fertilizers and during harvest a GPS satellite system with the correction signal of RTK VRS was used. For machines steering an assisted steering system AgGPS EZ-STEER (Trimble) was used. Table 1 documents field operations and machines used for work operations.

**Table 1.** Field operations and machines (2013/2014)

| Field operation | Machines | Working width (m) | Distance of tracks (mm) | Tyre width (mm) |
|---|---|---|---|---|
| Sowing of winter wheat (18.10.2012) | NEW HOLLAND + VÄDERSTAD Rapid 600P | 6 | 2,150 | 500 x 2 |
| Mineral fertilizers application (19.3.2013) | ZETOR 10145 + AMAZONE 1000 | 18 | 1,800 | 300 x 2 |
| Pesticide application (27.4.2013) | CASE JX 1100U + AGRIO NAPA 18 | 18 | 1,800 | 320 x 2 |
| Pesticide application (11.6.2013) | CASE JX 1100U + AGRIO NAPA 18 | 18 | 1,800 | 320 x 2 |
| Winter wheat harvest (2.8.2013) | CLAAS Lexion 460 | 6 | 2,750 | 650 x 2 |
| Shallow loosening, 0.08–0.10 m (4.8.2013) | CASE 335 + FARMET Hurikan 600 | 6 | 2,220 | 720 x 2 |
| Medium deep loosening, 0.14–0.16 m (15.11.2013) | CASE 335 + Simba SLD 600 | 6 | 2,220 | 720 x 2 |
| Sowing of spring pea (7.4.2014) | NEW HOLLAND + VÄDERSTAD Rapid 600P | 6 | 2,150 | 500 x 2 |
| Pesticide application (26.4.2014) | CASE JX 1100U + AGRIO NAPA 18 | 18 | 1,800 | 320 x 2 |

Weather data of experimental years are in Table 2.

**Table 2.** Weather data of experimental years

| Year | Month | Air temperature (°C) | Total precipitation (mm) |
|---|---|---|---|
| 2013 | 1 | 1.7 | 18.8 |
| | 2 | 2.8 | 10.8 |
| | 3 | 3.0 | 15.2 |
| | 4 | 9.8 | 35.4 |
| | 5 | 13.7 | 70.4 |
| | 6 | 17.6 | 145.0 |
| | 7 | 21.4 | 26.8 |
| | 8 | 19.4 | 10.2 |
| | 9 | 13.6 | 0.2 |
| | 10 | 10.2 | 47.7 |
| | 11 | 5.4 | 17.5 |
| | 12 | 2.6 | 7.2 |
| 2014 | 1 | 1.5 | 22.0 |
| | 2 | 3.2 | 1.4 |
| | 3 | 7.7 | 29.0 |
| | 4 | 11.3 | 8.8 |

## RESULTS AND DISCUSSION

In the fourth year of the field trial, in 2013, physical properties of soil were determined at sites with different intensity of the wheel traffic action on soil (variants 1 to 4). Graph in Fig. 2 show total porosity of soil in the topsoil layer. Before winter wheat harvest, as expected the highest soil porosity was found out at sites without wheel tracks (variant 3) while the values of soil porosity were lowest in variant 1 with the highest intensity of wheel traffic. At a depth of 0.35–0.40 m there were no larger differences in the values of soil porosity between the variants any more – average values of total porosity: 38.9 (Var. 1), 38.3 (Var. 2), 38.6 (Var. 3), 39.5 (Var. 4). Confirmed the results of previous years: in the CTF system were favorable indicators of soil physical properties on the most area of field. This is consistent with the results of McHugh et al., (2009) whereby controlled traffic is an opportunity for restoration of physically degraded soil after random field wheeling. According Hamza & Anderson (2005) increasing of soil porosity is a tool of reduction even elimination of soil compaction. We prefer the use of controlled traffic but further measures can be recommended: addition of organic matter, selecting appropriate crop rotation, suitable mechanical loosening.

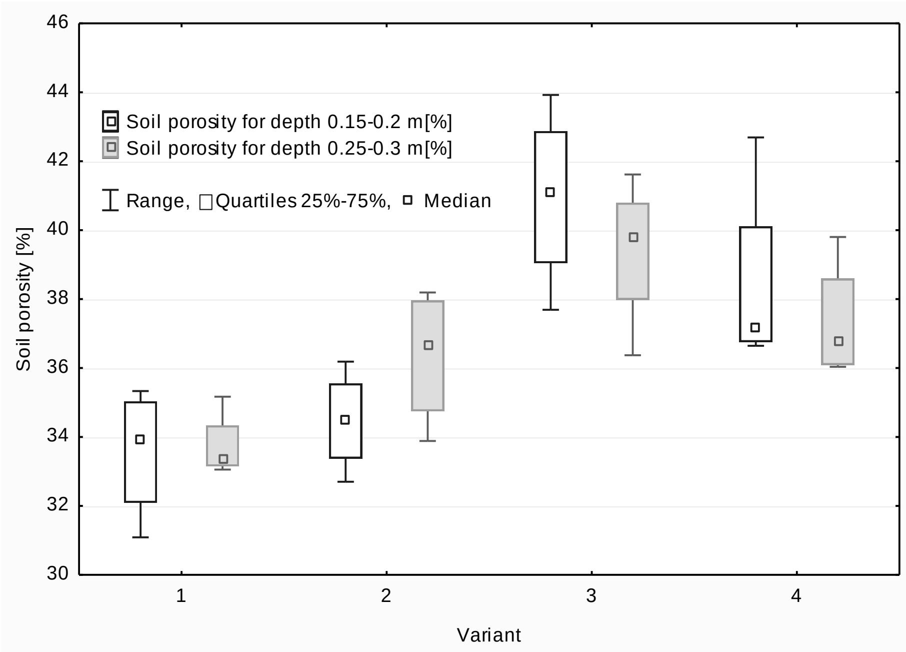


**Figure 2.** Total porosity of soil at a depth of 0.15–0.20 m and 0.25–0.30 m (2nd July. 2013). Variants: 1 – Traffic lanes including application of chemicals for plant protection and mineral fertilizers; 2 – Traffic lanes without application of chemicals for plant protection and mineral fertilizers; 3 – Outside the traffic lanes; 4 – Random traffic.

Fig. 3 illustrates the values of the surface soil layer resistance to the penetration of the cylindrical body of a penetrometer. On the summer date of measurement differences in the values between variants 1, 2 and 4 were statistically insignificant while penetration resistance in the variant without wheel traffic (variant 3) was statistically significantly lower than in all the other three variants (Tukey HSD test). A similar conclusion was drawn for the statistical significance of differences in penetration resistance measured during the crumbling of clods that originated by autumn soil tillage. The distinctly lowest resistance of clods to crumbling at sites without long-time wheel traffic is shown in Fig. 4. At sites without passes the topsoil crumbling was good without formation of large clods (variant 3) – Fig. 5. On the contrary, at sites with concentrated wheel tracks (variants 1 and 2), and also at sites with random wheel traffic, large clods were formed that are undesirable for the quality of sowing of subsequent winter crop. On an experimental land the area without wheel tracks accounted for 68% of the area of this land. At random machinery traffic 86.1% of the total field area was run-over at least once a year, when using conventional tillage for winter wheat, and 63.8% of the total field area was run-over when using conservation tillage (Kroulík et al., 2011).

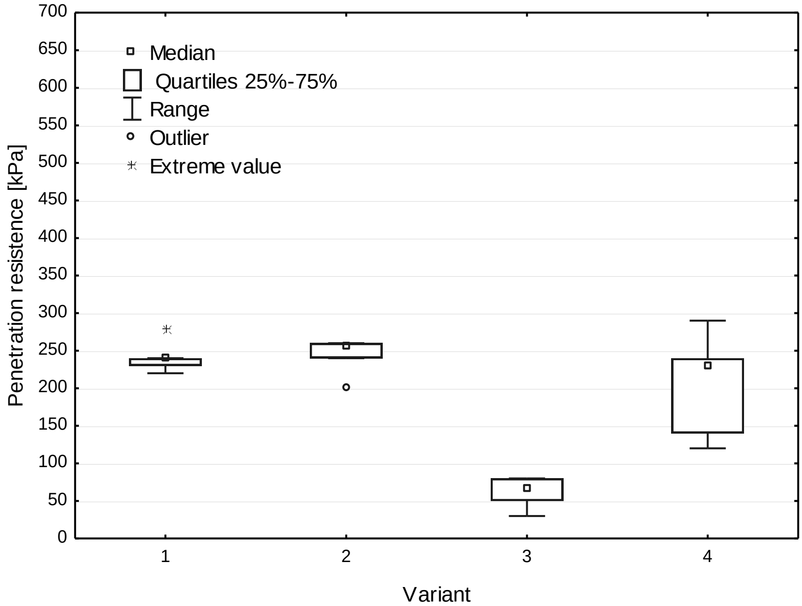


**Figure 3.** Penetration resistance at a depth of 0.05 m (2nd July. 2013) – soil moisture content (weight%): 18.7 (Var. 1), 20.1 (Var. 2), 19.6 (Var. 3), 20.1 (Var. 4). Variants: 1 – Traffic lanes including application of chemicals for plant protection and mineral fertilizers; 2 – Traffic lanes without application of chemicals for plant protection and mineral fertilizers; 3 – Outside the traffic lanes; 4 – Random traffic.

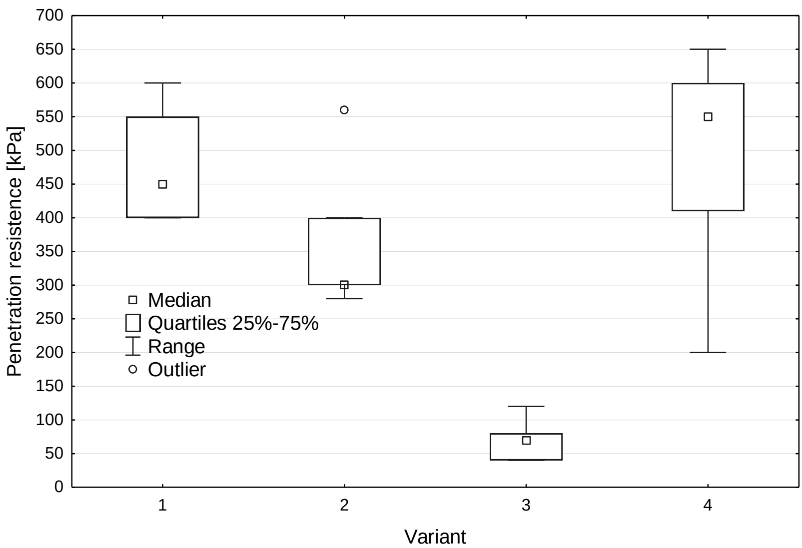


**Figure 4.** Penetration resistance of clods (31st October 2013) – soil moisture content (weight%): 18.4 (Var. 1), 18.2 (Var. 2), 20.8 (Var. 3), 17.1 (Var. 4). Variants: 1 – Traffic lanes including application of chemicals for plant protection and mineral fertilizers; 2 – Traffic lanes without application of chemicals for plant protection and mineral fertilizers; 3 – Outside the traffic lanes; 4 – Random traffic.

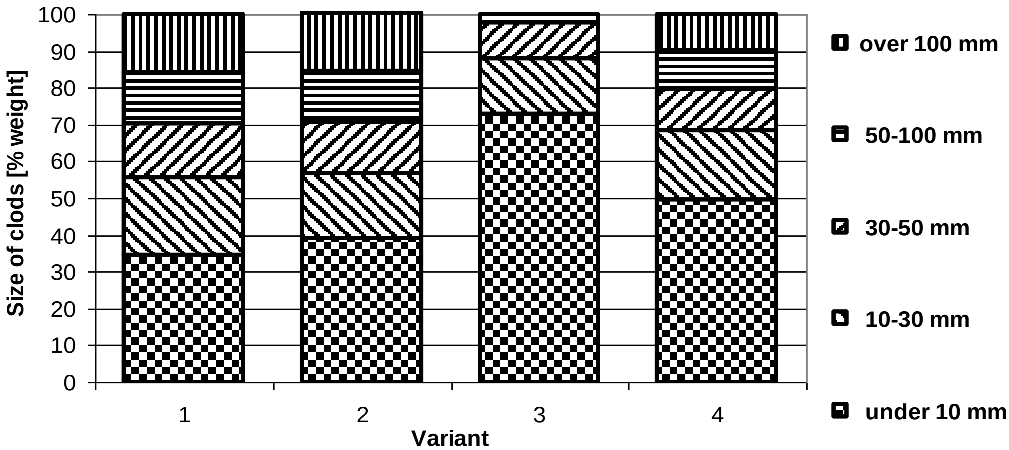


**Figure 5.** Size of clods after loosening (0–0.10 m) (31st October 2013). Variants: 1 – Traffic lanes including application of chemicals for plant protection and mineral fertilizers; 2 – Traffic lanes without application of chemicals for plant protection and mineral fertilizers; 3 – Outside the traffic lanes; 4 – Random traffic.

It is to assume that differences in physical properties of soil and quality of soil tillage can be reflected in different capacity of the soil to take up water under intensive rainfalls. The results of measurements with a rainfall simulator in April 2014, after four years from the beginning of the field trial, are documented in Fig. 6. The graph shows a surface runoff under artificial rainfall made at a rate of 88 l $m^{-2}$ $h^{-1}$, which is 88 mm of rainfall per hour. Surface runoff at sites with confined wheel traffic to permanent tracks (variants 1 and 2) and on a part of the land with random passes (variant 4) was substantially different from variant 3. An important indicator is the onset of surface runoff. In variant 3 (outside the wheel tracks) surface runoff began in almost 40 minutes from the beginning of artificial rainfall, until then all water was infiltrated into the soil. At sites with permanent wheel tracks, and also at sites with random passes, surface runoff started within a more than twice shorter time than on the land without lanes. This result is consistent with the conclusions drawn by Yuxia et al., (2001) and Li et al., (2004). The results of measurements with a rainfall simulator indicate a contribution of the controlled traffic farming technology to the improved capacity of soil to take up water under intensive rainfall.

Surface runoff water is related with a risk of soil erosion. Fig. 7 shows the soil loss by wash under artificial rainfall. The measurement with a rainfall simulator showed the highest soil loss by wash in variant 4 (random passes) – 24.9 g $m^{-2}$ $h^{-1}$. The almost tenfold lower soil loss was observed at sites without wheel traffic. The low soil loss by wash was also measured at a site of permanent tracks (variant 1). This result supports a hypothesis about the contribution of a system with permanent traffic lanes to a reduction in the water erosion of soil.

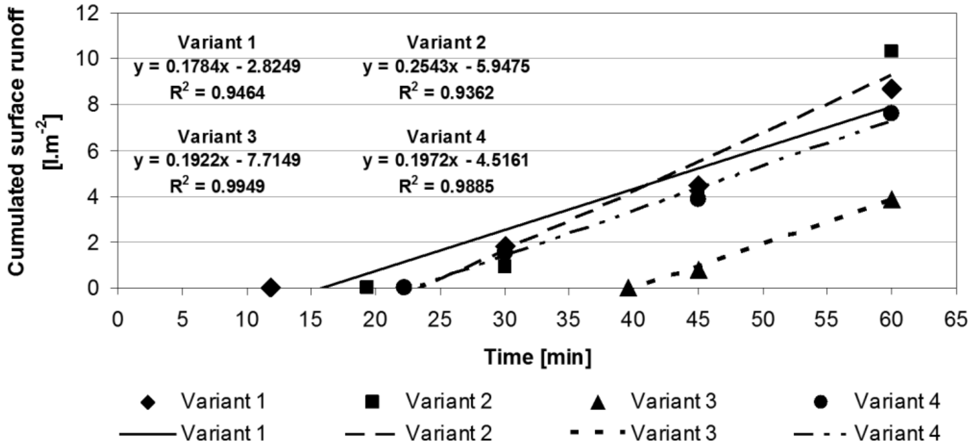


**Figure 6.** Cumulative surface runoff under artificial rainfall (rainfall simulator) – 29th April 2014, four years after the founding of the field experiment (*x* – time, *y* – cumulative surface runoff). Variants: 1 – Traffic lanes including application of chemicals for plant protection and mineral fertilizers; 2 – Traffic lanes without application of chemicals for plant protection and mineral fertilizers; 3 – Outside the traffic lanes; 4 – Random traffic.

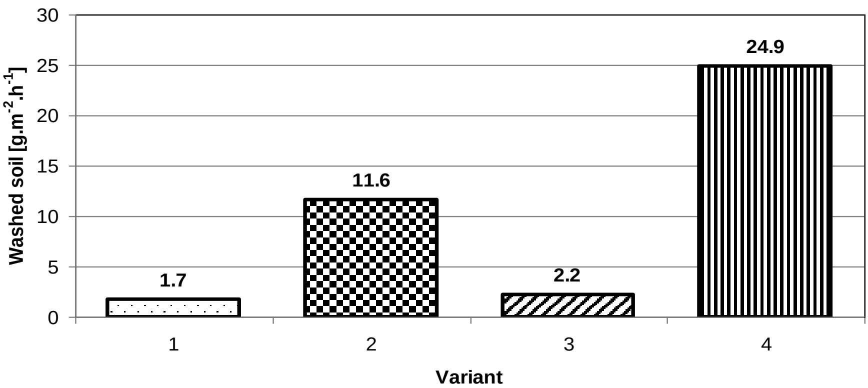


**Figure 7.** Soil loss by wash under artificial rainfall – 29th April 2014. Variants: 1 – Traffic lanes including application of chemicals for plant protection and mineral fertilizers; 2 – Traffic lanes without application of chemicals for plant protection and mineral fertilizers; 3 – Outside the traffic lanes; 4 – Random traffic.

The results of measurements of water surface runoff under artificial rain made with a rainfall simulator are consistent with the results of the authors who evaluated the influence of soil compaction on water infiltration into the soil (Hamza & Anderson, 2005; Raper & Kirby, 2006). Crop residues have a great importance on the soil surface. According to Tullberg (2010) maximum runoff and soil loss occurred on compacted, non-tilled plots unprotected by plant residues. For this reason, it is appropriate to keep the crop residues in place of traffic lanes for the benefit of erosion control measures.

It shows that a major barrier to adoption of controlled traffic farming in practice is the lack of compatibility in equipment as reported Tullberg (2010).

## CONCLUSIONS

The results of evaluation of physical properties of soil four years after the establishment of a field trial indicated favourable physical properties of soil on a part of the field without wheel tracks – the area without wheel tracks accounted for 68% of the land area when the working width module of 6 m was used. The work quality of machines for soil tillage operations was also higher on a part of the field without wheel tracks. An important finding is that the wheel traffic confined to permanent traffic lanes made it possible to substantially increase the soil capacity of taking up water under intensive rainfall – compared to a part of the land with random passes. The soil loss by wash during water surface runoff was also lower with controlled traffic farming compared to the variant with random passes. Hence it is to assume that suitable application of the CTF system may be a contribution to soil protection from water erosion.

ACKNOWLEDGEMENTS. Supported by the Ministry of Agriculture of the Czech Republic under the institutional support for long-term strategic development of RIAE, p.r.i., RO0614.

## REFERENCES

Chamen, W.C.T., Alakukku, L., Pires, S., Sommer, C., Spoor, G., Tijink, F. & Weisskopf, P. 2003. Prevention strategies for field traffic – induced subsoil compaction: a review, Part 2. Equipment and field practices. *Soil & Tillage Research* **73**, 161–174.

Chamen, W.C.T. 2006. Controlled traffic farming on a field scale in the UK. In*: Horn, R. – Fleige, H. – Peth, S. – Peng, X.H., (Eds.): Soil Management for Sustainability. Advances in geoecology* **38**, 251–260.

Hamza, M.A. & Anderson, W.K. 2005: Soil compaction in cropping systems. A review of the nature, causes and possible solutions. *Soil & Tillage Research* **82**(2), 121–145.

Kovaříček, P., Šindelář, R., Hůla, J. & Honzík, I. 2008. Measurement of water infiltration in soil using the rain simulation method. *Research in Agricultural Engineering* **54**(3), 123–129.

Kroulík, M., Kvíz, Z., Kumhála, F., Hůla, J. & Loch, T. 2011. Procedures of soil farming allowing reduction of compaction. *Precision Agriculture* **12**(3), 317–333.

Li, Y.X., Tullberg, J.N., Freebairn, D.M. & Ciesiolka, C.A. 2004. Effect of controlled traffic and conservation tillage on runoff and crop yield. Paper No. 041071 ASAE, St Joseph, MI, USA.

McHugh, A.D., Tullberg, J.N., Freebairn, D.M. 2009. Controlled traffic farming restores soil structure. *Soil & Tillage Research* **104**, 164–172.

Raper, R. & Kirby, J., 2006. Soil compaction: How to do it, undo it, or avoid it. In.: *Agricultural Equipment Techonology Conference*. Louisville, Kentucky, USA, 2006. 14 pp.

Tullberg, J.N., Yule, D.F. & McGarry, D. 2007. Controlled traffic farming – From research to adoption in Australia. *Soil & Tillage Research* **97**, 272–281.

Tullberg, J. 2010. Tillage, traffic and sustainability – A challenge for ISTRO. *Soil & Tillage Research* **111**, 26–32.

Valla, M., Kozák J., Němeček J., Matula S., Borůvka L. & Drábek O. 2008. *Pedological practicum* . ČZU v Praze, Praha, 151 pp. (in Czech).

Yuxia L., Tullberg J.N. & Freibairn D.M. 2001. Traffic and residue cover effects on infiltration. *Australian Journal of Soil Research* **39**, 239–247.

*Agronomy Research* **13**(1), 73–82, 2015

# Investigation of the technological spring harvesting variants of the industrial hemp stalk mass

S. Ivanovs*, A. Adamovics and A. Rucins

Latvia University of Agriculture, Ulbroka, LV-2130, Latvia
*Correspondence: semjons@apollo.lv

**Abstract.** One of the simplest technological solutions of hemp harvesting applied in practice in Latvia and some other countries is harvesting of the hemp stalks in spring. Implementation of this technology does not require expensive specialised machinery. However, there are significant losses of the mass and quality of the product. The loss of hemp stalk mass in two-stage harvesting (Option A: harvesting of the seedy part of the yield by means of grain harvesting combines and subsequent gathering of the stalks in spring) constitutes approximately 50–80%. The basic possible solution for reducing these losses is raising the cutting height of the stalks when the seedy part of the yield is harvested. With spring harvesting, Option B, the mass of the stalks is preserved, while the seedy part of the yield is completely lost. A rational solution for spring harvesting can be established by calculations, considering the crop volume and the prices of the seeds and stalks sold, as well as the value of technological losses. In the tests conducted during a subsequent harvest in spring the tensile strength of the fibres of the uncut hemp stalks was 25–52% lower than the strength of the fibres harvested in autumn.

**Keywords:** industrial hemp, spring harvesting, loss of stalks.

## INTRODUCTION

Over the past 25 years, an active increase in areas under industrial hemp cultivation can be observed throughout the world (Struik, 2000). In addition, the EU has imposed strict control, only allowing the cultivation and subsidising of those varieties whose tetrahydrocannabinol (THC) content – it being a psychoactive ingredient – does not exceed 0.2%. For hemp to have such a content of THC, a narcotic substance, is practically ruled out (Jankauskiene & Gruzdeviene, 2010). In Latvia the cultivation of this crop started in 2009. In EU countries, industrial hemp (*Cannabis sativa* L.) is considered as one of the important renewable resources for the production of a wide range of industrial products (as evidenced by the Resolution of the EU Commission 'COM/2008/03/07') (*Cannabis sativa* L. Hemp., 2009).

At present a search for optimal technological options for growing and harvesting hemp is underway in various farms; new innovative technologies for the use of the raw material are being developed to make it possible to extend the range of application of this product (Burczyk & Kaniewski, 2005). For the time being, the stalks of industrial hemp are traditionally used to produce fibre and wood shives, while the seeds are a raw material for the production of oils, foodstuffs and medical preparations. In recent years investigations have been undertaken in order to create new building materials on the basis of hemp stalk mass. The most complicated factor to determine the production economy of this crop lies in the field harvesting operations (Ivanovs et al., 2014). Among the considerable number of technological harvesting options there is one that attracts the interest of practical growers – namely, the spring harvesting of industrial hemp. However, an apparent drawback of spring harvesting of industrial hemp, in contrast to autumn harvesting, consists in significant losses in the amount of crop yields (the seeds or stalks) and the quality of the product (tensile strength of the fibres). The aim of the investigation was to determine the value of the potential yield of different varieties of industrial hemp, to assess the quantitative losses and strength of the hemp stalk mass when the technological option of spring harvesting is applied.

## MATERIALS AND METHODS

The objectives of this study were:

- to determine the potential yield of the stalks of different varieties of industrial hemp;
- to provide an analytical assessment of the degree of quantitative losses of the stalks in two-stage harvesting of industrial hemp due to the use of grain combine harvesters for harvesting the seedy part of the yield;
- to determine the rate of strength degradation of the hemp fibres at the time of its spring harvesting;
- to determine the rate of the operating costs related to the implementation of the spring harvesting technology of hemp.

Field trials were carried out in 2014, in a Research and Study farm 'Pēterlauki' that is supervised by the Latvia University of Agriculture, according to an established methodology (Adamovičs et al., 2012). 11 industrial hemp (*Cannabis sativa* L.) cultivars – 'Bialobrzeskie', 'Futura 75', 'Fedora 17', 'Santhica 27', 'Beniko', 'Ferimon', 'Epsilon 68', 'Tygra', 'Wojko', 'Felina 32' and 'Uso 31' – were sown in the sod calcareous soil ($pH_{KCl}$ 6.7, containing available P 52 mg kg $^{-1}$, K 128 mg kg $^{-1}$, organic matter content in the soil from 21 to 25g kg$^{-1}$). The overall seeding rate was 50 kg ha$^{-1}$. The plots were fertilised as follows: N: 120 kg ha$^{-1}$, $P_2O_5$: 90 kg ha$^{-1}$, $K_2O$: 150 kg ha$^{-1}$. The biometrical indices of the hemp seedlings, the height and stem diameter at harvesting time, the amount of green and dry above-ground mass, and the fibre content were evaluated. The trial data were processed using descriptive statistics with Microsoft Excel for Windows (Arhipova and Balina, 2006). The mean values were obtained with an LSD test.

The following hemp harvesting options were investigated in this study:

**Option A:** harvesting of hemp on the field where the seedy part is cut in autumn using grain combine harvesters. A flowchart of this harvesting option (Ivanovs et al., 2014) can be applied in case the most important product is the hemp seed. With this option, the stalks are cut in autumn by means of a grain combine harvester at the maximum possible height, and the seeds are threshed. The stalk mass passing through the combine harvester goes to waste. Any stalks in the passage zone of the wheels of the combine harvester are pressed into the soil and can no longer be used. The uncut part of the stalks, 0.9–1.6 m tall (depending on type of the harvester used), remains in the field and is removed in the spring.

**Option B:** harvesting of hemp on the field where nothing is done in autumn. The flowchart of the spring operations is similar to that in Option A (except that the various operations are performed during a different time of the year). With this option, the seedy part of the harvested crop is lost completely (it drops off, is eaten by the birds, etc.). However, the amount of harvested stalk mass per hectare of the area is substantially greater – in practice it is approximately 2…3 higher than in Option A.

The loss of hemp stalk mass in two-stage harvesting (where the seedy part of the crop is harvested in autumn and the commercial part of the stalks in spring) was determined in an analytical way, based on the technical and operating indicators of combine harvesters.

An experimental investigation into the springtime hemp stalk harvesting technology was conducted on the farmstead 'Zalers' (Kraslavas reg., Latvia). On an experimental field of one hemp variety ('Futura 75'), the tensile strength (breaking strength) of the fibres was determined after the autumn field-retting (control option S) and then after the winter field-retting of the same variety of hemp. The breaking strength was determined by means of equipment from the laboratory of the Kraslava Flax Factory, using methods corresponding to the standard 'Scutched hemp. Specification' (GOST 10379-76), according to which 30 samples of a specified size were taken with each option. Their breaking strength was tested on the equipment DKB-60. This standard is currently used in Latvia by hemp processing factories in order to determine the quality of the purchased product.

The daily average air temperatures in the period from November 2012 till September 2014 are given in Fig. 1; other weather parameters can also be seen from the statistical data of the Latvian Meteocentre (www.meteo.lv).

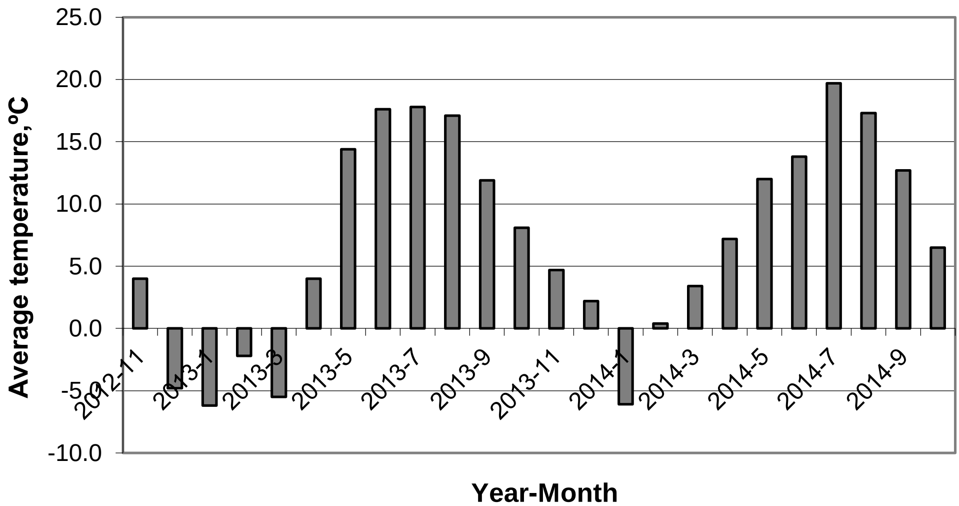


**Figure 1.** The monthly average air temperatures in the period from November 2012 till October 2014 (Riga, Latvia).

In the winter season of 2012–2013 sub-zero temperatures were dominant within the range of -2…-6 C. Only in November and April was the daily average temperature +4 C. At sub-zero temperatures any biological processes in the stalks (including rotting) are practically suspended or proceed very slowly. In the winter season of 2013–2014 the prevailing temperatures were +1…+5 C, and only in January was the daily average temperature below zero, i.e. -6 C.

The operating and economic indicators of machine performance were determined on the basis of experimental data (efficiency, fuel consumption), taking into account the operating costs (wages paid to the staff, the cost of fuel, repairs and depreciation), according to established methodologies (Kopiks & Viesturs, 2010, Barwicki et al., 2014).

Under Latvia's weather conditions hemp is ready for fibre harvesting at the end of August or the beginning of September. The seeds take longer to mature and are ready for harvest in the second half of September and the beginning of October. The weather conditions in such late autumn season are usually not favourable to a further processing of the hemp stalks. It is a venture to spread the stalks on the field for retting: in rainy or cold weather the process is slow and prolonged; besides, it is very difficult to obtain stalks that are suitable for baling with a moisture content less than 16–18%. Specialised machinery for harvesting the hemp stalks in autumn (specialised combine harvesters or mowers) is very expensive, and its use is justified only at a full load, i.e. for a large amount of work (Ivanovs et al., 2014). Therefore, rational solutions are being sought for the preservation of the hemp yield and a reduction in costs. One of the simplest and cheapest technological solutions already applied in practice is harvesting the hemp stalks in spring. The hemp stalks left uncut till spring (or with the upper part cut off) maintain a position close to vertical (Fig. 2) and at favourable temperatures undergo biological processes that ensure a further separation of the fibre from the wooden part (i.e. the so-called retted stems are produced).

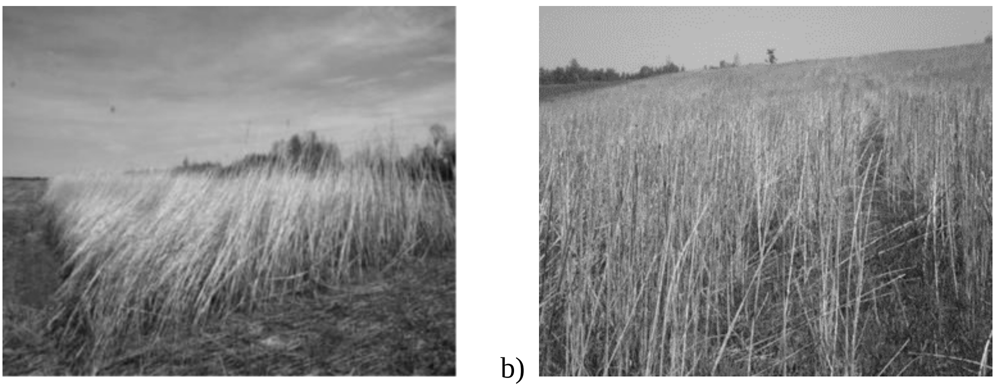

a) b)

**Figure 2.** A hemp field in spring: a) without previous harvesting of the seedy part, b) with harvesting of the seedy part in autumn.

A natural field-retting process takes place under the impact of moisture and the sun before the frost and in spring. Decomposition of pectin substances occurs during this process, ensuring an easy separation of the fibre from the wooden part. Furthermore, under a prolonged influence of the sun (about 5 months), a natural bleaching of the fibre takes place, producing a specific beautiful colour that is required for the production of several kinds of products. A drawback of this retting method is a partial loss of fibre strength due to the fact that the winter period the retting process cannot be regulated.

Harvesting takes place after the soil has dried and the machines can pass through (in Latvia this usually occurs at the end of April or the beginning of May). There is no need to cut such stalks in spring – instead, the stalks are rolled down using rollers, because the part of the stalks in contact with the soil becomes brittle (it starts rotting) and the stalks can break easily. In addition to rolling down the stalks, the technology of the spring operations also includes swathing (gathering the stalks into swathes) and harvesting by means of pickup balers. The essence of the two-stage hemp harvesting technology is the following: in stage one, the upper part of the plants is removed using grain combine harvesters in order to obtains seeds; in stage two, the remaining stalks are harvested (this may be done in autumn or in spring). The use of a grain combine harvester for harvesting the seedy part of the plants entails a specific quantitative loss of the stalks (some of the plants perish under the impact of the wheels, and some of the tops of the stalks gathered with the seeds go to waste).

Let us define the analytical expressions of the quantitative losses.

With spring harvesting, Option A, the total technological loss of stalks $W$ (%) is:

$$W = W_m + W_r \tag{1}$$

where: $W_m$ – the loss of the upper parts cut off by a grain combine harvester that go to waste after the threshing of the seeds, %; $W_r$ – the loss of the upper parts of the stalks pressed into the soil under the wheels of a combine harvester, %,

$$W_m = [(H - m)/H]100 \tag{2}$$

where: $H$ – the technical height of the hemp stalks, cm; $m$ – the cutting height of the stalks harvested by a combine harvester, cm.

$$W_r = (B/L)100 \tag{3}$$

where: $B$ – the width of the imprint zone formed by the combine wheels (as a rule, equal to double width of a big driving wheel), cm; $L$ – the width of the harvester header, cm.

After the corresponding expressions are inserted, we obtain a formula for the determination of the total technological loss of stalks:

$$W = W_m + W_r = 100[(H - m)/H] + B/L \tag{4}$$

In order to estimate the efficiency of the spring harvesting options, it is necessary to compare the possible earnings from the sales of the product under particular conditions (prices, productivity, etc.), including the technological losses mentioned above.

## RESULTS AND DISCUSSION

The yield of industrial hemp stalks depends on the variety, the used fertilisers and the nutrients available in the soil, as well as a number of other factors. In order to find out the possible volume of harvesting operations, experiments have been conducted to determine the stalk yield of the most widespread hemp varieties in Latvia. The industrial hemp cultivars ‘Bialobrzeskie’, ‘Futura 75’, ‘Fedora 17’, ‘Santhica 27’, ‘Beniko’, ‘Ferimon’, ‘Epsilon 68’, ‘Tygra’, ‘Wojko’, ‘Felina 32’ and ‘Uso 31’ could be successfully grown in Latvia for biomass and fibre production. The highest biomass yield during the trial years was obtained from cv. ‘Bialobrzeskie’. The experimental results obtained under equal circumstances with the aim of establishing the average green mass and dry matter yields of different varieties of industrial hemp as well as their averaged values are presented in Table 1. The highest crop yields in Latvia are produced by the varieties ‘Bialobrzeskie’, ‘Epsilon 68’ and ‘Futura 75’. On the whole, these crop yield values are, to a certain degree, evidence for the potential productivity of hemp stalks. We can conclude from the data that the growing season and the industrial hemp cultivars chosen had a significant ($p < 0.05$) effect on the hemp yield. However, in practice the crop yield values on large agricultural farms are usually 20–25% lower.

With Option A, a grain combine harvester is used in autumn to harvest the seedy part, whereas with Option B the combine harvester is not used at all. Therefore, in order to obtain results that are comparable with the expected income in Option A, the operating costs of the combine harvester should be deduced. Due to a lower actual crop yield of the harvested mass in Option B (due to the losses) the machines perform harvesting at a lower efficiency by mass in t $h^{-1}$ (with a similar efficiency by area in ha $h^{-1}$). The operating costs consist in the depreciation of the machinery and repair deductions, as well as fuel and electric energy expenses, wages and the cost of crop transportation to the processing sites.

**Table 1.** The yields of green biomass and dry matter with different hemp cultivars

| Hemp cultivars | Yield of green mass, t $ha^{-1}$ | Yield of dry matter, t $ha^{-1}$ |
|---|---|---|
| \`Bialobrzeskie\` | 60.99 | 15.86 |
| \`Futura 75\` | 49.65 | 14.81 |
| \`Fedora 17\` | 42.87 | 12.78 |
| \`Santhica 27 \` | 45.07 | 13.47 |
| \`Beniko\` | 39.96 | 11.96 |
| \`Ferimon\` | 43.24 | 12.93 |
| \`Epsilon 68\` | 48.67 | 14.47 |
| \`Tygra\` | 45.07 | 13.40 |
| \`Wojko\` | 39.59 | 11.79 |
| \`Felina 32\` | 42.98 | 12.80 |
| \`Uso 31\` | 40.43 | 11.98 |
| Average | 45.32 | 13.30 |
| $LSD_{0.05}$ cultivars | 6.35 | 2.69 |

The operating costs (rolling down of stalks, swathing by loosening rakes, picking and baling) in different spring harvesting options of hemp are shown in Fig. 3. The expenses are calculated using actual performance data and fuel consumption. With

Option A the specific operating costs are approximately 62–78% higher than with Option B. This is due to the fact that the amount of stalks harvested from one hectare, the harvested areas being equal, is at least two times smaller, which affects the efficiency in t $h^{-1}$.

In experimental tests the upper part of the hemp stalks was harvested for seeds in autumn by the combine harvester Class Mercator 75 (Option A1) or New Holland (Option A2).

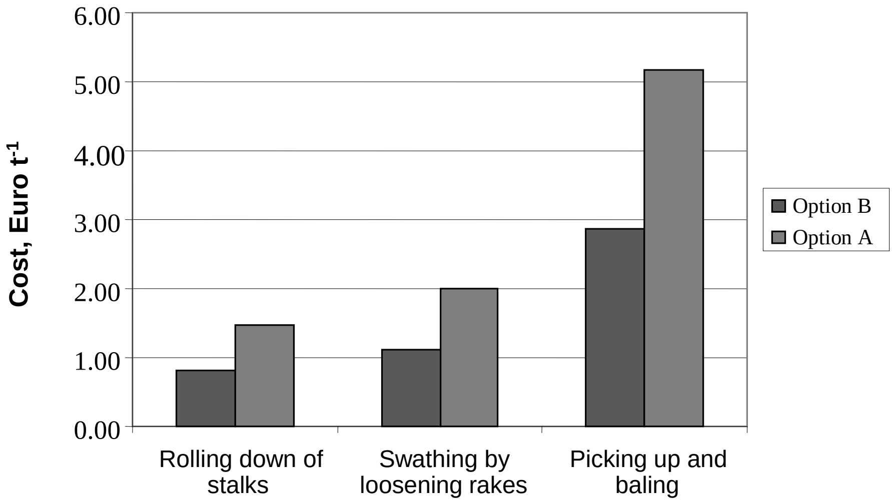


**Figure 3.** Operating costs in different spring harvesting options.

The average height of the stalks remaining on the field was 89 cm (combine harvester Claas Mercator 75) or 155 cm (combine harvester New Holland). Such a height was determined by the design parameters (technical possibilities) of a particular combine harvester. With the brands of grain combine harvesters that are widespread in Latvia, the value of the maximum height setting of the header varies within the range of 90...160 cm, representing the lowest and highest values available (Sheichenko & Lukjanenko, 2013).

After the technical data are inserted into Formula 4, we find that the total value of stalk loss is 79% with Option A1 and 47% with Option A2. The correlation between the width of the wheels of the combine harvester and the width of the header with different brands of combine harvesters varies to an insignificant degree (Ivanovs et al., 2014). Therefore, the use of grain harvesting combines with a higher setting of the cutting apparatus (header) might prove a real solution for reducing the loss of stalks in two-stage hemp harvesting. With spring harvesting, Option B, the stalk mass is preserved, while the seedy part of the yield is completely lost. In order to give an economic estimation of the advantages of this or that harvesting option, we need to know the potential crop yield and harvesting loss; in addition, a calculation is needed on the basis of the actual indicators of the purchasing prices of the hemp stalk mass and seeds, the distance of the farm from the marketing sites of the products, the operating costs of a particular set of harvesting machinery, and so on.

Among all the parameters of hemp fibre quality (length, colour, linear density, etc.) the most characteristic property of the fibre is its breaking strength.

Studies on the influence of winter retting on fibre strength were carried out for two seasons. Three options were tested:

S) standard – autumn retting and harvesting;

A) only the lower part of the stalks was left in winter, the upper part was cut by a combine harvester to obtain seeds;

B) the stalks were left in autumn on the field in the natural environment without any processing.

On the experimental field of the variety 'Futura 75' the breaking strength (tensile strength) of the fibre was first determined after autumn retting and then after winter retting.

**Table 2.** Tensile strength of the fibre with different retting options

| Stalk retting option | Mean value of breaking strength, N | Variation coefficient | Relative value of breaking strength in relation to the standard option |
|---|---|---|---|
| | Spring harvesting May 4, 2013; | standard harvesting – November 2, 2012. | |
| S (standard) | 202 | 28.3% | 100% |
| B | 148 | 32.1% | 73.2% |
| A | 136 | 34.5% | 67.3% |
| | Spring harvesting April 29, 2014; | standard harvesting – October 21, 2013. | |
| S (standard) | 181 | 25.2% | 100% |
| B | 87 | 39.3% | 48.0% |
| A | 94 | 35.7% | 51.2% |

As evident from the data obtained, by the time of spring harvesting the fibre had lost 27…33% of its breaking strength in the year 2013 and 49…52% in 2014. No substantial difference in the strength of the fibre was found between Options A and B; however, the strength varies significantly by season (year). Apparently, a prolonged (more than 4 months) impact of temperatures +1…+5°C on the hemp stalks in the winter season of 2013–2014 had an unfavourable effect on their strength. That period saw not only decomposition processes on the organic bonds between the fibrous and wooden parts of the stalks, but also active destruction processes on their structure (rotting). With all the options, the values of the variation coefficient were quite high (25–39%); however, this is due to the fact that hemp fibre is not a homogeneous material and, in relation to the initial stalk strength, many various random factors exert continual influence on the biological processes.

In order to achieve short fibre and wood shives, Latvian hemp processing enterprises purchase their hemp stalks after spring harvesting (in 2013 their average price, depending on quality, was approximately 110–140 EUR $t^{-1}$).

It should be noted that a significant loss (12–23%) of wood shives occurs during baling in spring (Ivanovs et al, 2014). This is due to the fact that after picking in spring the wood shives start separating from the fibres, breaking into small pieces when turned into a cylindrical bale, and drop out onto the soil surface through the gaps between the baling rollers. In autumn the retted stems separate from the fibres only under mechanical coercion, and therefore the dropout-related losses constitute no more than 3%.

Another limiting factor for the application of the spring harvesting technology of hemp stalks is the short period of time that is left in the spring for soil preparation and sowing of a new crop on a particular field (in Latvia's weather conditions no more than 15–20 days are usually left for these operations).

In spite of these drawbacks, the spring harvesting of hemp is not cost-intensive and, as practice shows, it can find some limited application in certain cases:

- if the seedy part of the crop yield ripens late and is harvested by grain combine harvesters, one might manage to harvest the seeds in autumn, preserving and gathering up to 50% of the stalks in spring;
- if the hemp stalks ripen and are harvested late, for instance, at the beginning of November (i.e. when there is great risk that the field-retting of the cut stalks and their picking up by pickup balers cannot be finished before winter sets in, and all the crop yield may be lost), one might manage to preserve and gather most of the stalks in spring;
- if hemp is grown for the main purpose of obtaining wood shives (as a building material), one might manage to preserve most of the stalks and obtain the necessary raw material;
- in the first stage of the adoption of the technology on farms that have insufficient technical means for autumn harvesting (a lack of specialised combine harvester or mower) one might manage to preserve and gather most of the stalk yield.

## CONCLUSIONS

In the experiments the average dry matter yield of the stalks of 11 cultivars of industrial hemp was 13.30 t $ha^{-1}$, while the highest yield, with the 'Bialobrzeskie' variety, was 15.86 t $ha^{-1}$. We can conclude from the data that the growing season and the selected industrial hemp cultivars had a significant ($p < 0.05$) effect on the hemp yield.

The loss of hemp stalk mass in two-stage harvesting (Option A: harvesting of the seedy part of the yield by means of grain harvesting combines and subsequent gathering of the stalks in spring) constitutes approximately 47–79%. The basic possible solution for reducing these losses is raising the cutting height of the stalks when the seedy part of the yield is harvested. With spring harvesting, Option B, the stalk mass is preserved, while the seedy part of the yield is completely lost.

In the tests conducted during a subsequent spring harvest the tensile strength of the fibres of the uncut hemp stalks was 25–52% lower than the strength of the fibres harvested in autumn.

ACKNOWLEDGEMENTS. The research was supported by a grant of the Ministry of Agriculture of the Republic of Latvia, Agreement No. 270314/S70.

## REFERENCES

Adamovičs, A., Balodis, O., Gaile, Z., Komlajeva, Ļ., Poiša, L., Slepitis, J., Straume, I., Strikauska, S., Višinskis, Z. 2012. Enerģētisko augu audzēšanas un izmantošanas tehnoloģijas. *Atjaunojamā enerģija un tās efektīva izmantošana Latvijā* (Technologies of production and use of production and use of energy crops. *Renewable energy and its effective use in Latvia*), Jelgava, pp. 88–91. (in Latvian).

Arhipova, I. and Balina, S. 2006. Economics statistics. Solutions with SPSS and Microsoft Excel, Riga, DC, 352 pp. (in Latvian).
Burczyk, H., Kaniewski, R. 2005. New Technology of Harvesting Hemp Grown for Seed. *Journal of Industrial Hemp – production, processing and products* **10**(1), 49–60.
Barwicki, J., Gach, S., Koprysz, K., Ivanovs, S., Adamovics, A., Valainis, O. 2014.Technical and economical analysis of harvesting and ensilaging of corn grain. *Agronomy research* **12**(1), 33–40.
*Cannabis sativa* L. Hemp. 2009. p 199 – 200. Available at: http://eur-lex.europa.eu.
Ivanovs, S, Adamovics, A., Rucins, A., Bulgakov, V. 2014. Investigations into losses of biological mass and quality during harvest of industrial hemp. *Engineering for rural development* Proceedings, Volume 13. pp. 19–23.
Ivanovs, S.; Rucins, A. 2014. Cutting of the biological mass of industrial hemp. *Journal of Research and Applications in Agricultural Engineering* **59**(3), 87–90.
Jankauskiene, Z. & Gruzdeviene, E. 2010. Evaluation of *Cannabis sativa* in Lithuania/. *Žemdirbyste = Agriculture.* Vol. 97. No. 3. pp. 87 – 96.
Kopiks, N., Viesturs, D. 2010. Research into models choice of tractor aggregates./ *Engineering for rural development.* Proceedings, Volume 9. pp. 139–143.
www.meteo.lv
Sheichenko, V., Lukjanenko, V. 2013. Definition of stem height of semiral hemp for harvesting by the combine DON-1500 / *Mechanization and Electrification of Agriculture*. Collected papers. Issue 98. Volume 1. Glevakha, pp. 230–235. (In Ukrainian).
Struik, P.C., Amaducci, S., Bullard, M.J., Stutterheim, N.C., Venturi, G., Cromack, H.T.H. 2000. Agronomy of fibre hemp (*Cannabis sativa* L.) in Europe. *International Journal Industrial Crops and Products* **11**, 107–118.
GOST 10379-76 'Scuted hemp. Technical specification', Moskow, 1987.12.p. (In Russian).

*Agronomy Research* **13**(1), 83–88, 2015

# Use of combined pneumatic conveying in the processing of granular waste materials

T. Jehlička* and J. Sander

Czech University of Life Sciences Prague, Faculty of Engineering, Department of Technological Equipment of Buildings, Kamýcká 129, 165 21 Prague 6 – Suchdol, Czech Republic; *Correspondence: jehlickat@tf.czu.cz

**Abstract.** This paper focuses on the structural design, verification and operational functions of combined pneumatic and mechanical transport systems in processing granular materials. A pilot plant was designed in laboratory conditions, and the combined pneumatic and mechanical transport system was tested in operation. Subsequently, transport possibilities for granular waste materials, which varied in size and specific particle weight, were evaluated. A combined pneumatic and mechanical transport system was designed as a transport line for pneumatic conveying at low pressure in combination with a mechanical towing component. The combination of both modes was designed so that the towing component in the form of an axis-less helix was inserted into the conveying pipe. Transport efficiency was monitored by comparing common pneumatic transport and combined pneumatic transport (pneumatic and mechanical transport). Both systems were tested under the same operating conditions with various granular waste materials, which varied in size and specific particle weight. Crushed electric waste was used as granular material to assess the operational functions used. Properties of the proposed transport system were tested by constructing and operating the system. The evaluation of transport options featuring pneumatic and combined (pneumatic and mechanical) transport systems proved that the system was reliable and highly efficient for the transportation of dry granular waste.

**Key words:** pneumatic conveying, mechanical conveying, granular waste.

## INTRODUCTION

Conveying granular material is a frequent part of production processes. The choice of specific equipment is always linked with the conveying conditions and properties of the material thus transported. There is a general requirement that the conveying equipment must allow vertical as well as horizontal transport, it must be dustproof and it must be able to convey granular material with a high degree of specific weight scattering with minimal energy costs. Pneumatic conveying meets such requirements. Material is conveyed in a closed pipeline either with negative pressure or overpressure of the air sucked in and ultimately released from the conveyor's surroundings (Mills, 2004). Ventilators are used for conveying air.

The previously defined pneumatic conveying is simple and functionally non-demanding without any specific constructional or material requirements. However, the simplicity of the system also limits the scope of applicability of such conveying. In practice this means that a lower pressure gradient and a smaller volume of air must be used, reducing the transport distance, elevation rise and lowering the output or weight scatter of the material conveyed (Mallick & Wypych, 2009).

The negative characteristics of low-pressure pneumatic transport suggested above can be neutralised in a variety of ways, while maintaining the functions of the processing lines prescribed in the project requirements. One option is changing the properties of the material conveyed (pre-sorting and reducing the size and weight spread of the particles conveyed), or adjusting the operation parameters of the conveying system, i.e., increasing the air flow volume and operating pressure (Baker & Klinzing, 1999). Affecting the material's properties or adjusting the operational parameters of the conveying system can be done in the framework of low-pressure transport only within a limited range and at the cost of increased energy requirements (Yan et al., 2012). This is why transport operation systems are often designed as combinations of pneumatic and mechanical conveying systems.

The incorporation of a mechanical conveyor before or after a pneumatic conveying unit can help to achieve a corresponding conveying output and reliability (Hilgraf, 1998).

This paper suggests a construction solution, discusses the verification of the operational function and assessment of conveying options in view of combined (pneumatic and mechanical) transport used in processing granular materials. A combined (pneumatic and mechanical) conveying system was designed and tested in pilot-plant laboratory conditions. Operating reliability was investigated in respect of conveying particles of a material with a high weight scatter, depending on the set operational conditions limited by the air flow volume and pressure gradient in a conveying pipeline.

## MATERIALS AND METHODS

The combined (pneumatic and mechanical) conveying system was designed and tested in operation in pilot-plant laboratory conditions. The conveying options of this combined transport were then assessed with granular waste materials, which differed in size and specific particle weight. The system was tested on a waste processing pilot-plant line. The line is situated in the laboratories of the Czech University of Life Sciences in Prague.

### Brief description of the design and functioning of the electric waste processing line

The electric waste is crushed in a two-roll crusher and then in a ring-type cutter. The material is conveyed into a dust-separator chamber from the cutter; the dust part is separated in the separator. The dust-free material is measured by a vibrating feeder into a fluid weir, where it is sorted by specific weight.

### Description of a pneumatic conveying system incorporated into the electric waste material processing

Pneumatic conveying is designed as a low-pressure, negative pressure transport system. The material is conveyed in a closed metal pipe with the circular profile diameter of 150 mm both horizontally and vertically. The radial ventilator URBAN Technik, Type VE-6000A is the source of negative pressure with an output of 4,500 $m^3 h^{-1}$ and with the negative operating pressure of 400 Pa.

**Design and construction of the combined (pneumatic and mechanical) conveying system**

A conveyer pipeline for low-pressure conveying in combination with a towing mechanical part is the main unit of the construction. The combination of the both types of conveying systems is designed in such a way that the towing part is in the form of an axis-less helix and it is inserted into the inner space of the conveying pipeline. The material is conveyed in this environment as a result of the dynamic effect of the flow medium, and, at the same time, it is carried forward by the mechanical movement of the turning axis-less helix. This technical solution allows conveying particles both by pneumatic and mechanical means in a single transport space (conveying pipeline).

**Verification of the operational function of the combined (pneumatic and mechanical) conveying system**

The operational function was verified by comparing the conveying reliability (i.e., the ability to convey material with specific physical properties at set operating conditions) of pneumatic and combined (pneumatic and mechanical) conveying systems. Conveying reliability was tested with two types of granular material that had various granular sizes and specific weight. Both materials were crushed and sorted into several granule-size groups. The first material was a mix metallic materials (electric conductor), grouped by grain size. The other material was a mix of plastic materials (electric insulating material), also grouped by grain size. Conveying reliability was tested individually in all material-size groups using pneumatic conveying followed by combined (pneumatic and mechanical) conveying. Different operational conditions were set for each subsequent grain-size group. The operational conditions were varied by setting different operational pressures to the conveying pipeline. The operational pressure was changed gradually by setting the ventilator revs. The value was measured by using the Testo 521-1 measure with a pressure sensor placed into the conveying pipeline at the distance of 1.9 m from the entering point of the conveyed material.

## RESULTS AND DISCUSSION

The influence of the operational pressure in the conveying pipeline upon the transportation of particles with a specific size (and a constant specific weight) was explored for the purpose of assessing conveying reliability. Tables 1 and 2 feature operational data, i.e., the particle sizes in case of which and operational pressures at which materials are reliably conveyed using both pneumatic and combined transport. Table 1 lists values in view of the transportation of metal waste (electric conductor), while Table 2 lists values in view of the transportation of plastics (of an electric insulator).

The ways in which the operational data depends upon the aforementioned influences are shown in Fig. 1 and Fig. 2. In Fig.1 the values from Table 1 have been plotted to a graph and interlaid with a trend connecting line. The curves thus obtained show the conveying reliability for the transport of metal particles using both pneumatic and combined conveying systems. The given value of pressure always corresponds to the minimal value at which the material particles can be still conveyed using pneumatic transport.

**Table 1.** Values of operational pressure for conveying particles with a specific size (metal)

| Pneumatic transport of metal | Combined transport of metal | |
|---|---|---|
| pressure (Pa) | pressure (Pa) | particle size (mm) |
| 970 | 970 | 6 |
| 940 | 970 | 8 |
| 910 | 970 | 10 |
| 880 | 970 | 12 |
| 850 | 970 | 14 |
| 830 | 970 | 16 |

**Table 2.** Values of operational pressure for conveying particles with a specific size (plastics)

| Pneumatic transport of plastics | Combined transport of plastics | |
|---|---|---|
| pressure (Pa) | pressure (Pa) | particle size (mm) |
| 970 | 970 | 6 |
| 965 | 970 | 8 |
| 965 | 970 | 10 |
| 960 | 970 | 12 |
| 960 | 970 | 14 |
| 955 | 970 | 16 |

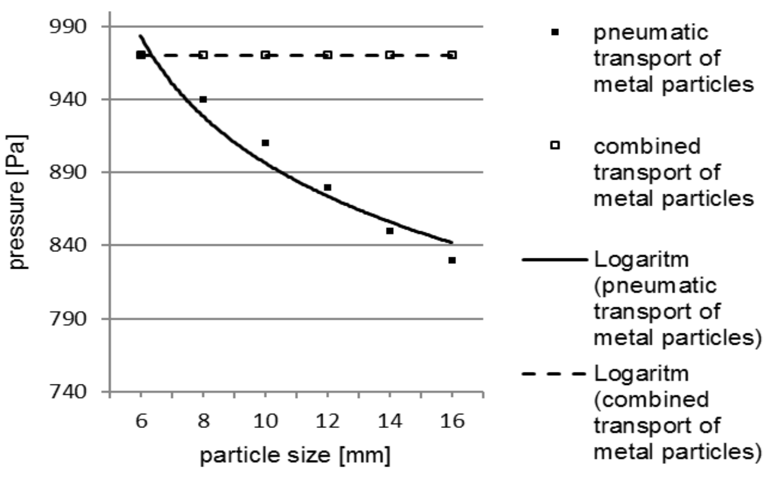


**Figure 1.** Dependence of operational pressure upon particle size (metal).

The course indicates that the pneumatic conveying of metal particles requires increasing the conveying sub-pressure depending on the size of the metal particles. Crushed plastics particles behaved similarly in the operational test, as shown in Fig. 2. As plastics are lighter to convey (their specific weight is smaller than that of metal), the transport pressures were lower. The course of pressures for conveying both metal and plastics is similar but the values of sub-pressure vary with particles of the same size.

As metal and plastics form a mixture during the processing of electric waste (electric cables), the operational pressure for the pneumatic conveying of same-sized particles must always be determined in view of transporting material with the higher specific weight (i.e., metal). This principle holds regardless of the proportion of the plastics and metal in the mix. In case the share of particles with a high specific weight is negligible in the mix (which is often the case in processing electric waste), the operational pressure must still accommodate conveying that share, i.e., it must be sufficiently high. Transporting such a mix in the given conditions is energy demanding.

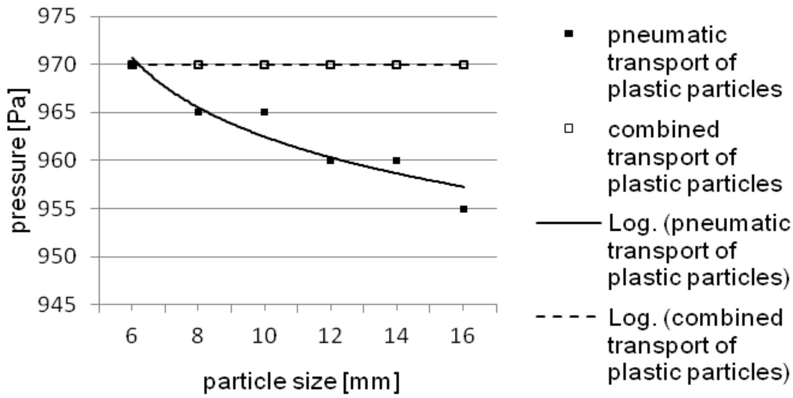


**Figure 2.** Dependence of operational pressure upon particle size (plastics share).

Adapting pneumatic conveying for combined (pneumatic and mechanical) transport allows both the metal and plastics share of the material to be conveyed in different operational conditions. Tables 1 and 2 list operational data, i.e., pressure, and the particle size which can be conveyed reliably at such a pressure while using combined conveying systems. The dependence of the data upon specific influences during conveying metal and plastics is shown in Fig. 1 and Fig. 2. The operational data show that the conveying reliability for both metal and plastics does not depend upon operational pressure. The transport of particles with a higher specific weight is facilitated by the inserted axis-less spiral. Operational pressure in the conveying pipeline allows conveying light, small and dust particles which emerge from the process of crushing the electric waste. For this reason it is possible to apply relatively low operational pressures in the combined transport system's conveying pipeline.

## CONCLUSIONS

The advantage of the proposed combined (pneumatic and mechanical) conveying system is the possibility of transporting material with a wide spectrum of specific-weight particles. Particles with a lower specific weight and higher aerodynamic resistance are carried forward by the air flow mainly through the centre of the pipeline. Heavier particles are carried forward by the mechanical energy of the axis-less helix. The construction of a combined (pneumatic and mechanical) conveying system can be used to cover short distances at horizontal and oblique levels.

The values measured thus indicate that the conveying reliability for metal and plastics does not depend upon the operational pressure of the combined (pneumatic and mechanical) transport system. The axis-less helix conveys particles with a higher specific weight. The operational pressure in the conveying pipeline allows conveying light, small and dust particles. For this reason the combined transport system can be used with relatively low operational pressures in the conveying pipeline. Combined (pneumatic and mechanical) conveying is less energy demanding compared with pneumatic conveying.

The combined (pneumatic and mechanical) conveying system has an operational advantage in that its construction is simple, it needs less energy for material transport (smaller flow of volume and operational pressure), has minimal space requirements (the towing component is inside the conveying pipeline) and a small number of mobile parts.

## REFERENCES


Baker, J.D., Klinzing, G.E. 1999. Optimal performance of pneumatic transport systems. *Powder Technology* **104**(3), 240–247.

Hilgraf, P. 1998. Energy consumption for pneumatic conveying compared with mechanical conveying. *ZKG INTERNATIONAL* **51**(12), 660–673.

Mallick, S.S. , Wypych, P.W. 2009. Minimum transport boundaries for pneumatic conveying of powders. *Powder Technology* **194**(3), 181–186.

Mills, D. 2004. *Pneumatic conveying design guide*. Butterworth-Heinemann, London, 629 pp.

Yan, F., Rinoshika, A., Nonaka, H. 2012. An experimental study on a horizontal energy-saving pneumatic conveying system with soft fins. *Powder Technology* **217**, 516–522.

*Agronomy Research* **13**(1), 89–94, 2015

# Continuous airflow rate control in a recirculating batch grain dryer

T. Jokiniemi*, T. Oksanen and J. Ahokas

University of Helsinki, Faculty of Agriculture and Forestry, Department of Agricultural Sciences, P.O. Box 28, 00014, University of Helsinki, Finland; *Correspondence: tapani.jokiniemi@helsinki.fi

**Abstract.** As the energy efficiency requirements in agriculture increase, offers grain drying opportunities for substantial energy saving. Earlier work indicated that energy savings in grain drying can be achieved by controlling the drying airflow rate during the drying process. Aim of this study was to design an embedded control system, based on microcontroller, for continuous airflow rate control in a recirculating batch grain dryer, and to test it in a scaled-down research dryer. The control system proved to be working as designed, reducing the dryer airflow rate smoothly towards the end of the process. However, additional research of the energy efficiency and performance of the dryer using the airflow rate control is needed.

**Key words:** grain drying, grain dryer, energy efficiency, airflow rate control, drying air temperature.

## INTRODUCTION

Grain drying is one of the largest energy inputs in arable farming in boreal and northern temperate climate zone countries (Mikkola & Ahokas, 2009). Considering the ever increasing energy efficiency requirements in agriculture, provides grain drying, and grain preservation in general, opportunities for substantial energy savings. Previous work of the authors indicated that controlling the airflow rate and drying air temperature during the drying process has potential to improve both the energy efficiency and the performance of the dryer (Jokiniemi & Ahokas, 2014). The energy savings were achieved by decreasing the dryer airflow rate towards the end of the process and elevating the drying air temperature concurrently. The energy savings were based on two factors: 1) using higher drying air temperature and 2) obtaining higher exhaust air humidity in the latter part of the drying process.

The effect of the elevated drying air temperature on the energy efficiency of the dryer has been reported by several authors (Morey, Cloud & Lueschen, 1976; Suomi et al., 2003). This is a consequence of the nonlinearity in the moist air equilibrium equations; the same amount of added heat energy increases the water binding capacity of air more in higher temperatures, as Fig. 1 indicates. Additionally, the elevated drying air temperature creates a greater pressure gradient of water vapor between the core and the surface of the whole grains, which enhances the water movement inside the grain and hence also the evaporation.

In addition to the drying air temperature, the humidity of the exhaust air has a significant effect on the energy efficiency of a dryer, as shown by Fig. 1. While the heating power of the dryer remains usually constant, the relative humidity of exhaust air indicates directly the efficiency of evaporation. When the exhaust air humidity is high, the majority of the applied heat energy appears as latent heat in the exhaust air, and the exhaust air temperature is typically low. When the relative humidity of the exhaust air is low, the applied heat appears as sensible heat. It is not thus used for evaporation, but it is lost with the exhaust air. In this case the exhaust air temperature is relatively high and the specific energy consumption in drying is high. When the airflow rate is reduced, the moisture in the grain has more time to diffuse to the surface of individual whole grains. Higher exhaust air relative humidity is thus obtained, leading to lower energy consumption in drying. The effect of the airflow rate on the energy consumption in grain drying has also been recognized by several authors in past. For example Morey et al. (1976) and Peltola (1988) suggested airflow rate control as one possible approach for reducing the energy consumption in grain drying.

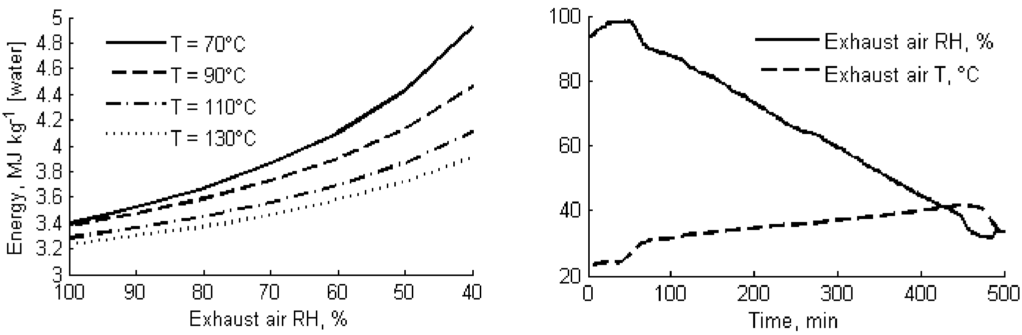


**Figure. 1.** The effect of drying air temperature *T* and exhaust air relative humidity *RH* on the energy consumption of adiabatic drying process (on the left) and typical exhaust air properties in practical grain dryer (on the right).

Another requirement for the control of grain dryer is to maintain the quality properties of grain, such as germination ability and baking qualities. Previous studies have proved that using high drying air temperature may severely damage these properties, but this vulnerability is also strongly affected by the moisture content of the grain. The grain can tolerate higher temperatures when its moisture content is reduced (Ghaly & Taylor, 1982; Ambardekar & Siebenmorgen, 2012). Therefore it is reasonable to assume that the grain is not so sensitive to heat damage in the latter part of the drying process, when some drying has already occurred, and the drying air temperature can be increased gradually. This is also a beneficial approach considering the energy use, since the dryer exhaust air humidity is inherently high in the beginning of drying, leading to efficient energy use, and begins to decrease towards the end of the process (Jokiniemi & Ahokas, 2014). The benefits of the reduced airflow rate and elevated drying air temperature, considering the energy use, are thus essential in the latter part of the process, which can also be concluded from the Fig. 1.

In the previous work of the authors, the airflow control was conducted by manual control of the speed of the drying air fans when the exhaust air humidity had decreased under a certain level. It was concluded that an automatic control system, which utilizes the exhaust air humidity and temperature information as control factors, would be relatively simple and easy to implement in new or existing grain dryers. (Jokiniemi & Ahokas, 2014) Aim of this work was to build a simple microcontroller based embedded control system for the continuous airflow control in a recirculating batch grain dryer, and test it in a scaled-down research dryer.

## MATERIALS AND METHODS

The study was conducted in a scaled-down research dryer at the research farm of the University of Helsinki. A measuring system for observing the essential process variables, such as air temperatures and humidities as well as the air flow rate, was installed into the dryer. A detailed description of the research dryer and the measurement system, including the used sensors and data acquisition, can be found in the previous work of the authors (Jokiniemi & Ahokas, 2014). The measuring system enabled the calculation of the essential process parameters, such as the amount of removed water and energy use in a point in time, as well as during the entire process in total. The amount of removed water was calculated from the changes in the air humidity, while it passed through the grain, and the air flow rate. The heat power was calculated from the changes in the enthalpy of the dryer supply air before and after the heaters, and the air flow rate. Energy consumption was calculated by multiplying the heat power with the measuring interval, and total energy consumption during each test run was received by summing the energy consumptions recorded for all of the measuring intervals.

The airflow rate in the research dryer was controlled by a frequency converter, which was used to control the speed of the drying air fans. The frequency converter could be controlled either manually from the control panel, or by using a 0–10 V external control signal. The 0–10 V input was used to supply the control signal from the microcontroller to the frequency converter.

The airflow rate controller was based on an Arduino Mega 2560 microcontroller development board. A simple setup of two Honeywell HIH-4000 humidity sensors and one LM35 temperature sensor was configured to the Arduino board, and a pulse width modulation (PWM) signal from the microcontroller was used as the control signal to the frequency converter. A control algorithm to generate the PWM-signal on the basis of the voltage readings from the humidity sensors was written in C-language and uploaded to the microcontroller. While the voltage range expressed by the PWM-signal from the microcontroller digital pins was 0–5 V, a power transistor circuit was built to repeat the PWM-signal with a higher voltage level. A supply voltage of 12V was used, and suitable coefficients in the microcontroller program were used to scale the control signal to the correct range for the frequency converter.

The aim of the control algorithm was to decrease the speed of the drying air fans smoothly when the humidity of the exhaust air started to decrease. The control rules were defined by Eq. (1):

$$u_{RH}(t) = u_{init} - (RH_{limit} - RH(t)\,) \cdot K \qquad (1)$$

where: $u_{RH}$ controller output; $u_{init}$ = constant term; $RH_{limit}$ = controller threshold RH; $RH$ = measured RH; $K$ = controller gain.

The threshold value $RH_{limit}$ for the RH of the exhaust air was set to 90%, i.e. the controller became active when the RH of the exhaust air reduced below this level. The constant term $u_{init}$ was the desired control value in the beginning of the drying process. The control algorithm was thus almost equal to the conventional P-controller. However, due to the nature of the process, the RH of the exhaust air decreases inevitably towards the end of the process, and the control algorithm will thus end up reducing the output while the process proceeds. Additional conditional expression was added to the microcontroller program to ensure that the control output $u_{RH}$ did not exceed the constant term value $u_{init}$ in the beginning of the process, when the RH was greater than 90%.

The drying air temperature was adjusted manually to 65 °C in the beginning of the drying process, and it was allowed to rise freely as the airflow was decreased. However, an upper limit of 90 °C was defined for the drying air temperature to avoid heat damage to the grain. The microcontroller program compared the temperature of the drying air to the upper temperature limit threshold value, and when it was reached, the temperature control rule became active:

$$u_T(t) = u_{RH}(t) - (T(t) - T_{limit}) \cdot K \tag{2}$$

where: $u_T$ = controller output; $u_{RH}$ = output from the RH controller; $T$ = measured drying air temperature; $T_{limit}$ = controller threshold temperature; $K$ = controller gain.

The controller gain value $K$ for both controllers was defined in the first test runs. The $K$ values used in the final setup were 1 for the RH-controller and 5 for the temperature controller. The aim for the RH-controller was to decrease the airflow smoothly in such a way that the upper temperature limit was not reached until close to the end of the process. For the temperature controller the aim was to react quickly when the temperature limit was reached, but to avoid the excessive fluctuation of the controller output caused by too high gain value.

Control system was tested in drying trials in the scaled-down research dryer. Altogether eight drying trials were accomplished: four with the airflow rate control system and four references without it. The airflow rate in the reference trials was equal to the initial airflow rate in the control system trials. The grain used in the trials was barley with the initial moisture content of ca. 20% (wet mass basis). The drying process was ended when the moisture content of the barley had decreased to ca. 13.5% in each trial.

## RESULTS AND DISCUSSION

Fig. 2 presents the operation of the controller during the drying process. In the beginning of the process the exhaust air humidity was high, and the initial set point for the controller output was used. When the decreasing exhaust air RH reached the threshold value of 90%, the controller started working. The controller operated as designed, reducing smoothly the airflow rate and increasing drying air temperature simultaneously. When the maximum drying air temperature limit was reached at 90 °C, the temperature controller in Eq. (2) became active, starting to increase the airflow. Some oscillation occurred in the control signal value in the end of the process, when the two control algorithms were alternating. This did not, however, have any significant practical effect on the drying air temperature or the airflow rate.

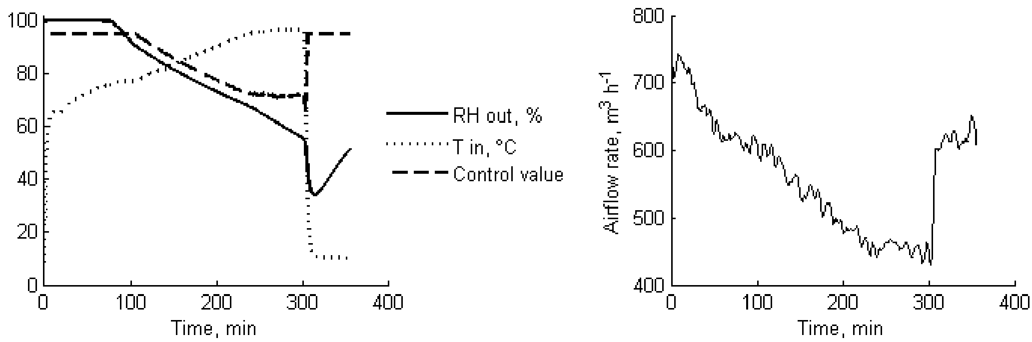


**Figure 2.** Dryer exhaust air humidity, control signal value and the effect of the control system on the drying air temperature (on the left) and dryer airflow rate (on the right).

Fig. 3 presents the specific energy consumption and the evaporation rate in each trial member. The results do not indicate a clear advantage for the airflow rate control considering the energy efficiency. The average energy consumption was 10% lower with the controller, compared to the conventional drying. However, the coefficient of variation for specific energy consumption in the airflow rate control trials was 17%, while the corresponding figure in the conventional process trials was only 9%.

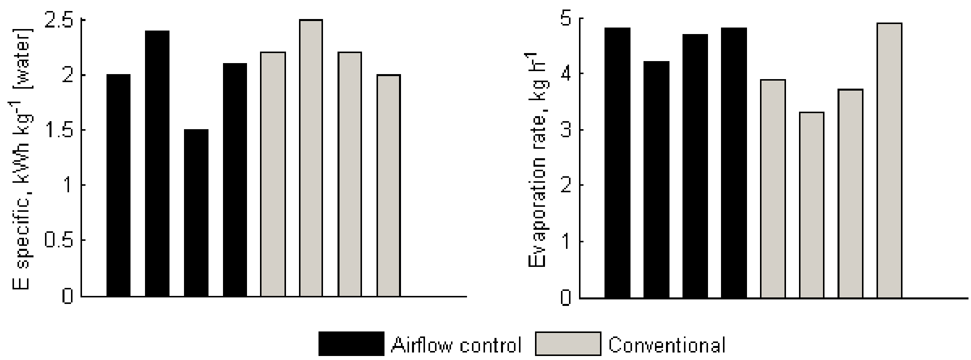


**Figure 3.** Average specific energy consumption and evaporation rates in each trial with airflow rate control and conventional drying without airflow rate control.

The relatively large variation in the airflow rate control trials is explained mainly by the third test run, which had an exceptionally low energy consumption compared to the other trials in the Fig. 3. This may be a consequence of a possible measurement error in this trial.

The evaporation rate for the airflow rate control trials was in average 15% higher compared to the conventional process, which indicates that the airflow rate control could be used to enhance also the performance of the dryer. However, the variation was large also here, and the last trial in the conventional process showed an exceptionally high evaporation rate compared to the others.

## CONCLUSIONS

The simple microcontroller based control system for controlling the drying airflow rate in a recirculating batch grain dryer operated as designed, reducing smoothly the airflow rate towards the end of the drying process. The results indicated that the control system enhanced both the energy efficiency and the performance of the dryer, but the variation in the results was also large. The simple and inexpensive control system could be easily installed in most of the dryers. In the current study the airflow rate was controlled by adjusting the speed of the drying air fans by a frequency converter, but a choke valve in the dryer supply air intake pipe could be used as well. The exhaust air temperature information could be used as a control input, instead of relative humidity, as there is a strong inverse correlation between the exhaust air humidity and temperature. Replacing the sensitive humidity sensors by robust temperature sensors would improve the reliability of the system considerably. However, further research about the effect of the control system on the energy efficiency and performance of the dryer is needed prior to the commercial applications.

ACKNOWLEDGEMENTS. This study was funded by the foundation of Marjatta and Eino Kolli.

## REFERENCES

Ambardekar, A.A. & Siebenmorgen, T.J. 2012. Effects of postharvest elevated-temperature exposure on rice quality and functionality. *Cereal Chemistry* **89**(2), 109–116.

Ghaly, T.F. & Taylor, P.A. 1982. Quality effects of heat treatment of two wheat varieties. *Journal of agricultural engineering research* **27**, 227–234.

Jokiniemi, H.T. & Ahokas, J.M. 2014. Drying process optimisation in a mixed flow batch grain dryer. *Biosystems engineering* **121**, 209–220.

Mikkola, H. & Ahokas, J. 2009. Energy ratios in Finnish agricultural production. *Agricultural and food science* **18**, 332–346.

Morey, R.V., Cloud, H.A., & Lueschen, W.E. 1976. Practices for the efficient utilization of energy for drying corn. *Transactions of the ASAE* **19**, 151–155.

Peltola, A. 1988. Viljankuivurin säätö kuivauksen aikana – hyödyksi vai hienostelua? *Työtehoseuran maataloustiedote*, **355**, 8 pp. (in Finnish)

Suomi, P., Lötjonen, T., Mikkola, H., Kirkkari, A.-M. & Palva, R. (2003). Viljan korjuu ja varastointi laajenevalla viljatilalla. *Maa- ja elintarviketalous* **31**, 100 pp. (in Finnish)

*Agronomy Research* **13**(2), 95–100, 2015

# Measurement of tensile force at the fundamental tillage using tractor's build-in sensor and external sensor connected between machines and their comparison

M. Kroulík*, J. Chyba and V. Brant

Czech University of Life Sciences Prague, Kamýcká 129, Prague 6 – Suchdol, 165 21, Czech Republic; *Correspondence: kroulik@tf.czu.cz

**Abstract.** The value of tensile force during soil tillage is crucial for estimating the energy performance of trailed machines.
For tensile force measurements, a mouldboard plough with working width of 4 m was used. The ploughing speed was approximately 7 km $h^{-1}$. Measurements were carried out on two plots with different soil texture. Loam-sandy soil dominated on the first plot, whereas clay soil dominated on the second one. The slopes of the plots are 1.1° and 2.4° respectively. Both plots have been left without stubble modification after harvest. The dynamometer LUKAS type S-38 was used for measuring tensile force. The dynamometer was placed on a hinge, which was positioned between two tractors. As a second method of tensile force measurement, electro-hydraulic hitch sensors were used, from which the values were recorded.
The obtained values of tensile force were approximately 30 kN on the first plot and 54.3 kN on the second plot. The interdependence values of tensile forces between internal and external sensors showed a high coefficient of determination $R^2 = 0.91$ in regression data analysis.
The comparison of tensile force measurements using a special dynamometer and electro-hydraulic tractor sensor proved that the outputs of serial sensors can be used for the continuous monitoring of tensile forces during operating the machine. The automated storage of data collected from tractor sensors during tillage can greatly simplify this work, while no additional expenses are incurred to obtain data. Thus, the findings can be used to determine the variability of the land.

**Key words:** force sensing, soil tillage, tensile force, soil variability, soil mapping.

## INTRODUCTION

The high price of sampling and laboratory analysis supports the development of sensors that will evaluate the required soil properties, for example, during towing sensors across a field (Adamchuk et al., 2004; Viscarra Rossel et al., 2011). The deployment of these sensors will facilitate an overall reduction of data collection costs and the optimization of the sampling grid.

Soil mechanical strength is an indicator of the mechanical properties of soil. This strength can be affected by compaction, soil texture, water content and other agricultural parameters (Adamchuk & Christenson, 2005). A number of prototype systems were developed for mapping soil mechanical strength during machine operation. The higher sampling frequency of these techniques provides a much more accurate representation of the variability of soil mechanical strength inside the field, compared with the data obtained from point-sampling with a cone penetrometer.

Barone & Faugno (1996), Sirjacobs & Destain (2000), Mouazen et al. (2002) and Novák et al. (2014) discuss sensors for measuring soil compaction and monitoring physical properties in order to gain knowledge of locally different soil properties. In their experiments, they measured the force necessary for drawing the tool or biting in the soil at constant speed. Mouazen et al. (2005) evaluated tensile forces in motion with a unilateral blade that was equipped with strain gauges. In those cases, the tool could be also called a horizontal penetrometer. These systems meet the requirements of continuous recording to a much greater extent.

Sirjacobs et al. (2002) used tools like the plough coulter in their experiments. During the measurement, physical parameters that affect the size of tensile force were monitored. Verschoore et al. (2003) compared the horizontal penetrometer with a measuring chevron chisel in order to investigate the forces acting on the working side of the chisel. On the basis of small differences in correlation coefficients, the authors see a great future for measurements in this field ,but emphasize that their findings must be confirmed with further measurements.

Van Bergeijk & Goense (2001) found that there is a relationship between tensile strength and different soil types on an experimental plot. The authors state in conclusion that it is possible to use a tractor's serial tension pins for measuring tensile force, if the proper calibration is performed prior to measurement.

As further stated by Kürsteiner (2003), force measurement at 3-pt. hitch is often performed using measuring frames that are inserted between the tractor and the implement. Working with and handling such frames can be very difficult. In addition to the results obtained with experimental frames, the standard force pins of the tractor, designed for electronic linkage control, can be also used for measurements (Schutte & Kutzbach, 2003).

The measurement of differences in soil properties during normal tillage is the basic tool for tensile force mapping. Moreover, as noted in the work of Rothmund et al. (2003), tensile force can be measured through an electronically controlled 3-pt. hitch, and automated data storage is available at no additional cost during tillage. Kutzbach et al. (2004) dealt with verifying experimentally detected values with values obtained from the tractor during field operations. The authors conclude that the findings can be used to determine the variability of the field.

## MATERIALS AND METHODS

A four-share reversible plough with the working width of 4 m was used for measuring tensile forces in field conditions. The operating speed of the plough was set to 7 km $h^{-1}$, which corresponds to the working speed recommended by the manufacturer. The seven-blade plough Kverneland was attached to the tractor John Deere 8320. Measurements were carried out on two plots which differed in particle size distribution composition of the soil. The experimental agricultural field is located in the central part of the Czech Republic. It represents intensively exploited arable land with commonly planted crops such as canola, spring barley, winter wheat and corn. The area is in a typical temperate zone climate with the average annual temperature ranging from 7 to 8.5 °C and with 500 to 750 mm of annual precipitation. Plot No. 1 contained mainly loam-sandy soil. The average slope of the plot was 1.1°. The landscape is gently rolling with an altitude ranging from 476 to 470 m. The main soil unit is *Eutric Cambisol* (classification system World Reference Base). Plot No. 2 contained mainly loamy to clayey soils. It also had a higher average slope of 2.4°.The landscape is gently rolling with an altitude ranging from 440 to 460 m. The main soil unit is *Dystric Cambisol* (classification system World Reference Base). Both plots were left without stubble modification after the harvest. The soil moisture ranged from 26.4 to 28.6 vol% during tillage.

For tensile force measurement, the tensile dynamometer LUKAS type S-38 with a measuring range of 200 kN was used. The dynamometer was placed in a hinge, which was positioned between two tractors (see Fig. 1). The dynamometer's outputs served as a reference value for measuring tensile force using an electro-hydraulic hinge sensor for a tractor. Data were simultaneously stored in a data logger. Position values of the machine collected from a GPS receiver were also recorded with the individual records.

**Figure 1.** The measuring set during the measurement of tensile force using the tensile dynamometer LUKAS type S-38.

The experiment started with the measurement of a two tractor set without ploughing to ensure the measurement of the rolling resistance of the whole drawn working set (tractor and plough).

As a second way of tensile force measurement, values from a three-point hitch electro-hydraulic sensor were used. Tensile force values were recorded with a 2 s interval. Tensile force was mapped using an electro-hydraulic hitch control for tractors (3-pt. hitch) only on plot No. 2.

## RESULTS AND DISCUSSION

The dependence of the tensile force of a 3-pt. hitch on the values received from the dynamometer LUKAS type S-38 is shown in Fig. 2. This dependence of tensile forces is supported by Fig. 3, which reveals that the tensile force values from both sensors were very similar.

Fig. 2 describes the dependence of tensile force values regarding the 3-pt. hitch on the tensile force values measured with the dynamometer. The comparison and evaluation of these two data sets were performed by means of regression and correlation analysis. The figure also shows the results of the discussed analysis. The determination coefficient value ($R^2 = 0.73$ and 0.91) is listed in the legend of the figure. The calculated value p was far lower than the chosen significance level $\alpha = 0.05$ in our case, thus, it may be claimed that the correlation coefficient is statistically significant. Generally, the whole regression model is classified as statistically significant. The regression formula is shown in Fig. 2 as well.

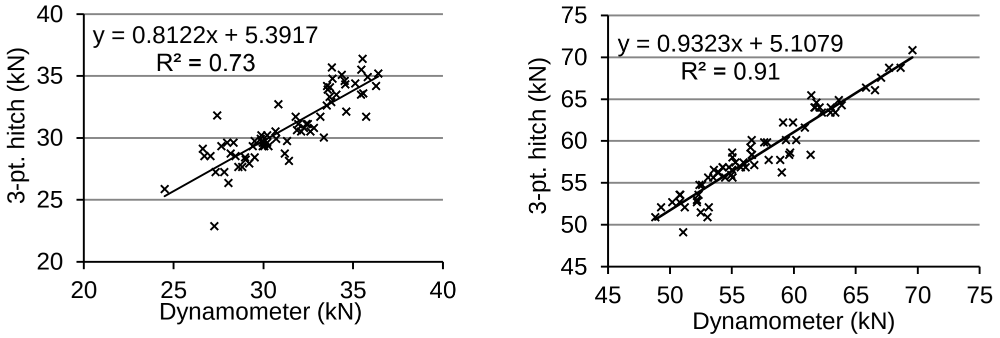


**Figure 2.** The dependence of the tensile force of a 3-pt. hitch on the values received from the dynamometer LUKAS type S-38 measured on field No. 1 (left side) and field No. 2 (right side).

The tensile force time records collected from both sensors are given in Fig. 3 and 4. This confirms the results of the correlation and regression analysis; it is possible to observe the progress of the values on the timeline.

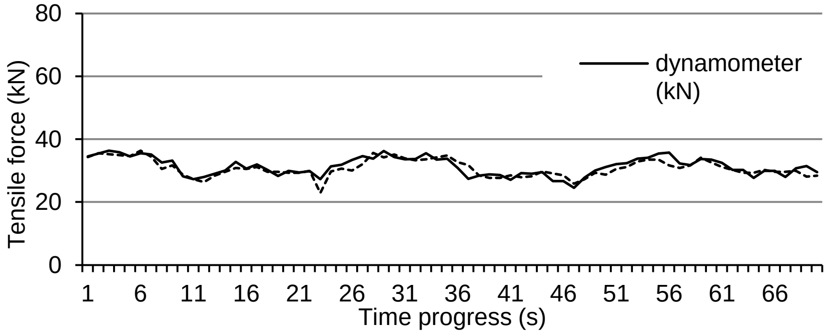


**Figure 3.** Time record of tensile forces measured with a tractor's in-built sensor and the dynamometer LUKAS type S-38 on plot No. 1.

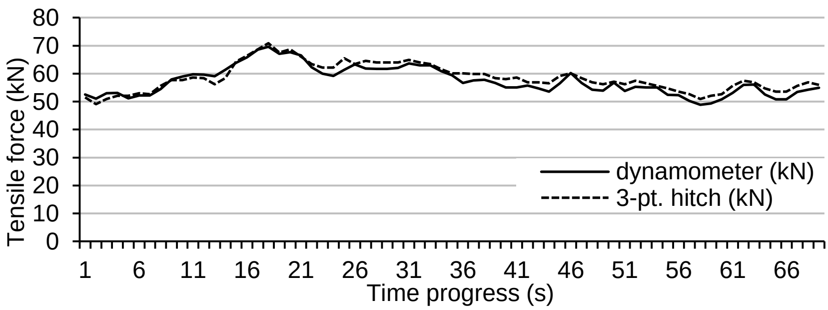


**Figure 4**. Time record of tensile forces measured with a tractor's in-built sensor and the dynamometer LUKAS type S-38 on field No. 2.

The trendline of tensile force values demonstrates the variability level of the observed properties at the monitored plot. Values fluctuate significantly on plot No. 2, where heavier soil prevailed. This fact supports the idea of introducing variable applications during tillage. Similarly, the causes for the changes in the values of tensile forces must be investigated further. Because tillage is a mechanical intervention in soil associated with a high energy demand, tillage technologies are subject to a concerted effort to reduce fuel consumption and labour intensity, which is related to achieving favourable costs per unit of production. Precision agriculture technologies are based on information. With the ability to measure tensile force directly with a tractor hitch, we can obtain information about the variability of land without significant additional inputs during machine operation. The map of tensile force, which was measured during ploughing, is in Fig. 5. Only the smallest values and extreme values were removed from the measured data (start and end of working passage).

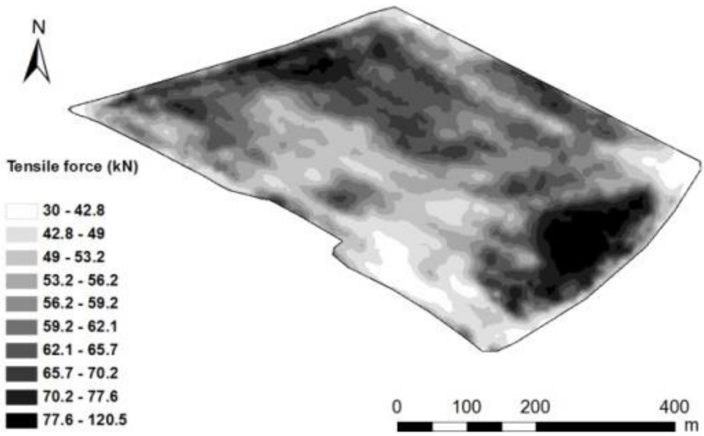


**Figure 5.** Map of the tensile force measured with a John Deere 8320 tractor.

The results of our measurement revealed possibilities for utilizing components of modern electronic tractors in tensile force measuring.

## CONCLUSIONS

Nowadays there are a number of prototypes that allow the continuous measurement of mechanical resistance but the commercial use of these sensors is minimal. In view of the fact that tillage is a mechanical intervention into the soil associated with high energy demands, tillage technologies are subject to a concerted effort to reduce fuel consumption and labour intensity, which is related to achieving favourable costs per unit of production. Current knowledge of tensile force could thus in many respects be a useful tool. The methods of measuring can be commonly used to compare the energy demand of the technologies used for assessing the technical changes in tillage machines or optimizing the tools, and for assessing the agronomic measures implemented on land. In view of management considering the spatial variability of a plot, spatial information on soil properties and their relations to the landscape is needed for the specific application of spatial management. Plenty of important information about the operation of machines could be obtained from the electronics of modern tractors.

ACKNOWLEDGEMENTS. This research project was supported by the research project IGA 2014:31160/1312/3120.

## REFERENCES

Adamchuk, V.I. & Christenson, P.T. 2005. An integrated system for mapping soil physical properties on the- go: the mechanical sensing component. In: *Precision Agriculture '05*, Wageningen Academic Publishers, pp. 449–455.

Adamchuk, V.I., Hummel, J.W., Morgan, M.T. & Upadhyaya, S.K. 2004. On-the-go soil sensors for precision agriculture. *Computers and Electronics in Agriculture* **44**(1), 71–91.

Barone, L. & Faugno, S. 1996. Penetration test for measurement of soil strength: Assessment of contribution of shaft friction. *J. agric.Engng Res*. **64**, 103–108.

Kürsteiner, B. 2003. Rahmenlose Messung der Dreipunktkräfte am Traktor. In: *Tagungsband VDI-MEG-Tagung Landtechnik*, Hannover, VDI-Berichte Nr. 1798, pp. 73–78.

Kutzbach, H.D. & Schutte, B. 2004. Mapping of soil tillage draught force to asses spatial variability of soil properties. In: *Actual Tasks on Agricultural Engineering*, Opatija, (Croatia) Nr.32, pp. 213–220.

Mouazen, A.M., De Baerdemaeker, J. & Ramon, H. 2005. On-the-go sensor for measurement of dry bulk density referring to soil compaction. In: *Precision Agriculture '05*, Wageningen Academic Publishers, pp. 523–528.

Mouazen, A.M., Dumont, K., Maertens, K. & Ramon, H. 2002. Sensing the Spatial Variation of Soil Compaction in a Sandy Loam Field. In: *AGENG EurAgEng*, Budapest 2002, Paper Number: 02–SW–018.

Novák, P., Chyba, J., Kumhála, F. & Procházka, P. 2014. The measurement of stubble cultivator draught force under different soil conditions. *Agronomy Research* **12**(1), 135–142.

Rothmund, M., Zipprich, M., Auernhammer, H. & Demmel, M. 2003. Zugkrraftmessung bei der Bodenbearbeitung als ergänzende Information zur Standortbeschreibung. In: *Proceeding of conference: Agricultural Engineering 2003*, Hannover, VDI Verlag GmBH, Germany, 305–310.

Schutte, B. & Kutzbach, H.D. 2003. Evaluierung von ortsspezifischen Zugkraftmessungen bei der Bodenbearbeitung. In: *Agricultural Engineering 2003*, Tagung Landtechnik, Hannover, ISSN 0083–5560, 299–304.

Sirjacobs, D. & Destain, M.F. 2000. A soil mechanical resistance sensor for on-line application in precision agriculture.In: *Conference AGENG*, Warwick 2000, Paper Number 00–PA–021.

Sirjacobs, D., Hanquet, B., Lebeau, F. & Destain, M. 2002. On-line Soil Mechanical Resistance Mapping and Correlation with Soil Physical Properties for Precision Agriculture. *Soil and Tillage Research* **64**, 231–242.

Van Bergeijk, J. & Goense, D. 2001. Soil Tillage Restiance as a Tool to Map Soil Type Differences. *Journal of Agricultural Engineering Research* **79**, 4, 371–387.

Verschoore, R., Pieters, J.G., Seps, T., Spriet, Y. & Vangeyte, J. 2003. Development of a Sensor for Continuous Soil Resistance Measurement. In: *Staffored, J. and A. Werner: Precision Agriculture–Proc. Of the 4th Europ*. Conf. on Prec. Ag., Berlin, 15.–19.06., 689–695.

Viscarra Rossel, R.A., Adamchuk, V.A., Sudduth, K.A., Mckenzie, N.J. & Lobsey, C. 2011. Chapter Five – Proximal Soil Sensing: An Effective Approach for Soil Measurements in Space and Time. *Advances in Agronomy* **113**, 243–291.

*Agronomy Research* **13**(1), 101–108, 2015

# Dependency of hop material fall through on the size of gaps between rollers of the roller conveyor in separating machine

M. Krupička* and A. Rybka

Czech University of Life Sciences Prague, Faculty of Engineering, Department of Agricultural Machines, Kamýcká 129, 165 21, Praha 9 - Suchdol, Czech Republic; *Correspondence: krupicka@tf.czu.cz

**Abstract.** This paper deals with a roller conveyor which forms a part of the separating machine for hops harvested from low trellises. One of the parameters that influences the correct operation of this conveyor is tested, namely the gap between the rollers. The aim of the test was to discover whether the fact that hop matter falls through the rollers depends on the size of the gap between the rollers. For testing purposes a model of the roller conveyor was designed, made, and subsequently tested in a series of experiments with the purpose of integrating it into a separating machine. The measurements were carried out using a sample of hop matter harvested from low trellises. The dependency of falling matter upon the gaps was determined in view of eight gaps between the rollers. The measurements revealed that the gap size has an influence on the falling of hop cones and small-sized admixtures only if the gap size is larger than the size of the hop cones. At the same time, this parameter has no substantial influence on the separation of medium-length and long stems which were separated perfectly.

**Key words:** hops, separating machine, roller conveyor.

## INTRODUCTION

At present, hops are used above all as one of the basic ingredients in beer brewing. Other purposes are not mentioned in world statistics. Yet, we know the plant is important in pharmacy as well as cosmetics (Vrzalová & Fric, 1994).

Extraordinary climatic and soil conditions contribute to the outstanding aromatic character of Czech hops. The Saaz semi-early red-bine hop is still the most widely recognized aromatic hop in the world (EAGRI, 2013).

One of the key problems of the Czech hop industry is that is complicated to hire labour for the most difficult operations such as hanging and sticking hop strings and training hop-bines. For these reasons, some growers tend to switch to growing hop on low trellises, where there is no need for performing these operations anymore. In the new growing system, hop bines spontaneously climb (wind) around a special plastic net, which forms a substantial part of the low trellis (Štranc at al., 2010; Štranc at al., 2012).

When grown on low trellises, traditional hop varieties (bred for high trellises) produce only approximately 63% of the yield compared to that gained from classic constructions. According to breeders and economic experts, new ‘dwarf’ varieties bred for low trellises should produce at least 80% of the yield gained from varieties grown on classic trellises (Lewis, 1990; Darby, 1999).

In the Czech Republic, low-trellis hop growing is in the experimental stage and the area covered by low-trellis hop fields is less than 50 ha today (EAGRI, 2013).

Other kinds of machinery are needed for this type of growing technology. The hops grown on low trellises are harvested by a mobile picker pulled by a tractor. The hop material collected by the mobile picker further undergoes separation on a machine line, which is adapted from a classic machine picking line. The aim of the separation is to separate hop cones from stems and leaves (Jech at al., 2011).

This paper focuses on the part of the separating machine which is placed behind the secondary picker, namely the roller conveyor, each roller of which can be meticulously adjusted. Its importance lies in separating hop cones from stems and leaves. This roller conveyor serves as a roller sieve. The main function of the roller conveyor is to separate the hop material into small-sized fractions such as hop cones, leaves and fragments with a size smaller than the gap between individual rollers, and into large-sized fraction such as stems, clumps and big leaves which cannot fall through the rollers.

The right functioning of the roller conveyor depends on several parameters: the rotational frequency of the rollers, roller profile, and the gap between individual rollers. To be able to determine the precise significance of these parameters, a model of the roller conveyor was made, an actual size copy of the real roller conveyor (Krupička & Rybka, 2014).

## MATERIALS AND METHODS

The first measurement, which was carried out in the laboratory of the Department of Agricultural Machines, dealt with the dependency of hop matter falling through the gap between the conveyor's rollers.

### Model of roller conveyor

The model (Fig. 1.) is an actual size copy of the roller conveyor which forms a part of the final separating machine for hops cultivated on low trellises. The separating machine is the first of its kind in the Czech Republic, it is still under development, and it will be constructed by Chmelarstvi, cooperative Zatec, Zavod mechanizace. The model has 9 rollers with a 60 mm diameter. The rollers are 600 mm long. The first roller is fixed to the frame, whereas it is possible to adjust the pitch of the remaining 8 rollers, thus changing the size of the gap between them. The space below the rollers was divided with KAPA boards so that we are able to determine the amount of hop material that fell through the rollers. The hops input is a belt conveyor which is 600 mm wide and 1,000 mm long.

The model's throughput is 450 kg $h^{-1}$ of hop material and it is derived from the throughput of the real 2 m wide roller conveyor. The throughput corresponds to the peripheral speed of the conveyor belt: 0.27 m $s^{-1}$, and the rotational frequency of the conveyor rollers: 40 $min^{-1}$. These values were set with the help of frequency inverters. The vertical distance of the belt conveyor from the roller conveyor corresponds to the actual device.

**Figure 1.** Model of roller conveyor.

**Methodology of measurement**

The measurements were done in September 2014 during the harvest of hops cultivated on low trellises. The hop material used for experimental measurements in the DAM laboratories was supplied by a hop grower from the town of Kněžice. The hops were collected and stored in high-capacity containers which were placed between the belt conveyor of the trailer—the trailer carried the hops forward from the mobile harvester, and the input belt conveyor of the separating machine.

The measurements were made using the Sladek variety, which is the best for profitable hop cultivation on low trellises, judged on the basis of a four-year long observation and findings from previous years (EAGRI, 2013).

The sample of hop material was chosen so that the percentage of individual components (hop cones, leaves and stems) was preserved. The throughput of the roller conveyor model, which is 450 kg $h^{-1}$, corresponds to the sample's (Fig. 2) weight: 450 g. The average hop cone size was determined on the basis of 100 sample pieces. The average hop cone length was 28.8 mm and the average cone diameter was 15.6 mm.

**Figure 2.** Sample of hop material evenly spread on the conveyor belt.

The measurement procedure was the following: the hop material sample was mixed and evenly spread on the conveyor belt. The sample layer was app. 40 mm high. Then the roller drive was switched on, followed by the belt conveyor drive. The hop material was steadily separated, and, owing to KAPA boards, which had been installed below each roller, the material fell through the roller gaps into seven containers. Individual components of the hop material that fell through the rollers were further weighed with a 1 g measurement accuracy.

The dependency of the hop material throughput on the size of the gap between the rollers was measured gradually in view of four different gaps between 60 mm rollers (gap sizes: 48, 53, 58 and 63 mm). Further on, the roller diameter was increased to 80 mm with Mirelon tubes (thermal insulating material made from foam polyethylene; Fig. 3). By increasing the diameter we obtained four more gap sizes (28, 33, 38 and 43 mm), which could not be fixed in the position with the current construction solution. The relationship between gap size and the amount of material falling through the gaps was also determined for these four gaps. The measurement was repeated five times for each gap size. A sample of hop material was used only for one set of measurements each time. A new sample was used for measuring each subsequent gap.

**Figure 3.** Increased roller diameter achieved with Mirelon tubes.

## RESULTS AND DISCUSSION

The measured values were processed and the results are depicted in the graphs of Figs 4 and 5. Both graphs clearly show the percentage ratio of hop material separated in the gaps between the rollers, as the hop material proceeded from the belt conveyor to the first separating gap between the second and third roller and on towards other rollers. The graphs depict the percentage of the total weight of the sample which fell through in-between the gaps, the rest that is short of 100% represents the material that was separated as waste.

The graph in Fig. 4 clearly demonstrates that the graphic courses are almost identical for the selected four gaps between the rollers (48, 53, 58 and 63) with the roller diameter of 60 mm, which might suggest that gap size has no influence on the separation across the entire roller conveyor. However, it needs to be considered that mixture composition and cone size vary within every hop field and separating technology needs to be adapted accordingly. The graph shows that approximately 65–80% out of the total weight of the hop material falls through the first two gaps and the rest through the other five gaps. Practically no cones were found in the material that had fallen through with all four gap settings. As for the admixtures, the tendency was decreasing: when the gap was 48 mm, 32% of the total weight of sample admixtures ended up in the drop-off, while when the gap was 63 mm, 23% of the admixtures finished among the drop-off material. The rest of the admixture fell through the roller conveyor with the cones.

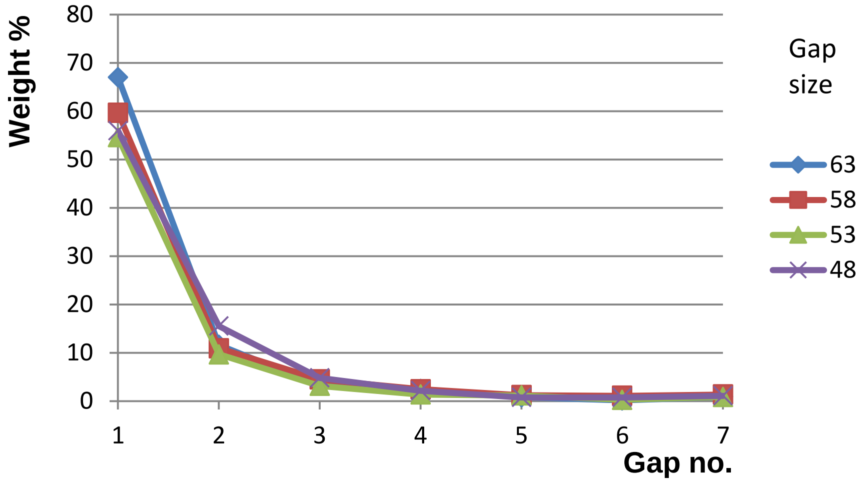


**Figure 4.** Weight percentage of material falling through each gap between the rollers, the roller diameter being 60 mm.

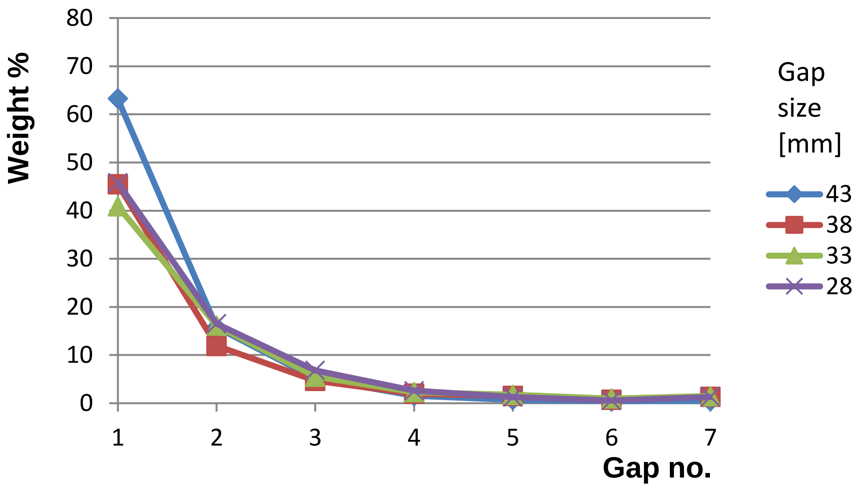


**Figure 5.** Weight percentage of material falling through each gap between the rollers, the roller diameter being 80 mm.

The graph in Fig. 5 illustrates the results of measurements similar to the previous case, only the roller diameter was increased to 80 mm with Mirelon tubes. Thus, the gaps between the rollers became smaller (28, 33, 38 and 43 mm). Graphic courses of the material falling through are similar to those represented in the graph from Fig. 4. The curves get notably closer from the second up to the seventh gap. When the gap size was set to the biggest value (43 mm), much more material fell through the first gap (contrary to the others), and percentagewise the figures are similar to the values of all the gaps in Fig. 4. Likewise, no cones detected in the drop-off here either. As for admixtures in the outlet, notable deviations (20–45%) were detected and no dependency can be observed. The remaining material again fell through with the cones.

To get a more detailed view of the composition of the mixture that fell through the individual gaps, the ratios of cones and admixtures, roller diameters and the smallest measured gaps between the rollers have been presented in the graphs of Figs 6 and 7. Distribution of ratios is similar to the other gaps. The admixture part in the material that fell through should be the smallest possible, the graphs, however, illustrate that both components (cones and admixtures) made up nearly half of the material that fell though the gaps, which is not the desired result. The largest part of the admixtures that fell through the gaps was made up of leaves, as proved by additional measurements which demonstrated that when the gap was 48 mm (rollers 60 mm in diameter) approximately 18% of the total weight fell through as drop-off and the remaining 82% of the total weight of leaves in a sample fell through the gaps. When the gap was 28 mm (rollers 80 mm in diameter) approximately 63% ended up in the waste and 37% fell through the gaps. This result proves the advantageousness of bigger diameters and smaller gaps. This conclusion cannot be taken too seriously since the measurements only had one variety and they were repeated a limited number of times.

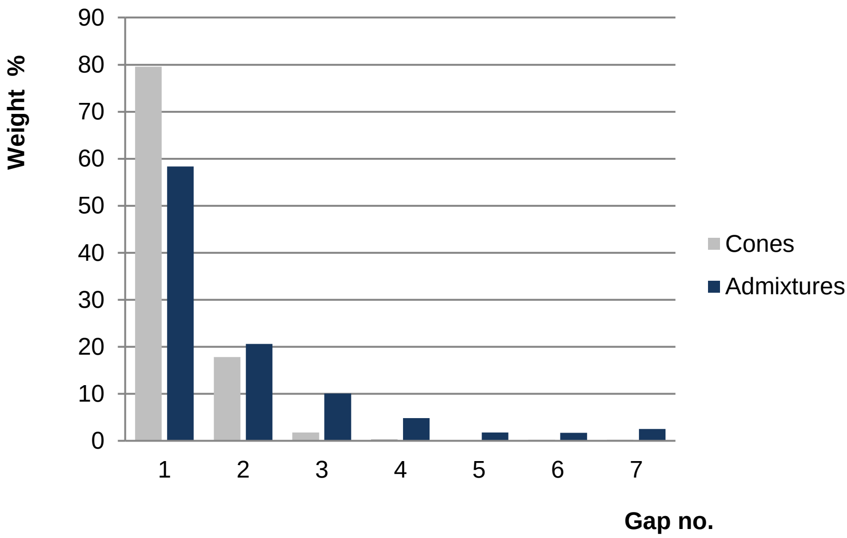


**Figure 6.** Cone and admixture weight percentage falling through individual gaps, the gap size being 48 mm and roller diameter 60 mm.

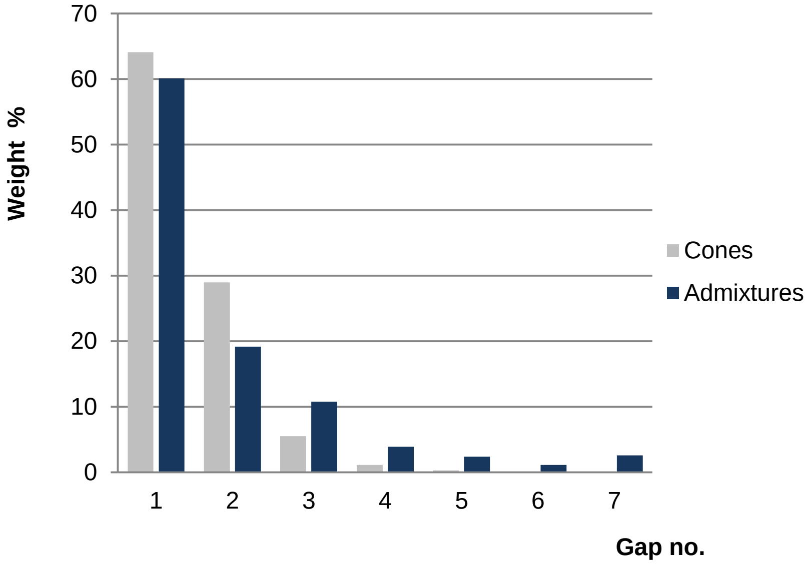


**Figure 7.** Cone and admixture weight percentage falling through individual gaps, the gap size being 28 mm and roller diameter 80 mm.

## CONCLUSION

These measurements were performed with a real sample of hop material, which also consisted of small-sized twigs, pieces of torn leaves and other small-sized admixtures, such as picked dry stalks from previous years besides hop cones, stems and leaves. It was determined that neither the roller diameter nor the gap size has any influence on the separation of medium-length and long stems, which were separated perfectly in all cases. The gap size has no influence on the hop cones and small-sized admixtures falling through if the gap size is larger than the size of the hop cones.

However, gap size influenced the amount of hop material falling through the gaps between the first two rollers. When the gap was 33 mm, only 41% of the total matter weight fell through. When the size of the gap was increased, the percentage hop material that fell through also increased. When the gap was 53 mm, 56% of hop material fell through and when the gap was 63 mm (the largest in this this test), 67% of the hop material fell through. Based on previous measurements the smaller gaps appear to be more convenient in view of the separation of bigger leaves.

Further measurements will follow in the season of 2015—these will be performed with samples of hop material the individual components of which will be precisely defined in terms of size. This way, more accurate results will be attained. The measurements will be focused, among other things, also on various roller profiles, which could have a positive influence on the separation of leaves.

ACKNOWLEDGMENTS. This article was written with the support of IGA TF CULS in Prague, project number 2014:31160/1312/313121.

## REFERENCES


Darby, P. 1999. *Economic yield potential of dwarf hop varieties. In: New Procedures in Hop Growing, Proceedings of International Symposium*, Hull, Bavaria, Federal Ministry of Food, Agriculture and Forestry, Germany

EAGRI: *Situation and Outlook Report of Hops 2013* (online). The last revision in December 2013 (cit.25.1.2015). Available from: http://eagri.cz/public/web/file/283356/SVZ_Chmel_a_pivo_12_2013.pdf (in Czech)

Jech, J., Artim, J., Angelovičová, M., Angelovič, M., Bernášek, K., Honzík, I., Kvíz, Z., Mareček, J., Krnáčová, E., Polák, P., Poničan, J., Rybka, A., Ružbarský, J., Sloboda, A., Sosnowski, S., Sypula, M., Žitňák, M., 2011. *Machines for crop production 3: machinery and equipment for post-harvest treatment of plant material,* Prague, Profi Press s.r.o., 368 p. ISBN 978-80-86726-41-0. (in Slovak)

Krupička, M., Rybka, A. 2014. *Parameters affecting the separation small fraction of the roller track machine lines for the separation of hops* 2014, XVI. International Conference of Young 2014, 9.–10.9 2014, Czech university of life sciences Prague, Faculty of Engineering, Str. 91–96. ISBN 978-80-213-2476-3. (in Czech)

Lewis, G.K. 1990. *Low Trellis Hop Production Systém*. Brewers Digest **65**(9), 22–29.

Štranc, P., Štranc, J., Holý, K., Štranc, D., Sklenička, P. 2012. *Growing conventional varieties of hops in low trellis*, Praha: FAPPZ, ČZU v Praze a Zemědělská společnost při ČZU v Praze, 96 pp. (in Czech).

Štranc, P., Štranc, J., Štranc, D., Holopírek, F., Podsedník, J., Zídek, J., Alt, A., Vent, L. 2015.: *The benefits of the technology of low trellis* (online). The last revision in 19.3.2010 (cit. 25.1.2015). Available from: http://zemedelec.cz/prinos-technologie-nizkych-konstrukci/ (in Czech)

Vrzalová, J., Fric, V. 1994. *Crop production – IV*. Prague: CULS Prague, FAPPZ, 80 s. ISBN 80-213-0155-4. (in Czech)

*Agronomy Research* **13**(1), 109–114, 2015

# Measurement of electrical conductivity of DAP fertilizer

J. Krupička*, P. Šařec and P. Novák

Czech University of Life Sciences Prague, Faculty of Engineering, Kamycka 129, 16521 Prague 6 – Suchdol, Czech Republic; *Correspondence: krup@tf.czu.cz

**Abstract.** Paper deals with the measurement of electrical conductivity of significant size groups of mineral fertilizer DAP divided in the air stream. Samples of these groups were dissolved in distilled water and the values of electrical conductivity recorded. Measurements will be used to monitor the electrical conductivity of other mineral fertilizers and to create a standard for qualitative assessment of fertilizer solutions.

**Key words:** electrical conductivity, air flow, fertilizer solution, concentration, DAP.

## INTRODUCTION

The concentration of fertilizers can be determined on the basis of the electrical conductivity (increasing the electrical conductivity). The value of the electrical conductivity can be used for precise application of fertilizers in liquid form. Monitoring the conductivity and knowing its value for target fertilizer concentrations enables to start the field application of fertilizers at an optimum moment. This would significantly increase the precision compared to the commonly used 'mass percentage method' where the concentration accuracy attains only ±10% according to fertilizer manufacturers. According to the electrical conductivity, the quality of the measured fluid can be assess accurately along with other data such as the level of pollution, the concentration of the various components of the solution, etc. (Kabeš, 1999). In that way, Electrical conductivity is the reciprocal of electrical resistance, is Indicated with the letter G and its basic unit is the Siemens (S).

The effectiveness of mineral fertilizers in crop cultivation depends on the particle stability and speed of their transformation to solution state to be acceptable by plants. This process depends on the particles dimensions, so that the dimension of particles is one of the main parameters that influence the fertilizer effectiveness.

Application of solid commercial fertilizers play important role in precision farming technologies. Quality of fertilization also significantly impacts the quality the final crops (Alaru et al., 2003). The application quality is depended on chemical composition and physical properties of fertilizer. Important from physical properties point of view is the grading of aggregate evaluation that is still performed by standard ČSN 01 50 30. The dimension of particulars only is characterized by this way.

In this paper we continue in the previous research program, in which the granulometric study mineral fertilizers were studied. In contrary to the similar study of other authors seat and airflow sorting were combined.

Experiments with particles can be designed differently. An elutriator was designed and constructed in which an airflow is supplied by a centrifugal fan (Csizmazia, 2000). Methods for measuring the coefficient of friction, the coefficient of restitution, the aerodynamic resistance coefficient, and the breaking force (particle strength) of fertilizers (Hofstee, 1992) were taken into account. The breaking force feature was skipped. The problem of particle destruction was overcome by fertilizer Superphosphate selection. The control of fertilizer discharge was studied for different designs of distributors and an experimental accurate fertilizer distributor with a rotary vessel type feeder was developed (Kudoh, 1989) what shows that dissolution of fertilizer also makes some problems. Consequent logistical problems are the same difficult for both pumping liquids, and transportation of particles by the air.

The size of particles makes the fertilizer's shelf life and stability of particulars behavior in the airflow more stable in storage and better acceptable by the plant. Therefore, experiments studying motion of particles through the air were accompanied by grading of particles.

This paper contains results obtained for DAP using the method developed previously.

## MATERIALS AND METHODS

Electrical conductivity was measured device Conductivity inoLab model WTW Cond 720. Instruments for the measurement of electrolytic conductivity, specifically electrical conductivity of liquids, consist of a measuring probe or conductivity sensor, transducer and evaluation unit. According to the manufacturer, accuracy of the device is 0.5% of value when measuring conductivity. Most of the apparatus is adapted for measuring the resistivity and weight concentrations of some components of the solution, which can be derived from the electrical conductivity. They are very sensitive and allow you to measure the content of various substances from small to very high concentrations and is often used to control a wide range of industrial processes. (Kabeš, 1999). Measurement was carried out for mineral fertilizer DAP (alternative trade name NP 18-46; manufacturer LIFOSA – Lithuania). The composition of DAP is the following: NP granular fertilizer with 18% ammonium nitrogen (NH4-N) and 46% water-soluble phosphorus (P2O5) and 2% magnesium (MgO). Fertilizer is suitable for basic fertilization of winter crops and spring crops. Distribution of the air stream was carried out in the laboratory of the Department of Agricultural Machinery using the laboratory air sorting machine K-293 (see Fig. 1).

The measurement procedure was as follows. First the laboratory sorting machine K-293 determined ranges of required amount of air, i.e. the minimum amount of air in which the particles are carried, and in the opposite a maximum amount of air in which the sample is completely sorted. With the help of graduated cylinders, interval of gradually increasing speed of the air flow is selected so that the number of classes was 7 to 10. It is necessary to ensure the right plane for the weights to ensure accuracy. Scales are calibrated and set to zero. Fertilizer is mixed because of the measurement accuracy and a sample of fertilizer weighing 500 g removed. An appropriate, predetermined, air speed is set for the laboratory device using graduated cylinders and adjusting screws. A sample of fertilizer is poured into the tank (1) with pre-set for the damper. With the help of a vibrator, fertilizer gets into the air flow in a vertical channel (see Fig. 2). Here comes the separation. Granules with larger than the critical speed set fall through the channel into the container (3). Granules with lower critical speeds are vertically entrained in air stream and in the extended portion of the channel are falling into the tray (4). The amount of fertilizer separated using air flow into the tank (4) is then placed in a pre-labeled bowl for later use. Emptied tank (4) is placed back into the machine and the speed of the air flow is checked. Then the fertilizer from the tank (3) is filled back to the tank (1) and the graduated cylinder is set to the next value of air stream speed. In this way, the experiment continues until the entire sample of fertilizer gradually falls into the tank (4).

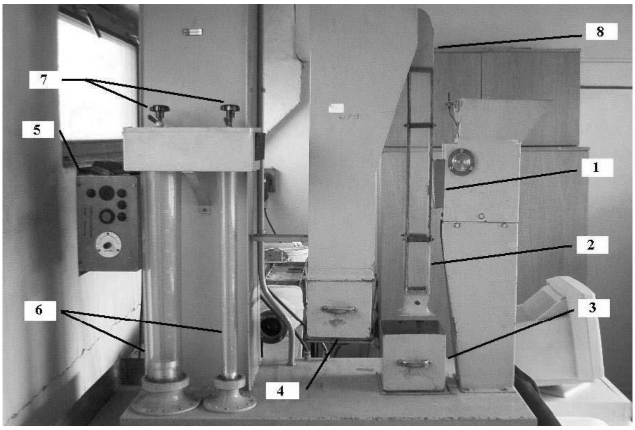


**Figure 1.** Laboratory Air sorter K-293. Labels: 1 – adjustable damper hoppers; 2 – vertical (aspiration) channel; 3.4 – tanks; 5 – control panel with buttons; 6 – small and large graduated cylinder; 7 – cylinder adjusting screws; 8 – fan.

The whole process is repeated with eight different samples of fertilizers to maintain the accuracy and reliability of statistical data measurements.

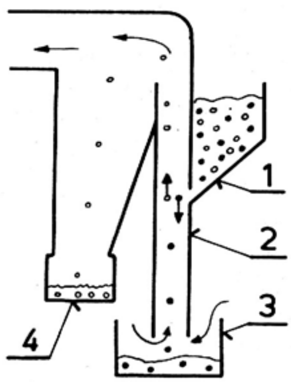


**Figure 2.** The vertical channel (detailed view). Labels: 1 – tray; 2 – vertical (aspiration) channel; 3 – stack; 4 – tray (particles of lower critical speed are carried into this tank).

Measurement was carried out in an air stream at a temperature of 22 °C and humidity of 22%. Electrical conductivity was measured on the machine Conductivity meter WTW inoLab model Cond 720. The measurements were carried out over ten hours in one-hour intervals. Before each conductivity measurement took place, the sample had been mixed to ensure its homogeneity.

## RESULTS AND DISCUSSION

From the samples measured in the air stream, samples weighing 5 grams were taken of significant proportions that were for the air stream 105, 115, 125 $m^3 h^{-1}$.

Therefore, these samples collected samples weighing 5 grams of six replications. Subsequently, 5 g samples were mixed and collected and then dissolved in distilled water to a volume of 50 ml. Table 1 shows the measured values. Conductivity measurements were performed after one hour. Electrical conductance G are given in units of electrical conductivity of G1, G2, G3 corresponding to granules of classes 105, 115, 125 (see Fig. 3).

**Table 1.** Measured values of electrical conductivity G of DAP fertilizer

| Time (h) | Temp. (°C) | G1 - for 105 $m^3 h^{-1}$ ($m^{-2} kg^{-1} s^3 A^2$) | Temp. (°C) | G2 - for 115 $m^3 h^{-1}$ ($m^{-2} kg^{-1} s^3 A^2$) | Temp. (°C) | G3 - for 125 $m^3 h^{-1}$ ($m^{-2} kg^{-1} s^3 A^2$) |
|---|---|---|---|---|---|---|
| 0:0 | 22.5 | 22.7 | 23.0 | 26.8 | 22.8 | 29.7 |
| 1:0 | 23.0 | 24.3 | 22.5 | 28.2 | 22.5 | 30.2 |
| 2:0 | 21.5 | 29.2 | 21.9 | 30.1 | 21.9 | 33.4 |
| 3:0 | 22.2 | 30.4 | 22.0 | 34.2 | 22.4 | 37.5 |
| 4:0 | 21.5 | 35.2 | 22.4 | 39.4 | 22.3 | 42.4 |
| 5:0 | 23.0 | 39.2 | 22.3 | 41.6 | 22.9 | 44.8 |
| 6:0 | 22.7 | 46.2 | 21.7 | 48.5 | 23.1 | 51.9 |
| 7:0 | 22.2 | 50.1 | 22.0 | 52.4 | 23.2 | 55.2 |
| 8:0 | 21.9 | 58.4 | 21.8 | 60.2 | 23.0 | 64.7 |
| 9:0 | 22.3 | 63.2 | 22.6 | 65.6 | 23.0 | 69.9 |
| 10:0 | 22.9 | 67.2 | 22.8 | 69.7 | 22.9 | 75.4 |

Undissolved residues were detected by using filter paper – the solution was filtered and the solids were weighed and dried in a dryer at a constant temperature of 105 °C to constant weight. These weights are not given here, because we cannot determine the amount of undissolved fertilizer.

This measurement was performed as indicative, and following additional measurements based on it were done where the sample was dissolved until it stopped to change its electrical conductivity, i.e. ended its dissolution. The undissolved remains of fertilizer were weighed. You could determine using nutrient analysis whether undiluted sample contains nutrients, or it is carrier roughage.

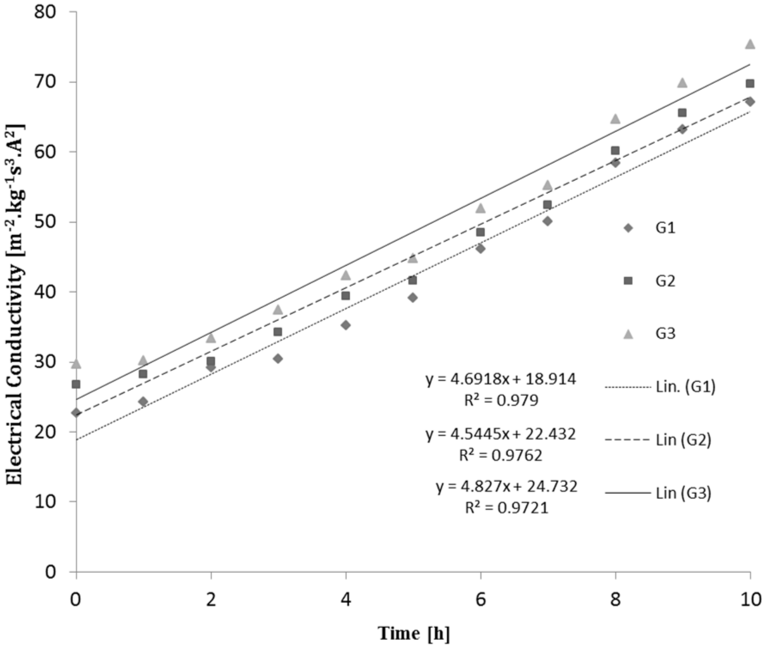


**Figure 3.** Graph of time dependence of electrical conductivity.

## CONCLUSIONS

On the basis of the electrical conductivity, the concentration of dissolved mineral fertilizer can be determined. Fig. 3 indicates that the values for the significant proportions are analogous. These values are crucial for the production of concentrated solutions of mineral fertilizers that can be applied by sprayers. Measurements are taken as the guidance for the methodology verification that will be used to measure other samples of similar fertilizers. These results will be used for the precise application of fertilizers and can be used as a reference for qualitative assessment fertilizer solutions. The research is about to continue with simultaneous measurement of concentrations in order to determine the relationship between concentration and electrical conductivity. Unfortunately, current measurement devices available to authors do not allow such approach.

ACKNOWLEDGEMENTS. This work was supported by Research Project of the Ministry of Education of the CR no. MSM 6046070905.

## REFERENCES

Alaru, M., Laur, Ü., Jaama, E., 2003. Influence of nitrogen and weather conditions on the grain quality of winter triticale. *Agronomy Research* **1**, 3–10.

Csizmazia, Z. 2000. Some physical properties of fertiliser particles.In: *Aspects-of-Applied-Biology*, Department of Agricultural Engineering, Faculty of Agricultural Sciences, Debrecen University, Hungary. 219–226.

Hofstee, J.W. 1992. Handling and spreading of fertilizers: part 2, physical properties of fertilizer, measuring methods and data. In: *Journal of Agricultural Engineering Research*, Wageningen Agricultural University, 141–162.

Kabeš, K. 1999. Instruments for conductivity measuring. *Automatization*, **42**(11), 826–832. (in Czech)

Kadlec, K. 1999. Sensors for electrolytic conductivity of liquids. *Automatization*, **42**(3), 823–825. (in Czech)

Kudoh, M. 1989. Flowability of fertilizers and development of an accurate fertilizer distributor. In: *Journal of Hokkaido College*, Department of Forestry & Landscape, Hokkaido College, Senshu University, Japan., Senshu University, 1–87.

*Agronomy Research* **13**(1), 115–123, 2015

# Plant remains distribution quality of different combine harvesters in connection with conservation tillage technologies

Z. Kviz*, F. Kumhala and J. Masek

Czech University of Life Sciences in Prague, Faculty of Engennering, Department of Agricultural Machines, Kamycka 129, Prague 6 – Suchdol, 165 21, Prague, Czech Republic; *Correspondence: kviz@tf.czu.cz

**Abstract.** Conservation tillage technologies are nowadays a part of modern agriculture. These technologies are used in plant production all around the world. Typical feature for these shallow soil tillage technologies is that all plant residues are left on the soil surface or in the treated (tilled) upper soil layer. The plant residues can significantly influence the next plant germination and growth, especially when they are unevenly placed on the field surface. Today's modern combine harvesters are able to crush and distribute all plant remains quite evenly with satisfactory results but all their mechanisms have to be properly set and sometimes some small improvements have to be done. This paper describes and evaluates the husk and straw distribution quality – the distribution pattern, on two very commonly used combine harvesters – CASE IH and JOHN DEERE. The measurement was carried out on serially manufactured machines without any change on them and with a small improvement on distribution mechanisms. The measurement of husk and straw distribution pattern was carried out on CASE IH combine harvester with an axial threshing system and on John Deere with a conventional tangential threshing system. Thereby it was possible to compare two completely different systems of threshing process and to observe a possible influence on straw and husk distribution quality (distribution pattern).
The most important outcome of the measurement of straw and husk distributors' work quality on combine harvesters is that cross irregularity of husk and straw distribution depends on instantaneous material feedrate through the harvester.

**Key words:** straw crushing, combine harvesters, conservation tillage, plant remains, distribution pattern.

## INTRODUCTION

Soil conserving tillage technologies, where ploughing by a mouldboard plough is replaced by tillers and shallow soil loosening, are used in agricultural practice as an alternative soil treatment. Besides the advantages of the application of this kind of soil cultivation, there are some problems and risks arising, which are not significant when ploughing is applied. It is typical for shallow soil tillage that all plant residues are left on the soil surface, or in the treated (tilled) upper soil layer. These plant residues can play an important role for the next plant cultivation and its yield. Based on the research of Johnson (1988), it can be said that all possible negative effects (effects on next plant seed germination, shedding growth, rodents spreading) can be eliminated or at least minimized as early as when the preceding crop is harvested (short stubble, small plant particles – maximum length of crushed straw particles up to 5 cm and regularity of plant residues left on the field surface after combine harvester passage). Furthermore, the negative effects can be minimized by appropriate technology and application time and, last but not least, by tools used for shallow tillage, seedbed preparation and seeding.

Sow et al., 1997 evaluated the influence of tillage and residue management practices on grain sorghum (*Sorghum bicolor* (L.) Moench), namely rooting depth and also changes in soil water content and cone index. Conservation tillage systems even increased sorghum grain yields by around 15% compared to conventional tillage system with ploughing. Root length in the 40 to 60 cm depth on reduced tillage plots was by 30 to 85% greater compared to the conventional tillage. Malhi at al., 2006 found out that different tillage and straw treatments had generally no significant effect on crop yield during the first three years observed. But after that time, reduced tillage plots produced 55, 32 and 20% greater canola seed, straw and chaff respectively than conventional tillage. There is also research evaluating different combinations of soil tillage and straw management including straw burning and their influence on next crop yield (Heege & Voßhenrich, 2000).

Placement of straw remains into the seeding layer, which is very often to happen when using only shallow tillage without ploughing, has an adverse effect and reduces plant germination up to 68% compared with 80% germination ratio when straw incorporating by a plough (Prochazkova & Dovrtel, 2000).

There is also research evaluating different combinations of soil tillage and straw management including straw burning and their influence on next crop yield (Heege & Voßhenrich, 2000). The best results were achieved exactly for straw burning technology and the worst for straw chopping and its shallow incorporation into soil.

From the previous crop harvest point of view, it has been revealed that cross irregularity of husk and straw distribution is a very significant point for the start of next crop planting. According to many authors, the basic precondition for good tillage and further crop growth is well performed harvest of preceding crop – short stubble, well chopped straw and evenly distributed plant remains on the field surface (Raoufat & Mahmoodieh, 2005; Bahrani, 2007).

The main subject of this article is the observation of the husk and straw distribution pattern by axial and tangential combine harvesters in real operation. Furthermore, the effect of this plant residues' irregular on-surface placement after harvest on residues placement in soil profile after treatment by a shovel tiller.

## MATERIALS AND METHODS

Soil conservation technology is a soil tillage system with certain benefits but also with specific prerequisites. One of the specific conditions is the quality of chopping and distribution of plant remains after preceding crop harvest. Good plant remains management means that the crushing mechanisms of combine harvesters have to ensure that 90% of plant remains particles must be shorter than 80 mm and the crushed straw and other organic remains (husk weed seeds, grain losses etc.) have to be evenly distributed along the working width of the machine Johnson (1988).

Plant remains distribution quality was observed after a passage of the combine harvester observed type. The observed area was 6 m wide strip behind the combine harvester passage with crop residues chopped and distributed on a field surface. This sampling area was at minimum 20 m from the point where the combine harvester started the passage in order to ensure that the combine harvester was completely full with the harvested material. The sampling area – 6 m long strip corresponded with machine's working width and was divided into twelve 0.5 m wide intervals. Then, all plant residues were collected from 0.1 $m^2$ area, which was considered as an 'interval sample'. Grain losses were separated from each sample and their placement across combine harvester working width was evaluated.

The measurement of husk and straw distribution pattern was carried out on CASE IH 2188 combine harvester with an axial threshing system and on John Deere 2266 with a conventional tangential threshing system. Thereby, it was possible to compare two completely different systems of threshing process and to observe a possible influence on straw and husk distribution quality (distribution pattern).

The following experimental arrangements and machines were evaluated:

Combine harvester John Deere 2266 was equipped with the engine power of 199 kW; header 5.90 m in width; threshing drum 660 mm in diameter and 1,670 mm in width; the total concave area 1.08 $m^2$; the total straw walker´s area 7.67 $m^2$; the total sieves area 5.083 $m^2$; the machine was equipped with a standard straw chopper and a twin vane-disc straw distributor mounted. (JD genuine equipment).

Combine harvester Case IH 2188 was of 196 kW engine power; 5.90 m header in width; rotor placed longitudinally; rotor 762 mm in diameter and 2,970 mm in length; the total cleaning area 5.12 $m^2$; a standard straw chopper and a two disc straw distributor mounted.

Combine harvester Case IH 2188 with 196 kW engine power; 5.90 m header in width; rotor placed longitudinally; rotor 762 mm in diameter and 2,970 mm in length; the total cleaning area 5.12 $m^2$; a standard straw chopper and two disc straw distributor mounted – with a specific improvement.

The straw distributor improvement consisted in elongation of husk distributing disc shafts by 20 cm. Due to this, the rotation surface of discs was lower, and therefore more small straw particles and husks, coming from sieves, could fall down onto both discs and could be distributed with more even pattern.

The number of repetitions of each measured variant was six at minimum. It means that we had 12 interval samples from one combine harvester passage with six or more repetitions.

Our experiments were realised during the standard harvesting season 2012 under ordinary field conditions on farms in the Czech Republic. The samples were being taken under normal operational conditions and therefore represent common machine setting, travelling speed and harvested plant state suitable for optimal harvest.

Measurement conditions:

- oil rape harvest – combine harvester setting according to the manufacturer's recommendations, working speed 6–8 km $h^{-1}$, grain moisture 7%, straw moisture 12%, yield 3.0 t $ha^{-1}$, 57 plants per 1 $m^2$;
- winter wheat harvest – combine harvester setting according to the manufacturer's recommendations, working speed 5–9 km $h^{-1}$, grain moisture 15%, straw moisture 17%, yield 5.2 t $ha^{-1}$, 590 plants per 1 $m^2$.

For plant residues' distribution quality evaluation, the Christiansen's coefficient was used. This coefficient determines a percentage deviation of each measurement and then an average value of these deviations from all measurements' arithmetic mean. When these deviations are small the value of Christiansen's coefficient is close to the value 1 (alternatively 100% if counting in percent) and vice versa.

This evaluation criterion was chosen because it perfectly and logically shows the variation size of the plant remains distribution values throughout the combine harvester header working width. The range of the Christiansen´s coefficient is within confined interval <0; > or <0; 100% > as opposed to other statistical variables possible to use for the distribution quality evaluation. And also this coefficient is used for the uniformity of liquid spreading and other liquid distribution characteristics evaluation on sprayers and sprinklers, which is very close to the distribution pattern of plant remains behind the combine harvesters. Coefficient of Christiansen´s is calculated using the following formula (1):

$$C_u = \left[1 - \left(\sum_{i=1}^{n} \left|i_{si} - i_m\right| / n \cdot i_m\right)\right] \tag{1}$$

where: $i_{si}$ – weight of an interval sample (g); $C_u$ range $<0;1>$; $i_m$ – arithmetic mean of $i_{si}$ values (g); $n$ – number of samples.

For every measurement the Christiansen's coefficient was counted separately for husk and for straw remains. It was assumed that the distribution quality of crop remains would depend also on their immediate amount, so the Christiansen's coefficient was calculated in dependence on the total weight of the sample from the area across the combine working width.

These values were processed separately for oil rape and winter wheat, each time for straw and husk and for all three kinds of evaluated combine harvesters. Graphical evaluation of our measurement was carried out by means of MS Excel charts.

Shallow tillage after harvest was performed by a shovel tiller after harvest on the examined plot. Number of plants germinated from grain losses was determined by manual counting.

Also plant residues placement evaluation after shallow tillage was carried out at the same places as grain losses were observed and by manual collecting of plant particles from the area of 0.1 m$^2$. The evaluation of crop residues placement after shallow tillage consisted of two measurement – firstly collection and weighing of crop residues remained on the field surface, and secondly collection and weighing of crop residues within the treated soil profile.

## RESULTS AND DISCUSSION

**Distribution regularity evaluation –** In all cases and variants it was found out that the irregularity of crop residues' distribution was always increasing with the increasing feed rate of combine harvester (mass going through the harvester). This fact was proved both for straw (Fig. 1) and for husk (Fig. 2) by winter wheat and oil rape harvest as well. The more material was harvested the worse Christiansen's coefficient was calculated.

There is a total weight of plant residues from one combine harvester passage (the sum of all interval samples) on the X-axis and there are Christiansen's coefficient values on the Y-axis. The presented charts are for winter wheat only.

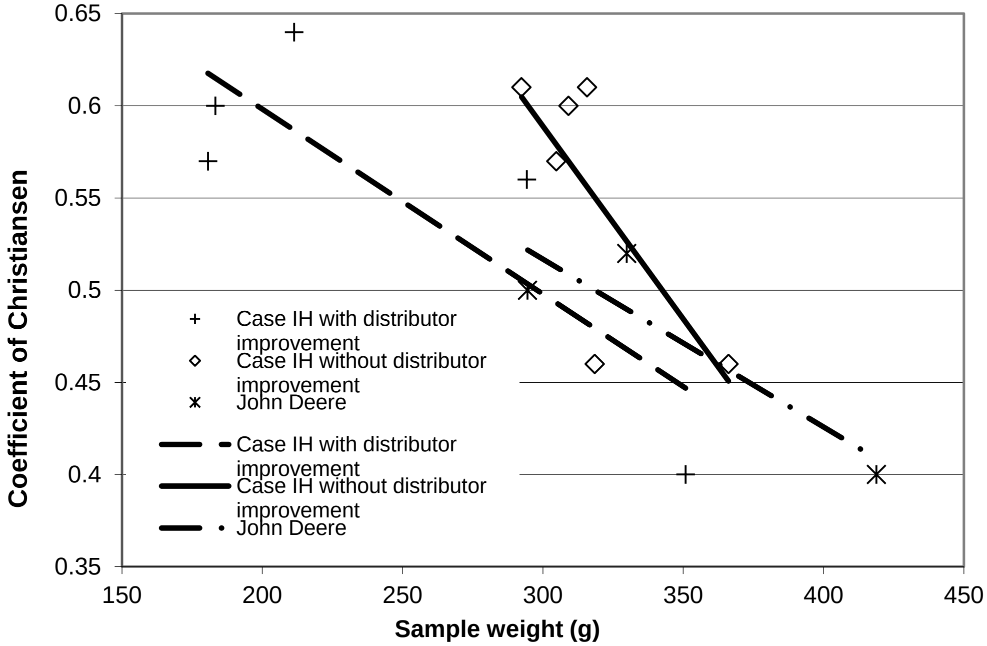


**Figure 1.** Straw distribution uniformity during winter wheat harvest.

The cleaning sieves on axial combine harvesters (CASE IH) gather more small plant particles in comparison with conventional tangential harvesters (John Deere). These particles flow from a threshing mechanism where material stays a certain time in the space between the threshing drum and the concave during threshing. When evaluating the axial threshing system, harvested material stays longer in the threshing space and the straw is therefore much more treated and broken up than by using a tangential threshing system. This fact was observed mainly during the oil rape harvest where the straw, very easy to break off, was not crushed so much in tangential threshing system as opposed to axial system. This resulted in better husk distribution on tangential combine harvester with mounted straw distributor because there were not so many small particles on the sieves going into the distributor.

However, there was the opposite situation in distribution of oil rape straw. Because a great amount of oil rape straw is going into a chopper, the distribution plate was overloaded and then the distribution quality was declining and was worse than on axial combine harvester.

For better plant remains distribution, a constructional change was proposed. The improvement on axial combine harvesters consists in elongation of husk and straw distributor shaft by 20 cm. This had a very significant effect on husk and straw distribution quality during the winter wheat harvest. This change could be highly recommended. During the oil rape harvest the effect on distribution quality was not very significant.

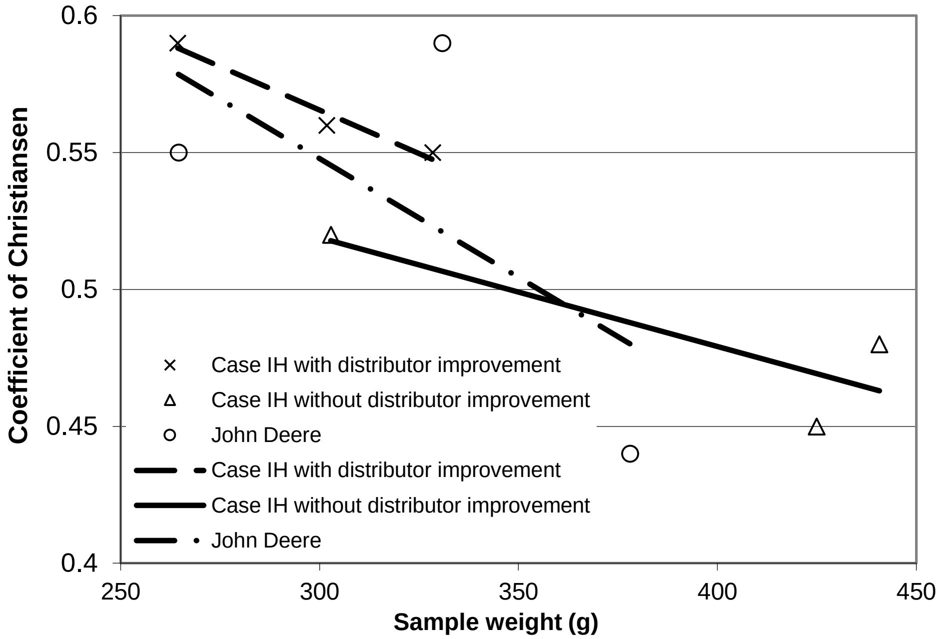


**Figure 2.** Husk distribution uniformity during winter wheat harvest.

**Plant residues' distribution after shallow tillage evaluation** – It can be seen on charts (Figs 3, 4 and 5) that there are some noticeable differences in plant residues placement after shallow tillage between different types of combine harvesters and also between standard design of the straw distributor and improved version.

Two variants are compared on charts (Figs 3–4), namely John Deere with the serial straw distributor mounted, and CASE IH without any straw distributor change/improvement. It means, regarding the regularity of straw distribution, the best and the worst measured variant. It follows from the charts that the overall regularity of the plant residues distribution after harvest had no influence on on-field-surface part of plant remains. This on-surface part of residues, consisted of straw and bigger particles and was a minor one. The vast majority of plant residues were incorporated into soil profile during tillage at a shallow depth.

This under-soil part of plant remains consisted mainly of husk and small straw particles. It turned out that the overall quality of husk and straw distribution corresponded with the amount of crop residues under the soil surface in the treated profile (irregular distribution) whilst the on-surface crop residues were always very balanced. Consequently, this fact can deteriorate conditions for the next plants germination and their growth.

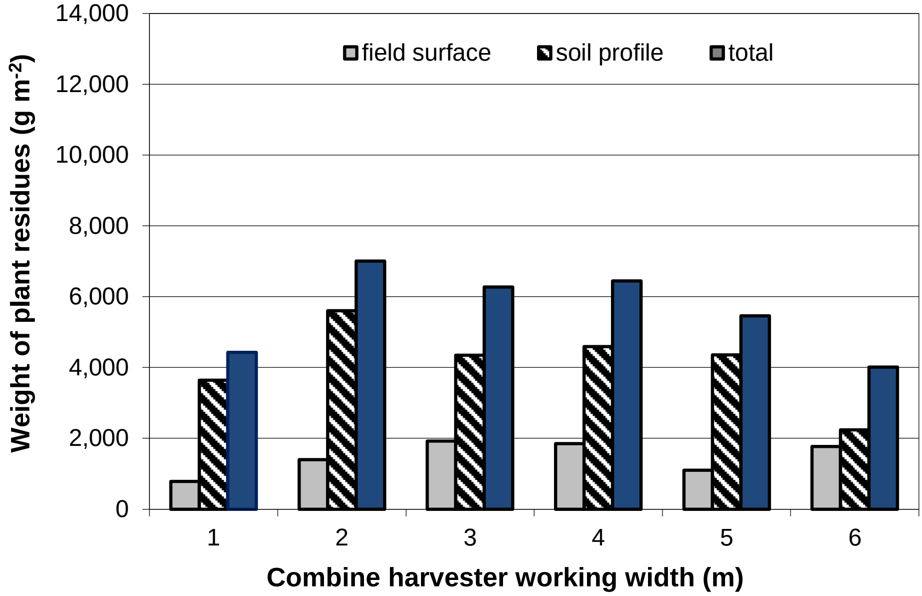


**Figure 3.** Plant residues distribution after shallow tillage (combine harvester John Deere).

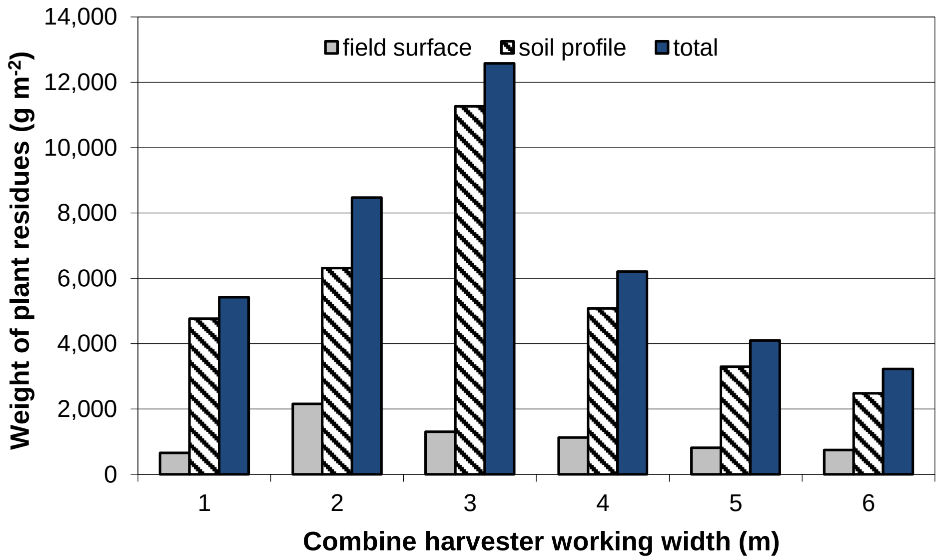


**Figure 4.** Plant residues distribution after shallow tillage (combine harvester Case IH without straw distributor improvement).

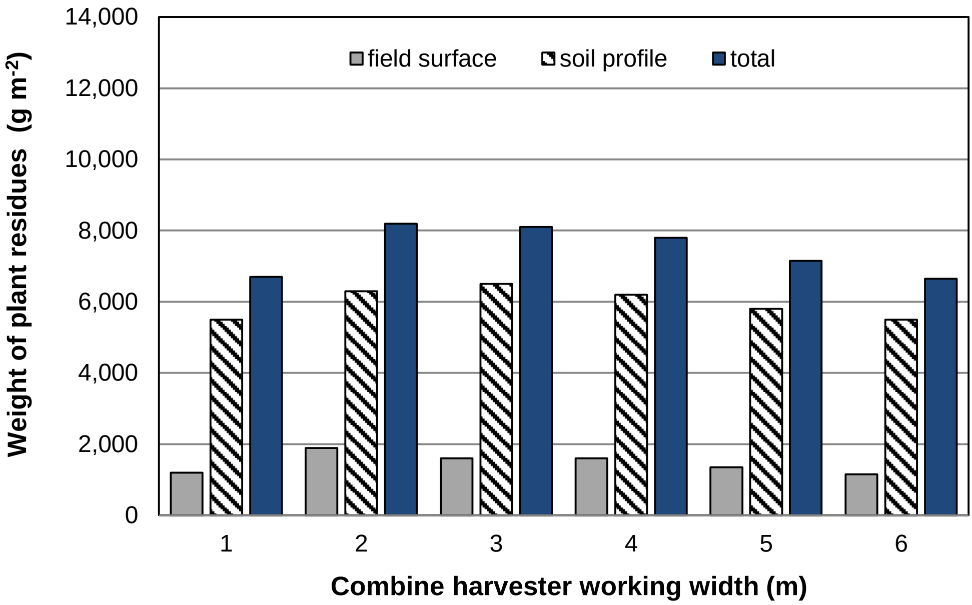


**Figure 5.** Plant residues distribution after shallow tillage (combine harvester Case IH with straw distributor improvement).

## CONCLUSIONS

The most important outcome of the measurement of combine harvesters husk distributors' work quality is that cross irregularity of husk and straw distribution depends on instantaneous material feedrate through the harvester. The more material, the worse regularity of husk and straw distribution. From a practical point of view it can be recommended to pay adequate attention to this problem especially when applying conservation tillage and when the preceding crop had a high yield and high amount of crop residues. Generally it is beneficial from that point of view to have optional possibility of settings for distributor deflection blades and for the angle of husk spreader as well. It is becoming necessary to set not only threshing and cleaning mechanisms on combine harvesters but also husk and straw distribution mechanisms.

The advantage of our change of distributor shaft on Case IH for better distribution quality was proved.

Axial combine harvesters, thanks to their technological process of threshing, break up straw more intensively then tangential combine harvesters. Straw crushers on tangential combine harvesters are therefore more loaded and need more attention from the crushing quality point of view. On the contrary, on axial combine harvesters most material goes on cleaning sieves and more attention should be paid to this small particles distribution.

The placement of all plant residues after tillage was almost even on field surface. Most small particles were mixed into soil when tilled and the placement of these particles corresponded with irregular distribution of all harvested plants' residues before tillage. To sum up this part of our research, the plant remains, mixed into soil after tillage, were placed as irregularly as they were before tillage. The plant remains left on the soil surface were placed more evenly, but the separation of small and big particles took place. The long and big particles stayed on the field surface and the majority of small ones were mixed into soil.

The mentioned irregularity of small plant remains in treated soil profile and so their great concentration at the particular place could affect next plant germination and growth.

This problem presented here is becoming very important nowadays because more and more farmers use conservation tillage systems on their fields and that is why it is necessary to pay proper attention to do the best from this point of view.

## REFERENCES


Bahrani, M.J., Raoufat, M.H., Ghadiri, H. 2009. Influence of wheat residue management on irrigated corn grain production in a reduced tillage system. *Soil and Tillage Research* **94**(2), 305–309.

Heege, H.J., Voßhenrich, H.H. 2000. Interactions between Soil Cultivation and Climate. ISTRO 2000, 15th Conference of the International Soil Tillage Research Organization, 2000, Fort Worth, Texas, Book of Proceedings, pp.125–133.

Johnson, R.R. 1988. Soil engaging tool effects on surface residue and roughness with chisel-type implements. *Soil Sci. Soc.* **52**, 237–243.

Malhi, S.S., Lemke, R., Wang, Z.H., Chhabra, B.S. 2006. Tillage, nitrogen and crop residue effects on crop yield, nutrient uptake, soil quality, and greenhouse gas emissions. *Soil and Tillage Research* **90**(1–2), 171–183.

Prochazkova, B., Dovrtel, J. 2000. The effect of different soil tillage on the yields of winter wheat. *Rostlinna vyroba* **46**(10), 437–442.

Raoufat, M.H., Mahmoodieh, R.A. 2005. Stand Establishment Responses of Maize to Seedbed Residue, Seed Drill Coulters and Primary Tillage Systems. *Soil and Tillage Research* **90**(3), 261–269.

Sow, A.A., Hossner, L.R., Unger, P.W., Stewart, B.A. 1997. Tillage and residue effects on root growth and yields of grain sorghum following wheat. *Soil and Tillage Research* **44**(1–2), 121–129.

*Agronomy Research* **13**(1), 124–129, 2015

# Sensitivity of capacitive throughput sensor to the change of material relative permittivity

J. Lev

Czech University of Life Sciences Prague, Faculty of Engineering, Department of Physics, Kamýcká 129, 165 21 Prague 6 Suchdol, Czech Republic; e-mail: jlev@tf.czu.cz

**Abstract.** The capacitive throughput sensors have been tested in many applications (e.g. the throughput measurement of potatoes, sugar beet, chopped maize and hops). The results showed that the capacitive throughput sensors can be very perspective in some cases. The capacitive sensor for the throughput measurement can be described as a parallel plate capacitor where the dielectric is a mixture of air and the measured material. The equivalent dielectric constant increases with the increasing thickness of the material layer between the plates and the electric capacitance of the capacitor is increasing as well. The thickness of the material layer between the plates can be then determined via the electrical capacitance measurement. The main goal of this work is to describe the relationship between the relative permittivity of the material and the sensor output. The sensor values output directly depend on the sensor impedance and it is influenced by the electric field between the electrodes. The electric field is most influenced by the dielectric properties of the material and the distribution of the material. It was found that the influence of the relative permittivity change is significant only for less values (approximately 10 and less). These results mean that the material with the higher relative permittivity is useful for the capacitive throughput sensor. Also this behaviour can explain why the influence of the moisture is less significant for the moister material, because moister materials have higher relative permittivity.

**Key words:** capacitive throughput sensor, relative permittivity, moisture content.

## INTRODUCTION

The material throughput measurement during the harvest is an important requirement of yield maps creating. However, the data obtained from these sensors can be used in other cases (e.g. an optimization of the material transport). Many yield sensors based on different principles were successfully tested for the combinable crops (Reinke et al., 2011; Reyns et al., 2002). Only few yield measurement systems are available for the non-combinable crops (Kumhála et al., 2009) and the research still continue in this area (Jadhav et al., 2014).

The capacitive throughput sensors have been tested in many applications. The Capacitive throughput sensor can be described as a parallel plate capacitor where the dielectric is the mixture of air and the measured material. The Equivalent dielectric constant increases with increasing thickness of the material layer between the plates. The thickness of the material layer between the plates can be then determined via the electrical capacitance measurement.

One of the earliest papers about the throughput measurement with the capacitive sensor was published by Stafford et al. (1996). Authors used the capacitive sensor to determine the grain mass flow. Other works were presented by Martel and Savoie (1999) and Savoie et al. (2002). Both papers deal with the measurement mass flow rate through a forage harvester. The testing of capacitive throughput sensors for potatoes, sugar beet, chopped maize and hops was presented in other papers (Kumhála et al., 2009; Kumhála et al., 2010; Kumhála et al., 2013).

The sensors based on capacitance measurement are commonly used for the moisture content determination because the dielectric properties of materials are highly correlated with the moisture content of the material (Nelson & Trabelsi, 2012). Many authors wrote about the techniques for the moisture content measurement (e.q. de Loor, 1983; Eubanks & Birrell, 2001; Lawrence, et al., 2001; Paz et al., 2011).

Stafford et al. (1996) presented that the capacitive throughput sensor is sensitive to the moisture content and this effect can be compensated by measuring of the capacitance at two widely spaced frequencies. However, authors state on the base of their measurement that the sensor output was much less sensitive to the moisture content than anticipated. Savoie et al. (2002) presented that their system was better correlated with the water flow rate ($R^2 = 0.624$) than with the wet mass–flow rate ($R^2 = 0.468$). Kumhála et al., 2010 performed a measurement where the influence of the moisture content was tested. The measurement was performed with four balsa blocks which were moistened to about 80% of moisture content and then slowly dried. Authors presented that the sensor was not sensitive to the change of the moisture content when the material moisture content of balsa bock varied from above 75% to 65%. However, in the case when materials with lower material moisture content are measured, the changes in the material moisture content itself can influence the results of the capacitive throughput measurement.

The main goal of this work is to describe the relationship between the relative permittivity of the material and the sensor output. If the electrostatic field in the sensor sensing area is assumed (Lev et al., 2013) the most important material parameter is the relative permittivity. Kumhála et al. (2010) presented interest results. However a theoretical rationale is missing.

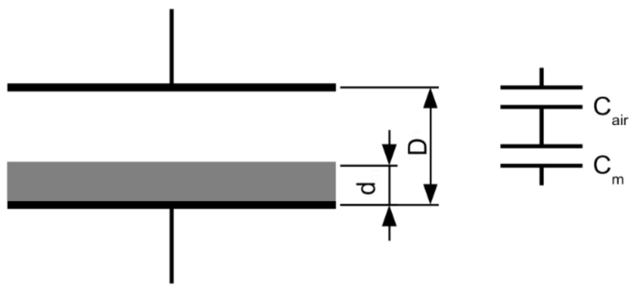


**Figure 1.** The diagram of the capacitive throughput sensor: *D* – the distance between electrodes; *d* – the thickness of the material layer, $C_{air}$; $C_m$ – the capacitance of the substituted capacitors.

## MATERIALS AND METHODS

In many cases the capacitive throughput sensor can be described by two parallel plate capacitors connected serially and with a different dielectric material (Kumhála et al., 2009). The first capacitor ($C_m$) represents the measured material and the second capacitor ($C_{air}$) represents the air above the measured material. The diagram of the sensor is in Fig. 1.

The total capacitance of the sensor can be calculated by this flowing equation:

$$C_T = \frac{C_{air} C_m}{C_{air} + C_m} = \frac{S \varepsilon_m \varepsilon_{air} \varepsilon_0}{d(\varepsilon_{air} - \varepsilon_m) + \varepsilon_m D} \tag{1}$$

where: $C_T$ – total electrical capacitance of the sensor; F; $S$ – sensor plate area, $m^2$; $\varepsilon_m$ –relative permittivity of the measured material; $\varepsilon_{air}$ – relative permittivity of the air; $\varepsilon_0$ – permittivity of vacuum; $\varepsilon_0$ = 8.85 $10^{-12}$ F $m^{-1}$; $d$ – thickness of material layer, m; $D$ – distance between electrodes, m.

The impedance magnitude of the sensor equals the capacitive reactance and it can be calculated:

$$X = \frac{1}{\omega C_T} = \frac{d(\varepsilon_{air} - \varepsilon_m)}{S \varepsilon_m \varepsilon_{air} \varepsilon_0 \omega} + \frac{D}{S \varepsilon_{air} \varepsilon_0 \omega} = dA + X_E \tag{2}$$

where: $X$ – capacitive reactance of the sensor; Ω; $\omega$ – angular frequency, rad·$s^{-1}$; $A$ – constant of the sensor; $X_E$ – capacitive reactance of the empty sensor, Ω.

The equation (2) is a linear equation. The constant $A$ is negative because $\varepsilon_m$ is always higher than $\varepsilon_{air}$. The positive capacitive reactance change magnitude of the sensor is:

$$X_{ch} = -dA = \frac{d(\varepsilon_m - \varepsilon_{air})}{S \varepsilon_m \varepsilon_{air} \varepsilon_0 \omega} \tag{3}$$

where: $X_{ch}$ – capacitive reactance change magnitude of the sensor, Ω.

The influence of the material relative permittivity change can be expressed as the error of the capacitive reactance change:

$$\Delta Xch = \frac{d(\varepsilon_m (1+\mu) - \varepsilon_{air})}{S \varepsilon_m (1+\mu) \varepsilon_{air} \varepsilon_0 \omega} - \frac{d(\varepsilon_m - \varepsilon_{air})}{S \varepsilon_m \varepsilon_{air} \varepsilon_0 \omega} = \frac{d\mu}{S \varepsilon_m \varepsilon_0 \omega (1+\mu)} \tag{4}$$

where: $\Delta X_{ch}$ – the influence of a material relative permittivity change, Ω; $\mu$ – a relative change of a material relative permittivity.

The relative error of the capacitive reactance change is:

$$\delta = \frac{\Delta X_{ch}}{X_{ch}} 100 = \frac{\mu \varepsilon_{air}}{(\varepsilon_m - \varepsilon_{air})(1-\mu)} 100 \tag{5}$$

where: $\delta$ – relative error of the capacitive reactance change, %.

## RESULTS AND DISCUSSION

The dependence between the capacitive reactance of the sensor and the material thickness layer was calculated based on the equation (2) and it is shown in Fig. 2. All values were calculated for: $\omega = 2\pi f$, where $f = 1$ MHz, $\varepsilon_{air} = 1$, $S = 1$ m$^2$ and $D = 1$ m. In the Fig. 2 there are five lines and each of them represents different relative permittivity of the measured material. All lines begin at the capacitive reactance value $X = 112$ kΩ where the sensor was without measured material. If the material thickness layer is $d = 1$ m, the sensor is wholly filled by the measured material. It is evident from Fig. 2 that the capacitive reactance of the sensor is significantly influenced by the relative permittivity, if the sensor is wholly filled by the material. Also it can be state that the influence of the relative permittivity increases with the increasing thickness of the material layer. However, the output values of the capacitive throughput sensor usually depend on the capacitive reactance change magnitude of the sensor (Kumhála et al., 2009; Lev et al., 2013) and these values are much less sensitive to the relative permittivity change of the measured material.

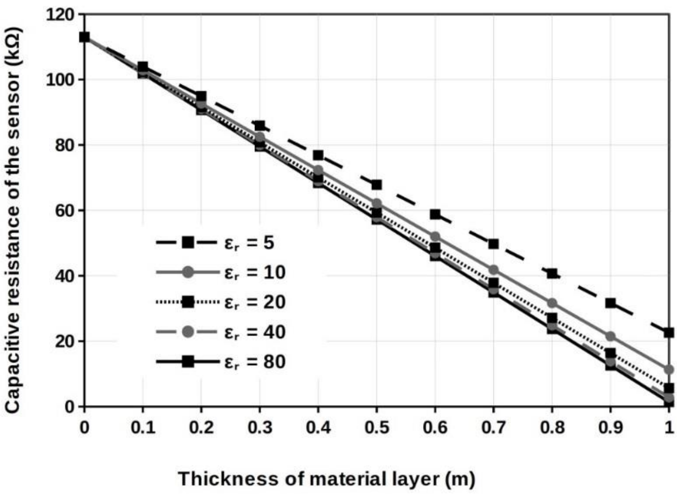


**Figure 2.** The dependence between the capacitive reactance of the sensor and the material thickness layer.

The equation (5) represents the relative error of the sensor capacitive reactance change. It is evident from this equation that the relative error of the sensor capacitive reactance change depends on the relative change of the material relative permittivity and on the relative permittivity of the measured material only. The relationship between the relative error of the capacitive reactance change and the relative permittivity of the measured material is shown in Fig. 3. In the Fig. 3 there are six curves and each of them represents different relative change of the material relative permittivity $\mu$. The values were chosen: $\mu$ = -0.5, -0.2, -0.1, 0.1, 0.2, 0.5. The negative or positive value means that the relative permittivity was decreased or increased, respectively.

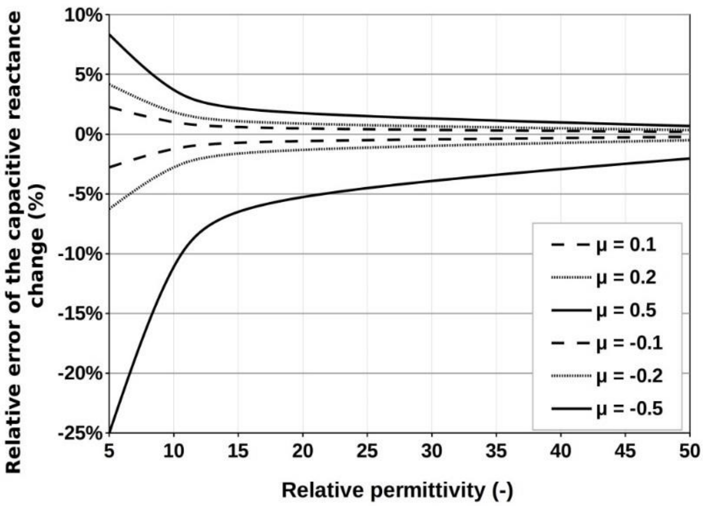


**Figure 3.** The relationship between the relative error of the capacitive reactance change and the relative permittivity of the measured material.

It can be seen in the Fig. 3 that the relative error of the sensor capacitive reactance change is decreasing very quickly with the increasing relative permittivity. If the relative permittivity of the measured material is for example 10 and $\mu$ = 0.5 (the relative permittivity increases to 15) the relative error of the capacitive reactance change is only about 4%. The negative or positive value of the relative error means that the relative error was caused by negative or positive relative change of the relative permittivity, respectively. It is logical that if the change of the relative permittivity is negative, the absolute value of the relative error of the sensor capacitive reactance change is bigger.

It is apparent that the influence of the relative permittivity change is more significant for small values. These results correspond with the paper of Kumhála et al. (2010) and they explain that behaviour. Savoie et al. (2002) presented different results. Nevertheless, their measurement method was quite different. Authors used the capacitance controlled oscillator and the output of their device directly depended on the sensor capacitance (not the capacitance/capacitive reactance change). Also it should be taken into account that the material distribution in their throughput sensor was fully random and the model presented in this paper would probably not be valid in that case.

## CONCLUSIONS

The sensitivity of the capacitive throughput sensor to the change of the material relative permittivity was studied in this paper. The mathematical model presented in this study is simple but it accords with previous works (Stafford et al., 1996; Kumhála et al., 2009; Kumhála et al., 2010) and it was not presented before. Results show that the influence of the capacitive throughput sensor on the change of the material relative permittivity is very quickly decreasing with the increasing relative permittivity. These results mean that materials with higher relative permittivity are useful for capacitive throughput sensors. Also the influence of the moisture is less significant for moister material, because moister materials have higher relative permittivity.

ACKNOWLEDGEMENTS. This work was supported by the Internal Grant Agency – Faculty of Engineering, Czech University of Life Sciences Prague, Project No. 2014:31160/1312/3122.

## REFERENCES

De Loor, G.P. 1983. The Dielectric Properties of Wet Materials. *IEEE Transactions on Geoscience and Remote Sensing*, **GE–21**(3), 364–369.

Eubanks, J.C., & Birrell, S.J. 2001. Determining Moisture Content of Hay and Forages using Multiple Frequency Parallel Plate Capacitors. *ASAE paper* No. 01-1072.

Jadhav, U., Khot, L.R., Ehsani, R., Jagdale, V. & Schueller, J.K. 2014. Volumetric mass flow sensor for citrus mechanical harvesting machines. *Computers and Electronics in Agriculture* **101**, 93–101.

Kumhála, F., Kavka, M., Lev, J. & Prošek, V. 2013. Measurement of hop material throughput by capative sensor. In: *Trends in Agricultural Engineering 2013*. Prague, Czech Republic, 3–6 September, 2013.

Kumhála, F., Prošek, V. & Blahovec, J. 2009. Capacitive throughputsensor for sugarbeets and potatoes. *Biosystems Engineering*. **102**(1), 36–43.

Kumhála, F., Prošek, V. & Kroulík, M. 2010. Capacitive sensor for chopped maize throughput measurement. *Computers and Electronics in Agriculture* **70**(1), 234–238.

Lawrence, K.C., Funk, D.B. & Windham, W.R. 2001. Dielectric Moisture Sensor for Cereal Grains and Soybeans. *Transactions of the ASAE* **44**(6), 1691–1696.

Lev, J., Mayer, P.,·Wohlmuthová, M. & Prošek, V. 2013. The mathematical model of experimental sensor for material distribution detecting on the conveyor. *Computing* **95** (Suppl.1), 521–536.

Martel, H. & Savoie, P. 1999. Sensors to measure forage mass flow and moisture continuously. *ASAE paper* No. 991050.

Nelson, S.O. & Trabelsi, S. 2012. Factors Influencing the Dielectric Properties of Agricultural Products and Food Materials. *ASAE paper* No. 12-1338239.

Paz, A., Thorin, E. & Topp, C. 2011. Dielectric mixing models for water content determination in woody biomass. *Wood Sci Technol* **45**, 249–259.

Reinke, R., Dankowicz, H., Phelan, J. & Kang, W. 2011. A dynamic grain flow model for a mass flow yield sensor on a combine. *Precision Agric*. **12**, 732–749.

Reyns, P., Missotten, B., Ramon, H. & De Baerdemaeker, J. 2002. A Review of Combine Sensors for Precision Farming. *Precision Agric*. **3**, 169–182.

Savoie, P., Lemire, P. & Thériault, R. 2002. Evaluation of five sensors to estimate mass-flow rate and moisture of grass in a forage harvester. *Applied Engineering in Agriculture* **18**(3), 389–397.

Stafford, J.V., Ambler, B., Lark, R.M. & Catt, J. 1996. Mapping and interpreting the yield variation in cereal crops. *Computers and Electronics in Agriculture* **14**, 101–119.

*Agronomy Research* **13**(1), 130–140, 2015

# Production of high quality hemp shives with a new cleaning system

C. Lühr*, R. Pecenka and H.-J. Gusovius

Leibniz Institute for Agricultural Engineering Potsdam-Bornim (ATB), Max-Eyth-Allee 100, 14469 Potsdam, Germany; *Correspondence: cluehr@atb-potsdam.de

**Abstract.** A shortage as well as a rise in costs for raw materials as used for production of derived timber products and fibre composites can be observed for quite some time. Especially the use of wood as energy source has led to an increased demand for cellulose raw materials. Non wood resources e.g. from agricultural production are coming into consideration as alternatives or as replenishment to conventional raw material stock. Therefore, there is an increasing demand for high-grade hemp and flax fibres as a raw material e.g. for production of natural fibre reinforced composites. Within this context also the non-fibrous fraction of fibre plants – shives or hurds – are suitable for different applications in composite or fibre board industry. At present, approx. 50% of the income of a hemp fibre processor is generated by marketing quality shives. There is still a substantial need for efficient shive processing and cleaning technologies. Cleaned high quality hemp shives can be used not only for animal bedding, but also for particle board or composite production. Hence, ATB has developed a simple but efficient technology for cleaning of shive-fibre mixtures. It allows classification and cleaning of shives as well as recovering of short fibres in only one processing step. On basis of these results, the developed fractionating system has been patented and scaled up to an industrial system in cooperation with a machine supplier for hemp processing equipment. The machine has been successfully tested with different machine settings as well as different varieties of input material.

**Key words:** hemp, fibres, shives, shive-fibre mixture, cleaning machine.

## INTRODUCTION

The share of decorticated fibre constitutes in hemp straw - dependent on the type of straw and growing conditions - averages at 30 mass-% (Höppner & Menge-Hartmann, 2000; Francken-Welz & Léon, 2003). Consequently, approx. 70 mass-% of by-products will accumulate during fibre production. Unclean shive-fibre mixtures with different compositions at different output stations in the decortication process are the biggest proportion of these by-products. These mixtures represent 50-60 mass-% of the total input material hemp straw (FNR, 2008).

Some of the biggest hemp producers are in Europe (approx. 8,000 ha year$^{-1}$ 2011), Canada (approx. 16,000 ha year$^{-1}$ 2011) and China (more than 80,000 ha year$^{-1}$ 2008) (Müssig, 2010; Kruse, 2012). Especially in Canada hemp is mainly cultivated for seed production. Therefore, the straw is available at reduced raw material prices for industrial applications if adequate processing technologies are available too. For efficient operation of a fibre decortication plant these accumulating by-products must be processed in ways that it can be marketed profitable like fibres.

The natural fibres from hemp can be used for production of insulation materials and fibre fleeces. Substitution of synthetic fibres (e.g. glass fibre) in composite materials by natural fibres, yet maintaining similar properties of the composite, is also considered feasible (Graupner & Müssig, 2009).

The shives have a stable market for application as animal bedding materials for pets and horses. Besides that, cleaned, high quality shives for particle boards are increasingly interesting as partial or complete substitution for shavings in the wood based panel industry. The high quality requirements of the wood based panel and composites industry regarding shives and fibres could only be met, if fibres can be effectively recovered from the material mixtures, and shives are cleaned properly from dust. Only two systems are currently available for cleaning of shives in fibre processing plants. These are either large screen drums or mixing shafts with fixed bars that turn the material undefined with high speed and transported it over a screen surface. These machines are primary developed for operation in a long fibre processing lines. Using these cleaning systems for processing of shive-fibre mixtures is connected to substantial modification of the machine design or high investment costs. However, a satisfactory cleaning result can often not be achieved.

In recent years, intensive research has been done in development of efficient technologies for fibre and shive cleaning (Fürll et al., 2008; Pecenka, 2008) at the Leibniz Institute for Agricultural Engineering Potsdam-Bornim (ATB). As a result of researching different processes for shive cleaning, a new variant has been developed, registered for patent (Fürll et al., 2010), and successfully tested under lab conditions (Fürll et al., 2008).

The biggest problems opposing a reliable separation of shive-fibre mixtures into its main components were shive locking in fibre flakes, partly entanglement, as well solid connections with fibres. Opening of fibre fluffs can only be achieved by an active mechanical intervention. This could be realized by using a paddle screw. Combining a paddle screw with a mesh strainer constitutes an effective separation system for cleaning of shive-fibre mixtures. In Fig. 1 the movement paths of the particles at the paddle as well as the respective material flows are schematically shown. The shive-fibre mixture is reliable separated into its main components by three different movement types. Thus, shives can pass the mesh strainer and fibres are moved over the screen in axial direction. Dust and ultra-short fibres are caught from the exhaust air on the top of the machine, transverse to the axial direction of the mass flow as well.

Based on this new technology a test plant for processing of shive-fibre mixtures was build and tested under practice conditions in an industrially operating fibre decortication plant.

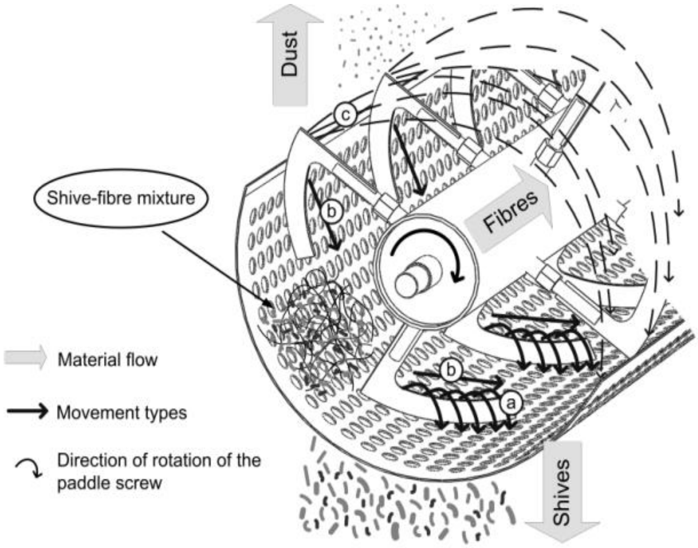


**Figure 1.** Material flow and straining process of a shive-fibre mixture in the cleaning system: a) flow over the paddle; b) flow along the paddle; c) dropping from paddle.

## MATERIALS AND METHODS

Different types of hemp straw (from slightly retted to strongly retted) were used for the screening experiments. Fig. 2 shows the typical shive-fibre mixture and the mass ratio of different particle fractions after screening. Generally, the mixture consists of dust, shives and fibres. The shive-fibre mixtures were produced in a fibre decortication plant, which is working with a hammer mill. Usually, in high capacity fibre decortication plants, hammer mills or sifter mills are used for the decortication of straw - the core process of the whole processing line (Munder et al., 2004).

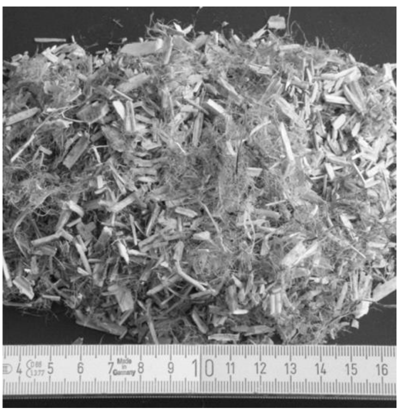

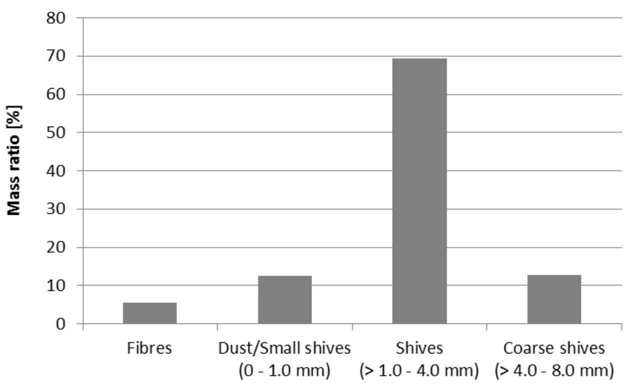


**Figure 2.** Shive-fibre mixture produced in a decortication plant by using a hammer mill.

The test plant and the experimental setup are shown in Fig. 3. The diameter of the used paddle screw is 1 m. The installed mesh types and the different screen lengths are shown in Table 1. The perforation of the sieves used was adjusted according to current market demands of purified shives. Depending on the particular end use there are the size range of shives or the remaining amount of dust and fibers in the purified shives of essential importance (OENORM S 1030:2008-01-01). The drive shaft of the paddle screw is separated into two parts. With this design parameter it is possible to use two different speeds ($n_1$, $n_2$) of the drive shaft at the same time. In the first part of the machine the loose shives are screened along sieve 1 & 2 at a slow shaft speed $n_1$. At a higher speed $n_2$ in the second part of the machine (sieve 3) the form-locking of the fibre flocks can be broken and the remained shives can be separated as well. At the end of the screen, clean and almost shive free short fibres can be recovered.

Under the strainer plate 21 boxes are installed to collect the material, which pass through the sieve. The first 20 boxes have a width of 0.3 m. That means, the whole strainer plate is 6 m. The last box is for collecting of recovered fibres. With this experimental setup it is possible to measure the mass ratio, which is passing through the sieve along the strainer plate.

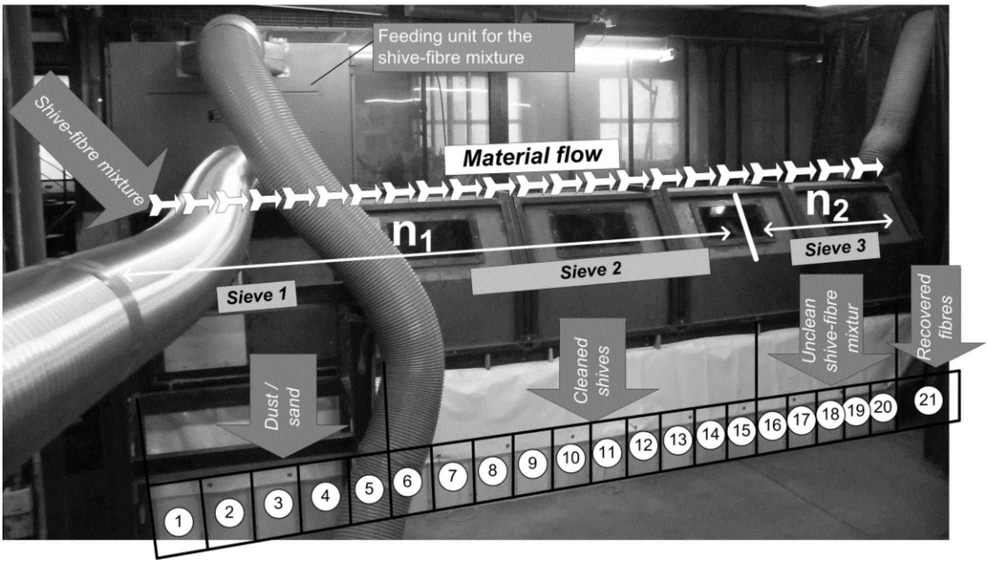


**Figure 3.** Experimental setup for cleaning of shive-fibre mixtures with a paddle screw over a sieve.

**Table 1.** Types of sieves used in the cleaning system (RMIG GmbH, 2010/2011)

| Description | ISO 7806:1983-12 | Perforation | Mesh aperture (mm) | Free space (mm) | Length (m) |
|---|---|---|---|---|---|
| Sieve 1 | Rv 1.1–2 | Round holes | 1.10 | 27.44 | 1.50 |
| Sieve 2 | Qg 10–12 | Square holes | 10.00 | 69.44 | 3.00 |
| Sieve 3 | Qg 20–25 | Square holes | 20.00 | 64.00 | 1.50 |

Fig. 4 shows the installed paddle auger and the used mesh types after a test run. The paddles are fixed with clamps at the drive shaft. The paddles are connected to the clamps with a screw thread. There is the possibility to fixe two paddles on each clamp. With this variability is it possible to define different paddle arrangements as well as different gradients of the paddle screw. Several different arrangements have been realised for the investigation of the screening behaviour of shive-fibre mixtures with this novel cleaning machine. Machine settings and operation parameters have been determined on the basis of a theoretical analysis and a model of the cleaning process has been developed as shown in the next chapter.

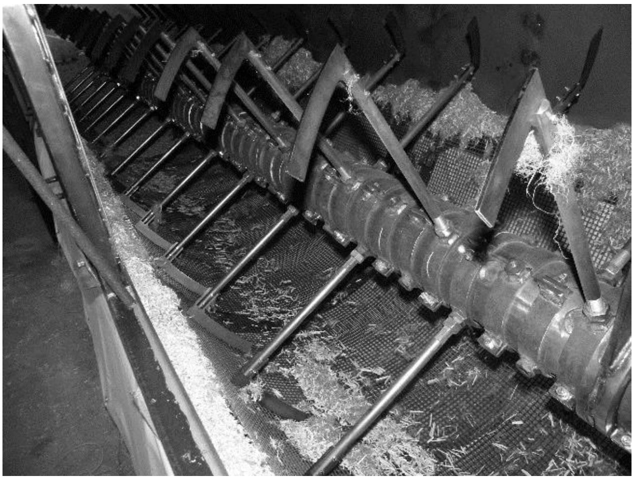

**Figure 4.** View inside of the cleaning system with the installed paddle arrangement.

**Theory and modelling**

Three different kinds of paddle arrangements have been investigated in practice experiments. The following variables can be used to describe exactly the differences in the paddle screw arrangements:

G – pitch;
a – intervention-wide of a paddle;
$\delta$ – angle distance between two successive paddles;
$\alpha$ – gradient of the paddle;
u – complete paddle screw rotation;
s – distance in the axial direction;
$\varphi$ – transit angle of the paddle screw.

First basic setup (S1) that has been investigated is the so called ‘trailing configuration’ (Fig. 5) with an angle $\delta$ of 90°. The material needs one complete rotation of the paddle screw to be transported over the distance of one G with this setting.

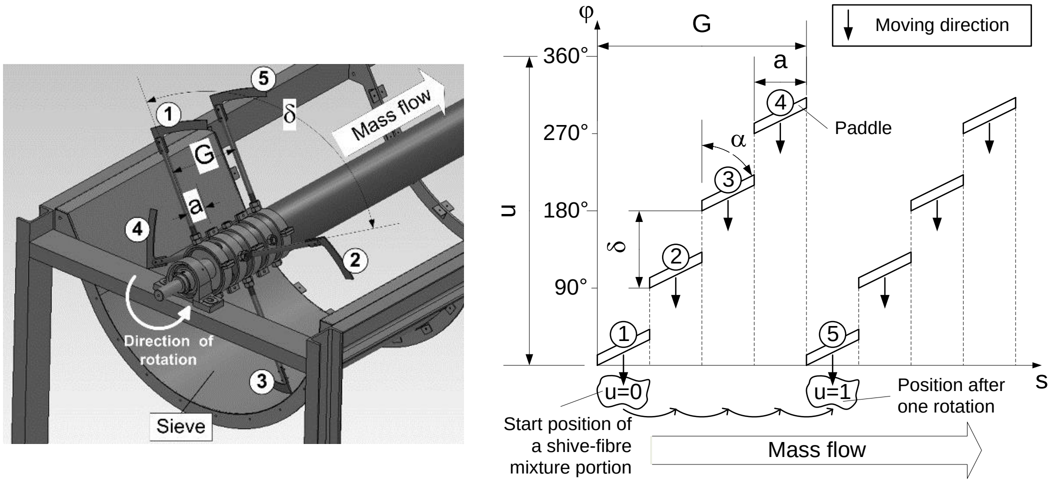


**Figure 5.** Installed paddles in the trailing configuration (left) and schematic drawing of material transport (right).

Second setup (S2) is the 'in-front configuration' with an angle δ of 270° (Fig. 6). There is also a distance of 90° between two paddles, but in backwards direction. In comparison to the trailing configuration, the material needs to be transported over the distance of one G three rotations of the paddle screw.

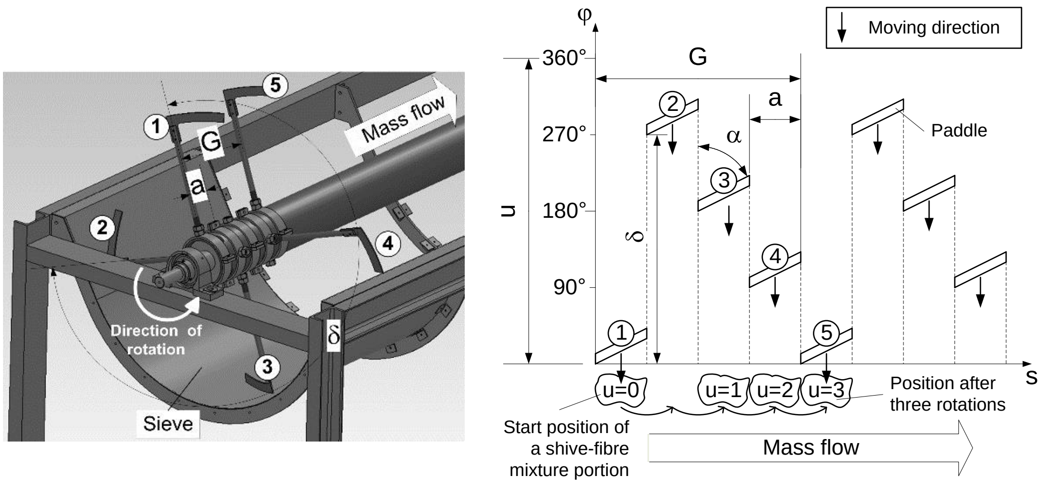


**Figure 6.** Installed paddles in the in-front configuration (left) and schematic drawing of material transport (right).

The third solution is a paddle screw with double-paddle numbers (setup S3, Fig. 7). This paddle arrangement is working like the trailing configuration, but with the doubled mass flow. That means, without changing the speed of the paddle screw more material can be transported in axial direction.

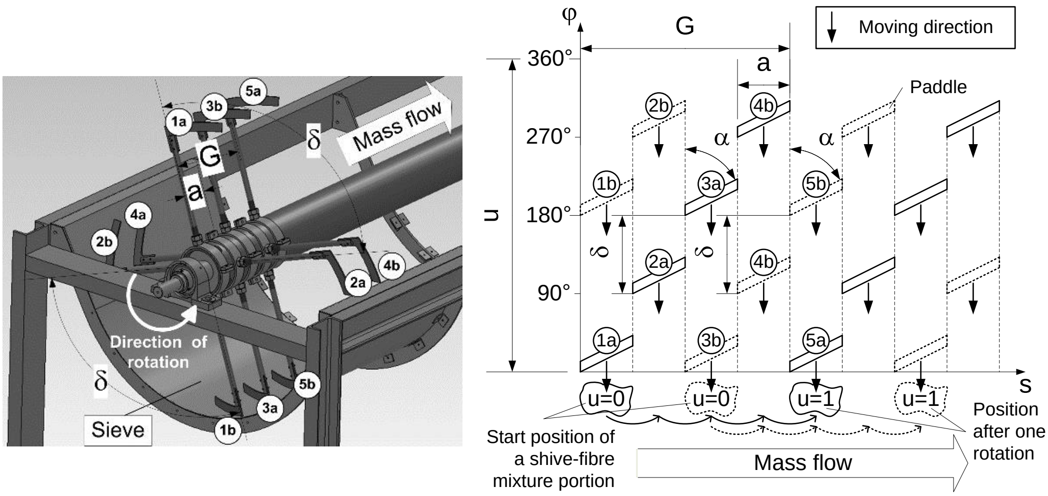


**Figure 7.** Installed paddles in the double-paddle numbers configuration (left) and schematic drawing of material transport (right).

The relation between material transport in axial direction and the parameters of the paddle screw in dependence to the numbers of rotations is shown in equation 1.

$$s_a = u \cdot \frac{G}{i} \cdot \frac{360°}{\delta} \tag{1}$$

where: $s_a$ – covered distance in axial direction; $u$ – number of complete paddle screw rotations; $G$ – pitch of the paddle screw; $i$ – numbers of paddles for one pitch; $\delta$ – angle distance between two successive paddles.

The relation between the velocity of material transport in axial direction in dependence to the drive shaft speed can be described by equation 2.

$$v_a = n \cdot \frac{G}{i} \cdot \frac{360°}{\delta} \tag{2}$$

where: $v_a$ – velocity of material flow in axial direction; $n$ – rotation speed of the paddle screw.

## RESULTS AND DISCUSSION

At first, the influence of the three different paddle screw setups on the separation of shive from fibres along the screen length should be investigated. Therefore, the input mass flow should be kept constant by the feeding system. This was not always possible and the realised mass flows varied between 2.42 t $h^{-1}$ and 3.16 t $h^{-1}$. Despite of these technical feeding problems typical differences in the screening efficiency could be clearly shown (Fig. 8). Setup S2 (In-front configuration) showed the best separation of shives along the shive screening section (screen 2). The disadvantage of this setting was that fibres haven't been transported over the screen at the required rotation speed of the paddle screw. Only at very high rotations speeds a reliable transport of fibres could be realised. Hence, the required gentle transport of shive-fibre mixtures through the cleaning machine is not possible at this paddle setup. Therefore, further investigations focused on the setups S1 and S3 only.

Despite a higher mass flow, the setup with the double number of paddles (S3) showed in comparison to the trailing configuration (S1) a better screening effect. The reason for this is seen in the higher number of paddles pushing the material over the screen.

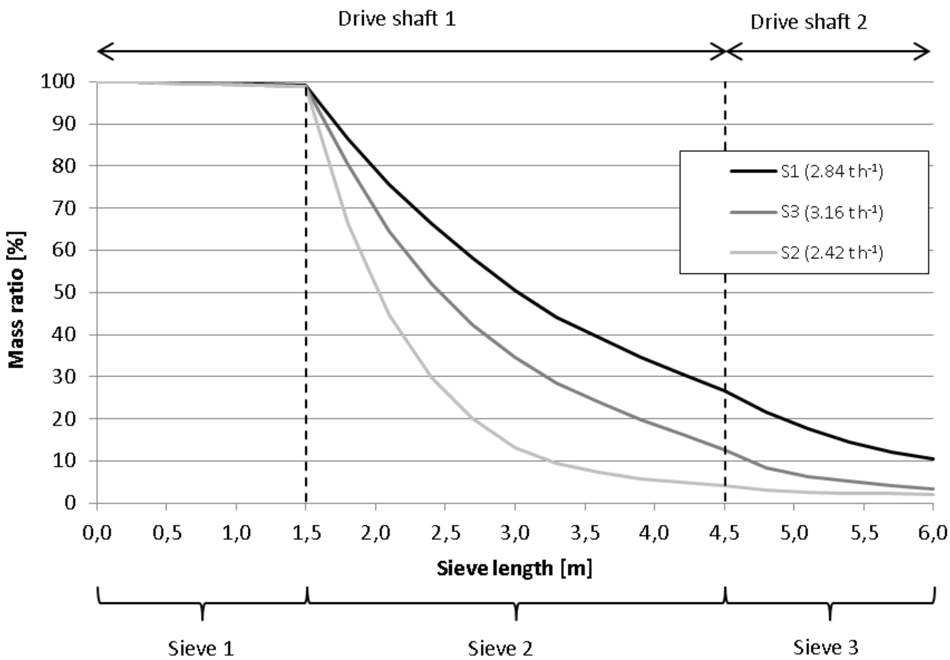


**Figure 8.** Sieving curve along the strainer plate with a rotation speed of 60 $min^{-1}$ for drive shaft 1 and three different paddle arangements.

In a next step, the dependence between paddle setup and input mass flow has been investigated. The rotation speed of the paddle screw has been kept constant for this purpose. At the same time, the mass flow has been increase at the feeder. An increase of the mass flow leaded to an impairment of the screening efficiency along shive sieve 2 for both paddle setups (S1 and S3). Furthermore, in all test the setup S3 showed the same screening quality as setup S1 but at doubled mass flow. Herby, the model assumptions regarding influence of the paddle setup on the mass flow could be confirmed.

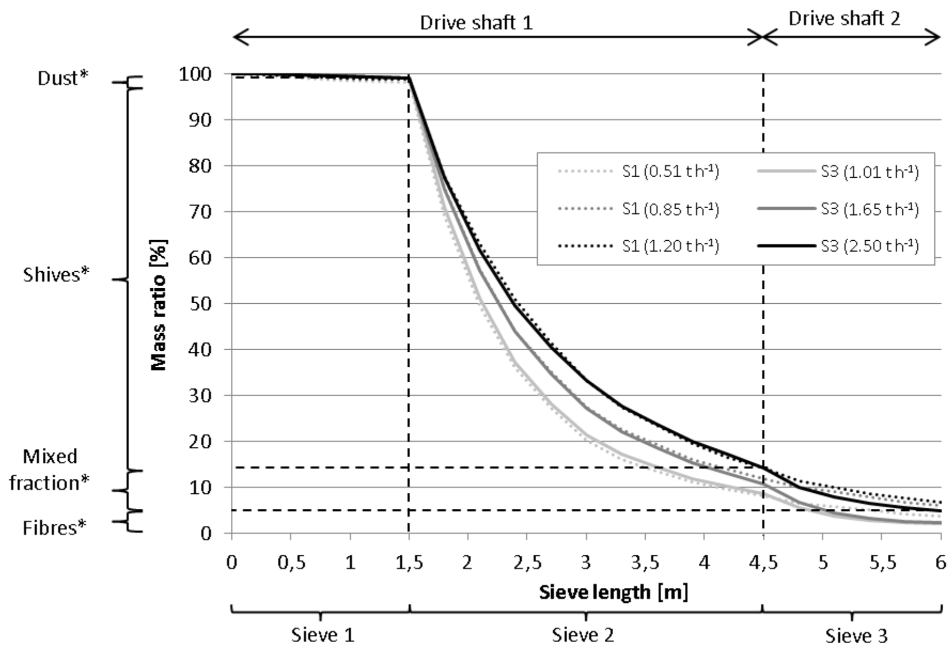


**Figure 9.** Sieving curve along the strainer plate depending of two paddle arangements and different mass flows.
*Mass ratios of the end products after the cleaning with the double-paddle numbers configuration and a mass flow of 2.50 t $h^{-1}$.

The influence of different rotation speeds of paddle screw 1 on the mass ratios of fractions of the three end products shives, a mixed fraction with fibres and dust is shown in Fig. 10. With an increase of the rotations speed the ratio of separated dust and clean shives declines. As a result, the ratio of the unclean mixed fraction and of recovered fibres increases. Due to the fact, that the cleaning effect of the paddle screw 2 working in the section of sieve 3 is not considered in this presentation, both fractions can be summarized. The important supplementary cleaning effect of paddle screw two on the end products cannot be shown in Fig. 10.

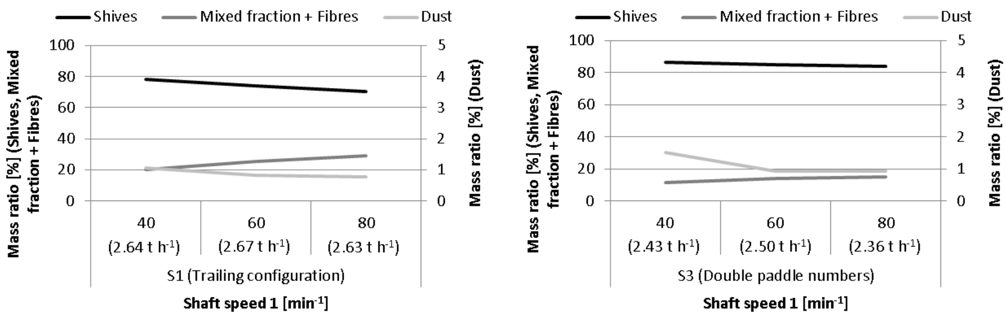


**Figure 10.** Mass ratios of end products depending of the rotation speed of shaft 1.

Finally, mass ratios of end products after processing in the novel cleaning machine have been determined using different types of hemp straw to provide basic information about the performance of the new cleaning concept. Representative results of all tests are compiled in Table 2.

**Table 2.** Cleaning results of a shive-fibre mixture after prior straw processed in a hammer mill and followed by a step cleaner

| End products | Mass ratio (%) |
|---|---|
| Dust | 1.0–5.0 |
| Shives | 80.0–90.0* |
| Mixed fraction | 5.0–10.0 |
| Fibres | 3.0–5.0 |
| Dust suction | 0.1–0.2 |

*almost free of dust and less than 0.7 mass-% short fibres in the cleaned shives.

## CONCLUSIONS AND OUTLOOK

The experiments with the novel cleaning technology have shown that the developed machine concept has the potential to clean shive-fibre mixtures in a single machine. On the basis of this concept a machine design has been developed fitting to modern powerful fibre processing lines using hammer mills for decortication of hemp straw (Fig. 11). For the industrial machine solution three hoppers and a suction pipe have been installed under the sieve for collecting the main outputs: dust, shives, mixed fraction and fibres. Furthermore, a suction pipe for the discharge of dust polluted air has been installed above sieve 2. It has been shown, that with this machine mass flows up to 2.5 t $h^{-1}$ can be reliable processed to clean, dust free shives as well as quality fibres can be recovered at the same process step. This mass flow corresponds to a throughput of 4 t $h^{-1}$ of hemp straw for the whole processing plant if a ratio of 60 mass-% of shive-fibre mixtures is assumed for the decorticated straw.

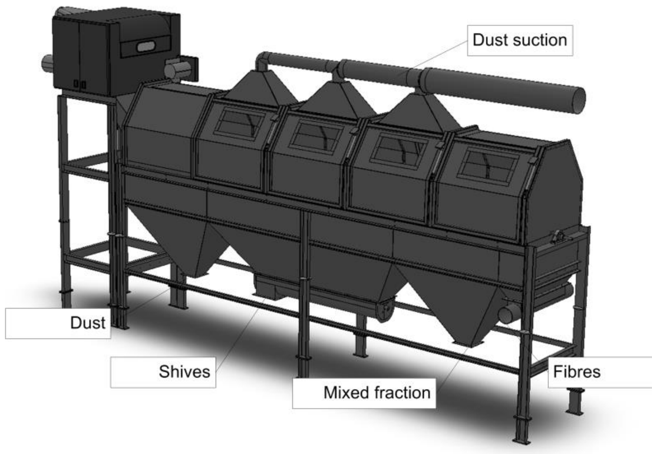


**Figure 11.** Machine concept for cleaning of shive-fibre mixtures in axial flow.

## REFERENCES

FNR. 2008. Studie zur Markt- und Konkurrenzsituation bei Naturfasern und Naturfaserwerkstoffen (Deutschland und EU). *Gülzower Fachgespräche*, Bd. **26**, Gülzow.

Francken-Welz, H. v. & Léon, J. 2003. *Faserqualität einheimischer Faserpflanzen (Hanf) – Bewertung von Rohstoff und Endprodukt-*. Landwirtschaftliche Fakultät der Rheinischen Friedrich-Wilhelms-Universität, Bonn.

Fürll, C., Pecenka, R. & Bojdzinski, B. 2008. The Potsdam-Bornim plant for separation of natural fibre with a new technology for cleaning and sizing of shives. *International Conference on Flax and other Bast Fibres.* Saskatoon, pp. 40–46.

Fürll, C., Pecenka, R. & Bojdzinski, B. 2010. EP2145988.

Graupner, N. & Müssig, J. 2009. Man-Made Cellulose Fibres as Reinforcement for Poly(lactic acid) (PLA) Composites. *Journal of Biobased Materials and Bioenergy* **3**, 249–261. http://dx.doi.org/10.1166/jbmb.2009.1032

Höppner, F. & Menge-Hartmann, U. 2000. Cultivation strategies of hemp for the use of fibres and oil. *Bioresource Hemp.* Wolfsburg.

ISO 7806:1983-12. *Industrial plate screens – Codification for designating perforations.*

Kruse, D. 2012. New Data on Hemp Food Market. *9th International Conference of the European Industrial Hemp Association (EIHA).* Wesseling.

Munder, F., Fürll, C. & Hempel, H. 2004. Results of an Advanced Technology for Decortication of Hemp, Flax and Linseed. *Molecular Crystals and Liquid Crystals* **418**(1), 165–179. http://dx.doi.org/10.1080/15421400490479253

Müssig, J. 2010. *Industrial Application of Natural Fibres: Structure, Properties and Technical Applications.* John Wiley & Sons, Ltd, Chichester, West Sussex, 75–pp. http://dx.doi.org/10.1002/9780470660324

OENORM S 1030:2008-01-01. *Animal bedding from renewable raw materials – Requirements, test specifications and classification.*

Pecenka, R. 2008. *Optimieren der Reinigung von Hanffasern auf Kammschütteln. Dissertation.* Brandenburgische Technische Universität, Cottbus.

RMIG GmbH 2010/2011. *Produkt und Leistungsübersicht. Catalogue.* FIBO Druck- und Verlags GmbH, Neuried.

*Agronomy Research* **13**(1), 141–147, 2015

# The effect of genotype on table grapes soluble solids content

M. Maante*, E. Vool, R. Rätsep and K. Karp

Department of Horticulture, Institute of Agricultural and Environmental Sciences, Estonian University of Life Sciences, Kreutzwaldi 64, EE51014 Tartu, Estonia;
*Correspondence: mariana.maante@student.emu.ee

**Abstract.** Sugar concentration in fresh consumed table grapes is mainly connected with technological maturity and primarily expressed by soluble solids content. The EU Regulation has laid down maturity requirements for *Vitis vinifera* L. cultivars (OJ L 157, 15.6.2011). The lowest allowed soluble solids content is 13 °Brix for seeded cultivars and 14 °Brix for seedless cultivars. In cool climate there are mainly cultivated grape hybrid cultivars which refractometric index is not regulated with this regulation. The aim of the present experiment was to investigate the accumulation dynamics and content of soluble solids from the beginning of veraison to harvest in table grapes with protected cultivation condition. The research was conducted with 3 black ('Osella', 'Kosmonavt', 'Mars'), 3 red ('Swenson Red', 'Somerset Seedless', 'Canadice') and 2 white ('Arkadia', 'Supaga') vine cultivars in 2013 and 2014. The results of the study indicated, that fruits of all table grape cultivars achieved the minimum content of soluble solids required for table grapes. Two years mean of soluble solids content varied among black, red and white grape cultivars respectively from 15.0 to 22.1 °Brix, from 15.6 to 22.5 °Brix and from 13.9 to 18.9 °Brix. The highest soluble solids content was observed in both years among black cultivars in Osella, among red cultivars in Somerset Seedless and among white in Supaga.

**Key words:** Brix, *Vitis* sp., hybrid cultivars.

## INTRODUCTION

The grapes (*Vitis* sp.) are used for making wine, raisin and for fresh consumption, intended for table use. In Europe traditional grape growing region lies between 30° and 50° N (Gustafsson & Mårtensson, 2005). But in spite of the harsh climate grapes are also cultivatied in cool climate condition above 50° N. In Estonia grapes are cultivated in open field contitions and protected areas. Table grapes for commercial consumption are mainly grown on protected areas because in northen countries there is a problem with late spring and early autumn frost. Protected cultivation helps to decrease frost injuries and also helps to get earlier yield (the temperature is higher than on open field).

Grapes should not be harvested until mature, because they do not ripen after harvest (Nelson, 1985). Indicator of grape maturity is the sugar content, determined as the total soluble solids content in the berry juice and it is measured on a degree-Brix scale (Nelson, 1985). Growers mainly use it as an indicator of ripness (Muñoz-Robredo et al., 2011). For winegrowers it is the most practical parameter to look at because the sugar concentration determines the potential alchol content in the wine (Liu et al., 2006; Nogales-Bueno et al., 2014). Also table grape growers need to measure the sugar content because it is connected with grape technological maturity.

Soluble solids content depends on the cultivar and production area (Nelson, 1985). In the world there are marketing standards for table grapes cultivars grown from *V. vinifera* L. Overall rule is that table grape production cultivars are harvested with a lower level of soluble solids than wine grapes (Liu et al., 2006). In the EU minimum soluble solids content levels are given as 12 °Brix for the cultivars Alphonse Lavalleé, Cardinal and Victoria, 13 °Brix for all other seeded cultivars, and 14 °Brix for all seedless cultivars (OJ L-157 15/06/2011). These standarts are same in Afghanistan, but the minimum °Brix for the Indian markets is 16 (ETN 300, 2004). In the United States, in California and early production areas the minimum soluble solids content is 16.5 °Brix (Rees et al., 2012). According to the International Organisation Vine and Wine (OIV, 2008) tabel grapes with a Brix degree equal to or above 16 is considered as ripe. Recommended soluble solids content in red wine grapes are from 20 to 23°Brix (Schalkwyk & Archer, 2000).

Proceeding from the previous, we can set up a hypothesis: in cool climate conditions table grapes ripen and achieve desired level of soluble solids on protected area faster. The aim of the study was to determine the accumulation dynamics and content of soluble solids from the beginning of veraison to harvest in table grapes with protected cultivation condition.

## MATERIALS AND METHODS

The research was conducted with 3 black (‘Osella’, ‘Kosmonavt’, ‘Mars’), 3 red (‘Swenson Red’, ‘Somerset Seedless’, ‘Canadice’) and 2 white (‘Arkadia’, ‘Supaga’) vine hybrid cultivars in 2013 and 2014. The berry samples were collected from the protected cultivation area in West-Estonia at Lüüste village (58° 37′ 42″ N, 25° 8′ 17″ E). The grapevines were propagated *in vitro* and grown as own-rooted. The protected cultivation vineyard plastic tunnels 45 m in length, 8 m in width and 4 m in height were used. The protected area was covered with 0.18 thick UV stable low density polyethylene, at the end of April. Vines were planted in 2010, in 1.65 × 3.5 m spaces and trained in high double trunk trellis. White polypropylene fabric and spruce (*Picea*) branches were used as vine winter cover no additional heating system was used in plastic tunnels. The vine rows were oriented from north to south and ground covered with 0.04 mm thick black polyethylene plastic. The experimental area soil was sandy loam, $pH_{KCl}$ 5.6 and 4.5% humus content. The soil P, K, Ca and Mg content was sufficient based on vine nutrients need and no additional fertilizers were used in experimental area. The experimental design was a randomized block with 3 replicates.

On the protected cultivation, in 2013 and 2014, the air temperatures were higher than open field and many years’ means (Fig. 1). In 2013, average air temperatures on the protected cultivation and open field were respectively 21.6 °C and 17.8 °C in June, 21.1 °C and 17.5 °C in July, 18.9 °C and 16.6 °C in August, and 12.8 °C and 10.8 °C in September. In 2014, average air temperatures on the protected cultivation and open field were respectively 17.2 °C and 13.4 °C in June, 22.9 °C and 19.3 °C in July, 18.7 °C and 16.4 °C in August, and 13.1 °C and 11.1 °C in September. In June 2013 on the protected cultivation the air temperature were 4.4 °C higher and in July 1.7 °C lower than 2014. The average temperatures in Estonia in the period from 1971–2000 were respectively 15.1 °C in June, 16.9 °C in July, 15.6 °C in August and 10.4 °C in September. It appears that, in June 2014, in the open field the temperature was 1.7 °C lower than usual. Both years in August and September air temperature were similar among protected cultivation and among open field.

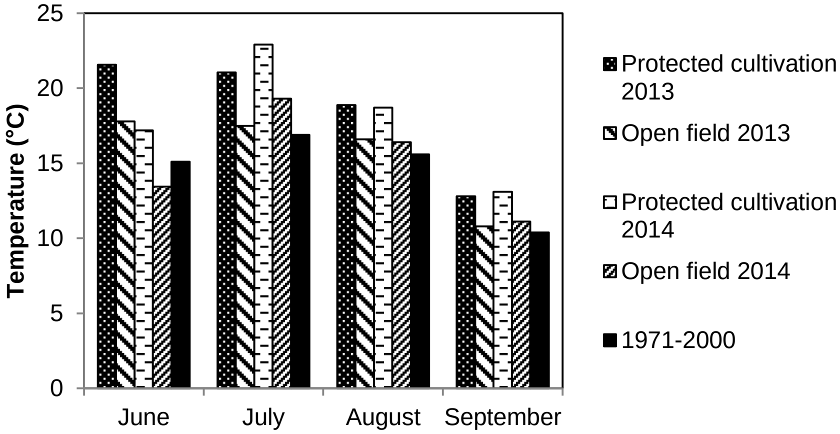


**Figure 1.** The mean air temperature in protected and open field in 2013, 2014 and the many years' means (1971–2000).

The soluble solids (SS, °Brix) measurements were carried out in 2013 from 08.08 to 20.09 and in 2014 from 7.08 to 12.09. The soluble solids content was measured from fresh berries by refractometer (Atago Pocket Refractometer Pal-1). For °Brix measurements, 30 grapes in 3 replications from the different parts of a cluster were picked and analysed.

The results of SS dynamics were tested by one-way analysis of variance. To evaluate significant influence, the least significant difference ($LSD_{0.05}$) was calculated. Different letters on figures mark significant differences at $P \leq 0.05$.

## RESULTS AND DISCUSSION

In 2013 grapes SS content varied from the beginning of veraison to harvest from 8.7 to 22.6 °Brix and received at the minimum required level of maturity (EU standards) in different times (Fig. 2). At the beginning of August SS content varied from 8.7 to 16.3 °Brix. SS content changed in August among the cultivars 0.1 to 6.2 °Brix. SS content increased the most in cultivar Kosmonavt (10.5 to 16.7 °Brix) and least in cultivar Osella (14.1 to 14.2 °Brix). At the beginning of September SS content varied 13.0 to 20.5 °Brix and the last day of harvest 15.0 to 22.6 °Brix. SS content changed in September among cultivars 1.6 to 5.6 °Brix. SS content increased the most in cultivar Canadice (3.0 to 18.6 °Brix) and least in cultivar Mars (13.4 to 15.0 °Brix).

In 2014 grapes SS content varied from the beginning of veraison to harvest from 9.0 to 19.6 °Brix and received at the minimum required level of maturity (EU standards) in different times (Fig. 3). At the beginning of August SS content varied from 9.6 to 16.1 °Brix. SS content changed in August among the cultivars 1.5 to 6.1 °Brix. SS content increased the most in cultivar Supaga (10.6 to 16.7 °Brix) and least in cultivar Kosmonavt (16.1 to 17.6 °Brix). At the beginning of September SS content varied 12.7

to 18.1 °Brix and the last day of harvest 13.9 to 18.3 °Brix. SS content changed in September among cultivars 0.2 to 0.7 °Brix.

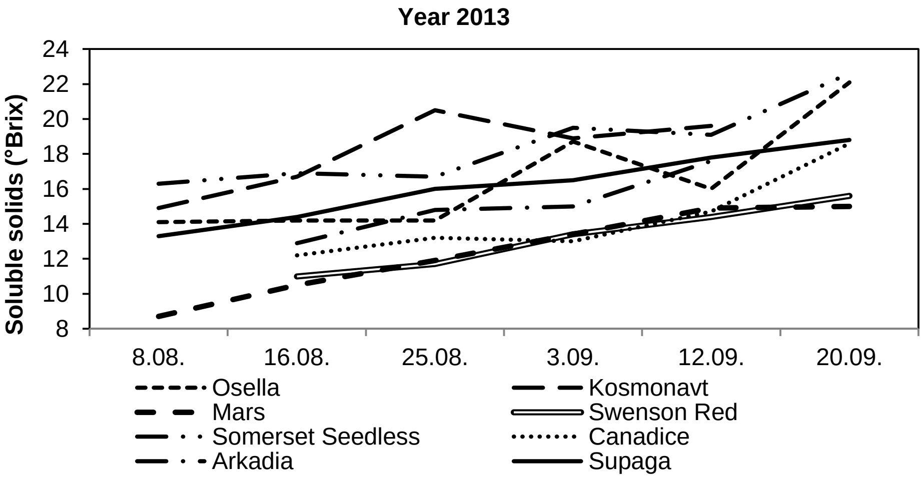


**Figure 2.** Table grape 'Osella', 'Kosmonavt', 'Mars', 'Swenson Red', 'Somerset Seedless', 'Candice', 'Arkadia' and 'Supaga' soluble solids content (°Brix) changes during the periods 08.08–20.09.2013.

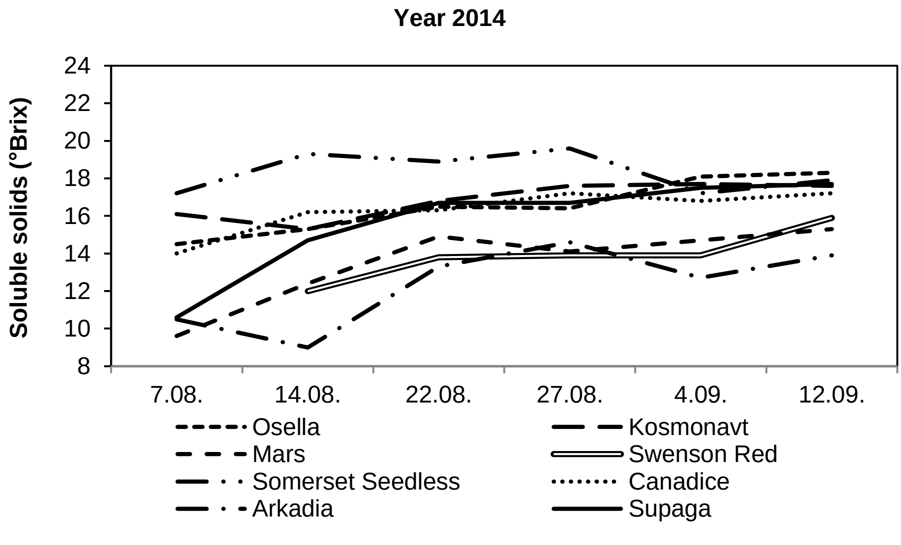


**Figure 3.** Table grape 'Osella', 'Kosmonavt', 'Mars', 'Swenson Red', 'Somerset Seedless', 'Candice', 'Arkadia' and 'Supaga' soluble solids content (°Brix) changes during the periods 7.08.–12.09.2014.

The rapid accumulation of sugars starts in grapes at the beginning of veraison and slows as maturity approaches (Bisson, 2001; Pedneault et al., 2013). It was also confirmed in our experiment. The beginning of veraison depends on the cultivar and growth conditions. The length of the veraison is 6 to 8 weeks (Plocher & Parke, 2008). For example in this experiment shorter ripening period has ‘Osella’ and ‘Kosmonavt’. In 2013 SS content in the cultivars Kosmonavt and Osella drops with some evaluation terms. It could be caused by the fact that SS content is not valuable with bare eye and collecting samples we focus on berry color. Different phenolic compounds are responsible for the grape color. It is known maximum accumulation level of sugars and phenols do not coincide (Maujean et al., 1983). Because of that into the berry samples could get some berries with lower SS content. In this experiment cultivars Mars, Swenson Red and Arkadia started to ripen later than other cultivars in both year. Earliest cultivars were Somerset Seedless, Kosmonavt and Osella. Also their SS content were highest at the end of veraison, because of longer ripening period. In 2014 grapes started to ripen earlier, this is due to higher temperatures in July. Also because of higher temperatures SS content could be reached an optimum level faster in 2014 than 2013, as demonstrated by the SS content stability in the measuring period (variation was less than in 2013).

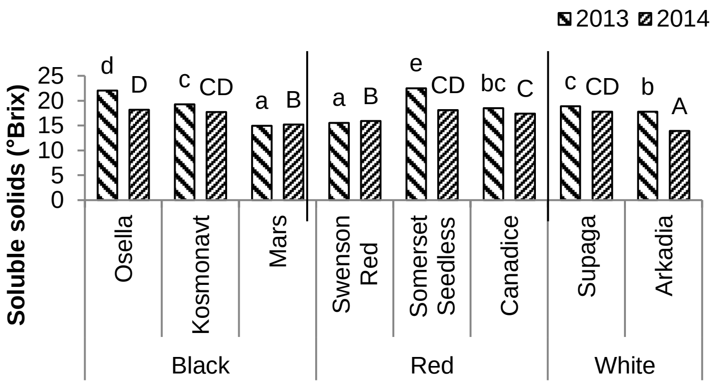


**Figure 4.** The grapes soluble solids (°Brix) content in the protected cultivation on cultivars Osella, Kosmonavt, Mars, Swenson Red, Somerset Seedless, Canadice, Supaga and Arkadia in 2013 and 2014. 2013 growing season cultivars effect PD%=0.9, 2014 growing season cultivars effect PD% = 0.8.

The content of SS ranged on the harvest from 15.0 to 22.6 °Brix in 2013 and 13.9 to 18.2 °Brix in 2014 (Fig. 4). In 2013 among black cultivars Osella had the highest value of SS (22.6 °Brix), but in both experimental year it was significantly lower in Mars (respectively 15.0 and 15.2 °Brix). Among red cultivars Somerset Seedless had the highest value of SS (22.1 °Brix) in 2013, but both experimental year it was lower in Swenson Red (respectively 15.6 and 15.9 °Brix). Among white cultivars Supaga had significantly higher values of SS in both years (respectively 18.9 and 17.8 °Brix). Year had a significant effect on table grapes SS content. In 2013 in several cultivars SS content was higher than 2014. In 2013 the harvest time was longer and because of that soluble solids accumulation period was also longer and °Brix values higher. Growing grapes on protected area we can extend the grape growing season, due to heat accumulation (Plocher & Parke, 2008). In Helsinki greenhouses accumulates 75 to 100% more heat than outdoor and because of that they can extend the growing season one month in the spring and in the autumn (Plocher & Parke, 2008). Fruits sugar concentration is higher in higher temperature conditions (Mira de de Orduńa, 2010) and it is also influenced by the genotype (Shiraishi et al., 2010). It was also confirmed in our study.

The EU Regulation provides maturity requirements for *V. vinifera* L. cultivars. The lowest allowed SS content is 13 °Brix for seeded cultivars and 14 °Brix for seedless cultivars. Compared to this requirement all our hybrid cultivars achieved these levels. But in the Nordic countries an important factor in the formation of taste are acids. Jayasena and Cameron (2008), on the Crimson Seedless cultivar, reported that the consumer acceptance increases with increasing SS content from 10 to 20 °Brix. In our experiment SS content was lowest in cultivars Mars, Swenson Red and Arkadia and highest in cultivars Osella, Kosmonavt and Somerset Seedless. Investigators of this experiment assessed better tasting cultivars Arkadia, Kosmonavt, Swenson Red and Somerset Seedless. This indicates that the taste is not determine only by SS content.

SS content differs among cultivars. For example optimum level for 'Arkadia' is find by Tairov National Research Centre for Viticulture and Winemaking 15 to 16 °Brix (Vinograd 'Arkadia', 2015), for 'Kosmonavt' is find by I.M. Filippenko 18.4 °Brix (Vinograd 'Kosmonavt', 2015), for 'Mars' find by J.N. Moore is 16 to 20 °Brix (Vinograd 'Mars', 2015) and for 'Swenson Red' find by E. Swenson is 17 to 18 °Brix (Myvinogradnik 'Swenson Red', 2015). In our experiment 'Arkadia' and 'Kosmonavt' reached that optimum level. 'Mars' and 'Swenson Red' SS content did not reach to optimum level, because they started to ripen later.

## CONCLUSIONS

The study results indicates that soluble solids content in table grapes on protected area depends on the beginning of ripening on the cultivar and temperature. SS content was highest in cultivars Osella, Kosmonavt and Somerset Seedless. For growers it means that planning table grapes harvesting time they need to take into account temperature and cultivar ripening time.

ACKNOWLEDGMENTS. This research was supported by Estonian Science Foundation Grant No. 9363.

## REFERENCES

Bisson, L. 2001. In search of optimal grape maturity. *Practical Winery Vineyard*, July/Aug 32–43.

ETN 003. 2004. Afghan Grapes: Grading for Quality. *http://afghanag.ucdavis.edu/a_horticulture/fruits-trees/grapes/fact-sheetsgrapes/ExtensionToolkitNotes3_GradingforQuality.pdf.pdf/view*. Accessed 21.01.2015

Gustafsson, J-G., Mårtensson, A. 2005: Review article: Potential for extending Scandinavian wine cultivation. *Acta Agriculturae Scandinavica, Section B – Soil & Plant Science* **55**, 82–97.

Jayasena, V., Cameron, I. 2008. °Brix/acid ratio as a predictor of consumer acceptability of Crimson Seedless table grapes. *Journal of Food Quality* **31**, 736–750.

Liu, H-F., Wu, B-H., Fan, P-G., Li, S-H., Li, L-S. 2006. Sugar and acid concentration in 98 grape cultivars analyzed by principal component analysis. *Science of Food and Agriculture* **86**, 1526–1536.

Maujean, A., Brun, O., Vesselle, G., Bureau, G., Boucher, J.M., Cousin, M., Feuillat, M. 1983. Investigations on grapevine maturation in the Champagne region: method of forecasting the harvesting date. *Vitis* **22**, 137–150.

Mira de Orduńa, R. 2010. Climate change associated effects on grape and wine quality and production. *Food Research International* **43**, 1844–1855.

Muñoz-Robredo, P., Robledo, P., Manriques, D., Molina, R., Defilippi, B.G. 2011. Characterization of sugars and organic acids in commercial varieties of table grapes. *Chilean Journal of Agricultural Research* **71**, 452–458.

Myvinogradnik ‘Swenson Red’. *http://myvinogradnik.ru/sorta-vinograda/s/svenson-red/*. Accessed 30.01.2015.

Nelson, K.E. 1985. *Harvesting and handling California table grapes for market.* Second Edition, UCANR Publications, 67 pp.

Nogales-Bueno, J., Hernándes-Hierro, J.M., Rodrigues-Pulido, F.J. 2014. Determination of technological maturity of grapes and total phenolic compounds of grapes skins in red and white cultivars during ripening by near infrared hyperspectral image: A preliminary approach. *Food Chemistry* **152**, 586–591.

OIV. 2008. Resolution VITI 1/2008. OIV Standard on Minimum Maturity Requirements for Table Grapes. Organisation Internationale de la Vigne et du Vin, Paris. *ftp://ftp.fao.org/codex/meetings/cac/cac36/if36_05e.pdf.* Accessed 21.01.2015

OJ L-157 15/06/2011. Marketing standards for fresh fruits and vegetables. *http://exporthelp.europa.eu/update/requirements/ehir_eu13_02v001/eu/auxi/eu_mktfrveg_annex1b_r543_2011_grapes.pdf*. Accessed 10.12.2014

Pedneault, K., Dorais, M., Angers, P. 2013. Flavor of cold-hardy grapes: impact of berry maturity and environmental conditions. *Agricultural and Food Chemistry* **61**, 10418–10438.

Plocher, T., Parke, B. 2008. *Growing grapes and making wine in cool climate*. Second Edition, Northern Winework, 208 pp.

Rees, D., Farrell, G., Orchard, J. 2012. *Crop Post-Harvest: Science and Technology, Perishables.* John Wiley & Sons, 480 pp.

Schalkwyk, H., Archer, E. 2000. Determining optimum ripeness in wine grapes. *Wineland* **130**, 90–91.

Shiraishi, M., Fujishima, H., Chijiwa, H. 2010. Evaluation of table grape genetic resources for sugar, organic acid, and amino acid composition of berries. *Euphytica* **174**, 1–13.

Vinograd ‘Arkadia’. *http://vinograd.info/sorta/stolovye/arkadiya.html*. Accessed 30.01.2015.

Vinograd ‘Kosmonavt’. *http://vinograd.info/sorta/stolovye/kosmonavt.html*. Accessed 30.01.2015.

Vinograd ‘Mars’. *http://vinograd.info/sorta/bessemyannye/mars.html*. Accessed 30.01.2015.

*Agronomy Research* **13**(1), 148–157, 2015

# Theoretical research into the frictional slipping of wheel-type undercarriage taking into account the limitation of their impact on the soil

V. Nadykto[1], M. Arak[2] and J. Olt[2,*]

[1]Tavria State Agrotechnological University, Khmelnytskoho pr. 18, Melitopol, 72312 Zaporozhye region, Ukraine
[2]Estonian University of Life Sciences, Institute of Technology, 56 Kreutzwaldi, EE51014 Tartu, Estonia; [*]Correspondence: jyri.olt@emu.ee

**Abstract.** The frictional slipping of the tractor's wheels causes great damage to the soil fertility. To ensure the minimal disturbance of its structure, it has been proposed to determine the maximum slippage of driving wheels taking into account the value of their permissible pressure on the soil in the horizontal plane. As a result, it has been established that for the substantial reduction of the soil structural damage during the spring agricultural field operations the maximum permissible frictional sliding $\delta_{max}$ of the wheel-type undercarriage of tractors classified into drawbar pull categories 5, 3 and 1.4 (drawbar pull based classification approach is used in Ukraine and some other countries) has to be equal to 15%, 12% and 9% respectively. In the summer/autumn period, the values $\delta_{max}$ can be greater and, accordingly, be equal to 20%, 16% and 13%. Wheeled tractors in drawbar pull category 5 equipped with single standard tyres can be used for field operations only in the summer/autumn period. For their operation in spring they must certainly be equipped with twin tyres. The implementation of this design solution is appropriate for all wheeled tractors.

**Key words:** agricultural engineering, tractor, undercarriage, driving wheel, tyre, drawbar pull category, slipping.

## INTRODUCTION

The slipping of the driving wheels of a wheeled tractor and power unit is known not only to cause the increased fuel consumption (Abraham et al., 2014) and tyre wear, but also to destroy substantially the structure of soil (Lang & Huder, 1985; Molari et al., 2012). This process is associated with the crushing and shearing deformations caused by the pressure on the soil of the sidewall of the currently rearmost ground lug on the wheel contacting the soil (Chyba et al., 2013; Chyba et al., 2014; Kutkov, 2014).

It should be noted that the crushing deformation of soil renders the active organic matter (or humus) inactive. In this process, the former is partially released in the form of separate thin films and partially remains on the separate mechanical elements of the destroyed clump of soil (Gudehus, 1981). The said thin films pass into the category of inactive humus, and no methods of reviving its properties are currently known to agrarian scientists. Moreover, soil shearing is accompanied by the sliding of ground lugs on the bearing surface, which results in the pulverisation of the soil medium up to erosion hazardous condition. Eventually, all these processes to a significant extent inhibit the process of development of various cultivated agricultural plants (Braunack et al., 2006; Kuht et al, 2012; Arvidsson & Hakansson, 2014).

Overall, the greater is the slipping of the undercarriage of the tractor and power unit, the more intensive is the process of soil structure destruction (Komandi, 2006; Schreiber & Kutzbach, 2008). At the same time, the smaller slipping rate translates into the smaller value of the tangential tractive force delivered by the wheel. According to the studies, the maximum value of this force is reached, when the undercarriage of the tractor operate with a frictional sliding rate of 22…24% (Guskov et al., 1988). Which, we believe, significantly exceeds the level that could be admissible in terms of the impact produced by the wheel on the soil structure.

This indicates the need to find the following compromise: the slipping rate limit for the wheel-type undercarriage must be set at such a level that at the minimum permissible degradation of soil structure the maximum possible tangential tractive force is delivered.

## MATERIALS AND METHODS

The problem with solving this task lies in the fact that at the moment any limitations of the pressure applied by the propelling units of tractor and power units to the soil in the horizontal plane stipulated by the agronomical requirements are absent.

At the same time, such limitations exist for the deformation of cultivated land by the undercarriage of tractor and mobile power units in the vertical plane. Namely, at the moment, for example, the following standard is in effect in Ukraine: DSTU 4521:2006 'Mobile agricultural machinery. Standard rates of impact on soil by undercarriage'. This standard stipulates the rates of permissible maximum pressure applied by the undercarriage of tractor and power units to the soil $[Q_{max}]$ depending on the latter's particle-size distribution and humidity as well as the timing of agricultural work in various edaphic-climatic zones.

If we assume a priori that the process of inhibition of the growth of plants does not depend on the choice of the plane, in which the soil structure is destroyed – be it the vertical or horizontal one – then the above-mentioned compromise can be reached by applying the following formula:

$$[Q_{max}] \geq Q_{eff}, \tag{1}$$

where $Q_{eff}$ – pressure applied by the driving wheel's ground lug to the soil in the horizontal plane (kPa).

To determine the value $Q_{eff}$, we take the following approach. The tangential tractive force $F_{tg}$ of a single wheel-type undercarriage is decomposed into two forces $P_{tg}$ (Fig. 1), each being equal to a half of force $F_{tg}$ and concentrated in its respective plane located at a distance of a quarter width of the tyre $b_t$ from the wheel's centre plane.

The generation of each of these forces can be the result of the action of one or several ground lugs. Their number $n_g$ is determined by the following formula:

$$n_g = \operatorname{int}\frac{L}{t_g}, \tag{2}$$

where: $L$ – length of the contact area between the driving wheel tyre and the soil; $t_g$ – pitch of the ground lugs on the tyre.

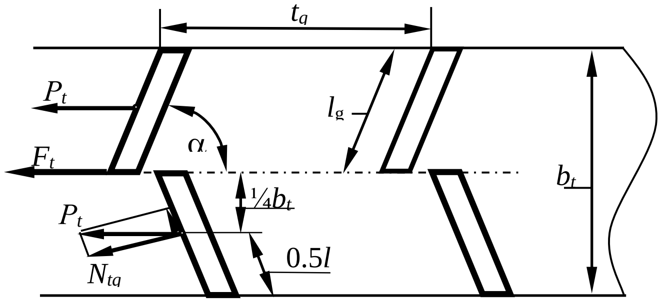


**Figure 1.** Analytical model of the forces acting on the soil via the tyre.

Each of the ground lugs in contact with the soil generates a tractive force $P_{tg}$ (Fig. 1), which, taking into account dependency (2), is equal to:

$$P_{tg} = \frac{F_{tg}}{2\operatorname{int}\frac{L}{t_g}}. \tag{3}$$

We assume a priori that the shift and shear deformations of the soil by a ground lug are produced mainly by the action of force $N_{tg}$ (Fig. 1), which, with the substitution of formula (3), can be found from the formula:

$$N_{tg} = P_{tg} \cdot \sin\alpha = \frac{F_{tg}\sin\alpha}{2\operatorname{int}\frac{L}{t_g}}, \tag{4}$$

where $\alpha$ – the angle between the centre planes of the ground lug and the wheel.

This force generates the following pressure in the horizontal plane:

$$Q_{eff} = \frac{N_{tg}}{l_g h_g}, \tag{5}$$

where $l_g$, $h_g$ – the length and height of the ground lug, respectively.

It can be concluded from Fig. 1 that:

$$l_g = b_t/(2\sin\alpha).$$

Taking into account this conclusion as well as formulae (4) and (5), requirement (1) assumes the following representation:

$$Q_{max} \geq \frac{F_{tg} \sin^2 \alpha}{2 \operatorname{int} \frac{L}{t_g} b_t h_g}. \tag{6}$$

In obtained limitation (6), the wheel-type undercarriage tangential tractive force $F_{tg}$ is an unknown quantity. To determine it's value, it is most appropriate to use the function proposed by Guskov et al. (1988):

$$F_{tg} = \frac{f_{cl} k_\tau G}{\delta L}\left[\operatorname{lnch}\frac{\delta L}{k_\tau} - f_{sup}\left(\frac{1}{\operatorname{ch}\frac{\delta L}{k_\tau}} - 1\right)\right] + 2\tau_{sh}\frac{h_g L}{t_g}, \tag{7}$$

where: $f_{sl}$ – the coefficient of sliding friction; $k_\tau$, $\tau_{sh}$ – the coefficient of deformation and rigidity modulus of the soil, respectively; $G$, $\delta$ – the vertical load on the wheel-type undercarriage and its slipping; $f_{sup}$ – the superficial friction factor.

Substituting expression of force $F_{tg}$ (7) into formula (6), we obtain a formula that provides the correlation between the slippage of the wheel-type undercarriage and the pressure exerted by it in the horizontal plane, but not in the vertical one:

$$[Q_{max}] \geq \left\{\frac{f_{sl} k_\tau G}{\delta L} \cdot \left[\operatorname{lnch}\frac{\delta L}{k_\tau} - f_{sup}\left(\frac{1}{\operatorname{ch}\frac{\delta L}{k_r}} - 1\right)\right] + 2\tau_{sh}\frac{h_g L}{t_g}\right\}\frac{\sin^2 \alpha}{\operatorname{int}\frac{L}{t_g} b_t h_g}. \tag{8}$$

Now we will analyse the components of obtained formula (8). According to Guskov et al. (1988), coefficient of soil deformation $k_\tau$ can be found with practically adequate accuracy from the formula:

$$k_\tau = 0.4 t_g. \tag{9}$$

The value of force $G$ is assumed equal to the maximum load specified for the respective tyre by standard GOST 7463-2003 'Inflated tyres for tractors and agricultural machines. Standard specifications'.

For the assessment of the length of the contact area between the tyre and the bearing surface Guskov et al. (1988) proposed the following relation:

$$L = R_w \cdot \operatorname{arctg}[(2 \cdot R_w \cdot h - h^2)^{0.5}/(R_w - h)] + (2 \cdot R_w \cdot h)^{0.5},$$

where: $R_w$ – the static radius of the wheel; $h$ – the depth of the track produced by the wheel-type propelling unit.

According to the data in (Kiss, 2003), the value of $h$ can be represented with a practically sufficient accuracy as follows:

$$h = 2 \cdot f_{roll}^2 \cdot R_w \cdot,$$

where $f_{roll}$ – coefficient of rolling resistance.

Taking this into account, after the transformations we finally obtain:

$$L = R_w \cdot \{\mathrm{arctg}[f_{roll} \cdot (1 - f_{roll}^2)^{0.5}/(0.5 - f_{roll}^2)] + 2f_{roll}^2\}. \quad (10)$$

The superficial friction factor can be found from the following function (Opeiko, 1960):

$$f_{sup} = 2.55 \cdot [(f_{st} - f_{sl}) / f_{sl}]^{0.825}, \quad (11)$$

where $f_{st}$, $f_{sl}$ – coefficients of static and sliding friction, respectively.

To calculate the values of coefficients $f_{st}$ and $f_{sl}$ we suggest using the relations obtained by means of approximating the experimental data presented in publication (Guskov et al., 1988):

$$f_{st} = 5.95 + 27.83q - 23.9\sqrt{q} \quad (12)$$

$$f_{sl} = 2.25 + 7.25q - 6.69\sqrt{q} \quad (13)$$

where

$$q = \frac{G}{b_t L} 10^{-6}. \quad (14)$$

Finally, the limiting value for the slipping rate $\delta_{max}$ of a wheel-type undercarriage taking into account that the limitation of its pressure on the soil can be obtained from the following set of equations (9), (10), (11), (12), (13), (14) and (8).
In this set of equations, the terms $G$, $t_g$, $h_g$, $b_t$, $R_w$ and $\alpha$ – design parameters of various wheel-type undercarriage. Their values are known for all tractors in any drawbar pull category. Further in our considerations we will concentrate on the following three categories: 5, 3 and 1.4[1].

Wheeled tractors and power units in lower drawbar pull categories (0.2, 0.6 and 0.9) are seldom used as parts of machine and tractor units. In the past they were considered non-system equipment, for which reason there even was no arrays of machines/implements designed for them.

Tractors in drawbar pull categories 6 and 8 achieve more or less acceptable traction and power ratings usually during the primary soil cultivation operations. But at this stage the resistance of the soil to shift and horizontal shear is significantly higher than that of the cultivated land prepared for seeding. At the same time, in work on soft soil the optimal loading of tractors of drawbar pull categories 6 and especially 8 is rather problematic. The working width of the machine and tractor unit in this case is limited not so much by the traction and power capacities of these propulsion and power units, as by the large overall widths of the applied machines/implements.

[1] For tractors in this traction category only the rear propelling units are taken into consideration

The values of the design parameters: vertical load on the wheel-type undercarriage $G$, pitch of the ground lugs on the tyre $t_g$, height of the ground lug $h_g$, width of the tyre $b_t$, static radius of the driving wheel $R_w$ and angle between the centre planes of the ground lug and the wheel $\alpha$ for the undercarriage of wheeled tractors of drawbar pull categories 5, 3 and 1.4 are assumed according to their technical specifications (Table 1).

**Table 1.** Design parameters of the undercarriage of the compared tractors and power units

| Drawbar pull category of tractor, series | Nominal size of tyre | Design parameter of undercarriage and its value | | | | | |
|---|---|---|---|---|---|---|---|
| | | $G$ (N) | $t_g$ (m) | $h_g$ (m) | $b_t$ (m) | $R_w$ (m) | $\alpha$ (deg) |
| 1.4 (MTZ-82) | 16.9R38 | 25,261 | 0.23 | 0.038 | 0.43 | 0.770 | 43 |
| 3 (KhTZ-170) | 23.1R26 | 35,807 | 0.23 | 0.045 | 0.59 | 0.715 | 47 |
| 5 (K-744) | 28.1R26 | 40,466 | 0.23 | 0.045 | 0.72 | 0.720 | 47 |

Terms $f_{roll}$ and $\tau_{sh}$ in set of equations (9, 10, 11, 12, 13, 14 and 8) represent the soil medium. The selection of their values will be based on the following considerations. According to the data in Guskov, et al. (1988), the $\tau_{sh}$ for clay loams varies within 1,260÷1,940 N m$^{-1}$, for sand loams within 1,500÷2,600 N m$^{-1}$. The estimation shows that the variation of $\tau_{sh}$ even within a range of 1,260÷2,600 N m$^{-1}$ has an effect only on the tenths in the value of the wheel-type propelling unit slipping rate. Therefore, for the further calculation we assume $\tau_{sh}$ to be equal to the mean of the range that is common for clay and sand loams: (1,500 + 1,940)/2 = 1,720 N m$^{-1}$.

As we already stressed above, the greatest shift and shear deformation occurs in soil prepared for planting, which features $f_{roll}$ = 0.16÷0.20 (Kutkov, 2014). At the same time, another sufficiently widespread type of cultivated land is broken stubble field, where the coefficient of rolling resistance varies within 0.12…0.16 (Kutkov, 2014). In light of that, for the following analysis we assume the value $f_{roll}$ = 0.16, which is common for both types of cultivated land – broken stubble field and field prepared for planting.

Finally, we have to decide on the value of $Q_{max}$. The above-mentioned DSTU 4521:2006 specifies two periods of field cultivation operations: spring and summer/autumn. We assume the first of them, when the soil is most vulnerable with regard to the deformations of shift and shear, as the basis for the following calculations. In the said period, when the structure of the cultivated land is moderately dense (0.9…1.0 g cm$^{-3}$) and its humidity is 0.4…0.5 times the minimum moisture-holding capacity, the level of permissible maximum pressure on soil of the tractor's driving gear may not exceed 160 kPa. This value of $Q_{max}$ we are going to use as the reference one.

## RESULTS AND DISCUSSION

As a result of solving set of equations (9, 10, 11, 12, 13, 14 and 8), it has been found that taking into account the limitation of the pressure on soil by a level of 160 kPa, tractors in drawbar pull categories 1.4, 3 and 5 have to comply with a slipping limit of 9%, 12% and 15%, respectively. Conceptually, this can be expressed as follows: the lower the drawbar pull category of the tractor is, the smaller the value of $\delta_{max}$ has to be.

To analyse the reached result, we will examine the relation between the slipping rate of a wheel-type undercarriage $\delta_{max}$ and those design parameters, which are used in set of equations (9), i.e. $G$, $t_g$, $h_g$, $b_t$, $R_w$ and $\alpha$. The undercarriage of the tractor of drawbar pull category 5 (series K-744) will be taken as an example.

The study of set of equations (9, 10, 11, 12, 13, 14 and 8) shows that the value of the slipping limit of the undercarriage very little depends on its radius ($R_w$, Fig. 2). Such a conclusion is due to the fact that the change of this parameter has effect only on the length of the contact area between the tyre and the bearing surface $L$. While this area, as the calculation proves, changes inessentially with the variation of wheel radius $R_w$ within the assumed range of 0.72 ± 0.04 m.

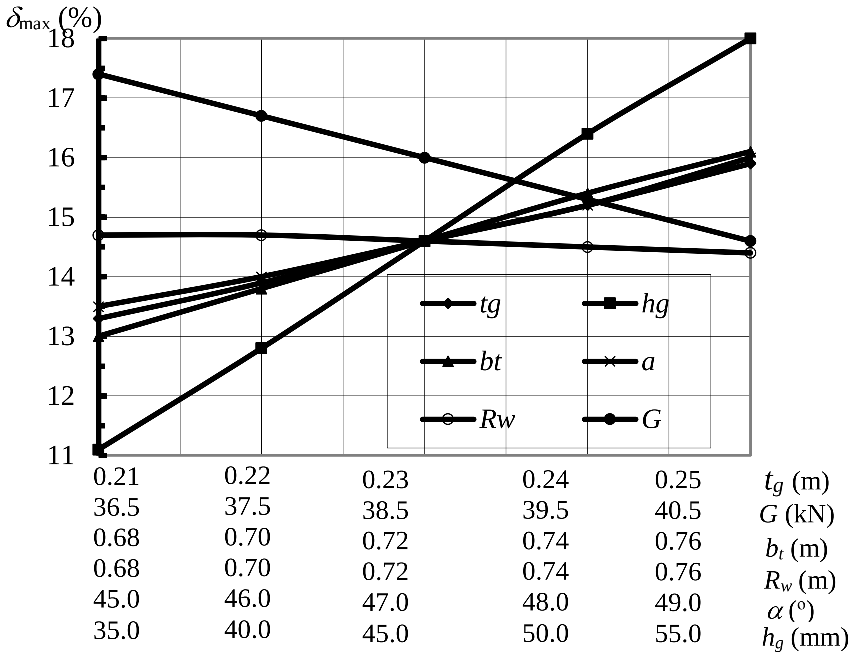


**Figure 2.** Relation between the maximum permissible frictional slipping $\delta_{max}$ of the undercarriage of a drawbar pull category 5 tractor and the wheel parameters ($G$, $t_g$, $h_g$, $b_t$, $\alpha$, $R_w$).

Increase of the undercarriages design parameters $t_g$, $b_t$ and $\alpha$ allows to set the level of its slippage limit higher (Fig. 2). At the same time, the intensity of their effect on value $\delta_{max}$ is insignificant and virtually the same.

The growth of the vertical loading $G$ of the tyre induces the reduction of the value of the undercarriages slippage limit. In principle, this effect is also fully consistent, because pursuant to relation (7) the increase of value $G$ is accompanied by the corresponding growth of the value of tangential force $F_{tg}$. Which, as formula (4) implies, results in the increase of force $N_{tg}$ and growth of the pressure applied by the ground lug's side surface to the soil (formula (5)).

The most significant influence on the value of the undercarriages slippage limit has the height of ground lug $h_g$ (Fig. 2). The greater it is, the greater $\delta_{max}$ can be and this is quite logical, since the said variation of parameter $h_g$ entails increase of the bearing surface area of the ground lug, which helps to reduce its pressure on the soil.

There is no need to consider separately how the undercarriage design parameters influence value $\delta_{max}$ in tractors of drawbar pull categories 1.4 and 3, because in essence they are similar to what has been described above.

The analysis of the values of the undercarriage design parameters of the compared propulsion and power units reveals that most significantly they differ only in two of them – the tyre width $b_t$ and the permissible vertical loading $G$ (see the Table 1). In our case at different values of the maximum vertical loading $G$ on the tyre each undercarriage exerts approximately the same pressure $q$ on the soil. For example, for tractors in drawbar pull category 5 $q$ = 210 kPa, drawbar pull category 3–230 kPa and drawbar pull category 1.4–210 kPa. Thus, there is virtually no difference between the values of $\delta_{max}$ for these tractor and power units as regards parameter $G$.

While the width $b_t$ of the undercarriage has essentially different and measurable influence on $\delta_{max}$. When it becomes smaller, the permissible slipping rate $\delta_{max}$ must also be set lower and vice versa (Fig. 3).

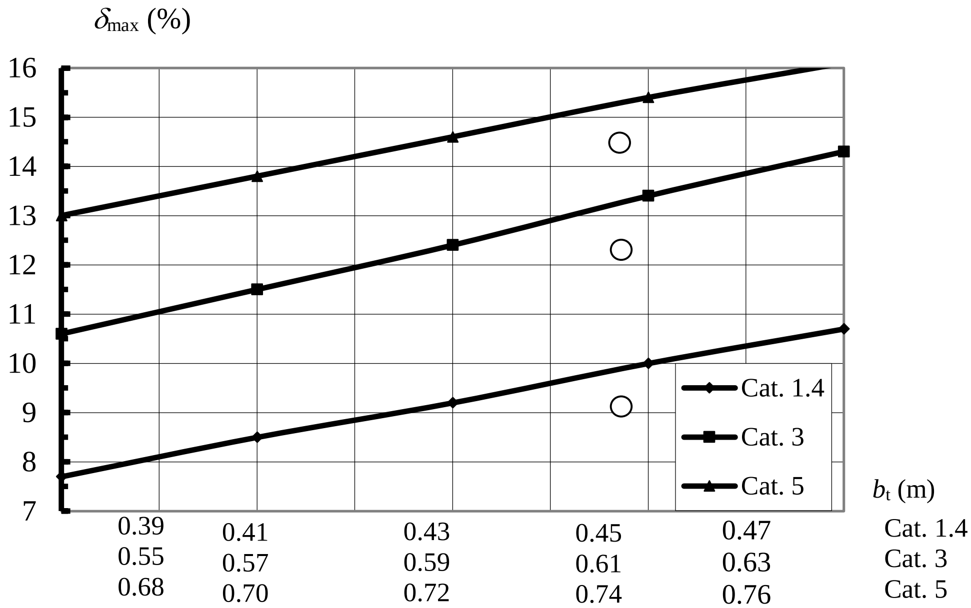


**Figure 3.** Dependence of the maximum permissible slipping $\delta_{max}$ rates of undercarriage of wheeled tractors in different drawbar pull categories on their tyre widths $b_t$.

Such a result can be explained as follows. The narrower the tyre is, the shorter its ground lug length $l_g$ is. As this, according to formula (5), results in the increase of pressure $Q_{eff}$, the undesirable probability of infringing requirement (6) increases.

The sizable difference between the tractors in drawbar pull categories 1.4; 3 and 5 as regards their undercarriage tyre widths $b_t$ is exactly what defines the result obtained above with respect to their ranking on the maximum permissible slipping rate (Fig. 3): 9%, 12% and 15%, respectively.

It should be stressed that the stated values of $\delta_{max}$ are defined at the maximum pressure $q$ of undercarriage on the soil in the vertical plane. The effective values $q_{eff}$ of this pressure are slightly lower. According to the calculations, for tractors in drawbar pull category 5 (series K-744) $q_{eff} \approx 200$ kPa, in drawbar pull category 3 (series HTZ-170) $q_{eff} \approx 160$ kPa and in drawbar pull category 1.4 (series MTZ-82) $q_{eff} \approx 100$ kPa.

From this we can conclude that with regard to the correlation between $q_{eff}$ and $Q_{max} = 160$ kPa the recommended maximum values for the undercarriage slippage hold true for tractors in drawbar pull categories 1.4 and 3.

For tractors and power units in drawbar pull category 5 $q_{eff} \approx 200$ kPa > $Q_{max} = 160$ kPa, therefore, with single standard tyres (see the Table 1) they can be used only in the summer/autumn period of field operations with the steady-state soil density of 1.2…1.3 g cm$^{-3}$ and the soil humidity at 0.4…0.5 of the minimum moisture-holding capacity. Pursuant to the requirements of DSTU 4521:2006, value $Q_{max}$ in this case may not exceed 210 kPa, while $\delta_{max}$, as our calculations show, may not exceed 20%. For tractors in drawbar pull categories 3 and 1.4 working in the summer/autumn period the maximum permissible propelling unit slipping rates are 16% and 13%, respectively.

In the spring period of field operations, tractors of drawbar pull category 5 can be used only with twin tyres installed. In this configuration their pressure on the soil is reduced almost twice. This implies that the coefficients $f_{st}$ and $f_{sl}$ increase and the superficial friction factor $f_{sup}$ decreases. This results, as follows from the analysis of formula (7), in the corresponding reduction of the undercarriage slippage.

In practice, it can occur that the effective values of the undercarriage slipping rates of tractors in drawbar pull categories 3 and 1.4 during their operation in the spring period exceed levels of 15% and 12%, respectively. In that case, the situation can be corrected by the installation of twin tyres on their wheels. At the same time, on tractors of drawbar pull category 1.4 the implementation of this design solution can be limited by the tyres of the rear axle only.

It should be emphasized that with twin tyres on the undercarriage the infringement of requirement (6) becomes possible at a considerably higher level of slippage. According to the calculations, under such conditions the value of $\delta_{max}$ for tractors in drawbar pull categories 5 and 3 is equal to 23%, while for tractors in drawbar pull category 1.4–16%.

Moreover, with the implementation of twin tyres a potential arises to increase the tractive force of the tractor and power unit by its ballasting. Nevertheless, this solution should be employed only with due consideration of the 'eco-friendliness' of the tyres, the technique of estimating that feature is rather comprehensively presented in study (Nadykto, 2013).

## CONCLUSIONS

In order to reduce considerably the destruction of soil structure in the spring period of field operations, the maximum permissible slipping rates $\delta_{max}$ of the wheel-type undercarriages of tractors in drawbar pull categories 5, 3 and 1.4 have to be 15%, 12% and 9%, respectively. In the summer/autumn period $\delta_{max}$ can have greater values and, respectively, be equal to 20%, 16% and 13%.

Wheeled tractors in drawbar pull category 5 equipped with single standard tyres can be used in field operations only in the summer/autumn period. For operation in spring they have to be equipped without fail with twin tyres. The implementation of this design solution is advisable for all wheeled tractors and power units.

## REFERENCES


Abrahám, R., Majdan, R., Šima, T., Chrastina, J. & Tulík, J. 2014. Increase in tractor drawbar pull using special wheels. *Agronomy Research* **12**(1), pp. 7–16.

Arvidsson, J. & Håkansson, I. 2014. Response of different crops to soil compaction–Short-term effects in Swedish field experiments. *Soil and Tillage Research* **138**, pp. 56–63.

Braunack, M.V., Arvidsson, J. & Håkansson, I. 2006. Effect of harvest traffic position on soil conditions and sugarcane (Saccharum officinarum) response to environmental conditions in Queensland, Australia. *Soil and Tillage Research* **89**(1), pp. 103–121.

Chyba, J., Kroulík, M., Krištof, K., Misiewicz, P.A. & Chaney, K. 2014. Influence of soil compaction by farm machinery and livestock on water infiltration rate on grassland. *Agronomy Research* **12**(1), pp. 59–64.

Chyba, J., Kroulík, M., Lev, J. & Kumhála, F. 2013. Influence of soil cultivation and farm machinery passes on water preferential flow using brilliant blue dye tracer. *Agronomy Research* **11**(1), pp. 25–30.

Gudehus, G. 1981. Bodenmechanik. Stuttgart, Enke, 268 S.

Guskov, V.V., Velev, N.N., Atamanov, J.E. 1988. Tractors. Theory. Moskow, Mechanical Engineering, 376 pp.

Kiss, P. 2003. Rolling radii of a pneumatic tyre on deformable soil. *Biosystems Engineering*, **85**(2), 153–161.

Komandi, G. 2006. Soil vehicle relationship: The peripheral force. Journal of Terramechanics, **43**(2), 213–223.

Kuht, J., Reintam, E., Edesi, L. & Nugis, E. 2012. Influence of subsoil compaction on soil physical properties and on growing conditions of barley. *Agronomy Research* **10**(1–2), pp. 329–334.

Kutkov, G.M. 2014. *Tractors and automobiles. Theory and technological properties*. Moskow, INFRA-M, 506 pp. (in Russian).

Lang, H.-J., Huder, J. 1985. *Bodenmechenik und Grundbau.* Das Verhalten von Böden und die wichtigsten grundbaulichen Konzepte. 3., überarb. u. erw. Aufl. – Berlin; Heidelberg; New York; Tokio: Springer, 252 S.

Molari, G., Bellentani, L., Guarnieri, A., Walker, M., Sedoni, E. 2012. Performance of an agricultural tractor fitted with rubber tracks. *Biosystems Engineering*, **111**(1), 57–63.

Nadykto, V.T. 2013. Problems of wheeled tractor ballasting. *Machinery and Technologies of Agro-Industry*, 2.

Opeiko, F.A. 1960. *Wheel and crawler*. Minsk, BSSR Academy of Agricultural Sciences Publishing House, 228 pp.

Sloboda, A., Ferencey, V., Hlavňa, V. & Tkáč, Z. 2008. *Construction of tyres and crawlers vehicles.* Vienala, Košice, 552 pp.

Schreiber, M. & Kutzbach, H. 2008. Influence of soil and tire parameters on traction. *Research in Agricultural Engineering* **54**(2), pp. 43–49.

*Agronomy Research* **13**(1), 158–166, 2015

# Application of overlaying material on surface of ploughshare for increasing its service life and abrasive wear resistance

P. Novák[1,*], M. Müller[2] and P. Hrabě[2]

[1]Czech University of Life Sciences in Prague, Faculty of Engineering, Department of Agricultural Machines, Kamýcká 129, 165 21 Prague, Czech Republic
[2]Czech University of Life Sciences in Prague, Faculty of Engineering, Department of Material Science and Manufacturing Technology, Kamýcká 129, 165 21 Prague, Czech Republic
[*]Correspondence: novakpetr@tf.czu.cz

**Abstract.** Soil processing is one of the most basic operations in vegetable production. This research project focuses on extending the service life of ploughshares by covering the tools with an oblique deposited overlaying material which is resistant to abrasive wear. The overlaying material was put in place parallel to the ploughshare's head, both to the front part as well as the back. The new functional profile of the conventional tool was created with overlaying electrodes so that the processed soil could drop from the tool. Carbide type (Soudokay A43-0, OK Tubrodur 14.70, OK Tubrodur 15.82) and martensitic type (Filarc PZ 6159) materials were used. Tested variants (overlays OK Tubrodur 15.82 and Filarc PZ 6159 above all) proved that the service life of the area at the top of the ploughshare's cutting edge was prolonged. This parameter is essential for effective ploughing.

**Key words:** soil processing, extending service life, functional profile.

## INTRODUCTION

Agricultural soil processing is a basic element in the process of crop production (Červinka & Fajman, 2013). Material type, thermal treatment and the geometry of exchangeable wear parts are essential characteristics for soil processing tools. The main problem connected with using soil processing devices is their wear owing to the components being embedded in soil (Doubek & Filípek, 2011; Müller & Hrabě, 2013; Müller et al., 2013).

Abrasive wear can be decreased to an acceptable level with suitable technologies and choosing the right material for the production of the whole tool or its part in the area of the highest wear (Votava et al., 2007; Liška & Filípek, 2012; Bednár et al., 2013). The ploughshare is one of the most stressed parts of the plough body (Müller & Hrabě, 2013). There are a lot of approaches to extending the service life of a ploughshare.

The most widespread method is hard faced overlaying but less known treatments have been increasingly tested in recent times (Legát et al., 2011; Müller et al., 2011). A significant problem is modifying the share geometry which also changes the impact of vertical force, enabling the plough to hollow furrows out from the soil (Müller et al., 2014). The functional surface properties of tools and parts can be purposefully changed, while keeping the original properties under the surface. An effective solution is increasing the wear resistance of tools that process soil with overlays (Novák et al., 2014). The aim is to improve the properties of a ploughshare.

## MATERIALS AND METHODS

Field research focused on the innovations connected to ploughshares in the area of conventional soil processing, namely on extending a ploughshare's service life by covering it with an oblique deposited abrasive wear resistant overlaying material. The overlaying material was put in place in parallel to the ploughshare head, both to the front part as well as the back. The new functional profile of the conventional tool was created with overlaying electrodes so that the processed soil could drop from the tool. The oblique depositing of the overlaying bead, i.e., the location of the overlays, was chosen in view of the direction of the abrasive particles' impact on the ploughshare during its relative motion through the soil.

Carbide type (Soudokay A43-0 (marked 1), OK Tubrodur 14.70 (marked 2), OK Tubrodur 15.82 (marked 3)) and martensitic type (Filarc PZ 6159 (marked 4)) overlaying materials were used. The etalon was marked with the number 5.

The new coating was created with overlaying, which is presented in Fig. 1 (an automatic welding machine ESAB, i.e.,an electric arc). Overlaying material was tube wire with the mean diameter of 1.6 mm. Welding parameters were the following: current 300 A, voltage 25 V, speed of overlaying 150 m min$^{-1}$.

The hardness of the coating layer was HV 751.46 ± 20.27 for Soudokay A43-0, HV 580.39 ± 15.65 for OK Tubrodur 14.70, HV 581.97 ± 3.08 for OK Tubrodur 18.82, HV 546.95 ± 15.82 for Filarc PZ 6159. The hardness of the basic material was HV 522.94 ± 8.13.

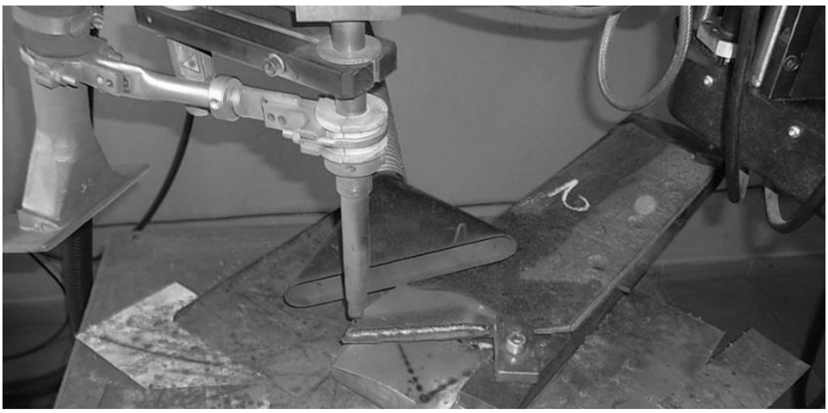

**Figure 1.** New surface created with overlaying. Automatic welding machine ESAB.

About 0.11 to 0.12 kg of the overlaying material was deposited on the plough surface. The new functional surface had a reinforced cutting edge and back part. The method of size and mass analysis was chosen for measuring the ploughshare's service life in field tests.

The location of the ploughshares on the plough was changed after 2 ha. The ploughshares were measured after 2 ha. Subsequently, the ploughshare was shifted to another position on the plough. This eliminated the factor of uneven wear in particular areas of the plough.

Fig. 2 shows a schematic presentation of the geometric solution and position of the measuring points.

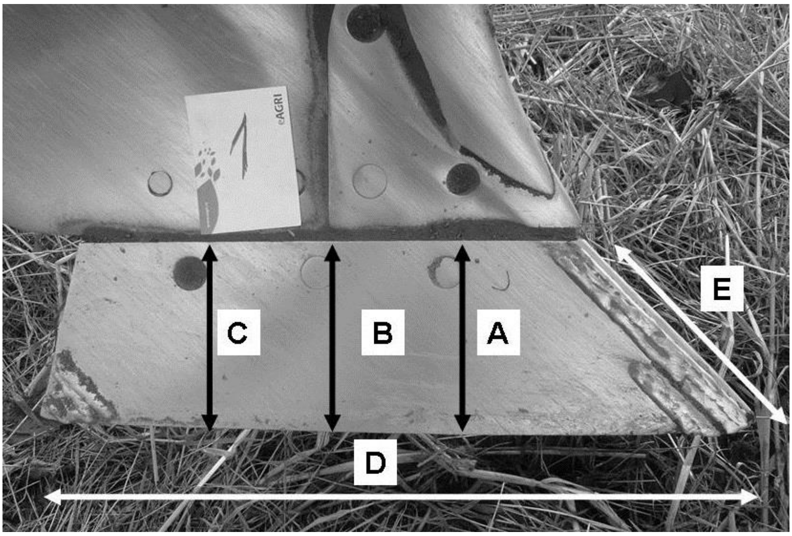


**Figure 2.** Ploughshare with oblique overlay and position of measuring points.

Parameters A, B and C were measured independently owing to the unevenness of the wear.

Changes in the tool shape (parameters A, B and C), mass loss (parameter M) and cutting edge shape (parameter D, E) were observed during testing the tool service life in field conditions. A five-share plough was used for the field tests. The tractor Zetor 120 45 (engine power 90 kW) was used for drawing the plough. The depth of ploughing was 0.22 m. The working speed was 6 km $h^{-1}$. Experiments were performed on a plot in Neperská Lhota near Benešov, which has mainly gravelly soil. The land plot had a predominantly light cambisol with the stoniness ranging from 1 (10% to 25%) to 2 (25% to 50%). The average humidity of the surface layer was 27% (measured with Theta Probe).

The ploughing resistance was very high and abrasive wear was above average. This type of soil was chosen on purpose owing to the extreme wear that occurred during ploughing in these conditions. The changes in the size, mass and geometry of the shares were measured after each 2 ha of ploughing. The entire area ploughed during the experiment was 14 ha. The reason for that was keeping approximately the same soil conditions within the chosen plot. All five ploughshares were measured and four of those had received an overlay (same overlay geometry but different types of overlaying material) and one was not treated (comparing etalon). The comparing etalon was a standard share.

## RESULTS AND DISCUSSION

The ploughshare mass increased from 2.1 to 2.6% owing to the overlaying. The results of single measurements are shown in Fig. 3 to Fig. 8. It is clear from the experiment results that the overlaying material has better properties than the etalon.

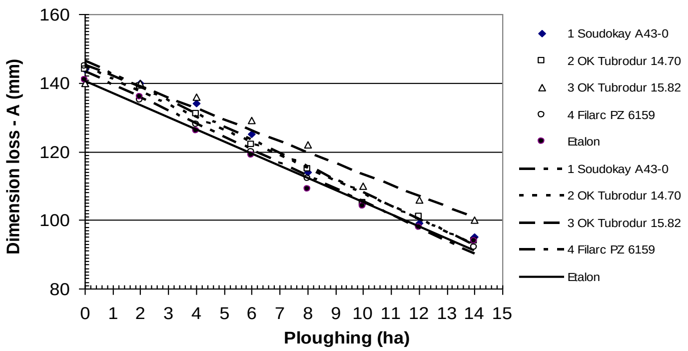


**Figure 3.** Course of share wear, dimension parameter A.

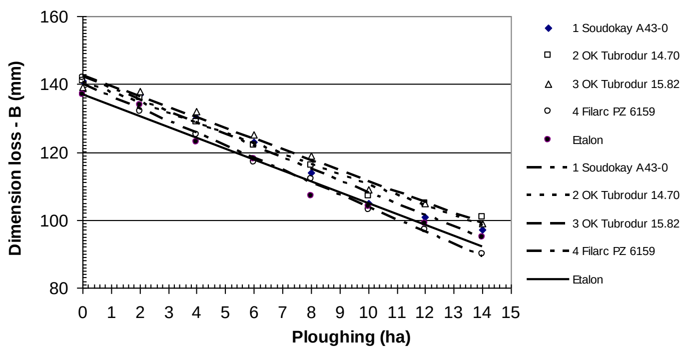


**Figure 4.** Course of share wear, dimension parameter B.

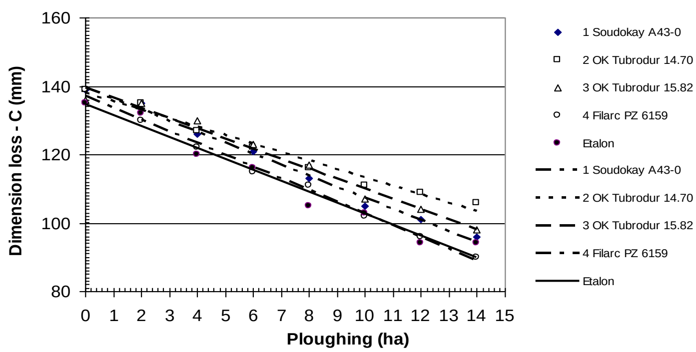


**Figure 5.** Course of share wear, dimension parameter C.

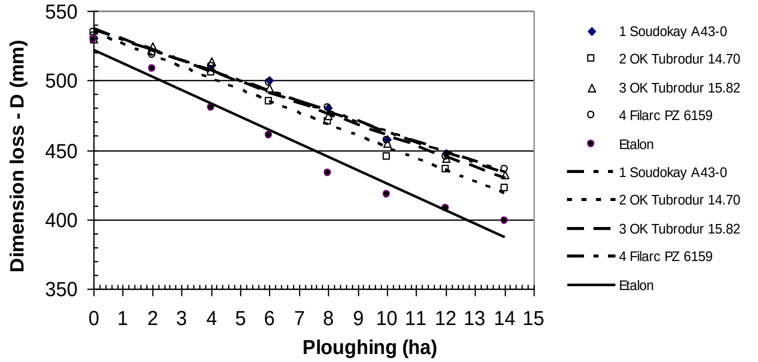


**Figure 6.** Course of share wear, dimension parameter D.

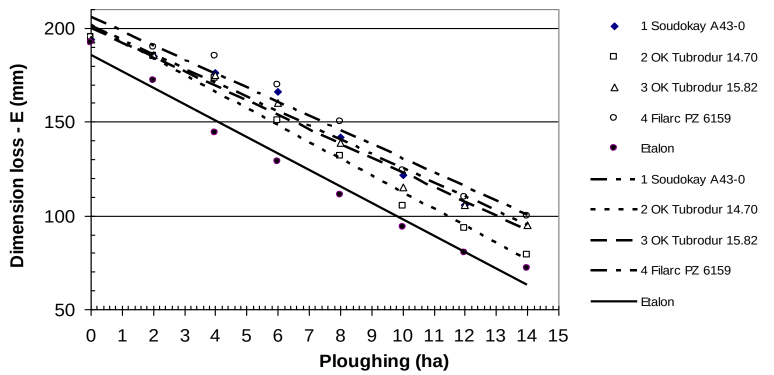


**Figure 7.** Course of share wear, dimension parameter E.

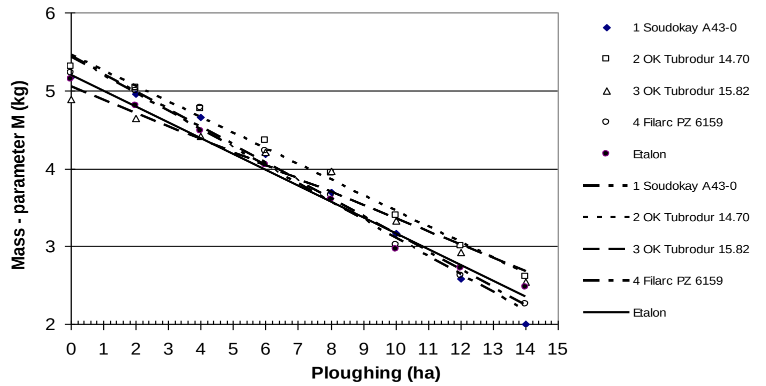


**Figure 8.** Course of share wear, mass.

The initial mass of the particular tested shares was slightly different. The percentage decrease remained in the interval of 48 to 60% for the shares with the overlay. The mass of the etalon decreased by 50%.

For correct evaluation, it is also important to verify the determination index $R^2$. This is problematic in terms of correlation analysis. The values of the determination index can be from 0 to 1. So far as $R^2$ equals 1, there is a perfect correlation in this sample (so there is no difference between the calculation and real values). The functions presented in Figs 3 to 8 are determined with the equations in Table 1. A strong dependence is revealed owing to the values stated in Table 1.

**Table 1.** Equations of linear functions: y–tested parameter, x–ploughing (ha)

| Description | | Functional equations | $R^2$ | Description | | Functional equations | $R^2$ |
|---|---|---|---|---|---|---|---|
| A | 1 | y = -3.8452x + 146.42 | 0.985 | D | 1 | y = -7.2857x + 536.57 | 0.978 |
| A | 2 | y = -3.7202x + 144.92 | 0.994 | D | 2 | y = -8.2619x + 534.83 | 0.992 |
| A | 3 | y = -3.1845x + 145.17 | 0.962 | D | 3 | y = -7.6667x + 537.42 | 0.983 |
| A | 4 | y = -3.7857x + 143.25 | 0.996 | D | 4 | y = -7.3512x + 536.33 | 0.988 |
| A | Etalon | y = -3.5417x + 140.67 | 0.987 | D | Etalon | y = -9.6607x + 522 | 0.972 |
| B | 1 | y = -3.4048x + 142.33 | 0.988 | E | 1 | y = -7.5714x + 201.29 | 0.967 |
| B | 2 | y = -3.0179x + 140.75 | 0.986 | E | 2 | y = -8.8988x + 201.42 | 0.987 |
| B | 3 | y = -3.0952x + 142.42 | 0.983 | E | 3 | y = -7.7024x + 200.17 | 0.982 |
| B | 4 | y = -3.631x + 140.17 | 0.996 | E | 4 | y = -7.5476x + 205.83 | 0.962 |
| B | Etalon | y = -3.1964x + 137 | 0.977 | E | Etalon | y = -8.7381x + 185.42 | 0.982 |
| C | 1 | y = -3.2262x + 139.58 | 0.992 | M | 1 | y = -0.2322x + 5.4253 | 0.982 |
| C | 2 | y = -2.4702x + 137.92 | 0.976 | M | 2 | y = -0.2002x + 5.454 | 0.991 |
| C | 3 | y = -2.9524x + 139.42 | 0.979 | M | 3 | y = -0.1702x + 5.0552 | 0.967 |
| C | 4 | y = -3.4345x + 137.17 | 0.994 | M | 4 | y = -0.2288x + 5.4507 | 0.983 |
| C | Etalon | y = -3.2083x + 134.83 | 0.968 | M | Etalon | y = -0.2037x + 5.2042 | 0.99 |

The F-test was used for statistical comparison. The zero hypothesis $H_0$ presents the state when there is no statistically significant differences ($p > 0.05$) between the mean values of the tested sets of data. In terms of the influence of various experimental variants (overlaying materials and etalon) on the measured parameters A to E, the results of the F-test are following: the hypothesis $H_0$ was proved to apply for all parameters: A ($p = 0.9437$), B ($p = 0.9117$), C ($p = 0.7799$), D ($p = 0.4803$) and E ($p = 0.6399$), so there is no difference between the particular tested variants at the significance level 0.05.

It is possible to claim the following on the basis of the results of the picture analysis: ploughshares with the overlays Soudokay A43-0 (marked 1), OK Tubrodur 14.70 (marked 2) and Filarc PZ 6159 (marked 4) kept their shape (primarily in the area of the cutting edge top) after 10 ha of ploughing. Results are shown in Fig. 9. The ploughshares were considerably worn after 14 ha of ploughing (Fig. 10).

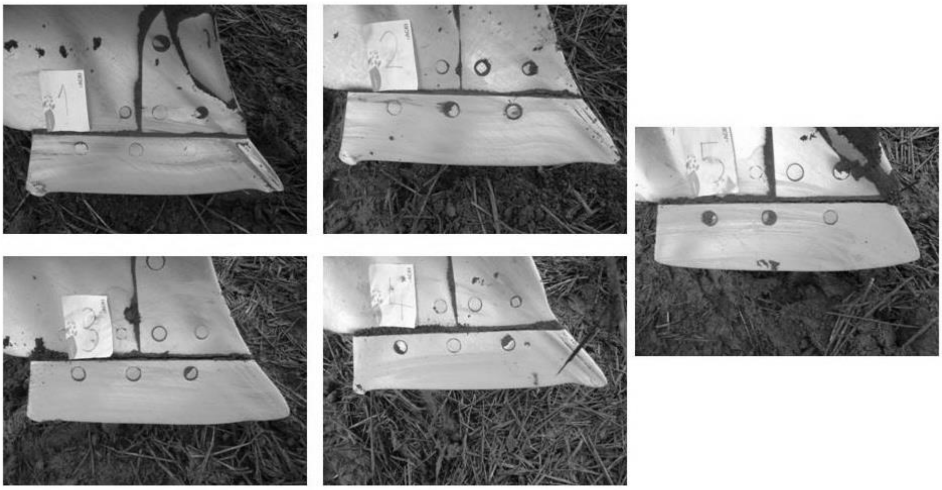

**Figure 9.** Wear of ploughshares after ploughing 10 ha.

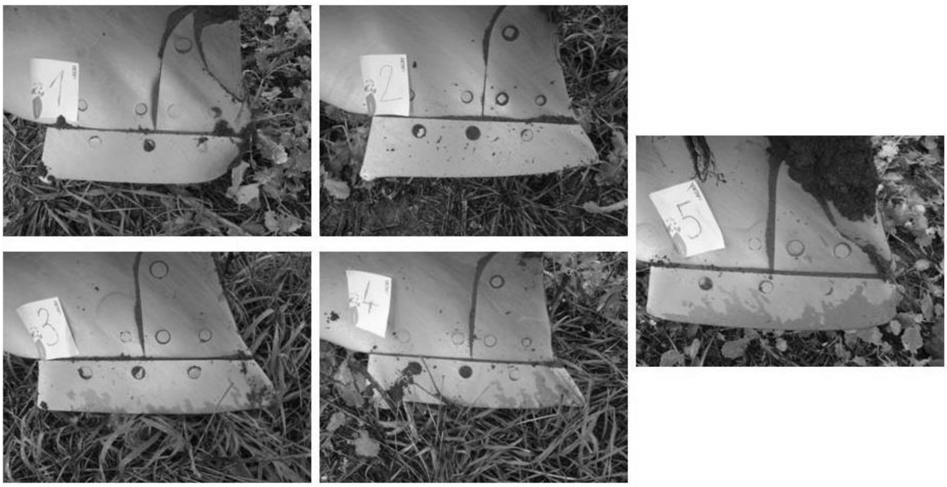

**Figure 10.** Wear of ploughshares after ploughing 14 ha.

The research results confirmed that it is necessary to conduct material and constructional research in the field of soil processing (Natis et al., 1999; Chotěborský et al., 2008; Natis et al., 2008; Doubek & Filípek, 2011; Hrabě & Müller, 2013; Kejval & Müller, 2013; Müller et al., 2013).

The reinforcement of the front and back part of the ploughshare is not sufficient for making the ploughshare more resistant to wear.

It is possible to create a wear resistant surface (overlay) and also use various geometrical positions of the covering layer (bead) with the aim of copying the course of the processed soil that drops of the share. A ploughshare with such a functional surface is worn unevenly during ploughing (Novák et al., 2014; Petrásek et al., 2014).

## CONCLUSIONS

Owing to the high prices of replacement parts, the research project focused on extending ploughshares' service life by covering their surface with an oblique deposited overlaying material which is resistant to the abrasive wear.

The research results led to the following conclusions:

- Results of changing the height at which the cutting edge is fastened to shanks, the length from the bottom edge to the cutting edge top, the ploughshare's head length and the mass of the cutting edge did not explicitly prove that performing the overlay has significant benefits for the ploughshares. The course of partial dependences was similar to minimum differences. The occurrence of a statistically significant difference was not proved with the statistical comparison of mean values in the F-test.
- Tested variants (number 3 and 4 above all) proved that the service life of the area at the top of the ploughshare's cutting edge was extended. This parameter is essential for effective ploughing.

ACKNOWLEDGEMENT. Supported by the Internal Grant Agency of the Faculty of Engineering, Czech University of Life Sciences in Prague.

## REFERENCES

Bednár, R., Votava, J., Cervinka, J., Fajman, M. 2013. Suitability of technical materials for machinery subsoilers for soil tillage. *Acta Universitatis Agriculturae et Silviculturae Mendelianae Brunensis* **61**(1), 9–16.

Červinka, J., Fajman, M. 2013. Suitability of technical materials for machinery subsoilers for soil tillage. *Acta Universitatis Agriculturae et Silviculturae Mendelianae Brunensis* **61**(1), 9–16.

Doubek, P., Filípek, J. 2011. Abrasive and erosive wear of technical materials. *Acta Universitatis Agriculturae et Silviculturae Mendelianae Brunensis* **59**(3), 13–21.

Hrabě, P., Müller, M. 2013. Research of overlays influence on ploughshare lifetime. *Research in Agricultural Engineering* **59**(4), 147–152.

Chotěborský, R., Hrabě, P., Müller, M., Savková, J., Jirka, M. 2008. Abrasive wear of high chromium Fe-Cr-C hardfacing alloys. *Research in Agricultural Engineering* **54**(4), 192–198.

Kejval, J. & Müller, M. 2013. Mechanical properties of multi-component polymeric composite with particles of Al2O3/SiC. *Scientia Agriculturae Bohemica* **44**(4), 237–242.

Liška, J., Filípek, J. 2012. The resistance of ledeburitic tool steels against the abrasive wear. *Acta Universitatis Agriculturae et Silviculturae Mendelianae Brunensis* **60**(6), 231–242.

Legát, V., Jurča, V., Aleš, Z. 2011. Contribution to plough shares and chisels useful life optimization. *Scientia Agriculturae Bohemica* **42**(2), 73–78.

Müller, M., Valášek, P., Novák, P., Hrabě, P., Paško, J. 2011. Overlays and composites application in technology of sugar beet cultivation and harvest. *Czech sugar and sugar beet jurnal* **137**(9), 304–307 (in Czech).

Müller, M., Chotěborský, R., Valášek, P. & Hloch, S. 2013. Unusual possibility of wear resistance increase research in the sphere of soil cultivation. *Tehnicki Vjesnik-Technical Gazette* **20**(4), 641–646.

Müller, M., Hrabě, P. 2013. Overlay materials used for increasing lifetime of machine parts working under conditions of intensive abrasion. *Research in Agricultural Engineering* **59**(1), 16–22.
Müller, M., Novák, P., Hrabě, P. 2014. Innovation of material design solutions of ploughshare in conventional tillage cultivation of sugar beet *Czech sugar and sugar beet jurnal* **130**(3), 94–99 (in Czech).
Natsis, A., Papadakis, A. & Pitsilis, J. 1999. The influence of soil type, soil water and share sharpness of a mouldboard plough on energy consumption, rate of work and tillage quality. *Journal of Agricultural Engineering Research* **42**(2), 71–176.
Natsis, A., Petropoulos, G. & Pandazaras, C. 2008. Influence of local soil conditions on mouldboard ploughshare abrasive wear. *Tribology International* **41**, 151–157.
Novák, P., Müller, M., Hrabě, P. 2014.Research of material and constructional solution in area of conventional soil processing. *Agronomy Research* **12**(1), 143–150.
Petrásek, Muller: Setting of Angle of Soil Flow on Ploughshare at traditional Processing of Soil. Manufacturing technology **14**(3). 2014, 407–412.
Votava, J., Černý, M. & Filípek, J. 2007. Abrasive wear of ploughshare blades made of Austempered Ductile Iron. *Acta Universitatis Agriculturae et Silviculturae Mendelianae Brunensis* **55**(1), 173–182.

*Agronomy Research* **13**(1), 167–172, 2015

# Laser scanner based collision prevention system for autonomous agricultural tractor

T. Oksanen

Aalto University, Department of Electrical Engineering and Automation, Otaniementie 17, 02150 Espoo, Finland; e-mail: timo.oksanen@aalto.fi

**Abstract.** In manned agricultural vehicles, the automated systems assist the driver by reducing the workload. This is achieved e.g. by using an automatic guidance system to steer the tractor along the desired path. However, increasing automation tends to cause a reduction of awareness, so risks to collide obstacles in the field are higher. In this study, an autonomous tractor was equipped with front side laserscanner (LIDAR) to sense the environment in front. The laserscanner scans the environment at 50 Hz rate. The theoretical maximum range of the sensor is 25 m, but it was found in the tests, that in agricultural field conditions, the feasible range is not more than 7 m, due to the sunlight disturbance. Agricultural vehicles weigh tons, so the deceleration is limited and the limited range causes challenges to detect the obstacle and decelerate without colliding it. The developed algorithm is able to detect solid objects, like electricity poles in the trajectory. The deceleration algorithm is based on the known dynamics and actuator delays of the tractor locomotion system, by taking into account the maximum deceleration rate. In field tests, the system was evaluated in grass fields. In the first test, the system was tested with real electricity poles with no implement. In the second test, the system was tested with a mower and by using artificial obstacles placed into the grass. The system was able to detect the obstacles with high accuracy and stop precisely, but in the corners of the field the system caused false positives when the sensor was sensing beyond the edges of the field plot.

**Key words:** tractors, vehicles, robotics, environment sensing, autonomous emergency brake, accidents, control systems.

## INTRODUCTION

Several kinds of obstacles may exist in agricultural fields and agricultural vehicles, like tractors, have to avoid hitting them. Some of the obstacles are permanent, like electricity poles or large rocks, while the others are temporary, like other vehicles and containers to store inputs and outputs.

Traditionally tractors and other vehicles have been in the full control of the driver and visual perception of the neighbourhood has been conducted continuously. However, nowadays automatic steering / guidance systems have emerged and the driver may not pay so much attention for the environment any more. Therefore the risk to hit the obstacles arises. Increased automation and fewer tasks for the human operator may cause a lack of attention, in any industry.

Modern passenger cars are equipped with radars or other sensors which are monitoring the area ahead. These systems are able to take emergency braking actions, in case the driver has lost concentration or something unexpected appears, to prevent rear-end collisions. Kaempchen et al. (2009) call the system as Autonomous Emergency Brake (AEB) and considers various possible trajectories in dynamic environment.

These systems are not yet installed on tractors, but they could be used for the same reasons. Agricultural tractors with heavy loads are used in on-road traffic and due to increased speed and mass the same requirements may be considered as for trucks, to prevent rear-end collisions on dynamic objects. However, in agricultural vehicles the on-road rear-end collision are not considered as usual as off-road collisions on static objects.

Various approaches to obstacle detection in agricultural context have been proposed. Yang & Noguchi (2012) used omnidirectional stereovision to detect humans, with machine vision methods. The motivation was a robot tractor where the safety needs to be secured. Backman et al. (2013) presented a collision avoidance system for a tractor with the automatic steering system; the laser scanner based object detection was integrated closely on the guidance algorithm which enabled manoeuvring around the obstacle.

In this paper, the developed collision prevention system for an autonomous system is presented. The objective was to study how to take the dynamic vehicle velocity model into account in the deceleration control system, in order to perform the (emergency) deceleration at last possible minute.

## MATERIALS AND METHODS

### Tractor

The autonomous tractor used in this study is equipped with 123 kW diesel engine and hydrostatic transmission with four wheel equal size. The weight of the tractor is about 6,000 kg without implements and each wheel is steerable. The tractor is equipped with four wheels and the overall width is 2.3 m. The maximum speed was limited electronically to 3 m $s^{-1}$, even though the transmission would give much more. The acceleration and deceleration were controlled electronically, in both directions the maximum rate was set to 1.0 m $s^{-2}$, to reduce pressure stress for the hydrostatic system. (Oksanen, 2012a; Oksanen, 2012b)

### Sensor

The environment was monitored with a 2D laser scanner, LIDAR, made by SICK. LMS100 model is designed for indoor use, but it was considered sufficient for this experimental system. The sensor sensed the environment with 50 Hz frequency and 0.5 degree resolution. The communication protocol is based on TCP/IP over Ethernet.

In the tests, the sensor was installed at first in front of the tractor and later on the front mounted mower. The scanner was installed on horizontal orientation. The installation of the laser scanner on the mower is presented in Fig. 1.

The scanner was specified to measure a maximum range of 25 m, but in outdoor with bright sunlight the maximum range was found to be limited to approximately 7 m. Therefore, the obstacles beyond 7 m cannot be detected reliably, even if in some conditions they are clear. The laser scanner senses the distance by sending an infrared light pulse to the environment and it measures the time-of-flight of reflection. In bright sunlight, the power of transmitted light is not sufficient to measure long ranges. However, the maximum range found was adequate for the maximum driving speed of m $s^{-1}$.

**Figure 1.** Installation of the laser scanner on the mower. The laser scanner is the blue component in the center.

**Object detection**

The algorithm was monitoring the area in front of the tractor. The region of interest is a rectangle or a bent rectangle. The width of rectangle equals to tractor or implement width and the length was 10 m ahead. The curvature or bent rectangle was equivalent to the current curvature of the vehicle. An illustration of the region of interest is presented in Fig. 2.

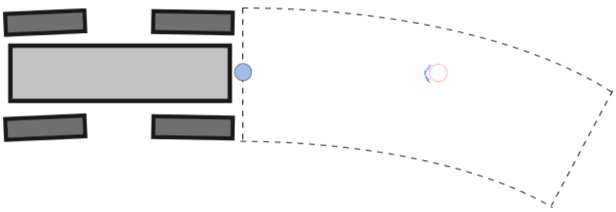

**Figure 2.** Illustration of the object detection region of interest. Red circle represents an obstacle and blue dots around are measurements the laser scanner get reflection from.

**Deceleration control**

As the tractor velocity control contains a control delay of magnitude 400 ms, this was taken into account in a predictive way. Also, the maximum deceleration rate of the vehicle needs to be known. From these factors, a model based control design was derived, to make a decision whether deceleration should be started, based on the object vicinity.

The faster the tractor is moving, the more distance and time is required to stop. When commanding the speed to zero, it takes 400 ms without any action and then the velocity starts to decrease at maximum rate of 1 m $s^{-2}$, which is the limitation of the tractor. From these figures it is possible to calculate the time required making a full stop and, furthermore, the distance the tractor has travelled after the stop was started. This is a function from the initial speed before full deceleration to the distance required to stop.

For deceleration control, an inverse function of that is required. For the parameters of this particular vehicle, the function is presented in Fig. 3. The obstacle detector system gives a distance from the nearest part of the vehicle to the obstacle in meters, or infinity when no obstacles exist in the region of interest. This distance is used as input to the function and the output gives the speed threshold when the deceleration must be done at maximum rate in order to prevent collision. For the distance, an offset is added as a tuning variable, to leave a safety zone between the obstacle and the vehicle.

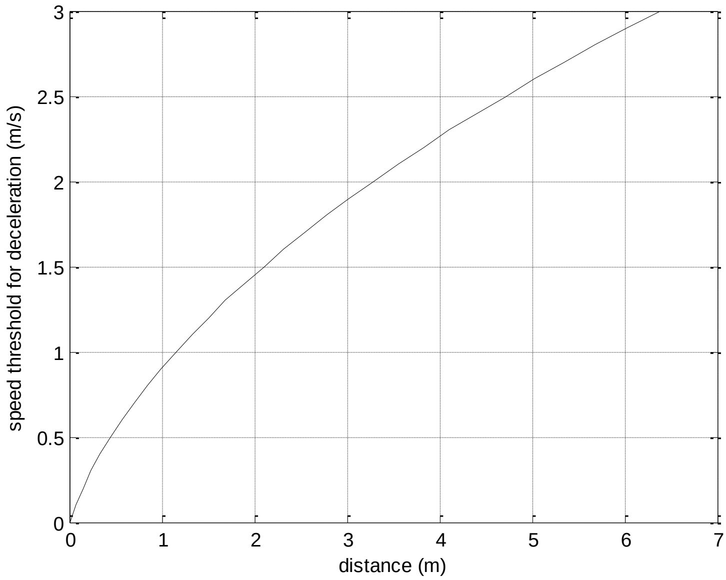


**Figure 3.** The function for deceleration control threshold. Below the curve is the safe zone, no deceleration action is necessary.

## RESULTS AND DISCUSSION

The system was evaluated by approaching the obstacle from a single direction repeatedly, and by varying the speed every time. The obstacle was an artificial round pole, made of dark foam. The diameter corresponds to the typical I-type wooden electricity pole. The situation is illustrated with Fig. 4. During the test the weather was cloudy, so the detection range of the laser scanner was not an issue. The safety offset for distance was set to 2.0 m.

**Figure 4.** Test setup, an artificial obstacle representing an electricity pole.

Each run was carried out by driving cruise control enabled towards to the obstacle and the system was decelerating automatically. An example of the deceleration test is presented in Fig. 5. The tractor approached the obstacle with cruise control enabled at 2.6 m $s^{-1}$ (bold line). At time step 3.5 s, the obstacle detector (solid line) started to limit the commanded speed (dashed line) and the command starts to follow this limit curve. The tractor stopped at time step 7.3 s and the distance to the object was 2.01 m in the end.

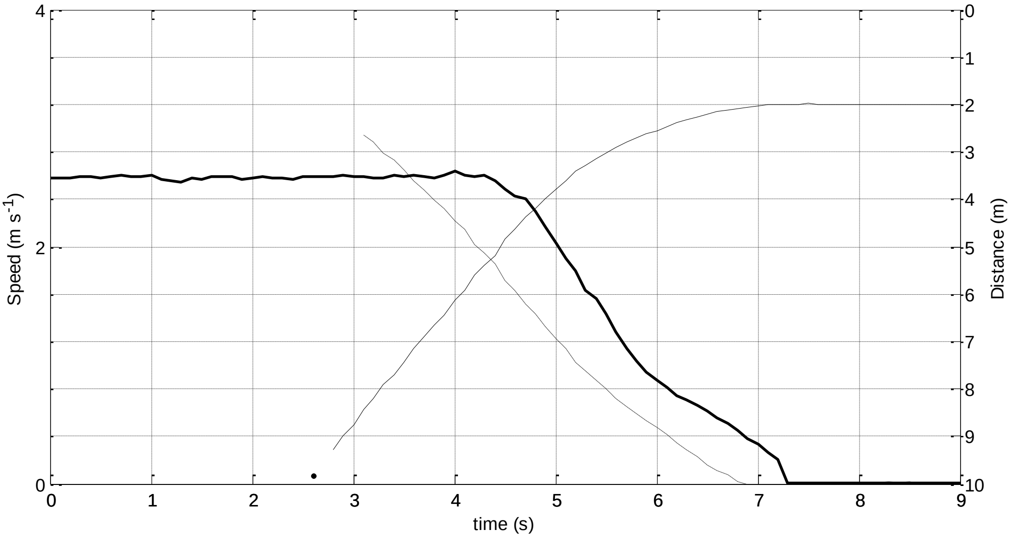


**Figure 5.** A sample deceleration. Bold line is the measured velocity, dashed line is the commanded deceleration and the solid line represents the measured distance to the obstacle.

The test was repeated 11 times, with varying speeds. The results are presented in Table 1. It can be seen that the tractor is able to decelerate automatically and stop within maximum error being 4 cm.

**Table 1.** Tests and results

| Initial speed (m $s^{-1}$) | Final distance to object (m) |
|---|---|
| 0.9 | 1.97 |
| 0.9 | 1.96 |
| 1.8 | 2.04 |
| 2.7 | 2.01 |
| 2.7 | 2.00 |
| 2.7 | 1.98 |
| 2.6 | 2.01 |
| 3.0 | 2.00 |
| 2.8 | 2.02 |
| 3.0 | 2.03 |
| 2.8 | 2.04 |

## CONCLUSIONS

A system with the automatic detection of solid obstacles in the field was developed and it was integrated into the tractors control system, to prevent collision by automatic deceleration. The deceleration is controlled by using a model based control of the tractor dynamics and control delay.

In the tests, the robot tractor was able to use full deceleration and it stopped to the safety margin from various speeds within accuracy level of two-inches.

The sensor used was intended for indoor use and the maximum range was found to be limited to 7 m in case of bright sunlight. Despite this was sufficient for the maximum driving speed of this tractor, even in bright sunlight, it cannot be used for higher speeds. Therefore, the sensor is not suitable for driving speed beyond 3 m/s. However, other sensor models of the same manufacturer should be used or other sensor types to overcome the sunlight problem.

ACKNOWLEDGEMENTS. This research was funded by ERA-NET ICT-AGRI project GrassBots. The research was supported by MTT Agrifood Research Finland, especially the author wants to thank Mr. Raimo Linkolehto and Dr. Juha Backman for the assistance and test environment during the research.

## REFERENCES

Backman, J., Oksanen, T. & Visala, A. 2013. Collision avoidance method with nonlinear model predictive trajectory control. In: *4th IFAC Conference on Modelling and Control in Agriculture, Horticulture and Post Harvest Industry (AgriControl2013)*, Espoo Finland, pp. 35–40.

Kaempchen, N., Schiele, B., & Dietmayer, K. 2009. Situation assessment of an autonomous emergency brake for arbitrary vehicle-to-vehicle collision scenarios. In: *IEEE Transactions on Intelligent Transportation Systems* **10**, 678–687.

Oksanen, T., 2012a. Modeling and Control of Hydraulic Drivetrain in Agricultural Tractor with Position Backlash in Speed Sensor Feedback. In: *Proceedings of Dynamics and Control in Agriculture and Food Processing*, Plovdiv, Bulgaria.

Oksanen, T., 2012b. Embedded control system for large scale unmanned tractor. In: *Proceedings of 5th Automation Technology for Off-road Equipment Conference (ATOE)*, Valencia, Spain.

Yang, L. & Noguchi, N. 2012. Human detection for a robot tractor using omni-directional stereo vision. *Computers and Electronics in Agriculture* **89**, 116–125.

*Agronomy Research* **XX**(1), 173–185, 2015

# Temperature distribution analysis inside the strawberry flower head

M. Pennar*, V. Palge, E. Kokin, K. Jürjenson, E. Ideon and A. Annuk

Estonian University of Life Sciences, Institute of Technology, Kreutzwaldi 56, EE51014 Tartu, Estonia; *Correspondence: madis.pennar@emu.ee

**Abstract.** Different studies by numerous researchers were carried out recently to describe different heat flux components of heat balance equations for radiation frost condition in plants. The aim of most of the papers was to present more simple and clear mathematical algebra to show the plant heat balance formulas. To achieve this aim several simplifications were made. Nevertheless there are studies reporting different flower damage rates during spring frost sessions that mentioned studies cannot explain. This leads us to the need to find the temperature distribution inside the flower to understand why during the similar energy flux conditions the flowers act against frost stress differently. It's easy to measure the flower surface temperature but rather difficult to measure temperature distribution inside the flower head due to very small flower head scale compared to sensor sizes. To help to overcome these difficulties the authors make simplification by substituting the strawberry flower head with spherical homogeneous body though it is clear that the flower head is not homogeneous because of varying flower structure. The aim of this study is to present mathematical formulas for temperature distribution calculation inside the spherical body in terms of heat transfer conditions characteristic to radiation frost. Transient numerical methods are implemented for different conditions in case of spherical body. This approach enables us to decide if suggested mathematical solution is usable for non-homogeneous body. Computer program was prepared to analyse the results.

**Key words:** radiation frost, temperature distribution, plant, transient numerical method.

## INTRODUCTION

In this paper the plant under the observation is strawberry and the specific plant part is the flower. In spring time the plants may be endangered by night frost in any part of the World depending on weather conditions. 'Freezing is a major environmental stress, inflicting economy ic damage on crops and limiting the distribution of both wild and crop species' (Pearce, 2001). Despite the numerous studies in this field by several generations of researchers of both engineering and botanical experience this is still continuing to be a problem in our days. In this paper the authors handle this subject from general and thermal engineering points of view starting by how it was evolving historically. As the subject is of practical nature there is a long history of scientific publications developing different aspects of it. A number of authors (Businger, 1965; Gerber & Harrison, 1964; Barfield et al., 1981; Hamer, 1986; Perry, 1986; Perry, 1998) have tried to compose the radiation night-frost heat balance equation for the bud or flower taking into account different members of the heat balance. The second objective was to change the mathematical expressions so that these would be solved simply and swiftly. Martsolf (1992b) summarized previous results by night-frost general protection theory in his handbook 'Energy in Farm Production'. Heinemann et al. (1992) suggested the prototype of the computer program meant to support the farmer in his decision making process for night-frost protection strategy selection. One of the four program modules predicts the temperatures for the following night, using the night-frost statistics from previous years weather reports giving the user the possibility to define the 'night-frost windows'. The program allows also saving measurement data from the specific field, creating thus more exact statistical database. Despite the previous publications Martsolf (2000) tries once more to explain the differences of night-frost protection strategies because Ferguson & Isreal (1998) publish surprising results of questioning by which the citrus growers in America use commercial weather forecasts to get the information about possible night-frost threat.

The earlier research performed by (Gerber & Harrison, 1964; Businger, 1965; Barfield et al., 1981; Hamer, 1986; Perry, 1986; Perry, 1998; Hollender et al., 2012; Issa, 2012; Maughan et al., 2015) and the theory, according to which the damage in plants by night-frost is a result of the nucleation and ice growth (Pearce, 2001) still lacks the possibility to produce the information about the time when the ice crystals start forming in the specific part of the plant it is necessary to observe the temperature distribution in it.

The idea to supply the consumers with the computer program supporting the decision making process (Heinemann et al., 1992) is very good, but too general for real-time applications. The further development would have been needed, but it has not been done in these years.

The radiation night-frost phenomenon is observed as a rule at dusk or night time on a large area, so, to react on time and in a most appropriate way, the farmer has to know, what kind of thermal processes are going on at his field. That information could be produced by a thermal processes simulation computer program with the possibility to predict the temperature changes of the specific parts of the plants and the ambient environment.

One of the essential phases in development of such a program is creation of temperature calculation algorithm for most endangered parts of plants, which is the main purpose of this paper.

## MATERIALS AND METHODS

### General description of plant part as a model

In this paper the plant under the observation is strawberry and the specific plant part is the flower.

The temperature changes and nucleation (ice crystals forming) assume the model where the cell solute temperature alteration of plant parts is observed in different aggregate states. The nucleation inside and between the cells is very complicated phenomenon because the cell solute temperature may often fell below 0 °C without the freezing which increases the ability of the plant to withstand the influence of chill (Pearce, 2001). The processes on the surface of the plant are also quite complicated as there may be found different nucleators, for example, INA (ice nucleation-active) bacteria species which produce a protein able to nucleate freezing (Warmund & English, 1998). There is no clear theory suggested describing the conditions, when the nucleation occurs and when not at the cell solute temperatures below 0 °C. Because of that in this paper for simplification purposes the process of temperature change is observed only until the beginning of nucleation. Suggested algorithms do not handle the aggregate state changes of the cell solute and temperature alteration after ice formation. Depending on the plant species and corresponding differences in cell solutes concentration the nucleation may occur at different temperatures: –0.6°C…–2.6 °C (Pearce 2001). In the model algorithm suggested here the temperature limit is chosen at 0 °C. In different research papers the thermal balance is analysed for different plant parts: the flower bud of the apple tree (Hamer, 1986), the plant leave (Businger, 1965), (Gerber & Harrison, 1964), (Barfield et al., 1981).

At the time when the strawberry flower may need frost protection its form may be different, depending on the stage of development. The authors presume the flower to be fully open as shown on Fig. 1.

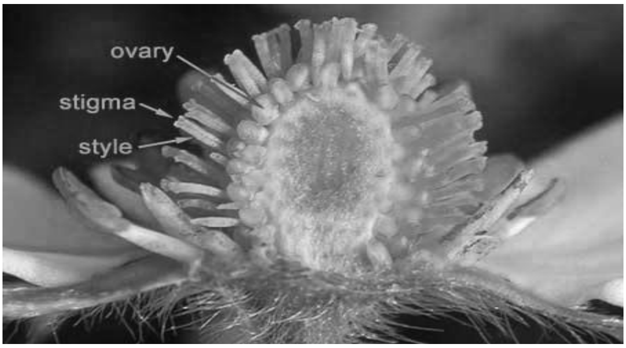


**Figure 1.** The cross-section of fully open strawberry flower.

The strawberry flower central part (receptacle) is practically entirely covered by spherical-shape ovaries (carpels) the number of which may vary between 100 and 400 depending on the species (Hollender et al., 2012). The ovaries have styles connected to them with the stigma at the end and are the most frost-endangered parts of the plant.

Defining as purpose the protection of the strawberry flowers from the night-frost it is necessary to provide the conditions that prevent the nucleation in the tissue of spherical-type ovaries.

## Theory and modelling

*Theory of spherically shaped body*

In spring-time in case of radiation night-frost the surface layer temperature of the spherical-shape ovary of the flower changes first of all due to the radiative heat exchange. But for this theoretical approach it is not important, of what character are the heat flows influencing the surface layer, as much more important is to know how the temperature changes in time between the inside layers of the spherical ovary.

For more clear explanation of the essence of mathematical algorithm of the process the most frost-endangered part of the plant, the ovary, is looked at as a spherically shaped body, devided for analysis purposes to large number of spherical layers with homogenious density (Fig. 2), where layer counting starts outside-in from outer radius *R*. The total number of layers is *N*. Here it is important to notice that in further calculations $r_{n-1}$ is the radius of the layer $n$–1, $r_n$ is the radius of the current layer $n$ and $r_{n+1}$ is the radius of the layer $n$+1.

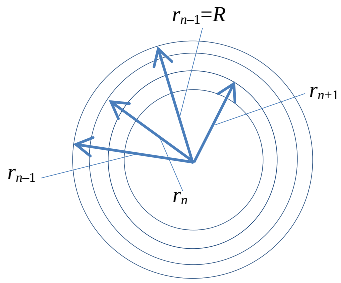


**Figure 2.** The description of the radiuses $r_{n-1}$, $r_n$ and $r_{n+1}$ of the body.

From these layers so small parts are chosen that it is possible to handle them as having not spherical but plain surfaces. Adjacent layers influencing each other are shown on Fig. 3.

Based on The Law of Conservation of Energy we can describe the heat balance equation for the layer $n$ (Fig. 3) as

$$m_n \cdot c_n \cdot dt_n = k_n \cdot F_{n-1} \cdot (t_{n-1} - t_n) \cdot d\tau - k_n \cdot F_n \cdot (t_n - t_{n+1}) \cdot d\tau \,, \tag{1}$$

where: $n$ is the number of the layer; $m_n$ – layer mass, kg; $c_n$ – specific heat capacity of layer material, J (kg °C)$^{-1}$; $dt_n$ – layer temperature change, °C; $k_n$ – heat transfer coefficient of the layer, W·(m$^2$·°C)$^{-1}$; $F_n$ – spherical surface area, m$^2$, separating layers $n$ and $n$+1; $F_{n-1}$ – spherical surface area, m$^2$, separating layers $n$–1 and $n$; $t_{n-1}$ – layer $n$–1 temperature, °C; $t_{n+1}$– layer $n$+1 temperature, °C; $t_n$ – layer $n$ temperature, °C; $d\tau$ – time step, s.

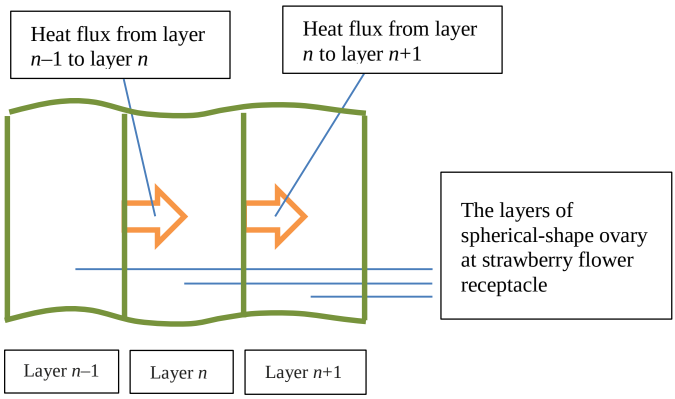


**Figure 3.** The heat-flows model of spherical-shape ovary layers at strawberry flower receptacle.

The layer mass definition expression looks like

$$m_n = \rho_n \cdot V_n \, , \tag{2}$$

where: $\rho_n$ is the density of the layer, kg m$^{-3}$; $V_n$ – the volume of the layer, m$^3$.

The heat transfer coefficient for the layer is:

$$k_n = \frac{\lambda_n}{\delta_n} \, , \tag{3}$$

where: $\delta_n$ is the thickness of the layer, m; $\lambda_n$ – thermal conductivity of the layer material, W·(m·°C)$^{-1}$.

As we noticed earlier that spherical surfaces are replaced with plain surfaces we can declare

$$F_{n-1} = F_n \, . \tag{4}$$

Transforming the formula (1) in appropriate way we get

$$\frac{m_n \cdot c_n}{k_n \cdot F_n} \cdot \frac{dt_n}{d\tau} = t_{n-1} - 2t_n + t_{n+1} \, . \tag{5}$$

In the expression (5) let

$$T_n = \frac{m_n \cdot c_n}{k_n \cdot F_n} \, , \tag{6}$$

where $T_n$ is the heating or cooling time constant of the layer, s.

The differential equation for temperature $t_n$ change is

$$T_n \cdot \frac{dt_n}{d\tau} + 2t_n - t_{n-1} - t_{n+1} = 0 \, . \tag{7}$$

As the functions $t_{n-1} = f(t_n)$ and $t_{n+1} = f(t_n)$ are not defined, we shall not try to find the analytical solutions for the differential equation but concentrate on numerical methods.

To define the equation (7) term

$$\frac{dt_n}{d\tau} = \frac{t_{n,j+1} - t_{n,j}}{d\tau} \, , \tag{8}$$

we have to introduce the index $j$ to formula (7), characterising the time dependence, which also enables the definition of calculation time interval length

$$d\tau = \tau_{j+1} - \tau_j . \quad (9)$$

Substituting the term in differential equation (7) by expression (8) we get

$$T_n \cdot \frac{t_{n,j+1} - t_{n,j}}{d\tau} + 2t_{n,j} - t_{n-1,j} - t_{n+1,j} = 0 . \quad (10)$$

After alteration

$$\frac{T_n}{d\tau} \cdot t_{n,j+1} = \frac{T_n}{d\tau} \cdot t_{n,j} - 2t_{n,j} + t_{n-1,j} + t_{n+1,j} . \quad (11)$$

Extracting the term $t_{n,j+1}$, we get

$$t_{n,j+1} = \frac{d\tau}{T_n} \cdot t_{n-1,j} + t_{n,j} - 2 \cdot \frac{d\tau}{T_n} \cdot t_{n,j} + \frac{d\tau}{T_n} \cdot t_{n+1,j} , \quad (12)$$

and finally,

$$t_{n,j+1} = \frac{d\tau}{T_n} \cdot t_{n-1,j} + \left(1 - 2 \cdot \frac{d\tau}{T_n}\right) \cdot t_{n,j} + \frac{d\tau}{T_n} \cdot t_{n+1,j} . \quad (13)$$

The calculation method here is based on the equality of time constant $T_n$ for all layers. In this case looking at the terms in equation (13), we can see that if the values in ratio $\frac{d\tau}{T_n}$ are chosen so, that

$$\frac{d\tau}{T_n} = \frac{1}{2} , \quad (14)$$

then expression (13) is reduced to arithmetic mean

$$t_{n,j+1} = \frac{t_{n-1,j} + t_{n+1,j}}{2} . \quad (15)$$

That is the $n$-layer temperature at the next time-step ($j$+1) equals to the mean temperature of the previous layer ($n$–1) and next layer ($n$+1) temperatures at given time-step $j$.

Expression (15) describes the situation, where temperature change $dt_n$ has maximal possible increase

$$dt_n = t_{n,j+1} - t_{n,j} . \quad (16)$$

In case of

$$\frac{d\tau}{T_n} > \frac{1}{2}, \tag{17}$$

the multiplier of $t_{n,j}$ in expression (13) becomes negative. In this circumstances the equation (3) describes the situation when the heat energy has to move from the body with lower temperature to the body with higher temperature which is conflictng with heat exchange laws. From that we can conclude that the term $\frac{d\tau}{T_n}$ in expression (13) should always be

$$\frac{d\tau}{T_n} \leq \frac{1}{2}. \tag{18}$$

The condition (18) becomes important when the temperature change in time is beeing sought.

The real body of spherical shape in our case is divided into layers so that the time constant is equal for all layers excluding the last, innermost one. The heat-balance for that layer differs from the equation (1):

$$m_n \cdot c_n \cdot dt_n = k_n \cdot F_{n-1} \cdot (t_{n-1} - t_n) \cdot d\tau. \tag{19}$$

After mathematical alterations similar to formulas (5) – (13) we get the differential equation

$$T_n \cdot \frac{dt_n}{d\tau} + t_n - t_{n-1} = 0. \tag{20}$$

Defining the term $t_{n,j+1}$ for the core layer, we get

$$t_{n,j+1} = \frac{d\tau}{T_n} \cdot t_{n-1,j} + \left(1 - \frac{d\tau}{T_n}\right) \cdot t_{n,j}. \tag{21}$$

The second special case is the surface layer of the sphere, the heat balance conditions for which are described by following expression:

$$m_n \cdot c_n \cdot dt_n = k_{n-1} \cdot F_{n-1} \cdot (t_{n-1} - t_n) \cdot d\tau - k_n \cdot F_n \cdot (t_n - t_{n+1}) \cdot d\tau. \tag{22}$$

This result is similar to the equation (1) but the essence of the terms $k_{n-1}$ and $t_{n-1}$ here should be described in more detail. As in this paper we are describing an algorithm for defining the temperature change of the inner layers of the spherical body, the ambient environment is looked at as a solid body with an initial temperature $t_{n-1} = t_0 = 0\,°C$, which stays constant during the whole process. The heat-exchange between the environment and the surface layer *n* of the sphere is considered to be conductive.

In case of spherical body we have to take into account some conditions:

$$F_{n-1} \neq F_n \,, \tag{23}$$

$$\lambda_n = const,\ n = 1..N \,, \tag{24}$$

where $N$ is a number of layers for which the body is divided.

Then the mathematical modifications of formula (1) differ from ones described above:

$$m_n \cdot c_n \cdot \frac{dt_n}{d\tau} = k_n \cdot F_{n-1} \cdot t_{n-1} - k_n \cdot F_{n-1} \cdot t_n - k_n \cdot F_n \cdot t_n + k_n \cdot F_n \cdot t_{n+1} \,. \tag{25}$$

Opening the term $dt_n$, we get

$$\begin{gathered} \frac{m_n \cdot c_n}{d\tau} \cdot t_{n,j+1} - \frac{m_n \cdot c_n}{d\tau} \cdot t_{n,j} = k_n \cdot F_{n-1} \cdot t_{n-1,j} - k_n \cdot F_{n-1} \cdot t_{n,j} - \\ - k_n \cdot F_n \cdot t_{n,j} + k_n \cdot F_n \cdot t_{n+1,j} \,, \end{gathered} \tag{26}$$

and extracting the variable $t_{n,j+1}$, we have

$$\begin{gathered} t_{n,j+1} = \frac{k_n \cdot F_{n-1} \cdot d\tau}{m_n \cdot c_n} \cdot t_{n-1,j} + t_{n,j} - \frac{k_n \cdot F_{n-1} \cdot d\tau}{m_n \cdot c_n} \cdot t_{n,j} - \\ - \frac{k_n \cdot F_n \cdot d\tau}{m_n \cdot c_n} \cdot t_{n,j} + \frac{k_n \cdot F_n \cdot d\tau}{m_n \cdot c_n} \cdot t_{n+1,j} \,. \end{gathered} \tag{27}$$

After grouping by $t_{n-1,j}$ , $t_{n,j}$ , $t_{n+1,j}$ we get

$$\begin{gathered} t_{n,j+1} = \frac{k_n \cdot F_{n-1} \cdot d\tau}{m_n \cdot c_n} \cdot t_{n-1,j} + t_{n,j} \left( 1 - \frac{k_n \cdot F_{n-1} \cdot d\tau}{m_n \cdot c_n} - \frac{k_n \cdot F_n \cdot d\tau}{m_n \cdot c_n} \right) + \\ + \frac{k_n \cdot F_n \cdot d\tau}{m_n \cdot c_n} \cdot t_{n+1,j} \,. \end{gathered} \tag{28}$$

Writing the formula (13) as

$$t_{n,j+1} = \frac{d\tau}{T_n} \cdot t_{n-1,j} + t_{n,j} \left( 1 - \frac{d\tau}{T_n} - \frac{d\tau}{T_n} \right) + \frac{d\tau}{T_n} \cdot t_{n+1,j} \tag{29}$$

we see, that expressions (28) and (29) have similar structure. Therefore, we have to find an answer to the question: can the parameters of the body layers correspond to the next relationship

$$\frac{k_n \cdot F_{n-1} \cdot d\tau}{m_n \cdot c_n} = \frac{k_n \cdot F_n \cdot d\tau}{m_n \cdot c_n} = \frac{1}{2}. \tag{30}$$

We can see that this relationship is not correct as

$$r_{n-1} \neq r_n , \tag{31}$$

where: $r_{n-1}$ is the radius of the layer $n$–1, m; $r_n$ is the radius of the layer $n$, m (Fig. 2).

In equation (29) the condition $\left(1 - \frac{k_n \cdot F_{n-1} \cdot d\tau}{m_n \cdot c_n} - \frac{k_n \cdot F_n \cdot d\tau}{m_n \cdot c_n}\right) = 0$, necessary for determining the arithmetical mean likewise in formula (15), is fulfilled when

$$\frac{k_n \cdot F_{n-1} \cdot d\tau}{m_n \cdot c_n} + \frac{k_n \cdot F_n \cdot d\tau}{m_n \cdot c_n} = 1. \tag{32}$$

In this case from

$$\frac{k_n \cdot F_{n-1} \cdot d\tau + k_n \cdot F_n \cdot d\tau}{m_n \cdot c_n} = 1 \tag{33}$$

we get

$$k_n \cdot F_{n-1} \cdot d\tau + k_n \cdot F_n \cdot d\tau = m_n \cdot c_n . \tag{34}$$

After substituting surface area in (34) we have

$$4 \cdot \pi \cdot k_n \cdot d\tau \cdot \left(r_{n-1}^2 + r_n^2\right) = m_n \cdot c_n \tag{35}$$

and then replacing heat transfer coefficient and mass as follows

$$\frac{4 \cdot \pi \cdot \frac{\lambda_n}{r_{n-1} - r_n} \cdot d\tau \cdot \left(r_{n-1}^2 + r_n^2\right)}{\frac{4}{3} \cdot \pi \cdot \left(r_{n-1}^3 - r_n^3\right)} = \rho_n \cdot c_n \tag{36}$$

we get finally

$$\frac{r_{n-1}^2 + r_n^2}{\left(r_{n-1} - r_n\right)\left(r_{n-1}^3 - r_n^3\right)} = \frac{\rho_n \cdot c_n}{3 \cdot \lambda_n \cdot d\tau}. \tag{37}$$

In the expression (37) the function of the term $r_n$ exists in implicit form. To resolve the problem the computer program is written for searching the suitable values of $r_n$. The term $r_{n-1}$ acts as a constant, because it is always already defined before $r_n$ (at the first run $r_{n-1} = R$, where $R$ is the radius of sphere). The members on the right side of equation

(37) are constants that express the physical parameters of the body and the process time $d\tau$. Giving different values to the radius $r_n$ we search such value for it in case of which the equality (37) is valid with sufficient accuracy.

The equation (37) is suitable also for the body with layers of different physical properties that is nonhomogeneous body. It is possible to describe the density $\rho_n$, specific heat capacity $c_n$ and thermal conductivity $\lambda_n$ for each layer *n*. These calculated $r_n$ values take into account physical parameters of nonhomogeneous body and the condition (37).

*Special cases*

The temperature change in the core layer of the sphere can be found from the heat-balance equation (19).

After mathematical modifications shown in (5) – (13) we get

$$t_{n,j+1} = t_{n,j} \cdot \left(1 - \frac{k_n \cdot F_{n-1} \cdot d\tau}{m_n \cdot c_n}\right) + \frac{k_n \cdot F_{n-1} \cdot d\tau}{m_n \cdot c_n} \cdot t_{n-1,j}\,. \tag{38}$$

More complicated is temperature change definition for the surface layer of the sphere. Very thin surface layer is allocated for that, which participate in the radiative, convective and sensible heate-exchange. The mathematics describing these three heat-exchange types is of complex nature and has been handled by many authors: (Gerber & Harrison, 1964; Businger, 1965; Barfield et al., 1981; Hamer, 1986; Perry, 1986; Perry, 1998; Martsolf, 1992b). Taking into account the scope of this paper, we do not elaborate on these heat-exchange processes and in such case, the form of equation (1), suitable for surface layer temperature change definition, similarly to the equation (28) takes the specific form

$$\begin{aligned} t_{n,j+1} = \frac{k_n \cdot F_{n-1} \cdot d\tau}{m_n \cdot c_n} \cdot t_{vk,j} + t_{n,j}\left(1 - \frac{k_n \cdot F_{n-1} \cdot d\tau}{m_n \cdot c_n} - \frac{k_n \cdot F_n \cdot d\tau}{m_n \cdot c_n}\right) + \\ + \frac{k_n \cdot F_n \cdot d\tau}{m_n \cdot c_n} \cdot t_{n+1,j}\,, \end{aligned} \tag{39}$$

where $t_{vk}$ is the surface temperature of the sphere, °C.

Thus, the mathematical algorithm describing temperature change inside the strawberry flower spherically shaped ovary, devided to $n = 1...N$ layers, can be described for different layers by following system of equations:

$$
\begin{cases}
n=1: \\
t_{n,j+1} = \dfrac{k_n \cdot F_{n-1} \cdot d\tau}{m_n \cdot c_n} \cdot t_{vk,j} + t_{n,j}\left(1 - \dfrac{k_n \cdot F_{n-1} \cdot d\tau}{m_n \cdot c_n} - \dfrac{k_n \cdot F_n \cdot d\tau}{m_n \cdot c_n}\right) + \dfrac{k_n \cdot F_n \cdot d\tau}{m_n \cdot c_n} \cdot t_{n+1,j}, \\
1 > n > N: \\
t_{n,j+1} = \dfrac{k_n \cdot F_{n-1} \cdot d\tau}{m_n \cdot c_n} \cdot t_{n-1,j} + t_{n,j}\left(1 - \dfrac{k_n \cdot F_{n-1} \cdot d\tau}{m_n \cdot c_n} - \dfrac{k_n \cdot F_n \cdot d\tau}{m_n \cdot c_n}\right) + \dfrac{k_n \cdot F_n \cdot d\tau}{m_n \cdot c_n} \cdot t_{n+1,j}, \\
n = N: \\
t_{n,j+1} = \dfrac{k_n \cdot F_{n-1} \cdot d\tau}{m_n \cdot c_n} \cdot t_{n-1,j} + t_{n,j} \cdot \left(1 - \dfrac{k_n \cdot F_{n-1} \cdot d\tau}{m_n \cdot c_n}\right).
\end{cases} \tag{40}
$$

## RESULTS AND DISCUSSION

To implement the algorithm, described by equations (40) the spherical body (in our case with strawberry flower ovary properties) has to be divided previously to virtual layers. Example results of such division defining the number of virtual layers depending on time-step length, which was performed using the equation (37), are shown in Table 1. To implement the algorithm, the computer program was composed.

**Table 1.** The numerical results for body division to spherical layers (body radius $R$ = 0.5 mm, number of spherical layers $N$, calculation time-step $d\tau$, density $\rho_n$ = 400 kg m$^{-3}$, specific heat capacity $c_n$ = 3,800 J·kg$^{-1}$·K$^{-1}$, thermal conductivity $\lambda_n$ = 0.8 W·m$^{-1}$·K$^{-1}$)

| Time-step | Number | Outside radius $r$ of layer $n$, mm | | | | |
|---|---|---|---|---|---|---|
| $d\tau$ length, s | of layers $N$ | 1 | 2 | 3 | 4 | 5 |
| 0.01 | 5 | 0.5 | 0.3969 | 0.2936 | 0.1894 | 0.0818 |
| 0.05 | 2 | 0.5 | 0.2636 | | | |
| 0.10 | 2 | 0.5 | 0.1476 | | | |
| 0.50 | 1 | 0.5 | | | | |

On Fig. 4 the change of temperatures in the body is shown with starting temperature 5° C and final temperature 0 °C. In reality, so rapid temperature changes are possible at some specific conditions, e.g. sunset or the change of atmospheric radiation heat flux depending on the cloudiness.

As the results of the modelling show that the temperature change is very fast process it could be useful to specify more precisely the physical properties of the strawberry flower ovary – the density, specific heat capacity and thermal conductivity. But in any case, as the internal temperatures change is much faster process than the speed of change of the heat fluxes producing this temperature alteration it will not have great influence.

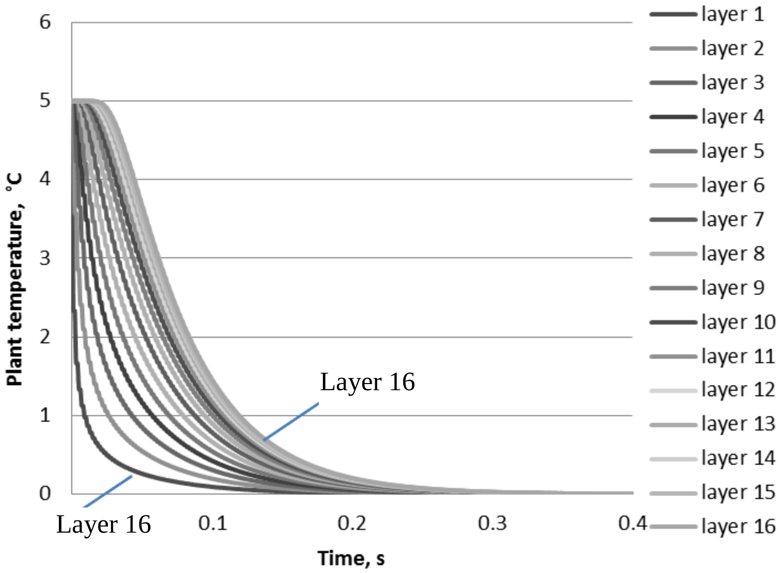


**Figure 4.** The calculated temperature change of different layers of strawberry flower ovary.

Choosing different time intervals in equation (37) we get different number of layers. If the interval is so long that the number of layers is small (2…5), the condition of the expression (32) is fulfilled with comparatively large error. Because of that it is important to select the time interval so short, that the number of layers would be larger than 15. The analysis of model errors due to the calculation method needs further investigation.

## CONCLUSIONS

The strawberry flower freezing or the ice crystals forming in the ovaries covering the flower receptacle is thermally very quick process. If this process is really so fast, then it is difficult to understand, how the strawberry flowers can survive in the night-frost conditions in spring. As a result of this analysis the phenomenon of 'super cooling' of cells solute needs more attention at radiative night-frost. Mathematical algorithm for the heat transfer analysis inside the ovaries is now available.

Further analysis of temperature distribution inside the ovary of strawberry flower is needed in the situation, when the surface layer of the ovary participate in real radiative, convective and sensible heate-exchange. The results of analysis presented in this paper enable us to suggest a new point of view on the night-frost problem. Instead of asking, when the flower will freeze, we should rather have to ask, is it really possible, that the flower will not freeze at night-frost?

## REFERENCES


Barfield, B.J., Walton, L.R. & Lacey, R.E. 1981. Prediction of sprinkler rates for night-time radiation frost. *Agricultural and forest meteorology* **24**, 1–9.

Businger, J.A. 1965. Frost protection with irrigation. *Agricultural and forest meteorology*, ISSN 0168–1923. Vol. **1** (1964)–30/1983).

Chesness J.L., Kidder E.H. & Dhanak A.M. 1968. Heat and Mass Transfer Study of Freeze Protection of a Leaf Model Subjected to water sprinkling. *Transactions of the ASAE* **11**(1), 0028–0033.

Ferguson, J.J. & Isreal G.D. 1998. Citrus cold protection: A 1996 Survey. *Proc. Fla. State Hort. Soc.*, **111**,117–121.

Finnikov, K.A., Minakov, A.V., Dekterev, A.A., Gavrilov, A.A., Korzun, A.M., Voinikov, V.K. & Kolesnichenko, A.V. 2010. Mathematical modeling of heat transfer between the plant seedling and the environment during a radiation frost. *Journal of Stress Physiology & Biochemistry* **6**(4), 2010, 108–125.

Gerber, J.F. & Harrison, D.S. 1964. Sprinkler irrigation for cold protection of Citrus. *Transactions of the ASAE*, pp. 464–468.

Hamer, P.J.C. 1986. The heat balance of apple buds and blossom. Part III. The water requirements for evaporative cooling by overhead sprinkler irrigation. *Agricultural and Forest Meteorology* **37**, 175–188.

Heinemann, P.H., Morrow, C.T., Martsolf, J.D. & Crassweller, R.M. 1992. A decision support program for design and management of frost protection systems. In: Watson, D.G., Zazueta, F.S. & Bottcher A.B. (ed.). Computers in Agricultural Extension Programs. *Proc. Of 4$^{th}$ International Conf.*, 28–31 Jan., Orlando, Fla., ASAE Publ. 1–92, pp. 135–140.

Heinemann, P.H. & Morrow, C.T. 1986. An Artificial Apple Bud for Frost Temperature Sensing. *Transactions of the ASAE* **29**(5), 1338–1341.

Hollender, C.A., Geretz, A.C., Slovin, J.P. & Liu, Z.C. 2012. Flower and early frukt development in a diplomid strawberry, Fragaria vesca. PLANTA. Volume **235**(6), 1123–1139.

Issa, R.J. 2012. Numerical Heat Transfer Model for Frost Protection of Citrus Fruits by Water from a Spraying System. *Thermal Science*, **16**(1), 31–42.

Martsolf, J.D. 2000. Diversity of frost protection methodology. *Proc. Fla. State hort. Soc*., **113**, 133–137.

Martsolf, J.D. 1992a. Cold Protection Mechanisms. Proc. Fla. State hort. Soc., **105**, 91–94.

Martsolf, J.D. 1992b. Energy Requirements for Frost Protection of Horticultural Crops. Chapter 15. Pp. 221–241. In: Fluck, R.C. (ed.). *Energy in Farm Production* **6**, 219–239.

Maughan, T.L., Black, B.L. & Drost, D. 2015. Critical temperature for sub-lethal cold injury of strawberry leaves. *Scientia Horticulturae* **183**, 8–12.

Pearce, R.S. 2001. Plant freezing and damage. *Annals of Botany* **87**, 417–424.

Perry, K.B. 1998. Basics of frost and freeze protection for horticultural crops. *HortTecnology*, January-March 1998, **8**, 10–15.

Perry, K.B. 1986. FROSTPRO, a model of overhead irrigation rates for frost/freeze protection of apple orchards. *HortScience* **21**(4), 1060–1061.

Warmund, M.R. & English, J.T. 1998. Ice Nucleation, Freezing Injury, and Colonization of ‘Totem’ Strawberry Flowers with Ice-nucleation-active (INA) Bacteria. J. Amer. *Soc. Hort. Sci.*, **123**(2), 234–238.

*Agronomy Research* **13**(1), 186–191, 2015

# Evaluation of measuring frame for soil tillage machines draught force measurement

P. Procházka[1], P. Novák[2], J. Chyba[2] and F. Kumhála[2,*]

[1]BEDNAR FMT s.r.o., Lohenická 607, Prague-9 Vinoř, 190 17 Prague, Czech Republic
[2]Czech University of Life Sciences, Faculty of Engineering, Department of Agricultural machines, Kamýcká 129, 165 21 Prague-6 Suchdol, Czech Republic;
[*]Correspondence: kumhala@tf.czu.cz

**Abstract.** The knowledge of energy demands of the machines for soil tillage is useful factor for machinery design and also farm management. Currently used methods of draught force measurement are based on the use of the measuring rod. Basic part of this measurement apparatus is strain gauge load cell which is protected against damage by steel cage so that the forces were applied only in tension or compression. The main disadvantage of this solution is the necessity of using two tractors for the measurement: pulling one and pulled one equipped with soil tillage machine.

To avoid this disadvantage, measuring frame for soil tillage machines draught force measurement was developed. For the evaluation of measuring frame function consequent measurement arrangement was used: crowled tractor John Deere 8320 RT as a pulling device, measuring frame mounted on its three point hitch, measuring rod connecting measuring frame and pulled wheel tractor New Holland T7050 and Köckerling Exact Gruber Vario soil tillage machine with 5 m working width.

When comparing draught force results from strain gauge load cell placed into measuring frame with those from measuring rod it was found that there existed no statistically significant difference between the data from measuring frame and measuring rod. Measuring frame can be used for the aim of soil tillage machines draught force measurement and pulled tractor is not necessary in this case.

**Key words:** soil tillage, draught forces, soil properties.

## INTRODUCTION

Root restricting soil layers reduce crop yield (Topakci et al., 2010). It’s usual to use subsoiling method to remove barrier of compacted soil which mainly caused by agriculture transport across the field (Hall & Raper, 2005). One of indicators of mechanical properties of soil is a soil mechanical resistance (Adamchuk & Christenson, 2005). Soil mechanical resistance involves soil compaction, texture, moisture etc. One of measurable parameters of soil mechanical resistance is drought force measurement. The drought force is affected mainly by soil conditions (soil type, compaction, relief etc.) (Schutte & Kutzbach, 2003) and by parameters of tillage machines (type of working tool, working width, working depth etc.). Current knowledge of draught force could be a useful tool in many ways. The results can be used in routine practice to compare the energy performance of the tillage technologies, verification of technical changes on working tool, working tool optimization and verification of agronomical measures (Kroulík, 2013).

Draught force measurement is a good tool for site mapping as evidenced from Paul (1992) measurements. During this measurement the data were logged from the strain gauge pins and from speed radar. Besides abovementioned the author recorded also overall slippage. Result of the measured values was in compliance of dependence of draught force on various soil types within experimental plot. Based on the results Paul (1992) concluded that soil moisture significantly influenced the overall slippage of the tractor.

Novák et al. (2014) performed the draught force measurement by load cell with measuring range up to 200 kN. This load cell was mounted between draw able and drawn tractor which was connected the measured cultivator. These measurements were carried out for three different speeds (6, 8, 10 km $h^{-1}$) and two working depths (0.1 and 0.15 m) at two different soil types (sandy and loam soils). The result of Novák et al. (2014) measurement was a confirmation of the influence of soil type on the draught force however the impact of speed on draught force was not proven.

Very important measurements were carried out by Droll (1999) who estimated the main sources of errors during measuring, such as: soil roughness, tractor and tool oscillations, speed differences, soil moisture content differences, variability of plot, etc. McLaughin et al. (2000) reached similar conclusions.

Another parameter which would indicate the mechanical strength of the soil is cone index measurement by penetrometer according to ASAE (2004). By penetrometer measurement can be estimated the depth of the compacted layer and then the subsoiler can be adjusted to the proper depth (Hall & Raper, 2005), than the subsoiler could break the compacted layer of soil. Penetrometers with vertical axis of cone penetration into the soil are standardly used nevertheless there are also available the penetrometers with horizontal axis of penetration called horizontal penetrometers. Horizontal penetrometers are good helpers for continuous mapping of the plots variability. There are a lot of types of horizontal penetrometers which do not always use the cone which penetrate the soil.

For example, Varga et al. (2014) used simple two blade horizontal penetrometer with load cell located on the three point hitch frame. Interesting measurement carried out by Hall & Raper (2005) where the sensing element was in shape of 30° wedge and also mentioned that penetrometer measurements are largely influenced by soil moisture.

The combine measurement of cone index by horizontal penetrometer and soil moisture content showed Lammers et al. (2007) and Naderi-Boldaji et al. (2012) both designed and constructed cone horizontal penetrometer where the cone already contained a capacitive sensor. These combined 'on the go' sensors confirmed significant influence of soil moisture content on the cone index measurement.

## MATERIALS AND METHODS

Field measurements took place in the field near to Městec Králové in Central Bohemia, N 50°10.88725', E 15°17.78900'. The measurements were taken in 30$^{th}$ of October 2014.The soil type was classified as clayey-sandy rendzina. Sugar beet was grown on the field before measurements with an average yield of 85 t·$ha^{-1}$ at 16% sugar content.

Tractor New Holland T7050 and cultivator Köckerling Gruber Vario was used to measure the draught force. The working width of the cultivator was 5 m. For actual measurement, two measuring instruments of draught force (stick and frame) developed in collaboration of BEDNAR FMT ltd. (formerly Stromexport) and Czech University of Life Sciences were used. As a pulling tractor means served crawler tractor John Deere 8320RT (Fig. 1). Tractor New Holland T7050 had engaged gear and was released during measurements and served only for lifting and lowering of the cultivator. The draught force was provided only by John Deere 8320RT tractor.

**Figure 1.** Measuring set. From left: pulling tractor John Deere 8320RT, measuring frame, measuring stick, pulled tractor New Holland T7050 for lifting and lowering of the cultivator, cultivator Köckerling Gruber Vario with 5 m working width.

Basic part of both measurement devices was strain gauge load cell S-38 with measuring range up to 200 kN. Detailed description of measuring stick can be found in Novák et al. (2014). Draught force measuring frame was newly developed instrument. Its design can be seen in Fig. 2. Measuring frame is connected to three point hitch (3) of pulling tractor. Strain gauge load cell (2) and horizontal penetrometer (4) are also integrated to the frame. Two point hitch (1) serves for the connection of soil tillage machine.

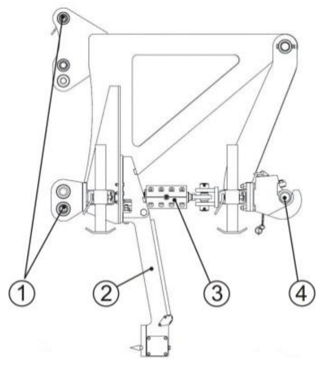


**Figure 2.** Draught force measuring frame: (1) connection to three point hitch of pulling tractor, (2) vertical penetrometer, (3) strain gauge load cell (200 kN), (4) two point hitch for soil tillage machine pulling.

The data from both load cells placed in measuring stick and frame were sensed with 6 Hz frequency by A/D converter NI USB-6008 and saved into notebook which was situated in tractor cab. This information was supplemented by machine location data from DGPS receiver Quectel L16 and signals form horizontal penetrometer.

Penetrometer used sensing element in shape of 30° conical wedge with 30 mm diameter and 56 mm length. Sensor Zemic B3G-C3-1.0t served as a force sensor on conical wedge sensing element. Measuring frame was also equipped with ultrasonic distance sensor UK1D-E1-0A for actual cultivator working depth measurement.

Prior field tests the area of 46 x 100 m was selected from the field and the measurements were done in order to characterise soil physical properties. Those measurements were carried out by horizontal penetrometer and by taking and evaluating samples of Kopecky's cylinders. Horizontal penetrometer PN-10 was developed at CULS Prague. It uses a probe with a cone angle of 30° and area of 100 $mm^2$. Penetrometer measurements were done at 204 places of above mentioned area up to 400 mm depth. Penetration resistance was estimated for each 50 mm depth during each measurement.

102 of Kopecky's cylinders samples were taken from the depth of 150 mm in order to as accurately as possible characterise soil bulk density, porosity and moisture content.

In order to evaluate the accuracy of draught force measurement by measuring frame in total three 100 m long measuring passes were performed with set cultivator working depth at 150 mm. Draught force signals from measuring stick and measuring frame together with vertical penetrometer resistance were observed in this case for next evaluation. Furthermore, the transverse profile of soil was uncovered for determination of quality parameters of tillage at the end of the measurements. Microsoft Excel and Statistica 12 computer programmes were used for statistical evaluation of the results obtained.

## RESULTS AND DISCUSSION

Fig. 3 shows a typical example of values obtained with lowered cultivator during one measuring pass. The figure shows similar progress of measured values for both the measuring frame and stick. Both curves can be considered as real progress of draught force caused by cultivator resistance. Small difference in the courses of values can be explained by the sensor sensitivity and its calibration. Also measuring frame is equipped with joint mechanism as opposed to purely draught dynamometer system (measuring stick).

From the graph in Fig. 3 it is also evident the course of measurement by horizontal penetrometer. This can be seen as complementary measurements to the measurements of draught force. It is also necessary to mention the fact that the curve of the horizontal cone index has a time offset against curves of draught forces. This was caused by displacement of horizontal cone index against the cultivator. The course of values in the early stages is also influenced by setting of measuring frame at the working depth in relation to the cultivator recessing. From the course of cone index values can be assumed the partial copying of the draught forces during measurement. The increase of cone index values follows the rise of the draught force values. Although the values of cone index and draught force cannot be simply compared, its resistance is undoubtedly one of the parameters that appropriately describe the draught strength.

Fig. 4 shows values of draught force at steady state (in the range of 30 to 80 s) using both measuring devices. As seen, the measurement using the measuring frame has a lower range of measured values (due to smaller oscillations) than the measuring stick. This is probably due to different imposition of sensor that has a lower tendency to oscillate. Another fact is the partial difference in the measured values. These can be caused by a slightly different design of the sensor, which cannot eliminate the influence of its imposition in relation to the construction of the measuring device. This may cause some distortion of values due to the transferred forces in the imposition. Nevertheless these deviations cannot cause significant distortion of values due to the high measured values and the errors are constant for each measuring devices.

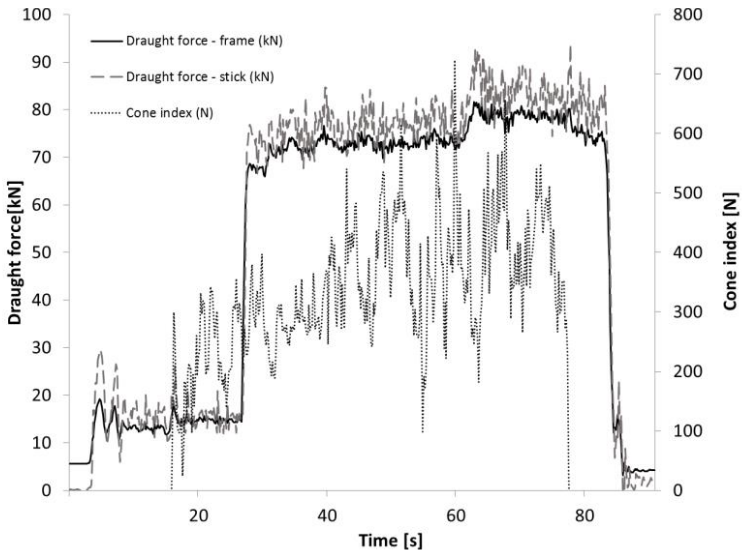


**Figure 3.** The course of measured values of draught force and cone index during one of three measuring passes.

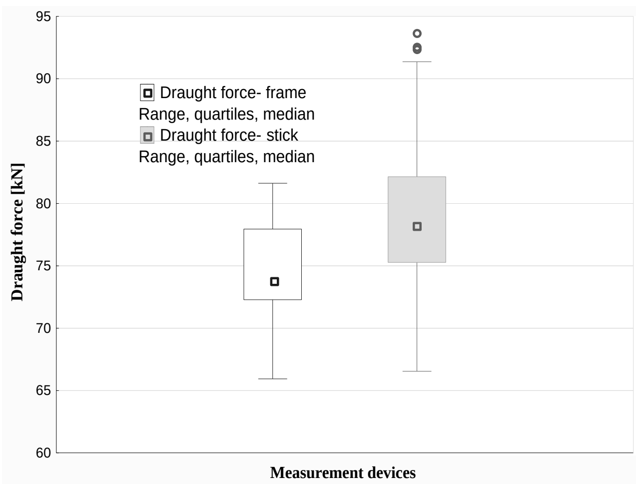


**Figure 4.** Draught force values between 30–80 seconds (constant measurement conditions).

Deep analysis of the influence of changing soil properties on horizontal penetrometer cone index and draught force measurements is unfortunately just out of the scope of this article. It will be discussed in some of forthcoming articles later.

## CONCLUSIONS

Measurement of draught forces is an important area at objective evaluation of agricultural technology. Using specialized measuring devices is the most accurate method of measurement so far. The alternatives (e.g. using data from tractor information system) do not reach accuracy of this basic method. The advantage of using the specialized frame is the possibility to use only one tractor instead of two ones. Drawn tools may be directly connected to measuring frame by two point hitch because draught force measurement results are similar. Additionally, this method is not distorted by a change of rolling resistance due to the fact that there is no preceding passage of the tractive tractor. Supplementation of the measuring frame by the horizontal penetrometer further expands the possibilities of using the measured values for rapid characterization of the soil surface layer state.

## REFERENCES


Adamchuk, V.I. & Christenson, P.T. 2005. An integrated system for mapping soil physical properties on the- go: the mechanical sensing component. **In:** *Precision Agriculture '05*, Academic Publishers, Wageningen, pp. 449–455.

ASAE, 2004. ASAE Standards Soil cone penetrometer. St. Joseph, Mich.: *American Society of Agricultural Engineers ASAE*, 49th Ed., ASAE S313.3.

Droll, P. 1999. Erstellung von geokodierten Karten mit Bodenkennwerten. Msc, thesis (Diplomarbeit Hohenheim), unpublished (unveröffentlicht). (in German)

Hall, E. & Raper, R. 2005. Development and concept evaluation of an on-the-go soil strength measurement system. *American Society of Agricultural Engineers ASAE*, **48** (2), 469–477.

Kroulík, M. 2013. Technique in precision agriculture technology. Thesis submitted in fulfilment of the requirements for the associate professor. Czech University of Life Sciences Prague. (in Czech).

Lammers, P., Sun, Y., & Ma, D. 2007. Using a combined sensor for mapping soil resistance force and soil water content. *Landtechnik*, **5**, 330–331.

McLaughin, N.B. & Burtt, S.D. 2000. Spatial Mapping of Tillage Energy. **In:** *the 5th Int. Conf. On Prec. Ag.* (2000), Bloomington, Minnesota/USA.

Naderi-Boldaji, M., Alimardani, R., Hemmat, A., Sharifi, A., Keyhani, A., Dolatsha, N. & Keller, T. 2012. Improvement and field testing of a combined horizontal penetrometer for on-the-go measurement of soil water content and mechanical resistance. *Soil & Tillage Research* **123**, 1–10.

Novák, P., Chyba, J., Kumhála, F. & Procházka, P. 2014. The measurement of stubble cultivator draught force under different soil conditions. *Agronomy Research* **12**(1), 135–142.

Paul, W. 1992. Zugkraftmessungen zur Teilschlagkartierung. *Landtechnik* **47**, 490–491.

Schutte, B. & Kutzbach, H.D. 2003. Evaluierung von ortsspezifischen Zugkraftmessungen bei der Bodenbearbeitung. **In:** *Agricultural Engineering 2003*, Tagng Landtechnik, Hannover, pp. 299–304.

Topakci, M., Unal, I., Canakci, M., Celik, H. & Karayel, D. 2010. Design of a Horizontal Penetrometer for Measuring On-the-Go Soil Resistance. *Sensors* **10**, 9337–9348.

Varga, F., Tkáč, Z., Šima, T., Hujo, Ľ., Kosiba, J. & Uhrinová, D. 2014. Measurement of soil resistance by using a horizontal penetrometer working with the two-argument comparative method. *Agronomy Research* **12**(1), 187–196.

*Agronomy Research* **13**(1), 192–201, 2015

# Taxonomic diversity of bacterial populations inhabiting gametophytes of *Sphagnum* mosses from different geographic regions of Russia

A.V. Shcherbakov[1,2*], E.Yu. Kuzmina[3], E.D. Lapshina[4], E.N. Shcherbakova[1,5], L.N. Gonchar[5] and V.K. Chebotar[1,2]

[1]All-Russia Research Institute for Agricultural Microbiology, Shosse Podbelskogo 3, 196608 Pushkin, St. Petersburg, Russia; [*]Correspondence: avsherbakov@bisolbi.ru
[2]ITMO University, Lomonosova Str. 9, St. Petersburg, 191002, Russia
[3]Komarov Botanical Institute, Professora Popova Str. 2, 197367 St. Petersburg, Russia
[4]Ugra State University, UNESCO chair, the Scientific and study centre 'Environmental dynamics and global climate change', Chehova Str. 16, 628012 Khanty-Mansiysk, Russia
[5]National University of Life and Environmental Science of Ukraine, Geroev oborony Str. 15, 03041 Kiev, Ukraine

**Abstract.** In this study we have analyzed the diversity of the endophytic bacterial community associated with Sphagnum mosses from Nort-West Region and Khanty-Mansiysk Autonomous District of Russia during the years 2009–2012. We isolated a more then 400 strains which were identified by means of phenotypic tests and by 16S rRNA sequences. The ribosomal data showed that the isolates belonged to genera *Pseudomonas* (20–57%), Colimonas (7–10%), Flavobacterium (6–8%), Burkholderia (5–6%), Serratia (3%). The data reported in this work are consistent with the results of research performed by the Berg group with samples of mosses of the Austrian Alps. It was found that *Sphagnum* mosses are a promising source for the isolation of beneficial microorganisms.

**Key words:** *Sphagnum* mosses, endophytic bacteria, microbial community, biodiversity.

## INTRODUCTION

Colonization of *Sphagnum* hyaline cells by heterotrophic bacteria was first mention in the works of Swedish researchers (Granhall & Hofsten, 1976). Their electron microscopic studies revealed, alongside with cyanobacteria, also heterotrophic ones. The possibility that internal tissues of *Sphagnum* plants may be colonized by methanotrophic microorganisms was first discussed in detail by Raghoebarsing and colleagues (Raghoebarsing et al., 2005; Raghoebarsing et al., 2006). These studies dealt with the symbiosis between *Sphagnum* mosses and methanotrophic bacteria ensuring carbon production for the plant construction. Dedysh (Dedysh et al., 1998; Dedysh et al., 2000; Dedysh, 2009) suggested that methanotrophic bacteria were not simply present in the bog water or peat deposits but inhabited *Sphagnum* mosses, including their internal parts. A recently coined the term 'Sphagnum-associated methanotrophy' (Larmola et al., 2010; Kip et al., 2011) is applied to the stable symbiosis between *Sphagnum* mosses and methanotrophic bacteria colonizing their inner parts. The latter assimilate methane and provide mosses with carbon.

The most complete body of information on the heterotrophic bacteria associated with *Sphagnum* mosses, including the data obtained by molecular-genetic methods, can be found in Opelt and Berg (2004); Opelt et al. (2007b); Vandamme et al. (2007) and Bragina et al. (2012). Detailed molecular-genetic studies of the total DNA extracted from the same moss species (*S. fallax* or *S. magellanicum*) and the analysis of clone libraries showed that non-culturable species of *Alphaproteobacteria* and *Gammaproteobacteria* were dominant in the microbial communities of *S. magellanicum* (Bragina et al., 2012). Microbial community of *S. fallax* was very different, the dominant species belonging to *Verrucomicrobia* and *Planctomyces*. The authors analyse the dependence of the composition of specific microbial communities of *Sphagnum* mosses on abiotic factors such as nutrient availability and water pH. They suggest that microbial community composition may change with the changing environmental conditions.

The aim of this work is study of the taxonomic composition of heterotrophic bacterial populations, associated with *Sphagnum* mosses from two geographically remote regions of Russia (Leningrad region (North-West of Russia) and the Khanty-Mansiysk Autonomous District (Western Siberia) and as well as some of their physiological properties to explain possible role in the functioning of plant-microbial symbiosis.

## MATERIALS AND METHODS

### Experimental Site and Sample Collection

In this study endophytic bacteria were isolate from *Sphagnum* moss gametophytes of two species: *Sphagnum fallax* (H. Klinggr.) H. Klinggr and *S. magellanicum* Brid. Samples of *Sphagnum* moss collected during expeditions in the two geographically distant regions of Russia: Leningrad Region (Northwest region) and the Khanty-Mansiysk Autonomous District (Western Siberia). In each region were selected 3 geographically distant points located at a distance of several tens of kilometers. One geographical point is not associated with other wetland ecosystems, often having its geographical name. List of sampling points is shown (Fig. 1). Identification of *Sphagnum* species was carried out in the field on the anatomical and morphological characteristics in accordance with the determinant of *Sphagnum* moss (Ignatov et al., 2006).

### Isolation of endophytic moss-associated bacteria

Endophytic moss-associated bacteria were isolated using original method of surface sterilization of plant samples. *Sphagnum* gametophytes 10–15 cm in an amount of 4–5 plants were weighed, placed in sterile 500 mL flask and washed three times in sterile water. The plant samples were sterilized for 10 min in 10% hydrogen peroxide, and then washed five times in sterile water. The surface sterilized plant fragments were crushed in sterile conditions, suspended with 10 ml sterile phosphate buffer, serially diluted in sterile water and plated onto R2A medium (Difco, USA). Plates were incubated for 5 days at 20°C, after which CFU were counted to calculate the mean number of colonies ($log_{10}$CFU) based on fresh weight. Isolates obtained by plating were purified and stored at -80 °C in sterile broth containing 20% glycerol.

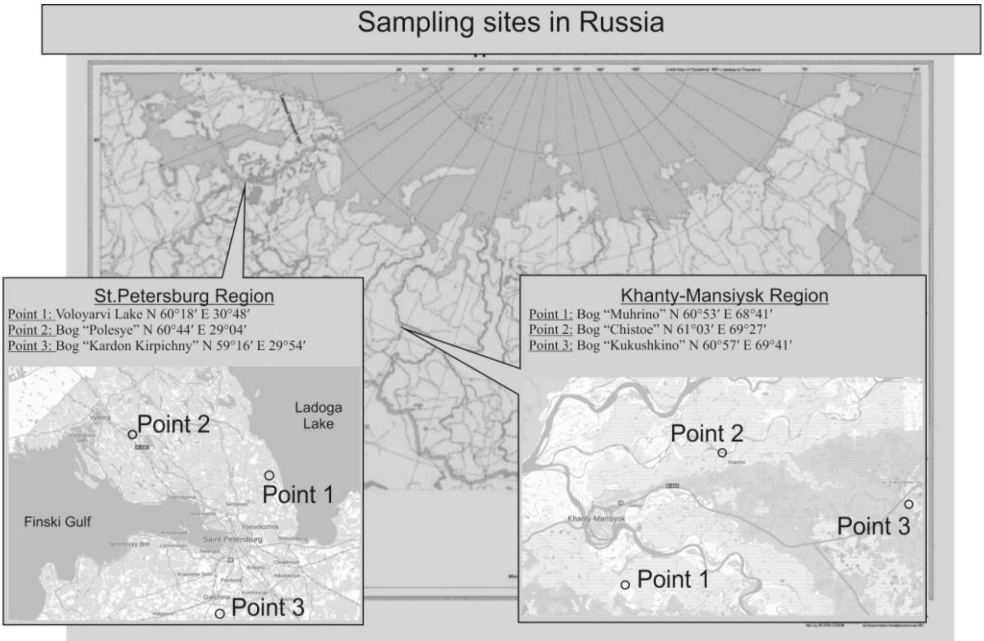


**Figure 1.** Geographic regions of *Sphagnum* mosses sampling.

**RFLP-analysis and identification of bacterial isolates**

Bacterial DNA from isolated bacterial strains was extracted using lysis by lysozyme and SDS, protein precipitation by 3M sodium acetate, purification by phenol:chloroform:isoamyl (24:24:1) and DNA precipitation by isopropanol. Briefly, portions of the 16S rRNA genes were obtained via PCR amplification with primers 27 fm (5′-AGA GTT TGA TCM TGG CTC AG-3′) and 1522R (5′-AAG GAG GTG ATC CAG CCG CA-3′) (Weisburget al., 1991). The amplified DNA fragments were subsequently digested with the two nucleases *Msp* I and *Hae* III. The resulting fragments were subsequently separated on a 2% agarose gel and the profiles of the endophytic strains were compared. For nucleotide sequence determination, PCR products were separated on a 1% agarose gel, recovered and purified from agarose using a QIAquick PCR Purification Kit (QIAGEN GmbH, Hilden, Germany). Sequencing was performed by manufacturer's recommendations for GS Junior (Roshe, The Switzerland). Similarity searches in GenBank were performed using BLAST (http://www.ncbi.nlm.nih.gov/blast/; Altschulet al., 1997).

**Phylogenetic analysis**

Computer-assisted evaluation of bacterial community profiles obtained by RFLP was performed by using the TotalLab program (version TL120; TotalLab Ltd, UK). Cluster analysis was performed with the UPGMA (unweighted pair group method with arithmetic averages) algorithm.

## RESULTS AND DISCUSSION

Altogether, more than 400 culturable bacterial strains were isolated from the tissues of *S. fallax* and *S. magellanicum* sampled in the St-Petersburg Region and Western Siberia. Their cultural and morphological properties were characterized. Most isolated bacteria (> 98%) were Gram-negative. They were represented by very small (< 1.5 µm) rounded or oval cells or short rods. On the R2A medium they formed fast- or slowly growing colonies, flattened and creeping, transparent or semi-transparent, brightly coloured (red, violet, pink, yellow, orange) or colourless (beige or milky white). The total abundance of microorganisms isolated on culture media varied in the range $10^5$–$10^6$ CFU $g^{-1}$ of plant tissue. Nitrogen-fixing and oligonitrophilic bacteria grew rather abundantly on the nitrogen-free medium but formed few morphotypes (not more than 5). They formed transparent colourless slimy colonies of middle size, either creeping on the agar surface or rounded and convex.

Molecular genetic identification based on analysis of the 16S rRNA gene fragments had allowed to study the taxonomic diversity of microorganisms isolated from two independent geographic regions (Figs 2, 3). Based on the presented results (more than 150 isolates were sequenced after RFLP-analysis) the major taxonomic branches in the composition of bacterial communities associated with *Sphagnum* mosses had been established. Class *Gammaproteobacteria* order *Enterobacteriales* included *Serratia, Enterobacter* and several others. A number of strains had classified as opportunistic forms of animals and plants pathogens (for example *Klebsiella sp.* – the opportunistic forms of animals and humans, *Erwinia rhapontici* – opportunistic bacterial plant pathogen), but some species can act as growth-stimulating and biocontrol agents (genera *Serratia, Klebsiella, Rahnella*) (Opelt et. al., 2007c; Mehnaz et al., 2010; Liu et al., 2014; Neupane et. al., 2015) *Serratia plymuthica* described as dominant specie isolated from *S. fallax*, and *S. magellanicum* gametophytes. Another equally dominant taxonomic branch *Burkholderiales* divided into two main families: the family *Oxalobacteraceae*, presented by *Collimonas* spp., and the family *Burkholderiaceae* presented by *Burkholderia* spp. The minor genera included *Janthinobacterium* sp., *Pandorea* sp. et al.

Phylum *Bacteroidetes* was presented by genera *Flavobacterium, Pedobacter, Chryseobacterium*. A characteristic feature here was the presence of *Flavobacterium sp*. in bacterial populations of *Sphagnum* mosses from different geographical origin, which formed on media characteristic bright–yellow colonies. It is possible that this specie of flavobacteria is specific for the *Sphagnum* mosses bacterial community. The largest taxonomic branch included the family *Pseudomonadaceae,* the number of which species reached 30–40% of all isolated bacteria. Among the characteristic species of *Pseudomonas* should be noted *P. poae, P. fluorescens, P. asplenii.*

The taxonomic composition of natural populations of heterotrophic bacteria associated with *Sphagnum* moss had the number of general patterns from different groups of bacteria (Figs 2, 3). One of the general observed trends was variation in the number of *Pseudomonas* and *Collimonas* for different types of *Sphagnum* moss. The genera *Pseudomonas* was the most numerous group of endophytic bacteria *S. magellenicum,* while *Pseudomonas* population for *S. fallax* was not so dominance, and the *Collimonas* and *Flavobacterium* here had large number of species (Table 1, Figs 2, 3).

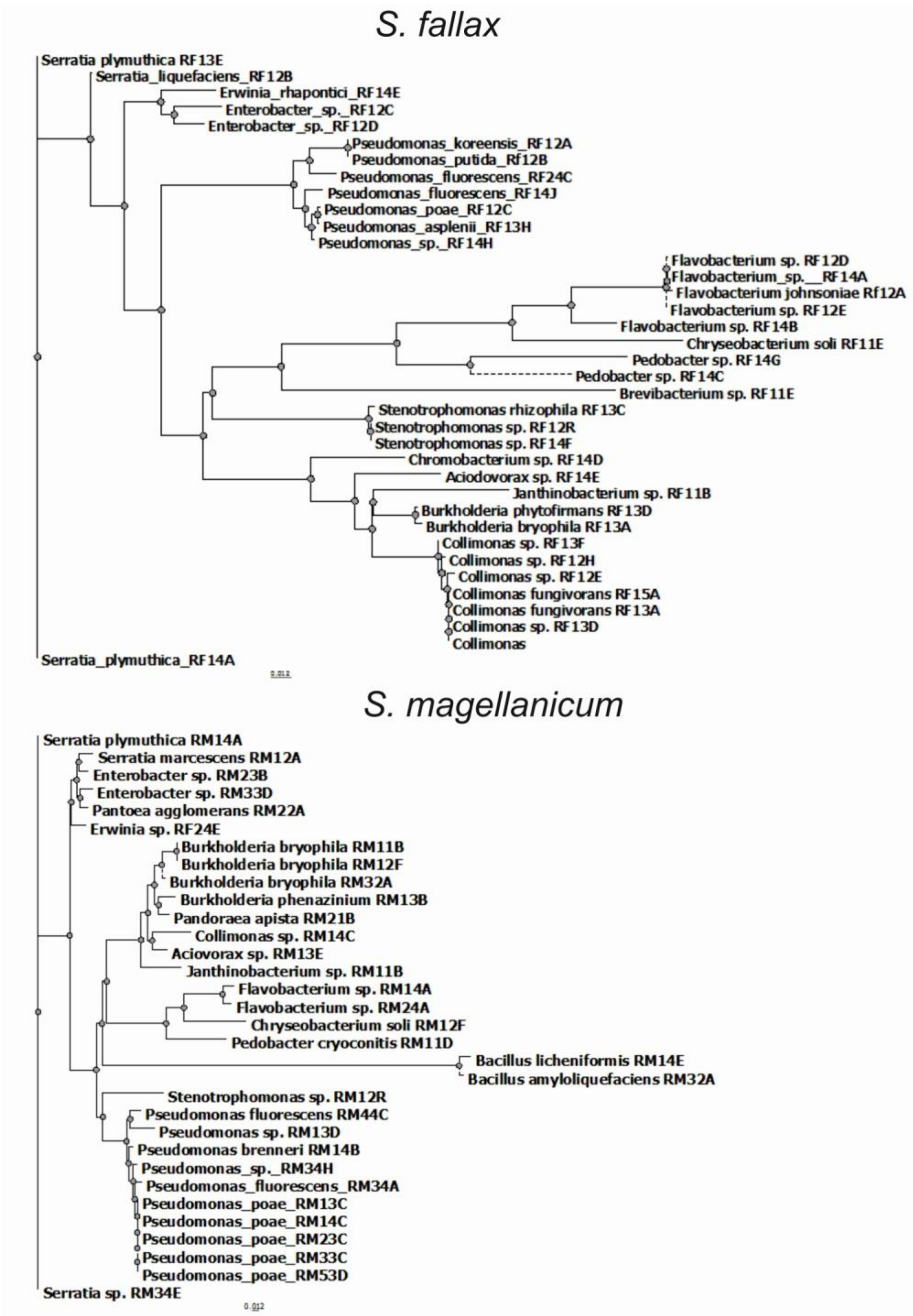


**Figure 2.** Phylogenetic trees obtained by maximum-likelihood analysis, reflecting the relationships of 16S rRNA gene sequences amplified from RNA isolated from *S. fallax* and *S. magellanicum*, sampled in the Leningrad region (Lake Voloyarvi, Vsevolozhsk District, 2010). Cluster analysis was performed with the UPGMA (unweighted pair group method with arithmetic averages) algorithm.

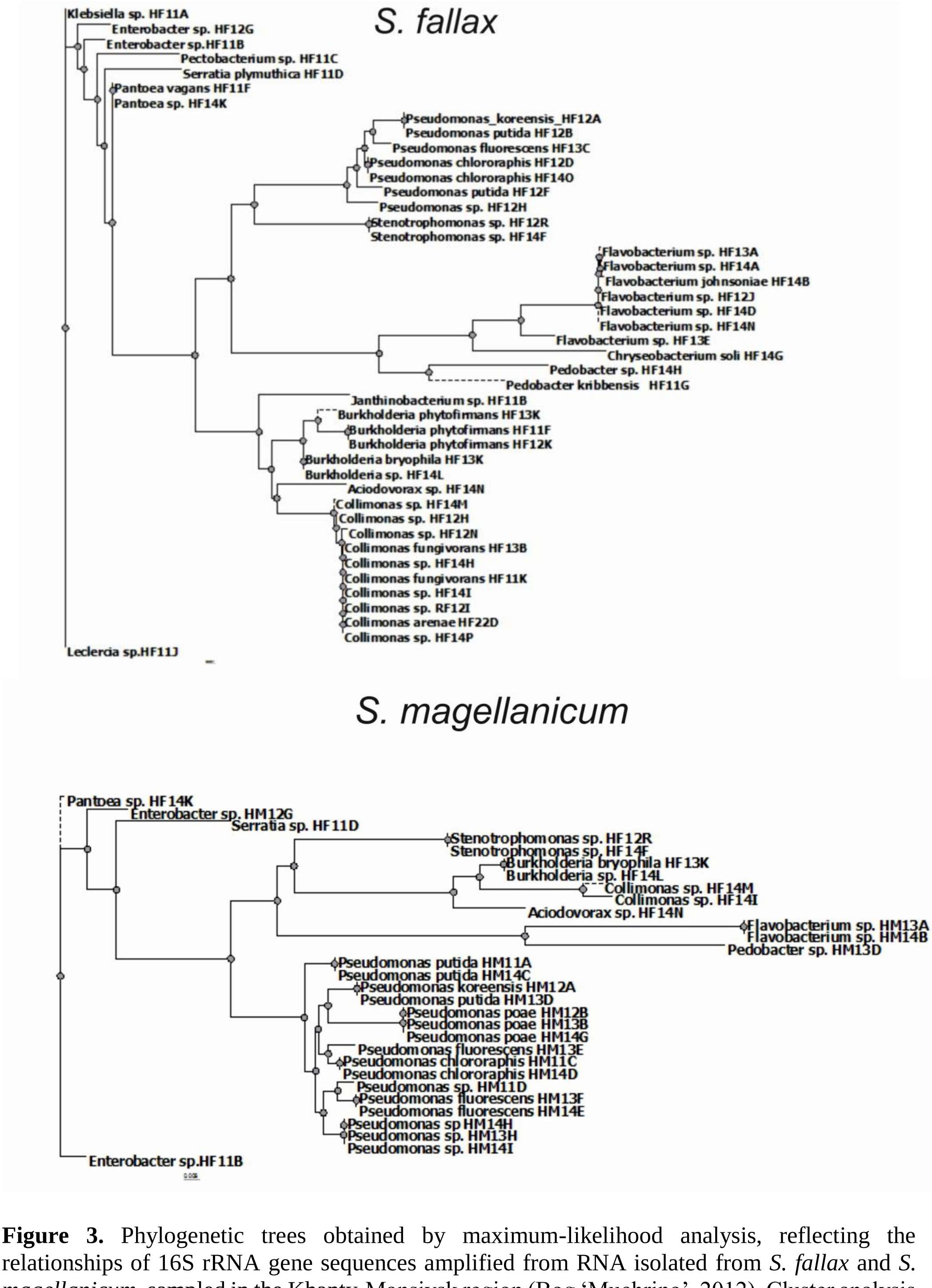


**Figure 3.** Phylogenetic trees obtained by maximum-likelihood analysis, reflecting the relationships of 16S rRNA gene sequences amplified from RNA isolated from *S. fallax* and *S. magellanicum*, sampled in the Khanty-Mansiysk region (Bog 'Muchrino', 2012). Cluster analysis was performed with the UPGMA (unweighted pair group method with arithmetic averages) algorithm.

**Table 1.** Number and distribution of genera *Sphagnum*-associated bacteria

| Genera | Nord-West Region | | | | | | Khanty-Mansiysk Region | | | | | |
|---|---|---|---|---|---|---|---|---|---|---|---|---|
| | Point 1[a] | | Point 2[a] | | Point 3[a] | | Point 1[b] | | Point 2[b] | | Point 3[b] | |
| | SM | SF | SM | SF | SM | SF | SM | SF | SM | SF | SM | SF |
| *Bacillus* | 2 | 0 | 1 | 1 | 0 | 3 | 0 | 0 | 2 | 1 | 2 | 0 |
| *Delftia* | 0 | 0 | 2 | 3 | 1 | 1 | 0 | 0 | 1 | 1 | 1 | 0 |
| *Rhodococcus* | 0 | 0 | 1 | 0 | 1 | 0 | 0 | 0 | 0 | 1 | 1 | 0 |
| *Chryseobacterium* | 1 | 1 | 3 | 1 | 1 | 0 | 0 | 1 | 2 | 0 | 0 | 3 |
| *Acidovorax* | 1 | 1 | 2 | 0 | 0 | 0 | 1 | 1 | 1 | 0 | 0 | 2 |
| *Erwinia* | 1 | 1 | 0 | 1 | 1 | 3 | 0 | 1 | 0 | 0 | 1 | 1 |
| *Enterobacter* | 2 | 1 | 0 | 3 | 3 | 5 | 1 | 2 | 1 | 0 | 5 | 3 |
| *Pedobacter* | 1 | 2 | 2 | 2 | 4 | 1 | 1 | 2 | 2 | 3 | 3 | 2 |
| *Serratia* | 3 | 3 | 1 | 3 | 2 | 5 | 1 | 1 | 3 | 5 | 2 | 1 |
| *Burkholderia* | 4 | 2 | 1 | 4 | 2 | 2 | 2 | 5 | 1 | 2 | 2 | 3 |
| *Stenotrophomonas* | 1 | 3 | 3 | 1 | 1 | 7 | 2 | 2 | 2 | 3 | 2 | 2 |
| *Flavobacterium* | 2 | 5 | 1 | 3 | 3 | 8 | 2 | 7 | 3 | 3 | 1 | 5 |
| *Collimonas* | 1 | 7 | 4 | 5 | 3 | 7 | 0 | 10 | 2 | 5 | 3 | 3 |
| *Pseudomonas* | 10 | 7 | 6 | 2 | 10 | 5 | 16 | 7 | 5 | 2 | 8 | 3 |
| *Other* | 3 | 4 | 5 | 6 | 8 | 7 | 4 | 3 | 4 | 1 | 6 | 7 |
| ∑ isolates | 32 | 37 | 32 | 44 | 40 | 60 | 30 | 44 | 29 | 27 | 37 | 35 |

[a]Point 1 – Voloyarvi Lake; Point 2 – Bog ‘Polesye’; Point 3 – Bog ‘Kardon Kirpichny’
[b]Point 1 – Bog ‘Muchrino’; Point 2 – Bog ‘Chistoe’; Point 3 – Bog ‘Kukushkino’

A characteristic feature was the low quantitative of gram-positive spore-forming bacteria from genus *Bacillus*: it was isolated and identified 2 species from the genus *Bacillu*s: *B. licheniformis* and *B. amyloliquefaciens*. The reasons of this phenomenon may be the waterlogging in the tall marsh ecosystems and habitat conditions *Sphagnum* or evolutionarily later appearance of spore-forming bacteria, when the foundations of the symbiosis between *Sphagnum* and other microorganisms have already been established. Since sporulation was formed in bacteria as an adaptation to adverse environmental conditions, especially a lack of moisture and the associated drying cells, it is logical to assume in the environment where the plant is only transferred to the terrestrial life, and much of it is in the water, plant-microbe symbiosis will occur with microorganisms that do not suffer from drying out and being in the aquatic environment. Such active microorganisms colonized the internal tissues and form a symbiotic relationship with *Sphagnum*, were the gram-negative bacteria.

**Discussion**

*Sphagnum* mosses are more dependent than other plants from the symbiosis with microorganisms, since this lack of root system and the ability to absorb nutrients from the soil substrate. The ability of mosses to the rate of photosynthesis, as well as high absorption activity and surface area are compensated these limitations of interstitial *Sphagnum* gametophytes. Products of photosynthesis thus can be used to support a variety of microorganisms providing food to their host, protection against phytopathogens, adaptation to abiotic stress and regulation of development.

Colonization of *Sphagnum* hyaline cells by heterotrophic bacteria was first mention in the works of Swedish researchers (Granhall & Hofsten, 1976). Their electron microscopic studies revealed, alongside with cyanobacteria, also heterotrophic ones. The most complete body of information on the heterotrophic bacteria associated with *Sphagnum* mosses, including the data obtained by molecular-genetic methods, can be found in Opelt and Berg (2004), Vandamme et al. (2007), Opelt et al. (2007) and Bragina et al. (2012).

In our studies, we present data on the diversity of microorganisms that were isolated from twospecies of sphagnum mosses selected in two geographically distant regions of Russia. The data reported in this work are consistent with the results of research performed by the Berg group with samples of mosses of the Austrian Alps. It was found that Sphagnum mosses are a promising source for the isolation of beneficial microorganisms.

According Opelt et al. (2007a; 2007b), with the use of SSCP method, the composition of microbial community was shown to vary depending on the moss species (two *Sphagnum* species, *Sphagnum magellanicum* and *S. fallax,* were studied), which collected in Austrian Alps. Samples of the same moss species from Germany and Norway had a similar composition of microbiota. The total of 1,222 strains of heterotrophic bacteria were isolated from surface-sterilized *S. fallax* and *S. magellanicum* samples by inoculation on solid cultural media.

Our data are consistent with the data on the species diversity of bacteria, isolated from Alps Sphagnum Mosses. Molecular-genetic identification of bacteria from Alps *Sphagnum* mosses revealed species of *Burkholderia*, *Serratia*, *Bacillus*, *Paenibacillus*, *Pseudomonas*, *Rahnella* and *Dyella* (dominant genera) as well as some representatives of *Moraxella, Microbacterium* and *Streptomyces*. According Opelt et al. (2007a; 2007b), more than 26% of the isolated strains had fungicidal activity against phytopathogenic fungi *V. dahliae* and *Rhizoctonia solani*. *S. fallax* had a higher percentage of strains with fungicidal activity than *S. magellanicum*. A special place among the isolated strains of *Sphagnum*-associated microorganisms was occupied by various *Burkholderia* species, bearing nifH genes and apparently possessing nitrogen-fixing activity.

Apparently, plants mosses form within its own hyalocytes certain conditions that are favorable for development of strictly selected genera of bacteria. These bacteria come into close relationship with the host-plant, supporting its metabolic activity. In this community of microorganisms we can identify key species, occurring in mosses of different geographical origin – for example, the characteristic species *Flavobacterium* sp.very common in the natural endophytic communities disribed in our work. This species is easily distinguishable morphologically in petri dishes from other colonies of microorganisms. Other abundant species identified during our study was *Pseudomonas poae*, found in large quantities (up to $10^4$–$10^5$ CFU $g^{-1}$ of plant tissue) in the microbial communities of *S. magellanicum*, rerely in the composition of endophytic microbiome of *S. fallax*.

During this work, regardless of Berg et al., from the same species of *Sphagnum* mosses we isolated representatives of *Burkholderia*, later identified as *B. bryophila* (Shcherbakov et. al., 2013). This species probably also is a characteristic in the composition of endophytic microbiome. In the composition of the microbial community of *S. fallax* one of the characteristic species were *Collimonas sp.*, not identified up to species (degree of genetic similarity of the sequences of the 16S rRNA gene with the closest species was 98%), forming morphologically homogeneous population, which have been actively developed on the surface of nutrient medium.

These isolates are likely to play an important role in the growth and development of plants *Sphagnum*. Requiring more detailed study of the mechanisms of interaction of these strains with the host-plant, their metabolic activity, chemical components produced by bacteria and the host-plant, we plan to continue the studies in the future.

## CONCLUSIONS

The studies of researchers (Raghoebarsing et al., 2005; Bragina et. al., 2012) had shown that tissue of *Sphagnum* mosses colonize diverse microbial communities, and that these bacteria can be used for practical purposes (Shcherbakov et al., 2013). In this work it was shown that the taxonomy composition of heterotrophic bacterial communities of *Sphagnum* mosses from different geographical origin include the genera *Pseudomonas, Serratia, Burkholderia, Flavobacterium, Collimonas, Stenotrophomonas*.

Our results confirm the validity of our strategy of sampling and high diversity and density of bacteria present in the tissues inside of *Sphagnum* mosses. In addition, we found a number of strains that can also represent a new species, and now require further investigation in our laboratory.

ACKNOWLEDGEMENTS. This study was financially supported by the Government of the Russian Federation, grant 074-U01 and performed on the equipment of the Centre for Collective Use ‘Genomic technologies and cell biology’ ARRIAM. The work of A.V. Shcherbakov and V.K. Chebotar was supported by the Russian Scientific Fund (project no. 14-16-00146).

## REFERENCES

Altschul, S.E., Madden, T.L., Schaffer, A.A., Zhang, J., Zhang, Z., Miller, W. & Lipman, D.J. 1997. Gapped BLAST and PSI-BLAST: a new generation of protein database search programs. *Nucleic Acid Res.* **25**, 3389–3402.

Bragina, A., Berg, C., Cardinale, M., Shcherbakov, A., Chebotar, V, Berg, G. 2012. *Sphagnum mosses* harbour highly specific bacterial diversity during their whole lifecycle. *The ISME Journal* **4** 6, 802–13.

Dedysh, S.N., Panikov, N.S., Tiedje, J.M. 1998. Acidophilic methanotrophic communities from Sphagnum peat bogs. *Appl. Environ. Microbiol.* **64**, 922–929.

Dedysh, S.N., Liesack, W., Khmelenina, V.N., Suzina, N.E., Trotsenko, Y.A., Semrau, J.D., Bares, A.M., Panikov, N.S., Tiedje, J.M. 2000. Methylocella palustris gen. nov., sp. nov., a new methane-oxidizing acidophilic bacterium from peat bogs, representing a novel subtype of serine-pathway methanotrophs. *Int. J. Syst. Evol. Microbiol*. **50**(3), 955–969.

Dedysh, S.N. 2009. Exploring methanotroph diversity in acidic northern wetlands: molecular and cultivation-based studies. *Microbiology* **78**(6), 655–669.

Granhall, U., Hofsten, A. 1976. Nitrogenase activity in relation to intracellular organisms in Sphagnum mosses. *Physiol. Plant*. **36**, 88–94.

Ignatov, M.S., Afonina, O.M., Ignatova, E.A. 2006. Check-list of mosses of East Europe and North Asia, *Arctoa* **15**, 1–130.

Kip, N., Ouyang, W., van Winden, J., Raghoebarsing, A., van Niftrik, L., Pol, A., Pan, Y., Bodrossy, L., van Donselaar, E.G., Reichart, G.J., Jetten, M.S., Sinninghe Damsté, J.S., Op den Camp, H.J. 2011. Detection, isolation and characterization of acidophilic methanotrophs from Sphagnum mosses. *Environ. Microbiol*. **77**(16), 5643–5654.

Larmola, T.E., Tuittila, S., Tiirola, M.H., Nykanen, P.J., Martikainen, Yrjala, K., Tuomivirta, T., Fritze, H. 2010. The role of *Sphagnum* mosses in the methane cycling of a boreal mire. *Ecology* **90**, 2356–2365.

Liu, W., Hou, J., Wang, Q., Ding, L., Luo, Y. 2014. Isolation and characterization of plant growth-promoting rhizobacteria and their effects on phytoremediation of petroleum-contaminated saline-alkali soil. *Chemosphere.* **117**, 303–308.

Mehnaz, S., Baig, D.N., Lazarovits,, G. 2010. Genetic and phenotypic diversity of plant growth promoting rhizobacteria isolated from sugarcane plants growing in pakistan. *J. Microbiol. Biotechnol.* **20** 12, 1614–1623.

Neupane, S., Finlay, R.D., Alström, S., Elfstrand, M., Högberg, N. 2015. Transcriptional responses of the bacterial antagonist Serratia plymuthica to the fungal phytopathogen Rhizoctonia solani. *Environ. Microbiol. Rep.* **7**(1), 123–127.

Opelt, K. & Berg, G. 2004. Diversity and antagonistic potential of bacteria associated with bryophytes from nutrient poor habitats of the Baltic Sea Coast. *Appl. and Envir. Microbil*. **70**, 6569–6579.

Opelt, K., Berg, C., Schonmann S., Eberl, L., Berg G. 2007a. High specificity but contrasting biodiversity of Sphagnum-associated bacterial and plant communities in bog ecosystems independent of the geographical region. *The ISME Journal* **1,** 502–516.

Opelt, K., Chobot, V., Hadacek, F., Schönmann, S., Eberl, L., Berg, G. 2007b. Investigations of the structure and function of bacterial communities associated with Sphagnum mosses. *Environ. Microbiol.* **9**(11), 2795–809.

Opelt, K., Berg, C., Berg, G. 2007c. The bryophyte genus Sphagnum is a reservoir for powerful and extraordinary antagonists and potentially facultative human pathogens. *FEMS Microbiol Ecol.* **61**(1), 38–53.

Raghoebarsing, A.A., Smolders, A.J., Schmid, M.C., Rijpstra, W.I.C., Wolters–Arts, M., Derksen, J.M. 2005. Methanotrophic symbionts provide carbon for photosynthesis in peat bogs. *Nature* **436**, 1153–1156.

Raghoebarsing, A.A., van de Pas–Schoonen, K.T., Smolders, A.J., Ettwig, K.F., Rijpstra, W.I., Schouten, S., Damsté, J.S, Op den Camp, H.J., Jetten, M.S., Strous, M. 2006. A microbial consortium couples anaerobic methane oxidation to denitrification. *Nature* **440**, 918–217.

Shcherbakov, A.V., Bragina, A.V., Kuzmina, E.Yu., Berg, C., Muntyan, A.N., Makarova, N.M., Malfanova, N.V., Cardinale, M., Berg, G., Chebotar, V.K., Tikhonovich, I.A. 2013. Endophytic bacteria of *Sphagnum* mosses as promising objects of agricultural microbiology. *Mikrobiologiya* **3**, 312–322.

Vandamme, P., Opelt, K., Knochel, N., Berg, C., Schonmann, S., Brandt, E., Eberl, L., Falsen, E., Berg, G. 2007. *Burkholderia bryophila sp. nov. and Burkholderia megapolitana sp. nov.*, moss-associated species with antifungal and plant-growth-promoting properties. *Int. J. of System. and Evol. Microbiol*. **57**, 2228–35.

Weisburg, W.G., Barns, S.M., Pelletier, D.A. & Lane, D.J. 1991. 16S ribosomal DNA amplification for phylogenetic study. *J. Bacteriol* **173**, 697–703.

*Agronomy Research* **13**(1), 202–211, 2015

# Development of in-store dryer model for corn for varying inlet conditions

Xu Ma, R.H. Driscoll and G. Srzednicki*

UNSW Australia, School of Chemical Engineering, Sydney NSW 2032 Australia; *Correspondence: g.srzednicki@unsw.edu.au

**Abstract.** Many thin layer drying models have been developed for constant inlet conditions. During deep bed drying, drying air conditions vary with position in the bed and also vary with time, so models developed for thin layers under constant conditions are not valid for deep bed drying analysis. A new thin layer drying rate model (called the two-layer model) is presented which allows for varying air conditions. The model was applied to corn by retro-fitting the model to Page's mode as fitted by Li and Morey (1984). The model was then incorporated into a deep bed simulation, and the results compared with pilot plant drying data. During drying experiments, constant air conditions and varying air conditions were both tested. For constant conditions, all models gave reasonable agreement, but for varying drying conditions, the diffusion model showed an ability to respond better to changes.

**Key words:** drying, corn, diffusion model, two layer model, varying air conditions.

## INTRODUCTION

Food dehydration is a unit operation consisting of removing moisture from a liquid, solid, or semi-solid feed material in order to control its bioactivity. Reduction of moisture reduces the risk of spoilage, so extends the shelf-life of foods. There are various mechanisms of food spoilage, which can be categorised as microbiological or chemical in nature. Microbiological causes of deterioration (such as bacteria, yeasts and moulds) need a wet substrate and a high water activity ($a_w$). The lower limits of $a_w$ for bacteria and moulds are 0.91 and 0.80 respectively (Smith, 2003). Dehydration reduces water activity, and after dehydration to below the microbial limits, the low $a_w$ environment is not suitable for bacterial and fungal growth. Chemical and biochemical causes of deterioration are also controlled by drying, including enzymic reactions, non-enzymic browning and lipid oxidation, which are not completely stopped but are significantly slowed down by the reduction in available water. Drying also helps preserves quality attributes of foods such as flavour and nutritive value, provided moderate drying temperatures are used. Moreover, dehydrated foods are easy to transport because of reduced weight or volume.

With a total production of 872 Mt in 2012 (Statista, 2015), corn is the highest volume grain crop produced in the world. Although in various parts of the world sun-drying of corn is still practiced, the fact that the drying performance is affected by weather conditions and that this process is often slow, leads to mould growing and results in production of mycotoxins (especially aflatoxins), which may harm human and animal health.

As a result, mechanical drying of corn is being increasingly adopted, especially among major producers of this crop. Various types of dryers are used for corn drying, for example column dryers or fluidised bed dryers for drying of very wet grain at high temperature with a continuous flow of grain or deep bed dryers with a static bed for grain at moisture content below 18% wet basis (wb). Deep bed dryers are often used for corn harvested under the prevailing climatic conditions in Australia, but since deep-bed models are based on thin-layer drying models, development of such a model for corn was the main focus of this study.

Dehydration of foods is a special challenge for food engineers, due to the complexity of food structure, texture and chemical composition. In order to predict dryer behaviour, mathematical models of the drying process have been developed. For accurate prediction of the drying behaviour of a food material these models are based on knowledge of drying principles, psychrometrics, product thermo-physical properties and the principles of heat and mass balance and transfer.

To reduce this complexity, in practise, many experimenters instead develop empirical or semi-empirical models of thin layer drying rates, which are then fitted to experimental data obtained under constant drying conditions. Drying models constructed for thin layers of a specific food product are then often applied to the deep bed dryers, commonly used for corn.

In a deep bed dryer, air passes from the inlet through successive layers of granular material before exiting the bed. Mathematically, each layer can be treated as a thin layer of material. Since each layer interacts with the drying air, air conditions are modified from inlet to outlet, and so each layer interacts with differing air properties.

Over time, successive layers will tend towards moisture equilibrium with the inlet air. Thus not only does each layer interact with different conditions, but those conditions are changing with time as the product dries.

The above discussion assumes the inlet air stays constant, but in commercial practice, this is not valid, as the inlet air is affected by changing ambient conditions or changing control setpoints. As a result, no layer in a deep bed receives the same air conditions over time. Thin layer drying models are normally developed using constant conditions only.

A number of thin layer drying models have been developed, and used for deep bed drying of grain. Among the most successful equations predicting the drying behaviour of corn are Page's (Li & Morey, 1984), a two-compartment (Henderson (1974) and a modified two-compartment model (Verma et al., 1985). However none of these takes into account changing air conditions, and so are not valid for application to deep bed drying.

A new thin layer drying model was developed by the Food Engineering Research Group at UNSW in Sydney, which has a theoretical basis in diffusion and surface transfer theory, but is able to respond to varying inlet conditions. The product is modelled as two separate compartments, only one of which interacts with the drying air, the other being buried within. No specific shape is assumed for the product, but the model can conveniently be represented by concentric spheres.

The aim of this study was to investigate the drying behaviour of a deep bed of corn using a form of diffusion model adapted for varying inlet conditions, and to test its responsiveness to changing conditions.

## THEORETICAL DEVELOPMENT

Page's (reference) empirical model is one of the most successful models for predicting drying time and moisture ratio, and has been widely used in food product drying. Li & Morey (1984) applied Page's model to corn drying data. Page's model can be expressed as:

$$MR = \frac{M - M_e}{M_0 - M_e} = \exp(-kt^n) \tag{1}$$

where: $MR$ is called the moisture ratio; $M$ is moisture content, % dry basis (%db); $M_o$ is initial moisture content, %db; $M_e$ is equilibrium moisture content, %db; k, n are drying constants; t is time.

The constant $k$ is normally assumed to exhibit Arrhenius temperature dependence, requiring determination of activation energy, $h$. The three drying constants $k$, $n$ and $h$ were obtained by Li and Morey (1984) by fitting the equation to experimental data.

Unlike Page's model, the new model is based on diffusion theory, with the product being composed of two layers (as for example was done by Verma et al., 1985). Fig. 1 represents the structure of the product. Layer 1 is the interior of the product and layer 2 is the layer in contact with the surface, and which interacts with the drying air. Note that the layers do not physically have to be spherical the only geometric requirement is that layer 2 wraps around layer 1 to prevent its contact with the drying air.

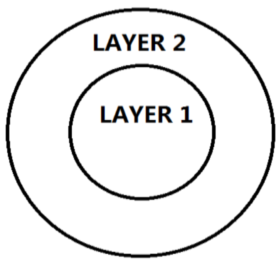


**Figure 1.** Structure of a product represented by two layers (Verma et al., 1985).

Define a mass ratio constant μ as:

$$\mu = m_{s2} / m_{s1} \tag{2}$$

where: $m_{s1}$, $m_{s2}$ are the masses for each layer on a dry basis.

The drying rates for each layer (using a first term approximation to the diffusion equation and including surface evaporation) are:

$$\frac{dM_1}{dt} = -k_1\mu(M_1 - M_2) \tag{3}$$

$$\frac{dM_2}{dt} = -k_1(M_2 - M_1) - k_2 A(M_2 - M_e) \quad (4)$$

The model moisture in the product can be calculated by equation (6).

$$M = \frac{M_1 + \mu M_2}{1 + \mu} \quad (5)$$

where: $M$ is the average moisture content; $M_1$, $M_1$ are the layer moisture contents; $k_1$, $k_2$ are rate constants.

The reason for inserting a factor μ on the right-hand side of equation (4) is to ensure mass balance is observed, which requires the mass leaving layer 1 to be equal to the mass entering layer 2 at the layer interface. The second term in equation (5) expresses the rate of evaporation from the surface. This could be estimated theoretically (for example from the wet bulb equation), but since product properties change during drying, it was thought best to leave this as a model parameter, determined by best-fit to drying data.

Since this model is in written in a differential form, it was implemented on computer using finite difference approximations.

Constants $k_1$ and $k_2$ are assumed to be dependent on temperature (Arrhenius):

$$k_1 = k_{10} \times \exp(-h_1/RT_k) \quad (6)$$

$$k_2 = k_{20} \times \exp(-h_2/RT_k) \quad (7)$$

where: $h_1$, $h_2$ are heat activation energies (J kmol.$K^{-1}$); $k_{10}$ and $k_{20}$ are constants; $T_k$ is temperature (Kelvin).

The method could be extended to further layers, but two layers was considered adequate, because integration of the resulting equations (4), (5) and (6) gives a form of equation similar to the standard two compartment model (Henderson, 1974), with two exponential terms and two constants. The integration is difficult, requiring successive elimination of $M_1$ and $M_2$ to give a final second order differential equation in M which when solved gives the two-term exponential form.

Equilibrium moisture content data published by Chen & Morey (1989) were used to estimate $M_e$ (see Table 1).

**Table 1.** Predicted final Me values required for drying runs (using Chen and Morey's equation, 1989)

| T (°C) | RH (%) | Me (%db) |
|---|---|---|
| 71 | 2 | 1.82 |
| 71 | 10 | 4.00 |
| 60 | 4 | 2.66 |
| 60 | 28 | 7.19 |
| 49 | 5 | 3.12 |
| 49 | 40 | 9.33 |

## MATERIALS AND METHODS

### Corn samples

The samples of hybrid waxy corn were supplied by Ingredion ANZ Pty Ltd in Lane Cove NSW 2066 (Australia). The initial moisture content (MC) was 12% wet basis (wb) or 13.6% dry basis (db). They were kept in a cold room at a temperature (T) of 3.5 °C and 55% relative humidity (RH) prior to rewetting pre-treatment.

### Conditioning of corn samples

Before conducting the drying experiments, the samples were taken out of the cold room and left in the lab to reach ambient temperature (about 23 °C). In order to prevent mould growth during rewetting, the samples were subjected to surface disinfestation by dipping them in a 1% hypochlorite solution for 1 min.

After harvest, corn has a moisture content between 23–26%wb (30–35% db) and such were the required levels for drying experiments. Thus, the seeds samples were rewetted by adding a calculated amount of distilled water. Then, the seeds were mixed daily and kept at a temperature of 2–5 °C for approximately 7 days to equalise the moisture content distribution and reduce the risk of spoilage. The moisture content of the seed samples was determined by the oven method in accordance with ASAE Standards. For moisture content determination, 15 g of corn seeds were dried at 103 °C for 72 h in a convection oven. The moisture content of seeds was calculated by using the weight loss after drying in the oven. A rapid method (11 min) using the infrared lamp (Mettler LP12) and a balance for ground samples was used for assessment of moisture content of samples during rewetting.

### Fitting the Two Layer model

The Page model was assumed to be a good description of the thin layer drying rate of corn for constant aeration conditions. The new Two Layer model was retro-fitted to the Page model, using the method of least squares to minimise the difference between the models. This allowed direct comparison of the capability of the two models to describe changing conditions. The calculated average moisture content M shows good agreement with Page's model. Comparison runs were generated for typical corn drying conditions, and an example is shown below (Fig. 2).

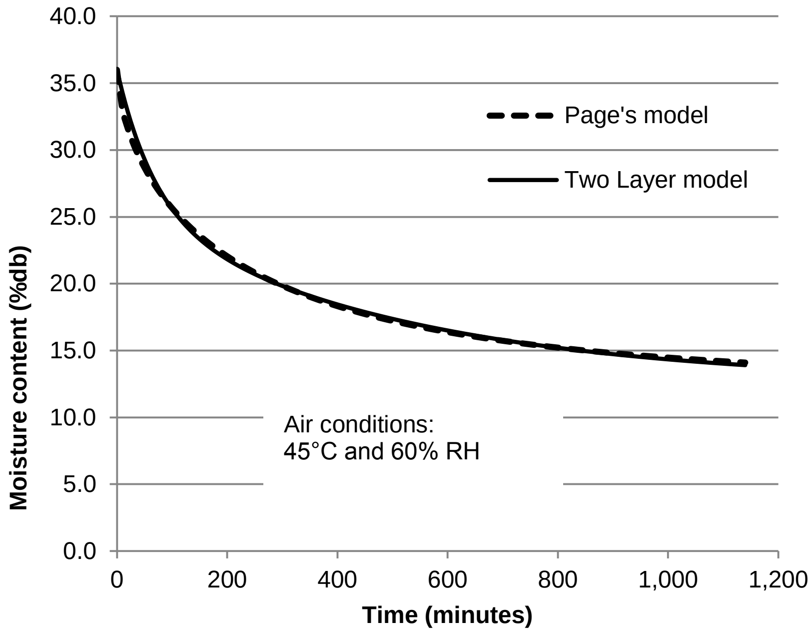


**Figure 2.** Example demonstrating agreement of retro-fitted Two Layer model to Page's model.

### Drying experiments

The in-store dryer built by the Food Engineering Group at the UNSW was used for the deep bed drying experiments (see Fig. 3).

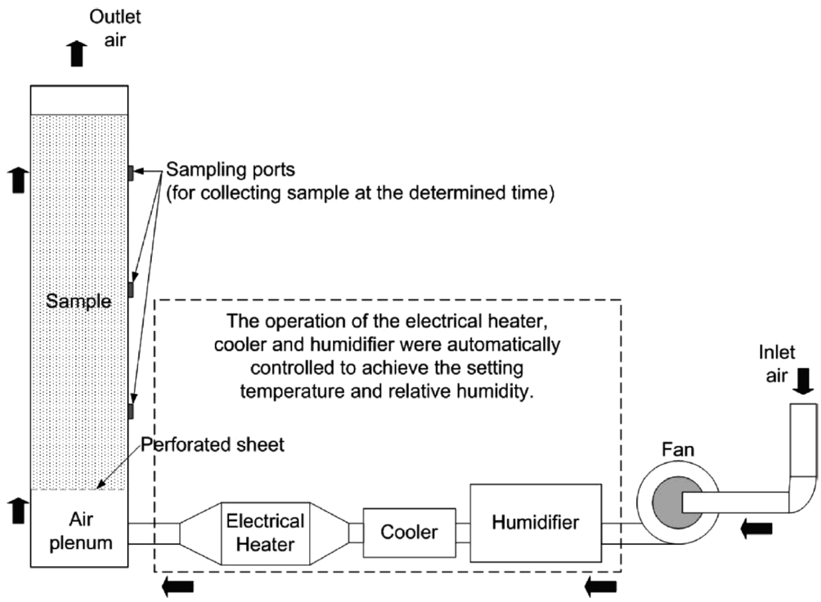


**Figure 3.** Schematic of the in-store dryer used in the experiments. Source: Jittanit et al. (2010).

The dryer is computer controlled and includes the following hardware:

- SWINNERTON centrifugal fan 7.5 kW with backwards curved blades
- Drying bin 1 tonne of corn capacity
- Heating unit (four heating steps: 7.5 kW, 1.5 kW, 0.75 kW and 0.75 kW)
- Air chilling unit (Carrier 30RQ005, 14.6 kW)
- Chilled water tank for cooler (not shown)
- Steam generator for humidifier (SIMONS model 25/100, 24 kW, not shown)
- Armstrong humidifier model FSA-1
- Landis & Staefa actuator model SKD62
- TOSHIBA variable speed drive model VF-S7 for fan control.
- T-type thermocouples, RH probes and RTD temperature sensors were fitted to the drying bin.

The drying conditions are shown in Table 2. In contrast to the conventional practise of keeping the process parameters constant (T and RH) during the whole run, this study used changing conditions where both temperature and relative humidity were changed during drying runs.

**Table 2.** Drying conditions for the five drying runs

| Run No | Condition 1 | | Condition 2 | | Condition 3 | |
|---|---|---|---|---|---|---|
| | T (°C) | RH (%) | T (°C) | RH (%) | T (°C) | RH (%) |
| 1 | 40 | 40 | 50 | 40 | 30 | 60 |
| 2 | 40 | 40 | 25 | 40 | 35 | 60 |
| 3 | 35 | 50 | 30 | 60 | 35 | 50 |
| 4 | 40 | 50 | 30 | 50 | 40 | 50 |
| 5 | 40 | 50 | 40 | 50 | 40 | 40 |

In spite of having a PID controller, the conditions could not always be precisely achieved due to the response time of the system controllers and actuators.

## RESULTS AND DISCUSSION

In all 5 runs, the corn was dried to a final moisture content of about 12% dry basis. The air speed was determined by hotwire anemometer traverses to be about 0.73 m $s^{-1}$ on average. Due to air vibration caused by the fan and poor relative humidity control, all data were smoothed (running average over 5 points) for presentation. However actual inlet data were used as input for the drying simulation.

Temperature data were chosen as the basis for comparison, as temperatures can be measured without disturbing the bed of corn. Five sensors were located at 20 cm intervals within the experiment bed, and these could be compared with simulated data.

Fig. 4 is an example comparison between the pilot plant (real) data and the simulation, for the first (inlet) layer of the deep bed. The dryer was operated empty for 4 hours, to allow the system to equilibrate, and then loaded over a period of 30 min (as can be seen by the temperature spike at 4 hours). For this run, changes in inlet drying conditions were made after 25 hours and again after 34 hours, as can be seen in the temperature data for layer 1. Also the effect of fluctuations in ambient conditions can be seen in the form of small perturbations in the drying data (dotted line).

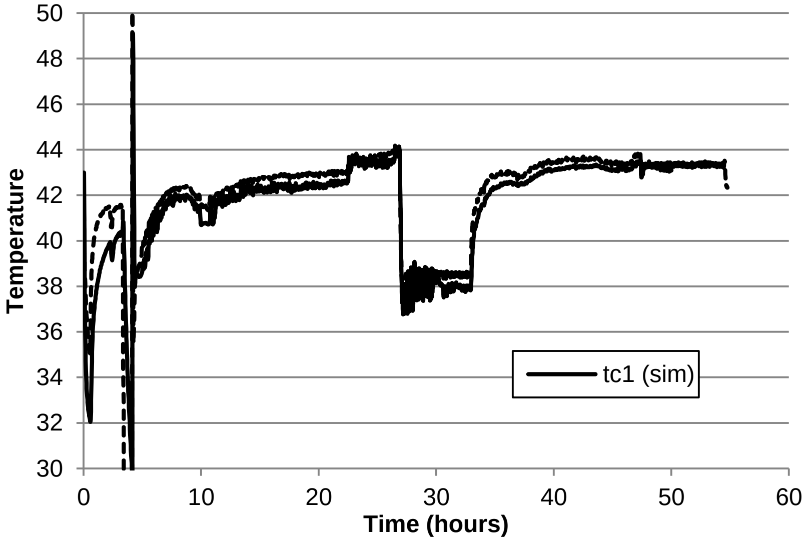


**Figure 4.** Comparison between data and model for layer 1 (near inlet) of first run.

Fig. 5 compares the data and simulation for the 5th layer (near outlet). Although the agreement is not as good as for Fig. 4, the simulation shows excellent responsiveness under changing conditions. The other four runs gave similar results.

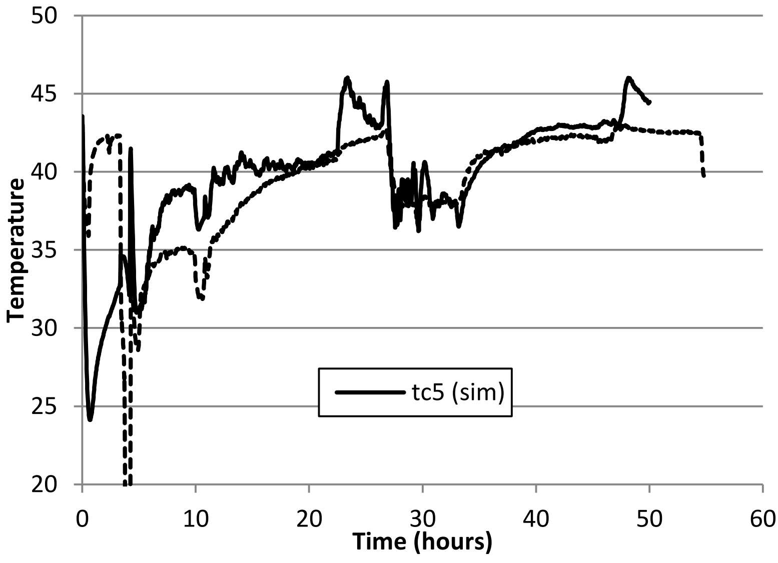


**Figure 5.** Comparison between data and model for layer 5 (near outlet) of first run.

Figs 6 and 7 show a comparison between the data and a different model, a two compartment model for a deep bed dryer using the Li and Morey (1984) model for thin layer drying. By comparing Figs 4 and 6 directly (for the first or inlet layer), and Figs 5 and 7 directly (for the outlet layer), the differences between the models can be seen. In both cases, the two layer model shows a better agreement between data and model. Similar results were obtained using other models for other experimental runs.

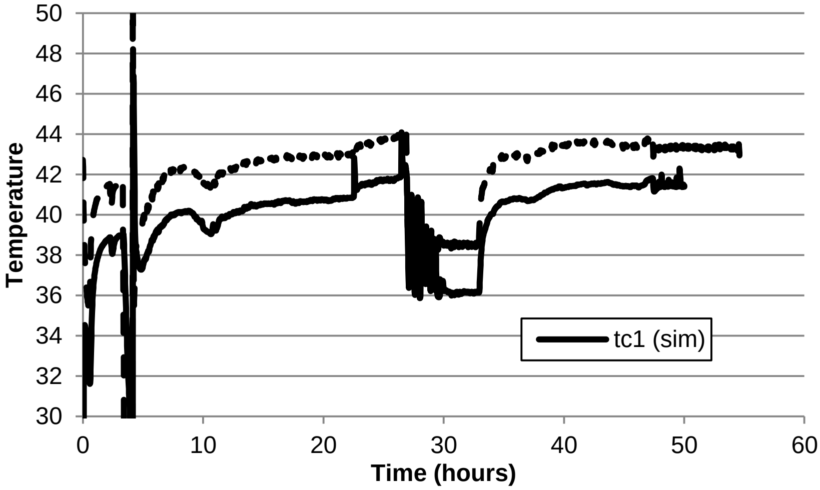


**Figure 6.** Comparison between data and Two Compartment model for layer 1 (near inlet) of first run.

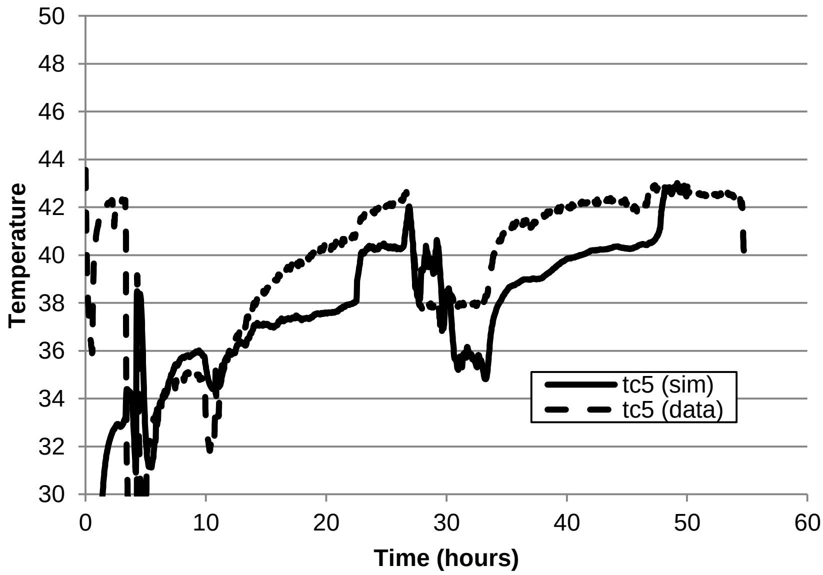


**Figure 7.** Comparison between data and Two Compartment model for layer 5 (near outlet) of first run.

## CONCLUSIONS

A new method for modelling thin layer drying rates has been presented, which uses differential forms of models to allow response to changing air drying conditions, and so giving a model which could be used for deep-bed simulation.

Two factors give an improved likelihood for correct modelling of drying rates through a deep bed, which are the differential form of the model and storage of moisture content information $M_1$ and $M_2$ for two layers. Further layers would give little benefit for the same reason that a two compartment model of thin layer drying rates is adequate for most practical situations, and in fact a single compartment model is often enough.

The results show that the model does respond correctly to changing inlet conditions, although agreement between the model and data is not always good. The model also provides a theoretical basis for understanding and predicting tempering effects during conditioning of grain in holding silos.

ACKNOWLEDGEMENTS. The contribution of Ingredion ANZ Pty Ltd, who provided the corn samples, is acknowledged.

## REFERENCES

ASAE 1988. ASAE Standards. ASAE S352.2: Moisture Measurement–Ungrounded Grain and Seeds, ASAE: St. Joseph, MI.

Chen, C.C. & Morey, R.V. 1989. Equilibrium relativity humidity (ERH) relationships for yellow-dent corn. *Transactions of the ASAE* **32**(3), 999–1006.

Henderson, S.M. 1974. Progress in developing the thin layer drying equation. *Transactions of the ASAE* **17**, 1167–1172.

Jittanit, W., Srzednicki, G. and Driscoll, R.H. 2010 Corn, Rice and Wheat Seed Drying by Two-Stage Concept, *Drying Technology* **28**(6), 807–815.

Li, H., & Morey, R.V. 1984. Thin layer drying of yellow dent corn. *Transactions of the ASAE* **27**(2), 581–585.

Smith, P.G. 2003. Introduction to Food Process Engineering, Kluwer Academic/Plenum Publishers, New York, p. 320.

Statista 2015. http://www.statista.com/statistics/263977/world-grain-production-by-type. Accessed 31.01.2015.

Verma, L.R., Bucklin, R.A, Ednan, J.B. & Wratten, F.T. 1985. Effects of drying air parameters on rice drying models. *Transaction of the ASAE* **28**, 296–301.

# II LIVESTOCK TECHNOLOGY

*Agronomy Research* **13**(1), 215–222, 2015

# Forced convection in drying of poultry manure

A. Aboltins[1,*] and P. Kic[2]

[1]Latvia University of Agriculture, Institute of Agricultural Machinery, Cakstes blvd. 5, Jelgava, LV–3001, Latvia; [*]Correspondence: aivars.aboltins@inbox.lv
[2]Czech University of Life Sciences Prague, Faculty of Engineering, Kamycka 129, 165 21, Prague 6, Czech Republic

**Abstract.** Pollution of environment by animal waste can be problem of intensive animal production in many countries with high density of animal farms. The aim of this paper is to inform about the experimental and theoretical investigations of moisture content reduction from poultry manure by forced convection. The experimental data created the background for calculation and modelling, which resulted in definition of the theoretical drying coefficient, useful for description and modelling of the drying process. The theoretical model has been verified and compared with experimental results obtained from the measurement. The laboratory equipment was used for test the forced convective drying of poultry manure due to vertical air streams going from bottom through supporting trays with holes and therefore through the manure up. Changed opened area of trays with different density has been used for definition of main parameters, which can serve especially in designing and construction of the new equipment for housing of poultry or improvement of the use of drying tunnel or in similar applications. The experimental data show that the air flow significantly increase the amount of moisture carried away from the material. Holes´ size does not significantly affect water runoff by convection without additional air flow.

**Key words:** air, bottom drying, drying coefficient, model, moisture.

## INTRODUCTION

The great problem of intensive animal production, especially in the countries with high density of population and also with high density of animal farms, is the animal waste management. Pollution of the environment by the animal waste can be a big problem which should be solved in the whole production and logistic chain. Modern farms with eggs production are typical with large capacity and concentration of laying hens in one location, which enable the use of industrial principles of technology but with respect to the animal welfare (Council Directive, 1999/74/EC).

Poultry manure can be a valuable resource of a significant amount of nitrogen, phosphorus, and many other components. The rapid growth of the animal breeding including the poultry industry in recent years and the application of waste to the agricultural land has resulted in excessive concentration of farms in many locations. Therefore direct fertilizing using fresh excrements is strictly limited by its consistence which does not allow a uniform spreading. Another limitation is the seasonality of application – it can be used only in a specific time-frame and is limited by the quantity (De Gobbi et al., 2012).

An application without treatment or non-appropriate disposal can become risky for environment and humans as such application might lead to the spread of diseases and may pollute soil and groundwater. Therefore the strong attention is paid to the technical solutions in the areas with intensive animal production (Chiumenti et al., 1993).

One of the reasonable solutions can be drying and reduction of water content in the manure, which can help to the solution of environmental problems and also reduce the costs of the logistics, storage and application for the farmers. Different technical principles of drying systems for poultry manure were used during the previous years. The producers of technological equipment for poultry usually apply the practical and empirical experience for the construction of drying equipment. The main principals are described in the literature, e.g. (Chiumenti, 2004). The investigations of characteristics of drying process of poultry manure at various temperatures have been done at the Faculty of Engineering CULS Prague (Liska & Kic, 2011).

In order to understand the drying process and find optimal drying regime it is necessary to understand transport mechanisms which take place within and on the surface of the product. Drying process is characterized by the existence of transport mechanisms such as surface diffusion, pure diffusion, capillary flow, evaporation, thermo-diffusion, etc. There are many different applications of drying for the agricultural (Jokiniemi et al., 2012; Aboltins & Palabinskis, 2013; Jokiniemi et al., 2014) or energetic purposes (Pasila, 2013).The forced convective drying of poultry manure by two air velocities going from tube to surface of trays with manure is given at (Kic & Aboltins, 2013).

The aim of this work is to bring some new experimental and theoretical investigations of drying of poultry manure with forced convective drying by air streams going from bottom through trays with different size of holes and therefore through manure up.

## MATERIALS AND METHODS

The laboratory measurements were carried out at the Faculty of Engineering CULS Prague during weather conditions from July to September. The technical equipment used for the experiments was forced convection system (Fig. 1) (Kic & Liska, 2012), simulating partly the real technical system used in some drying tunnels with belt conveyer (Fig. 2) for drying in the poultry farms.

The moisture content in the manure was identified by gravimetric measurement in regular time intervals. Samples were weighed on the digital laboratory balance KERN-440-35N with maximum load weight 400 g and with resolution 0.01 g. The total drying time was adapted to the need for a determination of final moisture content.

Samples were weighted during the drying on a laboratory balance (Fig. 3) and values were recorded. Each measuring tray was weighed during the first 3 hours every 15 min, later during the next 2.5 hours every 30 min and after that every 60 min. To research the drying kinetics manure samples were placed on trays with three different hole sizes (3, 4, 5 mm) and sieve with mesh 3 x 4 mm.

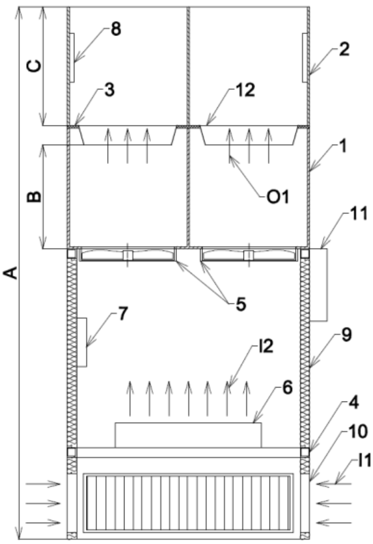


**Figure 1.** Apparatus used for manure drying (Kic & Liska, 2012): 1 – lower drying chamber; 2 – upper drying chamber; 3 – underlay; 4 – structure; 5 – fans; 6 – air heating; 7 – sensors; 8 – sensors; 9 – thermal insulation; 10 – inlet air; 11 – control panel; 12 – perforated tray with measured manure; I1 – inlet of fresh air; O1 – air passing through perforated tray with measured manure; A – overall height; B – height of the lower chamber; C – height of the upper chamber.

Air speed was measured by anemometer CFM 8901 Master with resolution 0.01 m $s^{-1}$ and accuracy ± 2% of final value. Air temperature and humidity was measured by the sensor FHA646-E1C connected to the data logger ALMEMO 2690-8.

**Figure 2.** Manure on the bell.


**Figure 3.** Measuring plates in experiment.

Assuming that the product is placed in thin porous layer it can be considered that the manure moisture W depends only on the drying time (at constant drying temperature). Taking into account the mathematical model of drying process of porous material layer (Aboltins, 2013) the manure drying process can be described by mathematical expression:

$$\frac{dW}{dt} = K(t) \cdot \left(W_p - W\right), \quad \text{with condition } W(0) = W_s \tag{1}$$

where: $W_s$ – manure moisture at the beginning of the experiment; %; $W_p$ –equilibrium moisture content; dry basis, %; $K(t)$ – drying coefficient, $h^{-1}$.

Lack of knowledge of drying coefficient K(t) makes difficult the drying process modelling. The K(t) expression depends not only on the drying product but also the drying temperature and conditions. In addition, the drying rate is variable during the drying due to different mechanisms of a moisture transport such as a surface diffusion, pure diffusion, capillary flow, evaporation, thermo-diffusion, etc. There is used the common transport coefficient K(t), which was found by the methodology (Aboltins, 2013).

## RESULTS AND DISCUSSION

The kinetics of manure drying process caused by forced convection was measured by manure samples placed on trays with three different hole sizes (3, 4, 5 mm) and sieve with mesh 3 x 4 mm with the air speeds 1.13 m $s^{-1}$ and 2.05 m $s^{-1}$. The results were compared with not forced drying.

Experimental results showed that the holes size does not significantly affect the water removal process from manure. The most significant acceleration of the drying process was observed through a sieve especially at higher air speeds (Figs 4, 5). Average air temperature during the drying process was 21.9 °C.

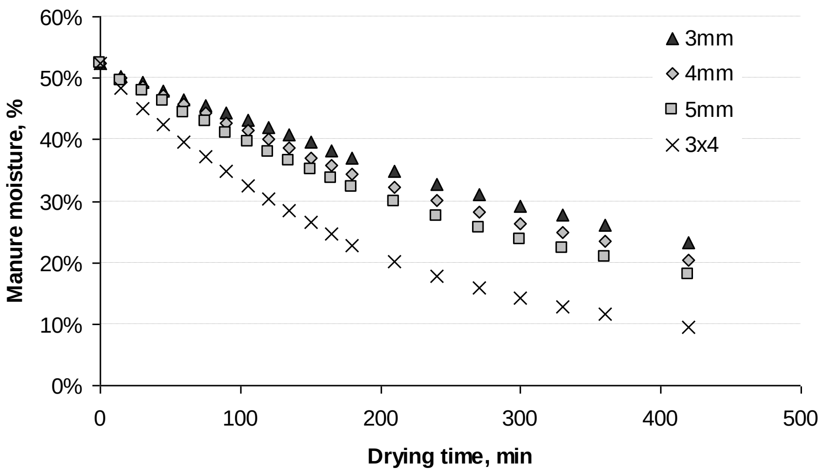


**Figure 4.** Moisture changes of manure samples placed on trays with different sizes of holes, by forced convection with air speed at bottom 2.05 m $s^{-1}$.

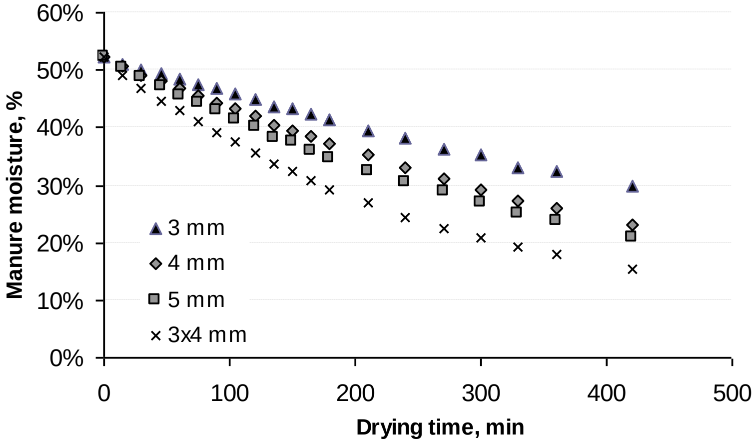


**Figure 5.** Moisture changes of the manure placed on trays with different sizes of holes, by the forced convection with the air speed at bottom 1.13 m $s^{-1}$.

It can be explained by the greater surface area of the manure through which is passing the air flow. Comparing the effects of air velocity, it can be seen that the higher air speed significantly increases the speed of drying at the beginning of the drying process. This can be explained by the migration of moisture from the surface of the product. Later, when the water runoff provides diffusion, the effect of air velocity on the product drying rate decreases.

The air flow velocity significantly affects the amount of water carried away, especially during the first 2–3 hours of drying (Figs 6, 7). During the first 3 hours of drying with all perforation holes and with the air speed 2.04 m $s^{-1}$is removed by 5% more moisture than with the air speed of 1.13 m $s^{-1}$. After 3 hours of drying on the sieve tray with the air velocity 2.04 m $s^{-1}$manure moisture is reduced to 22.7%.

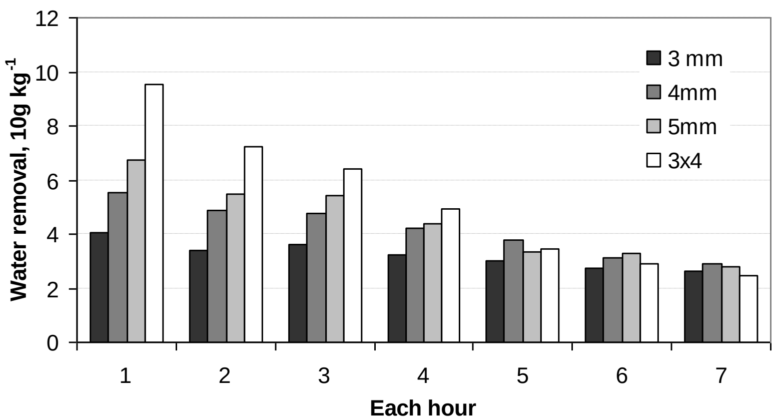


**Figure 6.** The moisture removal from the manure (10g $kg^{-1}$) with the initial manure moisture 52.4%, at each hour of drying with the air speed at bottom 1.13 m $s^{-1}$.

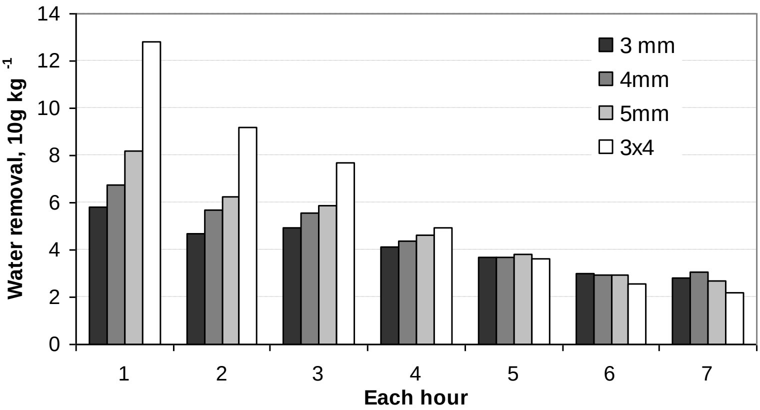


**Figure 7.** The moisture removal from the manure (10g kg$^{-1}$) with initial manure moisture 52.4%, at each hour of drying with air speed at bottom 2.04 m s$^{-1}$.

The results show that the forced air flow significantly increases the drying speed. Free convection is ineffective in manure drying especially during the first hours of drying (Fig. 8).

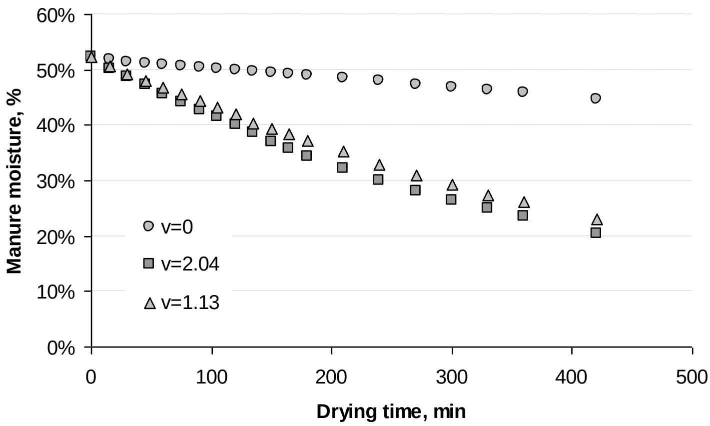


**Figure 8.** Changes of the manure moisture at tray with holes size 4 mm and with different forced air speeds v (m s$^{-1}$).

Using the experimental data and according to the methodology described in (Aboltins, 2013), there is in the case of manure drying by forced convection at sieve with mesh 3 x 4 mm with air velocity 1.13 m s$^{-1}$ obtained variable drying coefficient:

$$K(t) = 0.71 \cdot 10^{-5} \cdot t + 39.3 \cdot 10^{-4}, \qquad (2)$$

with the coefficient of determination $\eta^2 = 0.89$, where $t$ is the drying time (min).

The theoretical changes of manure weight can be calculated using (1)as

$$W = (W_s - W_p) \cdot exp[-(\frac{0.71 \cdot 10^{-5}}{2} t^2 + 39.3 \cdot 10^{-4} \cdot t)] + W_p, \qquad (3)$$

The theoretical and experimental results of changes of manure mass are shown in Fig. 9.

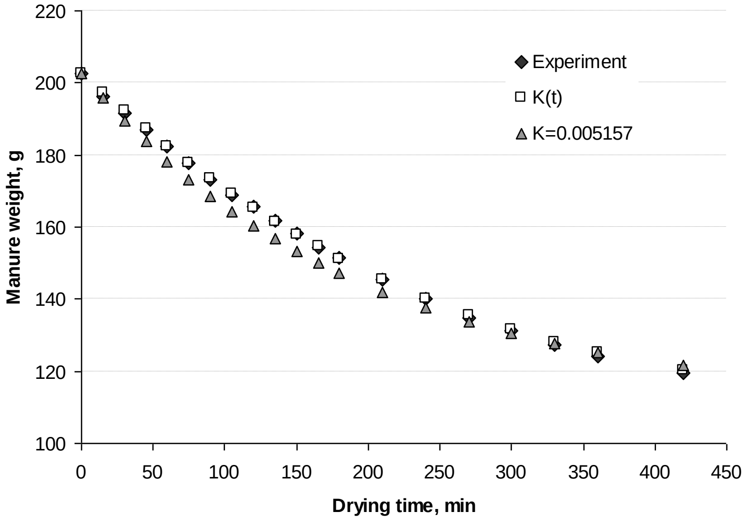


**Figure 9.** The theoretical (with constant and changing drying coefficients) and experimental changes of manure moisture at sieve with mesh 3 x 4 mm with forced air speed 1.13 m $s^{-1}$.

The constant drying coefficient was calculated as an average of drying coefficient values at each point of time. The average value of difference between the corresponding theoretical and experimental data was 1 g with standard deviation 0.7 g (for linear K(t)) and 2.6 g with standard deviation 1.6 g (for the constant drying coefficient). The equilibrium moisture content of manure in experiment was 16%.

The drying coefficient in the case of manure placed in a tray with holes 5 mm with the forced air by the velocity of 1.13 m $s^{-1}$, was

$$K(t) = 0.23 \cdot 10^{-5} \cdot t + 27.77 \cdot 10^{-4}, \qquad (4)$$

with the coefficient of determination $\eta^2 = 0.88$, with holes 4 mm was

$$K(t) = 0.22 \cdot 10^{-5} \cdot t + 23.23 \cdot 10^{-4}, \qquad (5)$$

with the coefficient of determination $\eta^2 = 0.95$ and with holes 3 mm

$$K(t) = 0.2 \cdot 10^{-5} \cdot t + 19.1 \cdot 10^{-4}, \qquad (6)$$

with the coefficient of determination $\eta^2 = 0.93$.

According to the equations (4–6) the hole diameter does not significantly affect the drying rate dependence on the time. Diameters have a significant impact at the beginning of drying process, which is characterized by free expression members at equations (4–6). Comparing the expressions (4–6) with (2) it is obvious that the tray with the sieve significantly increases the drying rate dependence of the time. This effect is more than 3 times larger than with the trays with holes.

## CONCLUSIONS

This research was useful for verification of the method for calculation of a drying coefficient in a thin layer of material for very special materials, like poultry manure. It has been found that the air flow has a strong influence on drying time, but the shape and dimensions of holes are not important from this point of view. The free convection is not efficient for the poultry drying.

In order to achieve the suitable moisture of manure for following applications with economic benefits, the optimization of drying time should be provided and respected.

Future research in this area of research should be focused on the study of other factors influencing the drying process partly described and expressed by drying coefficient.

## REFERENCES


Aboltins, A. 2013.Theoretical study of material drying coefficient. In Vartukapteinis, K.: *12th InternationalScientific Conference Engineering for Rural Development*. Latvia University of Agriculture, Jelgava, pp. 153–158.

Aboltins, A., & Palabinskis, J. 2013. New types of air heating solar collectors and their use in drying agricultural products. *Agronomy Research* **11**, 267–274.

Council Directive 1999/74/EC of 19 July 1999 laying down minimum standards for the protection of laying hens. Official Journal of the European Communities L 203/53

Chiumenti, R., Da Borso & Guercini, S. 1993. *Technical guide for the management of livestock manure.*Provincia di Padova, Padova, 160 pp. (In Italian)

Chiumenti, R. 2004. *Rural buildings*. Edagricole scolastico, Milano, 479 pp. (In Italian)

De Gobbi, R., Mezzalira, G., Santacroce, F.C. & Ruol, G. 2012. *Nitrates from problem to resource*. Veneto Agricoltura, Azienda Regionale per i Settori Agricolo, Forestale e Agroalimentare, Legnaro, 150 pp. (In Italian)

Jokiniemi, T., Mikkola, H., Rossner, H., Talgre, L., Lauringson, E., Hovi, M. & Ahokas, J. 2012. Energy savings in plant production. *Agronomy Research* **10**, 85–96.

Jokiniemi, T., Jaakkola, S., Turunen, M. & Ahokas, J. 2014. Energy consumption in different grain preservation methods .*Agronomy Research* **12**, 81–94.

Kic, P. & Liska, R.: *Apparatus for drying loose or bulk materials.* Utility model No. 23841. Industrial property Office, Prague, 2012, 5 pp. (In Czech)

Kic, P. & Aboltins, A. 2013.Convective drying of poultry manure by different air speeds. In Vartukapteinis, K.: *12th International Scientific Conference Engineering for Rural Development*. Latvia University of Agriculture, Jelgava, pp. 121–125.

Liska, R. & Kic, P. 2011. Characteristics of drying process of poultry manure at various temperatures. *Scientiaagriculturae Bohemica* **42**, 79–86.

Pasila, A. 2013. Changes, challenges and opportunities in the wood energy supply chain. *Agronomy Research* **11**, 529–532.

*Agronomy Research* **13**(1), 223–230, 2015

# Comparison of dairy potential in Europe and its effect on assessment of milking systems

M. Gaworski[1,*] and A. Leola[2]

[1]Department of Production Management and Engineering, Warsaw University of Life Sciences, Nowoursynowska str. 164, 02-787 Warsaw, Poland
[2]Institute of Technology, Estonian University of Life Sciences, Kreutzwaldi 56, EE51014 Tartu, Estonia
[*]Correspondence: marek_gaworski@sggw.pl

**Abstract.** The development of milking systems is one of the most important examples proving the dynamic improvement of dairy production on the basis of a technical infrastructure. Farm milking systems incorporate many technical solutions—this provides a basis for analysing and assessing different milking systems in use today. Milking systems can be evaluated on the basis of a set of data and indices directly connected with the work of milking installations. The purpose of the analysis is to show how different kind of milking systems can be assessed in view of milk and its selected features, especially the value of the milk.

**Key words:** assessment, milking system, dairy production, technical equipment.

## INTRODUCTION

It is possible to list many research problems concerning the assessment of dairy production systems as a set of elements, and the relationship between the elements.

The assessment involves most of the activities undertaken in a dairy system to identify advancement in the technical, technological, biological, economic and social aspects of dairy production.

Technical equipment, one of the most important elements in assessing the efficiency of a farm's dairy production, has provided the basis for many research analyses. A broad range of research projects indicate to the significance of technical facilities in barns and their substantial effect on the assessment of aspects like the level of comfort of dairy cows in the lying (Drissler et al., 2005), feeding (Fregonesi et al., 2004), milking (Wendl et al., 2000), and walking area (Haley et al., 2001) as well as the level of comfort resulting from microclimatic conditions created for animals in the buildings (Reppo & Pals, 2002).

Moreover, the technical equipment in a barn is investigated to find the most effective conditions for developing a farm's dairy production. The importance of equipment is highly evident in the area of milking. The analysis involves different kinds of milking systems. For example, milking parlour performance has been evaluated using primarily time and motion studies (Armstrong & Quick, 1986). Some procedures have also been used to evaluate the effect of different factors on milking parlour performance, i.e., pre-milking hygiene, level of milk production, type of parlour, level of mechanization as well as construction (Armstrong et al., 1992).

The abovementioned examples of aspects to be considered emphasize that the individual assessment of technical potential in dairy production includes two categories, i.e., direct or non-direct contact with milk. The first category involves milking systems where the milk stream flows directly through the technical installation.

The milking systems can be evaluated with a set of data and indices directly connected with the work of a milking installation, while the purpose of this paper is to show how different kind of milking systems can be assessed in view of milk and its selected features.

## MATERIALS AND METHODS

A detailed analysis on milk may include qualitative and quantitative aspects. In this paper, only quantitative aspects are taken into account to explore some trends and their relations to milking systems.

Based on quantitative and economic data, some indices have been proposed in specialist literature for a comparative analysis of dairy production and its efficiency; for example, the index of dairy production development delay (Fernandes et al., 2014). The general formula for calculating the index of dairy production development delay ($i_{dpd}$) is as follows:

$$i_{dpd} = \frac{v_{\max} - v_c}{v_{\max}} \tag{1}$$

where: $v_{max}$ is the maximum value of the parameter in the set of countries and $v_c$ is the value of the parameter for the considered country.

The index can be used to compare differences between the biological and economic potential of dairy production in a selected country with the data of a set of other milk-producing countries. The index expressing dairy production value is based on data like annual milk yield per cow and price paid for the unit mass of purchased milk.

By extending some analyses concerning the developments in dairy production on the international scale, it was proposed to juxtapose the value of produced milk per cow in particular countries with the potential dairy production of these countries. Potential dairy production can be expressed with the index of dairy production share ($i_{ps}$), i.e., a quantitative share of the produced milk in a particular country in relation to the total amount of milk produced in the set of considered countries. Based on the milk value (produced by cow per year) and the index of dairy production share ($i_{ps}$), it is possible to calculate the value of dairy production significance ($v_{dps}$) according to the following formula:

$$v_{dps} = v_{dp} \cdot i_{ps} \tag{2}$$

where: $v_{dps}$ is the value of dairy production significance (in monetary units) per cow and per year; $v_{dp}$ is the value (in monetary units) of milk produced by cow per year, while $i_{ps}$ is the index of dairy production share (-).

In order to compare countries and their dairy production the next proposed step is to calculate the index of dairy potential diversification ($i_{dpd}$) according to the formula:

$$i_{dpd} = 1 - \left( \frac{v_{dps\max} - v_{dps}}{v_{dps\max}} \right) \tag{3}$$

where: $v_{dpsmax}$ is the maximum value of dairy production significance in the set of countries and $v_{dps}$ is the value of dairy production significance for the considered country.

The set of 28 EU countries was taken into account for this analysis. The FAO database (www.faostat.fao.org) was used to collect the following information about each country: total dairy production, annual milk yield per cow and price paid for one tonne of purchased milk. The data about the year 2012 were considered.

## RESULTS AND DISCUSSION

The set of data concerning dairy production in 28 EU countries is available in Table 1. Croatia is a member of the EU since 01 July 2013 but it was included in Table 1 and all the calculations.

The index of dairy production development delay was calculated on the basis of milk value data (Table 1) according to the general formula (1). The results of the calculated delay for the set of 28 EU countries are presented in Fig. 1.

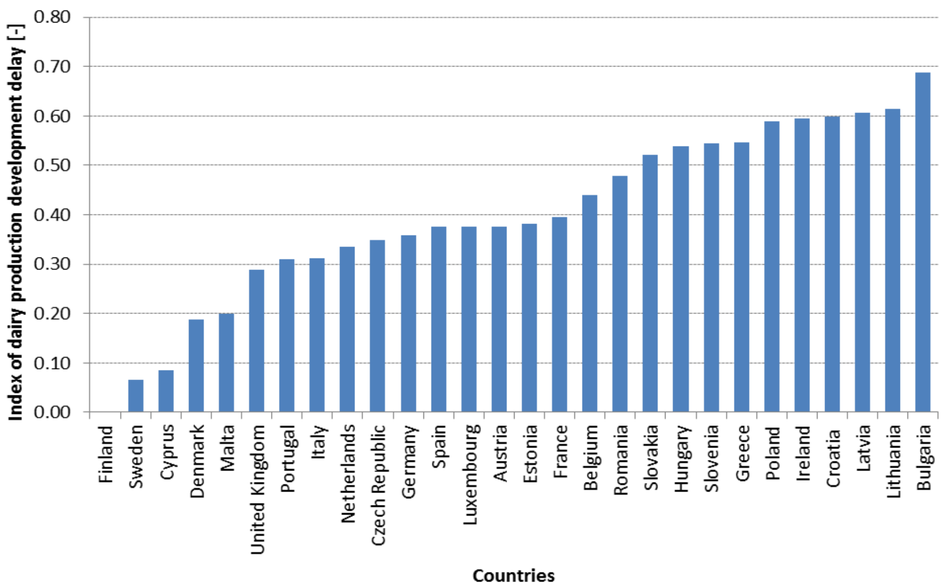


**Figure 1.** Index of dairy production development delay (Source: author).

**Table 1.** Dairy production data for 28 EU countries in 2012

| Country | Total amount of produced milk | Milk yield | Milk price | Value of milk |
|---|---|---|---|---|
| | tonne year$^{-1}$ | kg cow$^{-1}$ (year)$^{-1}$ | USD tonne$^{-1}$ | USD cow$^{-1}$ (year)$^{-1}$ |
| Austria | 3,382,076 | 6,418 | 452.6 | 2,904.6 |
| Belgium | 3,432,000 | 7,075 | 369.0 | 2,610.5 |
| Bulgaria | 1,093,034 | 3,562 | 409.1 | 1,457.3 |
| Croatia | 786,000 | 4,421 | 423.9 | 1,873.9 |
| Cyprus | 153,000 | 6,323 | 674.4 | 4,263.9 |
| Czech Republic | 2,814,680 | 7,633 | 398.2 | 3,039.6 |
| Denmark | 5,008,300 | 8,529 | 443.9 | 3,786.1 |
| Estonia | 720,718 | 7,492 | 384.5 | 2,880.6 |
| Finland | 2,296,676 | 8,098 | 575.6 | 4,661.1 |
| France | 23,983,197 | 6,583 | 428.0 | 2,817.3 |
| Germany | 30,506,929 | 7,280 | 410.3 | 2,987.0 |
| Greece | 800,000 | 3,738 | 566.7 | 2,118.5 |
| Hungary | 1,798,174 | 5,499 | 391.3 | 2,151.8 |
| Ireland | 5,379,700 | 4,716 | 401.0 | 1,891.0 |
| Italy | 10,579,572 | 5,921 | 541.8 | 3,208.0 |
| Latvia | 870,633 | 5,291 | 347.3 | 1,837.4 |
| Lithuania | 1,774,529 | 5,361 | 334.8 | 1,794.7 |
| Luxembourg | 289,395 | 7,266 | 399.9 | 2,905.5 |
| Malta | 43,360 | 5,940 | 628.2 | 3,731.3 |
| Netherlands | 11,675,448 | 7,577 | 409.2 | 3,100.3 |
| Poland | 12,667,773 | 5,189 | 368.6 | 1,912.7 |
| Portugal | 1,938,000 | 7,846 | 410.3 | 3,219.3 |
| Romania | 4,329,713 | 3,701 | 656.1 | 2,428.0 |
| Slovakia | 973,000 | 6,232 | 357.4 | 2,227.4 |
| Slovenia | 601,591 | 5,516 | 385.0 | 2,123.5 |
| Spain | 6,313,014 | 7,471 | 389.7 | 2,911.5 |
| Sweden | 2,901,000 | 8,717 | 499.3 | 4,352.4 |
| United Kingdom | 13,884,000 | 7,683 | 431.7 | 3,316.9 |

Source: faostat.fao.org

The general principle of the index was also used to calculate the index of annual milk yield per cow delay and index of milk price delay based on the data in Table 1. The two mentioned indices are displayed in Figs 2 and 3, respectively.

It is characteristic of the calculation method concerning different kinds of delays as well as for the results presented in the graphs (Figs 1–3) that the index amounts to 0.00 for the first country in the classification. Calculated values of delay show differences between a particular country and the best country in the set of data collected from 28 EU countries. This way it was possible to show the 'distance' (development gap) between regions of dairy production in Europe, including in view of important factors like annual milk yield per cow and price paid for raw milk, which have a decisive influence on a farm's dairy production efficiency.

On the basis of the analysis of some results gained through the calculations expressed with the three indices of delay discussed in this paper it can be claimed that Scandinavian countries have the lowest value of delay in view of the index of annual milk yield per cow, while the Balkan countries have the highest index values. The results indicate to a clear regional diversification of certain dairy production conditions in Europe.

The group of countries with the lowest index of milk price delay includes countries with the smallest potential dairy production, i.e., Cyprus and Malta. The results suggest that small scale dairy production can inspire to implement more attractive economic tools, like the price paid for raw milk.

The comparison of dairy production development delay index values reveals considerable differences between the countries in view of existing premises for effective dairy production.

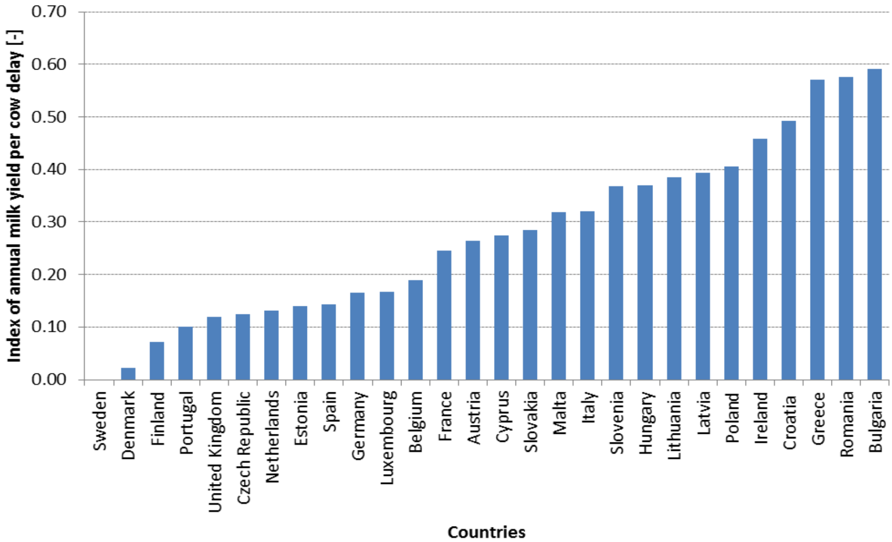


**Figure 2.** Index of annual milk yield per cow delay (Source: own elaboration).

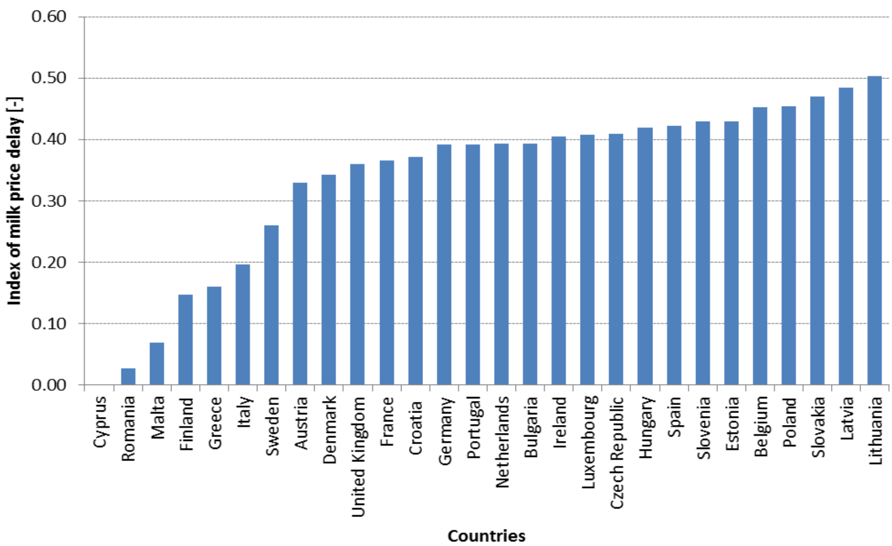


**Figure 3.** Index of milk price delay (Source: own elaboration).

The index of dairy potential diversification for 28 EU countries in Fig. 4

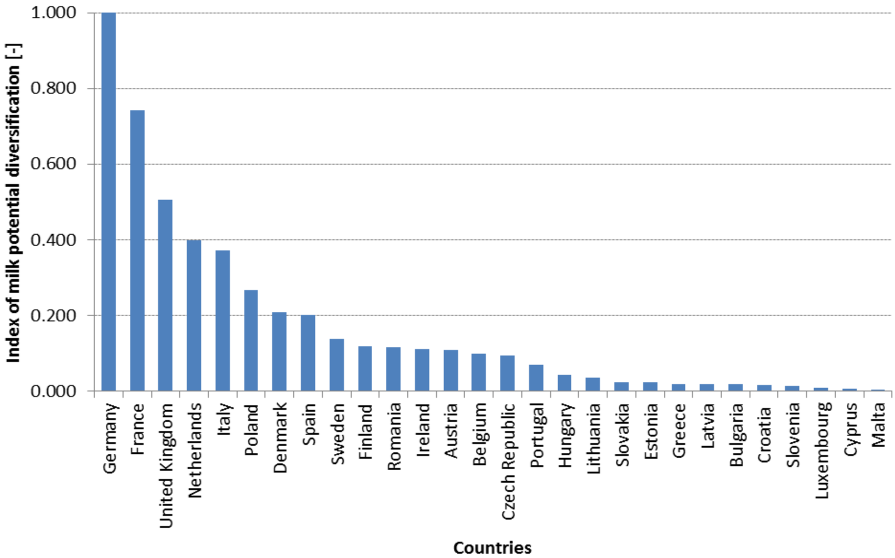


**Figure 4.** Index of dairy potential diversification (Source: author).

The index of dairy potential diversification concentrates on the most important features of dairy production on the national scale, including the value of produced milk by cow and amount of produced milk in comparison to the set of countries. Results of the index comparison (Fig. 4) indicate to considerable differences in potential dairy production in the 28 EU countries. Although the smallest countries are characterized by an attractive price for raw milk (Fig. 3), they have the lowest index values for dairy potential diversification. The differences between the countries primarily result from production potential expressed in the amount of produced milk.

The presented results confirm the differences between regions that produce dairy in Europe, including in view of some criteria of evaluation. The differences concern dairy production potential as well as the effects of using technical equipment like AMS (Gaworski et al., 2013) and other types of milking systems (Gaworski & Priekulis, 2014) in particular countries. In view of the efficiency of using milking systems, there are also other important factors that are manifested in the difference in dairy production. Dairy production can be stabile (month by month) in terms of the amount and value of milk collected from the farms. This is one of the most important factors confirming the effective use of technical potential in dairy production (Gaworski & Leola, 2014). Moreover, milk production regionalization (Parzonko, 2013) is a significant factor in dairy production assessment also within a specific country.

In order to underline the importance of some relationships between dairy production potential and different types of milking systems, the author presents the results of their calculations about Polish dairy farms equipped with the following milking systems: bucket, pipeline, milking parlour and AMS. The following data were collected from each of the investigated dairy farms: cow herd size, annual milk yield per cow, number of milking devices (or milking stalls for milking parlour and AMS), price paid for raw milk, current value of milking installation, etc. Some results concerning the aforementioned relationship, i.e., the value (in PLN) of produced milk (per year) in proportion to the current value of the milking installation (in PLN) in the investigated Polish dairy farms have been presented in Fig. 5.

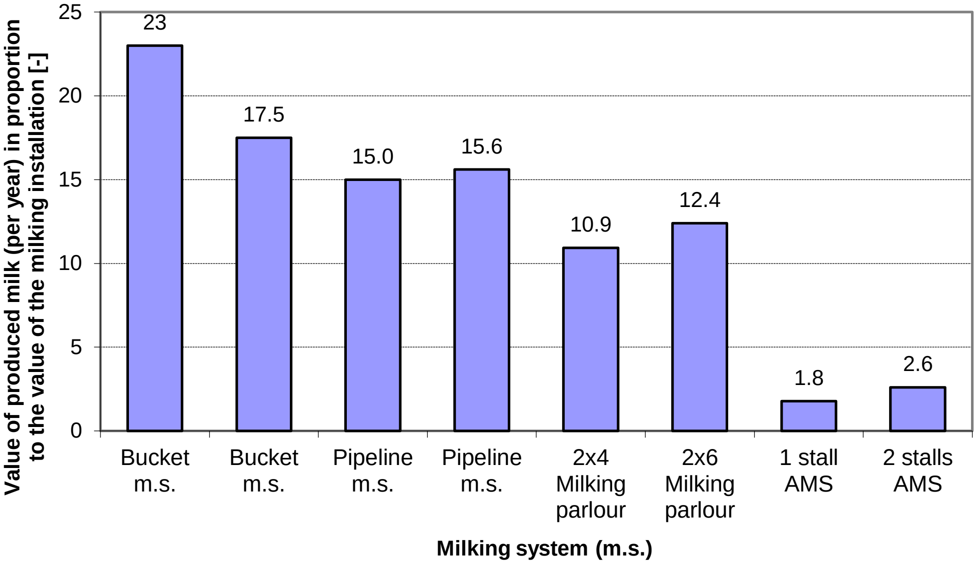


**Figure 5.** Value of produced milk (per year) in proportion to the value of the milking installation for Polish dairy farms (Source: author).

Analysis results (Fig. 5) contribute to the discussion on the significance of the value of produced milk in dairy farms in relation to such aspects as milking installations and data characterizing the technical equipment in dairy farms. It can be claimed that when milking equipment is modernized, the two types of values, i.e., that of produced milk and milking installations, become less closely connected.

## CONCLUSIONS

Results of the performed analyses show many possible comparisons of dairy potential can be made in the European dairy production sector to outline differences between countries and their dairy production. The proposed index of delay shows that some elements of the dairy production systems in the set of 28 EU countries are on completely different developmental levels.

The indices of delay as well index of dairy potential diversification are a possible approach for the assessment of dairy production systems on the international scale. Comparisons can also be made on a national or regional scale to find out ways how to increase potential dairy production as a result of using milking systems more efficiently.

Analysing milking systems in view of the value of milk in milking installations can be considered a necessary additional element of assessment to guarantee more precise results for comprehensive milking system assessments.

## REFERENCES


Armstrong, D.V. & Quick, A.J. 1986. Time and motion to measure milking parlor performance. *Journal of Dairy Science* **69**(4), 1169–1177.

Armstrong, D.V., Smith, J.F. & Gamroth, M.J. 1992. Parallel parlor efficiency as related to number of operators, construction, milking interval, and automatic detachers. *Journal of Dairy Science* **75**(Suppl. 1): 351 (Abstr.).

Drissler, M., Gaworski, M., Tucker, C.B. & Weary, D.M. 2005. Freestall maintenance: Effects on lying behavior of dairy cattle. *Journal of Dairy Science* **88**(7), 2381–2387.

Fernandes, F., Pereira, P., Silva, V.R., Borowski, P. & Gaworski, M. 2014. Premises of dairy systems development on an example of Polish and Portuguese conditions. *Annals of Warsaw University of Life Sciences – SGGW, Agriculture (Agricultural and Forest Engineering)* **64**, 49–57.

Fregonesi, J.A., Tucker, C.B., Weary, D.M., Flower, F.C. & Vittie, T. 2004. Effect of rubber flooring in front of the feed bunk on the time budgets of dairy cattle. *Journal of Dairy Science* **87**(5), 1203–1207.

Gaworski, M. & Leola, A. 2014. Effect of technical and biological potential on dairy production development. *Agronomy Research* **12**(1), 215–222.

Gaworski, M., Leola, A. & Priekulis, J. 2013. Comparative analysis on effectiveness of AMS use on an example of three European countries. *Agronomy Research* **11**(1), 231–238.

Gaworski, M. & Priekulis, J. 2014. Analysis of milking system development on example of two Baltic countries. *13th International Conference on Engineering for Rural Development*, Proceedings **13**, 79–84.

Haley, D.B., de Passillé, A.M. & Rushen, J. 2001. Assessing cow comfort: effects of two floor types and two tie stalls designs on the behaviour of lactating dairy cows. *Applied Animal Behaviour Science* **71**, 105–117.

Parzonko, A. 2013. Global and local determinants the development of milk production. Wyd. SGGW, Warsaw. (*in Polish*).

Reppo, B. & Pals, A. 2002. Inner climate of a cowshed in winter. *Agraarteadus*. *Journal of Agricultural Science* **XIII**(2), 87–95. (in Estonian).

Wendl, G., Harms, J. & Schön, H. 2000. Analysis of milking behaviour on automatic milking. In: Hogeveen, H., Meijering, A. (ed.) *Robotic milking*. Wageningen Pers, Wageningen, The Netherlands, 143–151.

*Agronomy Research* **13**(1), 231–236, 2015

# Security methods for livestock buildings including assessment aspects

J. Hart[1,*], Z. Štěrbová[2] and V. Nídlová[3]

[1]Czech University of Life Sciences Prague (CULS), Faculty of Engineering, Department of Technological Equipment of Buildings, Kamýcká 129, 165 21 Prague, Czech republic; [*]Correspondence: janhart77@gmail.com
[2]Czech University of Life Sciences Prague (CULS), Faculty of Engineering, Department of Mechanical Engineering, Kamýcká 129, 165 21 Prague, Czech republic
[3]Czech University of Life Sciences Prague (CULS), Faculty of Engineering, Department of Electrical Engineering and Automation, Kamýcká 129, 165 21 Prague, Czech republic

**Abstract.** The problem of security methods affects a large proportion of intrusion and hold-up alarm systems (I&HAS). In a time of increasing property crime, it is highly important for the security methods of livestock buildings to be able to achieve efficiency, reliability and faultlessness. In case it is proposed to place detectors, it is essential to determine the position of the detectors, the types of the detectors, but also to guarantee their capability of detection for use in livestock production buildings. The security proposals, which have been conducted, examine both the normal security methods in livestock production as well as cost and long-term financial expenses (investment in the communicator, private security guards etc.). These security proposals are important both from an informative perspective and also because of the possibility of using individual proposals in securing livestock production in practice. The aim was to compare the two kinds of security methods for a livestock building object. The compared values become the acquisition costs of security system.

**Key words:** security risks, sabotage, intrusion and hold-up alarm systems, glass break detector.

## INTRODUCTION

Intrusion and hold-up alarm systems serve primarily for the protection of buildings against unlawful conduct of third parties, and can be used as monitoring and control systems. Therefore, they are primarily a tool for ensuring a state of security. They operate in the material realm (physical protection of property, life and health) and in the emotional realm (providing a feeling of peace, safety and certain security). As a result, it is important for them not to malfunction and to be sufficiently resistant to attack.

The procedure for the design of the placement of detectors in livestock buildings is a very relevant part that precedes the actual installation of the entire electrical security system, and it a part of the overall design of the security alarm and emergency systems (hereinafter SAES). This usually regards the part of security process which determines where individual detectors will be located. The process that we selected when designing the SAES will decide on how difficult the installation will be, and the price of the final system.

## MATERIALS AND METHODS

Nowadays, several methods are used that provide a sufficient level of the building's security (Staff & Honey, 1999; Uhlář, 2005; Křeček, 2006). However, only two methods comply with the applicable standards related to ČSN EN 50 131. These are the method of perimeter procedure and the procedure using nodal points.

The perimeter procedure is a frequently-used procedure in the process of securing a building. Detectors are installed around the perimeter of the building, thereby almost perfectly securing the building which cannot be entered without triggering an alarm. The closer to the centre of the building a detector is located, the less important it is for the correctness of the operation of the system – see Fig. 1.

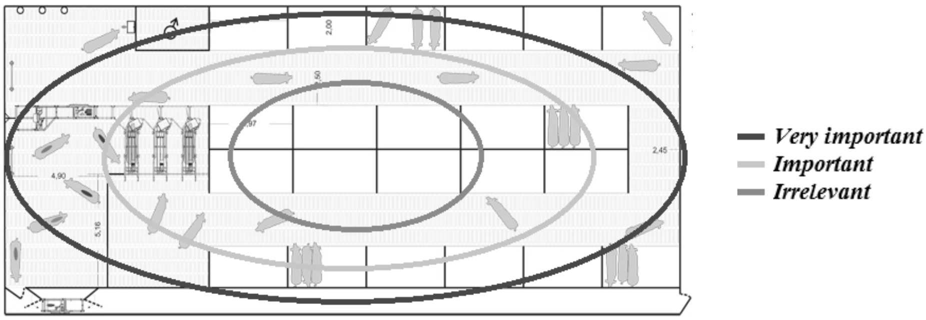


**Figure 1.** Floor plan showing the perimeter security procedure.

The procedure using nodal points is very different from the perimeter procedure. Here, the security of the perimeter of the building is not dealt with, but the most frequently used places, and places with the greatest probability of disturbing the building are selected and then secured – see Fig. 2. During this procedure, it is necessary to be experienced and have a certain amount of imagination, as the security design becomes complicated in determining the nodal points. Like with the perimeter procedure, three degrees of security priorities are also defined for this method, but herein this priority is defined for every room (by points) and not for the perimeter.

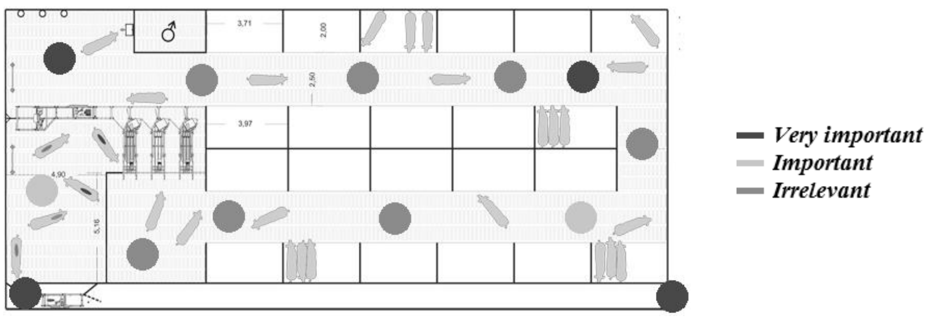


**Figure 2.** Floor plan showing the nodal points.

Nodal points are most often located in entrance areas and in all of the locations where the movement of an attacker is expected most probably. This mainly involves corridors, staircases to other floors, rooms that can be entered, etc.

Compared to the standard security of family homes, the security of buildings for livestock production is a complicated matter. This is due to the movement of animals, which can cause false alarms in the building. However, it is possible to use various specific detectors that allow for even such complicated spaces to be guarded.

The first alternative is to deploy infrared barriers and microwave barriers (Petruzzellis, 1993; Capel, 1999; Uhlář, 2005; Křeček, 2006). Although this alternative is efficient and effective, it is also costly, and it is relatively difficult to find a location where they can be placed in order to be usable.

Another alternative is the use of dual detectors, or detectors with PET immunity. Dual detectors combine the properties of PIR (passive infra-red) detectors and usually one representative from active space detectors (Petruzzellis, 1993; Capel, 1999; Uhlář, 2005; Křeček, 2006). This alternative is acceptable, but in view of the fact that the detector may set off an alarm anyway when animals are untethered, it is gradually being waived. The alarm is caused by the movement of accumulated heat and its movement, which in principle works with the surrounding spaces in the same way as it does for heat exchangers (Šeďová et al., 2013; Neuberger et al., 2014).

Thus, the only alternative for securing indoor spaces is the use of detectors with PET immunity. If these detectors are correctly selected and installed, they are able to accept the movements of animals whilst reliably detecting a human being. This is due to certain immunity to movement that occurs below a certain height level. These movements can also be limited by certain weight ranges that the detector can ignore up to a defined height level (Petruzzellis, 1993; Capel, 1999; Uhlář, 2005; Křeček, 2006).

In order to compare the design of security via the perimeter procedure and the nodal points procedure, a building for stabling pigs at a pig farm near Jablonné nad Orlicí was selected. This is a classical smaller stable with several partition walls (Syrový et al., 2008). The wall is located in the centre of the building and it separates individual pens (See Fig. 3), and the exit is also separated from the building via a long corridor.

**Figure 3.** Pig pens.

The security for the given building was designed according to the perimeter procedure (Fig. 1). The overall costs for the purchased material are shown in the following Table I.

**Table 1.** Price calculation of the system resolved by the perimeter procedure

| | pcs | Price per item (EUR) | Total price (EUR) |
|---|---|---|---|
| Detector of opening | 26 | 1.86 | 48.29 |
| Glass break detector | 2 | 17.82 | 35.64 |
| PIR detector with PET immunity | 7 | 21.39 | 149.75 |
| MainUnit +Keyboard | 1 | 167.46 | 167.46 |
| Zone expander | 1 | 46.39 | 46.39 |
| GSM communicator | 1 | 189.25 | 189.25 |
| Cost of installation (approx) | 45 | 12 | 540 |
| Total | | | 1176.79 |
| Total without GSM communicator and MainUnit | | | 820.07 |

Detectors of opening were designed for each pen and passage through the building. The glass break detectors were designed for the front of the building, as it has a glass surface. PIR detectors with PET immunity were designed for both sides of the passage serving as the entrance to building, and for both sides of both aisles with pens.

The security for the given building was designed according to the procedure using nodal points (Fig. 2). The overall costs for the purchased material are shown in Table II.

**Table 2.** Price calculation for the system resolved using nodal points

| | pcs | Price per item (EUR) | Total price (EUR) |
|---|---|---|---|
| Detector of opening | 3 | 1.86 | 5.57 |
| Glass break detector | 1 | 17.82 | 17.82 |
| PIR detector with PET immunity | 4 | 21.39 | 85.57 |
| MainUnit +Keyboard | 1 | 167.46 | 167.46 |
| Zone expander | 0 | 46.39 | 0.00 |
| GSM communicator | 1 | 189.25 | 189.25 |
| Cost of installation (approx) | 20 | 12 | 240 |
| Total | | | 705.68 |
| Total without GSM communicator and MainUnit | | | 348.96 |

With regard to nodal points, is was first necessary to mark the areas in the floor plan of the building where security is very important, followed by the areas that are important, and, finally, the areas that are unimportant in order for the system to operate correctly. The placement of nodal points follows the estimation of the designer, and is therefore not applicable for everyone who installs such a system. The floor plan marked in this way is shown in Fig. 2.

The following nodal points were marked as **very important: the access corridor** (from both sides) and the **top aisle between the pens** (from both sides). These were selected due to the most probable entry by an intruder. The following nodal points were marked as **important**: the **bottom aisle between the pens**. The **remaining spaces** were selected as **unimportant**.

## RESULTS AND DISCUSSION

If we disregard the repeated costs for both security designs (MainUnit + keyboard and GSM communicator) and subtract them from the resulting comparison, the resulting price difference between individual designs is 471.11 EUR – see Table 3.

**Table 3.** Comparison of the price of the system designed with the perimeter procedure and nodal points

| | Price (EUR) | Price (%) |
|---|---|---|
| Perimeter procedure | 820.07 | 100 |
| Nodal points | 348.96 | 42.55 |
| Difference | 471.11 | 57.45 |

Using nodal points will save approx. 62% of the acquisition costs while the resulting degree of security will not be decreased. The long-term costs are the same for both proposals. Estimated useful lives of the systems are tens of years. Although the method of nodal points does not give great variability of settings, it saves on the cost of the system.

The correct determination of nodal points in the building can decrease the costs for securing the building whilst maintaining the degree of security. Therefore, it is important not to refrain from this method, in particular in livestock production, where it is reasonable due to the efficiency of the security design, the fact that it can be assembled by on one’s own or the resulting savings.

As stated in ‘Security Systems & Intruder Alarms’ (Capel, 1999), the security design is one of the most important parts of the entire installation. This can minimize false alarms and lower the costs of acquiring the system. The same is stated in ‘Security: A Guide to Security System Design and Equipment Selection and Installation’ (Cumming, 1994), and that is why the author recommends primarily using the nodal points procedure.

## CONCLUSIONS

Correct installation is one of the essential factors that can directly affect the security and functionality of the security system. It is necessary that the companies providing the installation of security systems always follow the manuals for the given system and pay attention to the correct installation procedure according to the relevant standards. If the installation company does not follow the manuals and standards, then no equipment installed by them will meet the parameters of security systems and it is not suitable to use them.

In livestock production, the use of the perimeter procedure is not financially feasible. It is always important to concentrate on the building that needs to be secured, and not to proceed, with regard to all structures, in a manner that overdoes the security. Maximum security is not necessary for pig breeding, and it is important to focus rather on the development on new types of protection, specifically for livestock production.

In terms of the security design, financial calculations clearly showed that the perimeter procedure for small and simple installations can increase costs by up to 62% compared to the nodal point procedure – and the nodal point method does not decrease the quality of security. The perimeter procedure may be able to perfectly secure a building, but this procedure is costly and increases the number of false alarms. Therefore, the question is whether or not to use the perimeter method.

## REFERENCES


Capel, V. 1999. Security Systems & Intruder Alarms. Elsevier Science, 301 p.

Cumming, N. 1994. Security: A Guide to Security System Design and Equipment Selection and Installation. Elsevier Science, 338p.

Křeček, S. 2006. Manual security equipment. Blatná: Circetus, 313 p. (in Czech)

Petruzzellis, T. 1993. Alarm Sensor and Security. McGraw-Hill Professional Publishing, 256 p.

Staff, H., Honey, G. 1999. Electronic Security Systems Pocket Book. Elsevier Science, 226 p.

Syrový, O., Bauer, F., Gerndtova, I., Holubova, V., Hůla, J., Kovařiček, P., Krouhlik, M., Kumhala, F., Kviz, Z., Mašek, J., Pastorek, Z., Podpěra, V., Rybka, A., Sedlak, P., Skalicky, J., Šmerda, T. 2008. Energy saving technologies in plant production, Research Institute of Agricultural Engineering, p.r.i. Prague, 101p. (in Czech)

Šeďová, M., Adamovský, R., Neuberger, P. 2013. Analysis of ground massif temperatures with horizontal heat exchanger. Research in Agricultural Engineering (Zemědělská technika), pp. 91–97.

Neuberger, P., Adamovský, R., Šeďová, M. 2014. Temperatures and Heat Flows in a Soil Enclosing a Slinky Horizontal Heat Exchanger. Energies, pp. 972–987.

Uhlář, J. 2005. Technical protection of objects, II. part, Electrical security systems II. Prague: PA ČR, 229 p. (in Czech)

*Agronomy Research* **13**(1), 237–244, 2015

# Cow crowding in waiting yard using mechanical drivers and its influence on productivity of rotary type milking equipment

M. Mangalis*, Dz. Jaundžeikars and J. Priekulis

Latvia University of Agriculture, Faculty of Engineering, Cakstes blvd.5, LV – 3001 Jelgava, Latvia; *Correspondence: maris.mangalis@inbox.lv

**Abstract.** At present rotary type milking equipment is popular in Latvia. It is used almost on all farms where there are 400 and more cows. Nevertheless, the maximal productivity of work can be reached if the cows are continuously driven from the waiting yard to the milking equipment and if sufficient intensity of animal traffic is ensured. Therefore, the rotary type milking equipment is usually supplemented with a mechanical cow driver that crowds the cows in the waiting yard at the same time driving them towards the milking parlour.In the research it has been stated that using the heavy type mechanical cow drivers Cow Mander 640 or Cow Mander 740 the maximal cow crowding in the waiting yard reaches 1.1–1.2 $m^2$ calculating per one cow and it ensures the cow traffic intensity 8–11 s $cow^{-1}$. If, in turn, the medium heavy driver Cow Mander 015 is used, the cow crowding is only 1.5–1.7 $m^2$ $cow^{-1}$ and the cow traffic intensity reaches 15–23 s $cow^{-1}$. Using rotary type milking equipment with 20–30 milking places such cow traffic intensity is sufficient but if the rotary milking equipment has 50 and more milking places the necessary cow traffic intensity cannot any more be ensured by increasing the cow crowding. Therefore, the exploitation work productivity of the rotary type milking equipment with 50 and more places is by 30–40% less than its technological productivity of work that is obtained by means of calculations.

**Key words:** cow crowding, cow traffic intensity, mechanical cow drivers, productivity of work, rotary type milking equipment.

## INTRODUCTION

In Latvia application of rotary type milking equipment develops fast. It is used almost on all large farms that have been built in Latvia in recent years. Besides, equipment with side-by-side (abreast) location of cows during milking is especially popular. The economic profitability of application of this equipment is confirmed also by our research that proves that usage of rotary type milking equipment becomes economically profitable if the size of the herd exceeds 300–400 milk cows (Priekulis & Kurgs, 2010).

Nevertheless, the productivity of this milking equipment depends on two independent factors: the productivity of the corresponding milking equipment and the intensity of cow traffic entering the rotary parlour platform. It is because in an ideal case the rotary type milking equipment platform rotates with a definite speed during milking but in a definite moment of time or during the so called limit time replacement of cows should be ensured – every milked cow should leave the rotary equipment platform but the cow to be milked should manage to occupy its place in due time. If replacement of cows is delayed the rotation speed of the platform has to be reduced or it has to be stopped for a while. But it reduces the productivity of the milking equipment.

In order to fasten the cow traffic entering the rotary platform today cow mechanical drivers are used (Mangalis, 2014) that crowd the cows in the waiting yard ensuring their continuous movement to the milking equipment.

The aim of the present research is to state to what extent cow crowding in the waiting yard influences their traffic speed entering the rotary type milking equipment platform and how it changes the rotary type milking equipment productivity.

## MATERIALS AND METHODS

Seven milk farms in which cow mechanical drivers and rotary type milking equipment are used were selected for the research. On all farms included in the research the cows were handled in cold barns using recreation boxes, and the cows were milked three times a day. But the size of the herd and types of rotary milking equipment, planning of the farms and organization of work in milking were different on these farms. The most important data characterizing every of the farms included in the research are summarized in Table 1.

**Table 1.** Characterisation of farms included in the research

| Specification | Farms | | | | | | |
|---|---|---|---|---|---|---|---|
| | A | B | C | D | E | F | G |
| Number of cows in herd | 300 | 670 | 390 | 600 | 575 | 1055 | 816 |
| Company producing milking equipment | GEA Farm Tehnologies | GEA Farm Tehnologies | GEA Farm Tehnologies | GEA Farm Tehnologies | DeLa-val | GEA Farm Tehnologies | GEA Farm Tehnologies |
| Applied milking equipment | Rotary milking herringbone Systems-20 | Rotary milking herringbone Systems-32 | Rotary milking herringbone Systems-36 | Rotary milking Side-by-Side Systems-50 | Rotary milking PR-50 | Rotary milking Side-by-Side Systems-60 | Rotary milking Side-by-Side Systems-80 |
| Number of milking places | 20 | 32 | 36 | 50 | 50 | 60 | 80 |
| Applied cow mechanical driver | Cow Mander 015 | Cow Mander 640 | Cow Mander 640 | Cow Mander 640 | HRS Herdsmann | Cow Mander 600/700 | Cow Mander 740 |
| Number of milkers | 2 | 2 | 2 | 2 | 3 | 4 | 4 |
| Number of drivers | 1 | 1 | 1 | 2 | 1 | 1 | 2 |

Cow crowding in the waiting yard and the intensity or rhythm of cow traffic were stated experimentally during the research on the farms given in Table 1. For this reason the distance along which the mechanical cow driver moved during milking was stated after every 10 cows entered the milking equipment.

For calculation of the average cow crowding the following formula was used.

$$\Delta = \frac{b_l \cdot (s_1 + s_2 + ... + s_x)}{z_g \cdot x} \qquad (1)$$

where: $\Delta$ – average cow crowding in the waiting yard considering the part of the yard occupied by one animal, m$^2$ cow$^{-1}$; $b_l$ – width of the waiting yard, m; $s_1$; $s_2$; $s_x$ – distance or step along which the mechanical cow driver moves during the first, second and n period of the research, m; $z_g$ – number of cows that entered the milking equipment in the corresponding period of the research (in our research $z_g$ = 10 cows); $x$ – total number of research periods.

In order to state the cow traffic rhythm the time was stated that is necessary for milking every 10 cows, i.e., for implementation of one research period, and it was stated registering the time intervals in which groups of 10 cows entered the milking parlour. After that the average cow traffic rhythm was calculated using the following formula.

$$t_{virz} = \frac{\sum^{n} t_{gr}}{\sum^{n} z_{gr}} \qquad (2)$$

where: $t_{virz}$ – average cow traffic rhythm, s cow$^{-1}$; $t_{gr}$ – length of milking every cow, s; $n$ – number of cow groups.

For testing the validity of the calculated results the mathematical statistics methods described in literature were used (Arhipova & Bāliņa, 2003).

Using the experimental research results and information given in literature the milking equipment limit time, technological productivity as well as productivity of the milking equipment operation $W_{eks}$ were stated.

The limit time characterizes the period of time during which the milking equipment moves along one milking place and it is calculated according to the formula.

$$t_{\lim} = \frac{T_c}{n_{ap}} \qquad (3)$$

where: $t_{lim}$ – limit time, s; $T_c$ – length of one milking cycle (equal to the length of one rotary platform revolution), s; $n_{ap}$ – number of milking machines or milking places on the rotary platform, pcs.

Length of one milking cycle (Priekulis et al., 2012)

$$T_c = t_{ieie} + t_o + t_{ap} + kt_{ap} + t_{izie} \tag{4}$$

where: $t_{ieie}$ – time for a cow to enter the rotary type milking equipment, s; $t_o$ – average length of milkers' working operations per one cow (includes the time consumed for preparation of the cow before milking and application of the milking machine), s; $t_{ap}$ – average milking length of one cow, s; $t_{izie}$ – time spent for one cow to leave the rotary platform, s; $k$ – milking length margin coefficient (includes the possible increase of the milking length compared to the average milking length, it is recommended to assume that $k$ = 0,5 (Priekulis et al., 2012, Timšāns et al., 1974).

Technological productivity of the equipment can be calculated according to the following formula:

$$W_{teh} = \frac{3600 \cdot n_{ap}}{T_c} = \frac{3600}{t_{\lim}} \tag{5}$$

where $W_{teh}$ – technological productivity of the equipment, cows $h^{-1}$.

Productivity of the milking equipment operation

$$W_{eks} = \frac{3600}{t_{virz}} \tag{6}$$

where $W_{eks}$ – productivity, cows $h^{-1}$.

Coefficient of the productivity of the milking equipment operation

$$k_{eks} = \frac{W_{eks}}{W_{teh}} \tag{7}$$

## RESULTS AND DISCUSSION

The experimental researc data and the calculation results are summarised in a joint Table 2.

The dynamics of the cow traffic stated in the experiments is shown in Fig. 1. It can be seen that this intensity depends on the kind of the cow driver and partly also on the correspondence of the people engaged in cow driving to the number of the cows to be milked.

**Table 2.** Summary of the research results and calculations

| Indices | Farms | | | | | | |
|---|---|---|---|---|---|---|---|
| | A | B | C | D | E | F | G |
| Number of milking places | 20 | 32 | 36 | 50 | 50 | 60 | 80 |
| Crowding of cows, $m^2$ $cow^{-1}$ | 1.7 | 1.24 | 135 | 1.2 | 1.45 | 1.5 | 1.1 |
| Cow traffic rhythm, s $cow^{-1}$ | 24.0 | 14.3 | 17.3 | 14.0 | 16.1 | 13.5 | 9.3 |
| Limit time, s $cow^{-1}$ | 24.90 | 15.56 | 13.83 | 9.98 | 9.98 | 8.30 | 6.23 |
| Technological productivity of the equipment, cows $h^{-1}$ | 145 | 231 | 260 | 361 | 361 | 434 | 578 |
| Productivity of the milking equipment application, cows $h^{-1}$ | 150 | 252 | 208 | 257 | 224 | 266 | 387 |
| Coefficient of the productivity of the milking equipment application | 1.03 | 1.09 | 0.80 | 0.71 | 0.62 | 0.61 | 0.67 |

Working in automatic regime the cow mechanical drivers Cow Mander 640 and Cow Mander 740 (Priekulis & Kurgs, 2010) can ensure that cow crowding in the waiting yard reaches 1.1–1.2 $m^2$ calculating per one animal. Nevertheless, it considerably exceeds the cow crowding recommended in literature 1.5–1.6 $m^2$ $cow^{-1}$. Therefore, on many farms the average cow crowding is 1.4–1.7 $m^2$ $cow^{-1}$.

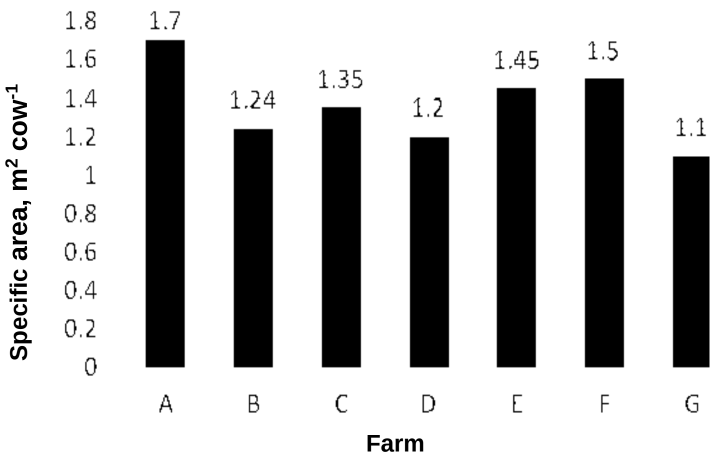


**Figure 1.** Cow crowding in the waiting yard using mechanical driver, $m^2$ $cow^{-1}$.

The influence of animal crowding on the intensity or rhythm of cow traffic is shown in Fig. 2. According to this it can be stated that if the crowding increases the cow traffic intensity has a tendency to increase.

But our observations prove that excess cow crowding promotes occurrence of stressful situations (Maton et al., 1985) when the cows are entering the rotary type milking equipment. It can cause situations that two cows are trying to occupy the milking place at the milking equipment entrance. But it causes jamming and a necessity to stop the rotary equipment as the cows have to be driven back. Therefore, in such cases the milkers are disturbed from doing their direct duties and the total length of milking cows increases.

It should be noted that using the heavy mechanical cow driver Cow Mander 015 cow crowding in the waiting yard does not exceed 1.6–1.7 $m^2$ $cow^{-1}$, but it is enough for ensuring the necessary traffic of cows if the rotary milking equipment has 20 milking places.

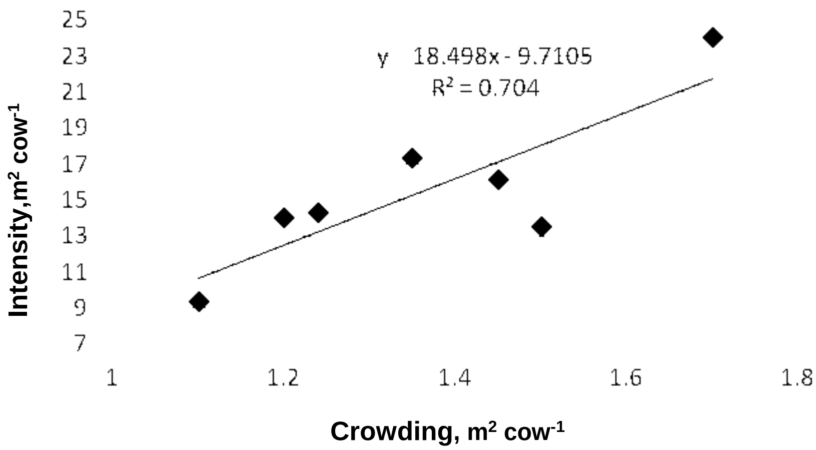


**Figure 2.** Changes of cow traffic intensity from the waiting yard to the rotary platform depending on the cow crowding in the waiting yard.

The cow traffic intensity is related to the milking equipment limit time. The bigger the number of the rotary equipment milking places, the less becomes the limit time, i.e., the interval of time in which the cow has to enter the rotary platform. If, for instance, the rotary type milking equipment has 20 milking places, the limit time is 24.9 s $cow^{-1}$, if there are 50 places, then 9.98 s $cow^{-1}$, but if 80 places, then only 6.23 s $cow^{-1}$.

In turn, our research shows that for rotary type milking equipment with 20–30 milking places the cow traffic intensity approximately corresponds to the limit time or even a little exceeds it (Table 2). But if there are more milking places, the cow traffic intensity starts to lack behind the limit time. It means that the cows cannot manage to occupy their place fast enough on the rotary platform so reducing the potential productivity of the milking equipment.

This situation is clearly shown in Fig. 3 which depicts the productivity of rotary type milking equipment depending on the number of milking places.

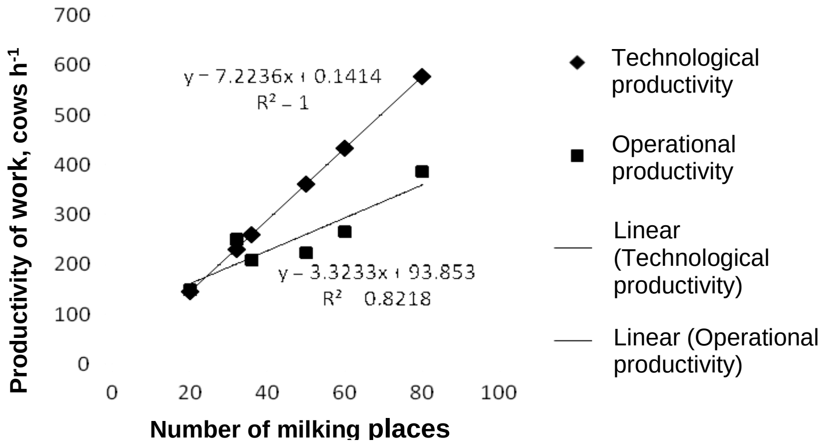


**Figure 3.** Technological and operational productivity of rotary type milking equipment depending on the number of milking places.

It can be judged from the figure that for rotary type milking equipment the operational productivity of work approximately corresponds to its technological productivity that is obtained by calculations. If the number of milking places is higher the operational productivity of work starts to lack behind the technological productivity as it is caused by lacking of the cow traffic intensity behind the limit time. This is surely dependent upon several factors: specifics of application of machinery (construction and the set operation regime of the cow mechanical driver, rotary equipment rotation speed), specifics of the cow herd (length of milking separate cows, character and health of the cows) as well as organization of work, (Brunsch et al., 1996), resourcefulness and skills of the people engaged in milking. Therefore, on every farm included in the research this difference between the technological and operational productivity was different. But for practical needs it can be considered that for rotary type milking equipment with 50 and more milking places the operational productivity coefficient is 0.6–0.7.

## CONCLUSIONS

Cow crowding in the waiting yard influences the intensity of animal traffic to milking. If, for instance, the crowding is 1.1–1.2 $m^2$, calculated per one animal, the traffic intensity reaches 9–13 s $cow^{-1}$, but if the crowding is 1.5–1.7 $m^2$ $cow^{-1}$, then 15–23 s $cow^{-1}$.

The maximal animal crowding can be achieved if the heavy type cow mechanical drivers Cow Mander 640 or Cow Mander 740 are used. If, in turn, the medium heavy driver Cow Mander 015 is used, the cow crowding is only 1.5–1.7 $m^2$ $cow^{-1}$ and the intensity of cow traffic reaches 123 s $cow^{-1}$.

To achieve correspondence of the milking equipment operational productivity with its potential resources the intensity of cow traffic from the waiting yard to the milking equipment should correspond to the calculated limit time, i.e., the period of time in which the rotary equipment moves ahead one milking place. If the rotary type milking equipment has 20–30 milking places, the necessary cow traffic intensity or the limit time is 15–25 s cow$^{-1}$ that can be ensured with medium heavy cow mechanical drivers, but if the rotary type milking equipment has more milking places, the cow traffic intensity starts to lack behind the limit time that reduces the operational productivity of the rotary type milking equipment.

For rotary type milking equipment with 50 and more milking places the coefficient of operational productivity is 0.6–0.7.

## REFERENCES


Arhipova, I., Bāliņa, S. 2003. Statistics in Economics. Rīga: Datorzinību Centrs, 349 pp. (In Latvian)

Brunsch, R., Kaufmann, O., Lupfert, T. 1996. Rinderhaltung in Laufstallen (Loose housing of cattle). Stuttgart: Eugen Ulmer, 132 pp. (in German).

Mangalis, M., Jaundžeikars, D., Priekulis, J. 2014. Cow Traffic Dynamics Using Mechanikal Movers. *13th International Scientific Conference 'Engineering for Rural Development'. Proceedings*, Volume 13. Jelgava, May 29–30, pp. 59–63.

Maton, A., Daelemans, J., Lambrecht, J. 1985. Housing of animals. Amsterdam, Oxford, New York, Tokyo: *Elesevier*, 458 pp.

Priekulis, J. 2012. Modern milk production farm: technology, machinery, operation. Jelgava: LLU, 240 pp. (In Latvian).

Priekulis, J., Kurgs, A. 2010. Economically most efficient equipment in milking parlours. /9th International Scientific Conference 'Engineering for rural development'. Proceedings, Volume 9. Jelgava, May 27–28, pp.93–96.

Timšāns, S. 1974. Technological processes on cow farms. Rīga: Liesma, 183 pp. (In Latvian).

*Agronomy Research* **13**(1), 245–252, 2015

# Heating and ventilation in milking parlours

J. Papez* and P. Kic

Czech University of Life Sciences Prague, Faculty of Engineering, Kamycka 129, 16521 Prague 6, Czech Republic; *Correspondence: papez@tf.czu.cz

**Abstract.** The aim of this paper is to show the results of the measurement of main microclimatic parameters (temperature and relative humidity) in milking parlours and compare the obtained results with values recommended in relevant standards. Temperature and relative humidity can affect animal welfare as well as the well-being of workers. These parameters were measured in three rotary milking parlours with herringbone type of stalls, each for 24 dairy cows. Two of these milking parlours were built in 2001 and one was built in 2009. Measurements were taken during the winter and summer periods, under extremely cold or high temperature conditions. Measurements were taken during the milking process for about two hours using suitable sensors for measurement of indoor temperature and relative humidity. The data of outside temperature and relative humidity were also obtained and compared with indoor data. The final results of the research were generalized. It is obvious from the results of measurements of selected milking parlours that heating and ventilation of milking parlours is insufficient. To set up adequate heating power, the heat balance of milking parlours was calculated. For adequate ventilation, the necessary flow of fresh air was calculated for both winter and summer periods. Also the methods of how to achieve these air flows are presented.

**Key words:** measurement, relative humidity, temperature, THI.

## INTRODUCTION

The aim of this article is to show the results of measurement of main microclimatic parameters (temperature and relative humidity) in milking parlours and to compare the obtained results with the values recommended in relevant standards.

Environmental conditions are determined by characteristic factors, especially by physical factors, chemical factors and biological factors. Thermal condition of the indoor environment is characterized by thermal and humidity variables which affect the resulting mental and physical state of an animal or person in agricultural buildings. The result of the analysis of thermal environment is the formation of optimal conditions for human and animal organisms. Required optimal temperature in milking parlour in the winter period is 14–16 °C (minimum 10 °C). In the summer period, the required optimal temperature should be in the range of 14–22 °C (maximum 26 °C). (Novy et al., 2006; Choupek & Suchy, 2008; Koznarova & Klabzuba, 2008; Zejdova et al., 2014)

Thermal condition of the indoor environment is also influenced by relative humidity. High water vapour content in the air reduces the possibility of cooling the body of a man or an animal by evaporation. It can cause heat stress already at a relatively low temperature of indoor environment. Relative humidity should by ideally in the range of 40–80%. The maximum allowable value of relative humidity according to Czech standard CSN 73 0543–2 is 85%. Wet air is a good conductor of heat. Long-term exposure of relative humidity above 85% adversely affects the organism and apparatus and could damage wooden elements of the buildings. (Kic & Broz, 1995; Kunc et al., 2007; Pavelek & Stetina, 2007; Papez & Kic, 2013; Zejdova et al., 2014)

The effect of combinations of temperature and humidity is included in the temperature–humidity index (THI). This index is widely used to describe the heat stress and it is also a good indicator of stress temperature environment conditions. THI value below 70 is considered comfortable for cattle. THI in the range of 70–78 is considered stressful and values higher than 78 cause extreme suffering (the organism is unable to maintain the thermoregulatory mechanisms, or normal body temperature). (Armstrong, 1994; Zejdova et al., 2014)

## MATERIALS AND METHODS

The basic assumption of this research is to perform measurements of main microclimatic parameters (temperature and relative humidity) in milking parlours and to compare obtained results with values recommended in relevant standards. The aim of this paper is also to find and define the methods for the improvement of indoor conditions in milking parlours in case of exceeding (or not reaching) allowable limits (setting up adequate heating power and necessary flow of fresh air).

To avoid big differences between the milking parlours from the point of view of other microclimatic parameters, the thermal comfort in the space was continuously measured by globe temperature (measured by globe thermometer FPA 805 GTS with operative range from –50 to +200 °C with accuracy ± 0.01 K and diameter of 0.15 m) together with temperature and humidity of surrounding air measured by sensor FH A646–21 including temperature sensor NTC type N with operative range from –30 to +100 °C with accuracy ± 0.01 K, and air humidity by capacitive sensor with operative range from 5 to 98% with accuracy ± 0.1%. All data were measured continuously and stored at intervals of three minutes to measuring instrument ALMEMO 2590–9 during the measurement (approximately 120 minutes).

Three milking parlours were measured during the winter and summer periods, under extremely cold or high temperature conditions. The measurement during the milking process lasted for about two hours. The data of outside temperature and relative humidity were also obtained and compared with indoor data. The results of measurements were processed by Excel software and verified by statistical software Statistica 12 (*t–test*, *ANOVA* and *TUKEY HSD Test*)

All three measured milking parlours are rotary with herringbone type of stalls, each for 24 dairy cows. Two of these milking parlours were built in 2001 and one was built in 2009. The differences are in heating and ventilation system.

### Milking parlour A

There is only natural ventilation in this milking parlour through the windows with a total area of about 14 m$^2$ and two skylights, each of size 2 x 2 m. This milking parlour is heated through four radiant heating panels with a total output of 9.6 kW.

**Milking parlour B**

Forced (over pressure) ventilation with a flow rate 3,240 $m^3\ h^{-1}$ is installed in this milking parlour. This system is equipped with an inlet air heater with power of 24 kW.

**Milking parlour C**

There is only natural ventilation in this milking parlour through the windows with an area of 6.48 $m^2$ and four ventilation chimneys; each of size 0.3 x 0.3 m. This milking parlour is heated through two radiant heating panels with a total output of 8 kW.

**Theory and modelling**

Thermal condition of the indoor environment can be controlled by operational temperature and relative humidity. The operational temperature is defined as a uniform temperature of enclosed space, black in terms of radiation, in which the heat shared by convection and radiation would be the same as in the real thermally unbalanced environment (Kabele & Veverkova, 2003). According to Novy (Novy et al., 2006) the operational temperature is determined by the following equation:

$$t_o = A \cdot t_i + (1 - A) \cdot \left[ \sqrt[4]{(t_g + 273)^4 + 1.855 \cdot 10^7 \cdot 1.4 \cdot \left( \frac{|t_i - t_g|}{D} \right)^{0,25} \cdot (t_g - t_i)} - 273 \right], \qquad (1)$$

where: $t_o$ – operational temperature (°C); $A$ – coefficient of velocity (for air velocity up to 0.2 m $s^{-1}$, $A$ = 0.5); $t_i$ – internal temperature of air (°C); $t_g$ – temperature measured by globe thermometer (°C); $D$ – diameter of globe thermometer (m).

Relative humidity is obtained directly by measuring. Effect of combinations of temperature and relative humidity is included in the THI. This index is widely used to describe the heat stress and it is also a good indicator of stress temperature environment conditions. According to Zejdova (Zejdova et al., 2014), the THI is determined by the following equation:

$$THI = 0.8 \cdot t_i + \frac{(t_i - 14.4) \cdot RH_i}{100} + 46.4\,, \qquad (2)$$

where: $THI$ – temperature-humidity index (–); $t_i$ – internal temperature of air (°C); $RH_i$ – internal relative humidity of air (%).

The average values, including standard deviation, were calculated from the results of measurements for each of the microclimatic parameters (operational temperature and relative humidity) and THI.

## RESULTS AND DISCUSSION

The main objective of this article is to show the results of the measurement of main microclimatic parameters (temperature and relative humidity) in milking parlours and to compare obtained results with values recommended in relevant standards.

**Summer period**

The results of the measurement of main microclimatic parameters and THI in the summer period are shown in Table 1.

**Table 1.** Average values and standard deviation of operational temperature ($t_o$), relative humidity ($RH_i$) and THI in milking parlours A–C in the summer period, including external temperature ($t_e$) and relative humidity ($RH_e$)

| Parlour | $t_o$ (°C) | $RH_i$ (%) | THI (–) | $t_e$ (°C) | $RH_e$ (%) |
|---|---|---|---|---|---|
| A | **28.81 ± 0.37** | 55.3 ± 3.2 | **76.40 ± 0.73** $^{a}$ | 28.86 | 52.7 |
| B | **28.88 ± 1.27** | 57.9 ± 3.0 | **76.81 ± 1.05** $^{a}$ | 29.57 | 54.8 |
| C | 20.20 ± 0.60 | 51.1 ± 4.5 | 65.05 ± 0.88 $^{b}$ | 18.53 | 41.4 |

*The results that exceed allowable limits are highlighted in bold.
**Different letters (a, b) in the superscript refer to statistically significant difference at level $P$ = 0.05 (*ANOVA* and *TUKEY HSD Test*).

The operational temperature in milking parlour A is corresponding with external temperature (*t–test*, $P$ = 0.83) as well as the operational temperature in milking parlour B (*t–test*, $P$ = 0.19). The maximum allowable temperature (26 °C) was exceeded in both of these milking parlours. The operational temperature in the milking parlour C is in the optimum range (14–22 °C) thanks to low external climatic condition during the measured period. According to the statistical evaluation (*t–test*, $P$ < 0.05) the indoor operational temperature in milking parlour C does not correspond with external temperature. Internal relative humidity was higher than external relative humidity in all three milking parlours (*t–test*, $P$ < 0.05), however, still below allowable maximum of 85%. THI values indicate stress condition for dairy cows (because of high external temperature) in milking parlours A and B and they could be considered as equal (*TUKEY HSD Test*, $P$ = 0.25).

Improving of the internal conditions could be ensured by the installation of overpressure forced ventilation, which increases air velocity (Kic & Gurdil, 1999). According to Czech standard CSN 73 0543–2, the required mass flow rate of fresh air for heat removal in the summer period for cows is determined by the following equation:

$$\dot{M}_{v,max} = 0.95 \cdot y \cdot z \cdot Z \cdot m_z^{0,74} \cdot 10^{-3}, \qquad (3)$$

where: $\dot{M}_{v,\max}$ – required mass flow rate of fresh air (kg $s^{-1}$); $y$ – coefficient, weight of the construction; $z$ – coefficient, area of translucent structures; $Z$ – average number of cows in milking parlour; $m_z$ – average weight of one cow (kg).

According to equation (3) it is necessary to ensure mass flow of fresh air for milking parlours for 24 dairy cows in range of 3.43–3.91 kg $s^{-1}$ (corresponding volume flow 10,284–11,732 $m^3$ $h^{-1}$), depending on '*y*' and '*z*'.

**Winter period**

The results of measurement of main microclimatic parameters and THI in winter period are shown in Table 2.

**Table 2.** Average values and standard deviation of operational temperature ($t_o$), relative humidity ($RH_i$) and THI in milking parlours A–C in the winter period, including external temperature ($t_e$) and relative humidity ($RH_e$)

| Parlour | $t_o$ (°C) | $RH_i$ (%) | THI (–) | $t_e$ (°C) | $RH_e$ (%) |
|---|---|---|---|---|---|
| A | **12.07 ± 1.60**[a] | 68.9 ± 3.2 [a] | 51.58 ± 1.71[a] | –1.07 | 79.46 |
| B | **11.82 ± 0.86** [a] | **94.0 ± 1.2** [b] | 52.26 ± 1.03[a,b] | –2.38 | 87.46 |
| C | **12.26 ± 1.03** [a] | **89.2 ± 2.8** [c] | 53.19 ± 1.65[b] | –1.33 | 94.00 |

*The results that exceed (or do not reach) allowable limits are highlighted in bold.
**Different letters (a, b, c) in the superscript refer to statistically significant difference at level $P = 0.05$ (*ANOVA* and *TUKEY HSD Test*)

The operational temperature is below the optimum range of 14–16 °C in all three milking parlours (*t–test*, $P < 0.05$). It is also possible to consider the operational temperature in all three milking parlours as equal (*ANOVA*, $P = 0.31$). Internal relative humidity exceeds allowable limit of 85% in milking parlours B and C (*t–test*, $P < 0.05$). In milking parlour A, the relative humidity is below allowable limit of 85% (*t–test*, $P > 0.05$). THI values do not indicate stress condition for dairy cows in the winter period.

Higher relative humidity in the milking parlour is probably caused by inadequate ventilation in the milking parlour. The Czech standard CSN 73 0543–2 calculates the required mass flow rate of fresh air in the winter period separately for exhaust of water vapour and separately for exhaust of $CO_2$.

According to Czech standard CSN 73 0543–2, the mass flow rate of fresh air for exhaust of water vapour is determined by the following equation:

$$\dot{M}_{vd} = \frac{Z \cdot (\dot{m}_{do} + \Delta\dot{m}_{do}) \cdot 10^{-3}}{\Delta x_{ie}}, \tag{4}$$

where: $\dot{M}_{vd}$ – mass flow rate of fresh air for exhaust of water vapour (kg s$^{-1}$); $\dot{m}_{do}$ – total production of water vapour (mg s$^{-1}$ pcs$^{-1}$) $\Delta\dot{m}_{do}$ – increased evaporation for underfloor heating (mg s$^{-1}$ pcs$^{-1}$); $\Delta x_{ie}$ – difference of specific humidity of internal and external air ($\mathrm{g\ kg^{-1}_{d.a.}}$)

According to Czech standard CSN 73 0543–2, the mass flow rate of fresh air for exhaust of $CO_2$ is determined by the following equation:

$$\dot{M}_{vu} = \frac{Z \cdot \dot{m}_u}{K_{ui} - K_{ue}} \cdot \rho_i\ , \tag{5}$$

where: $\dot{M}_{vu}$ – mass flow rate of fresh air for exhaust of $CO_2$ (kg s$^{-1}$); $\dot{m}_u$ – $CO_2$ production of 1 dairy cow (mg s$^{-1}$); $K_{ui}$—design value of the concentration of $CO_2$ in the internal air (mg m$^{-3}$); $K_{ue}$ – design value of the concentration of $CO_2$ in the external air (mg m$^{-3}$); $\rho_i$ – internal air density (kg m$^{-3}$).

The required mass flow rate of fresh air in the winter period is determined by the following equation:

$$\dot{M}_v = \max(\dot{M}_{vd}; \dot{M}_{vu}), \tag{6}$$

According to equations (4) to (6), it is necessary to ensure in milking parlour A the mass flow rate 0.79 kg $s^{-1}$ (volume flow rate 2,375 $m^3$ $h^{-1}$), in milking parlour B 0.81 kg $s^{-1}$ (volume flow rate 2,439 $m^3$ $h^{-1}$) and in milking parlour C 0.89 kg $s^{-1}$ (volume flow rate 2,696 $m^3$ $h^{-1}$). It is possible to achieve these mass flows by natural ventilation. According to various authors (Chysky et al., 1993; Novy et al., 2006) the calculation of required buoyancy for natural ventilation is determined by the following equation:

$$\Delta p = \Delta p_i + \Delta p_o = g \cdot (\rho_e - \rho_i) \cdot h, \tag{7}$$

where: $\Delta p$ – total pressure difference (effective buoyancy) (Pa); $\Delta p_i$ – the pressure required to overcome the resistance in inlet openings (Pa); $\Delta p_o$ – the pressure required to overcome the resistance in outlet openings (Pa); g – gravitational constant (m $s^{-2}$); $\rho_e$ – external air density (kg $m^{-3}$); $\rho_i$ – internal air density (kg $m^{-3}$); $h$ – height difference of axes of inlet and outlet openings (m)

In practice, the effective buoyancy is divided to the pressures required to overcome the resistance in inlet and outlet openings in the ratio 1:1. The required areas of inlet and outlet openings are determined by the following equations (Chysky et al., 1993; Novy et al., 2006):

$$S_i = \frac{\dot{M}_v}{\mu_i \cdot \sqrt{2 \cdot \rho_e \cdot \Delta p_i}}, \tag{8}$$

$$S_o = \frac{\dot{M}_v}{\mu_o \cdot \sqrt{2 \cdot \rho_i \cdot \Delta p_o}}, \tag{9}$$

where: $S_i$ – required area of inlet openings ($m^2$); $S_o$ – required area of outlet openings ($m^2$); $\mu_i$ a $\mu_o$ – coefficients of flows in inlet and outlet openings.

An overview of required and installed inlet and outlet openings according to the equations (7) to (9) is shown in Table 3.

**Table 3.** Overview of required and installed inlet and outlet openings for natural ventilation in milking parlours A–C in the winter period

| Parlour | Required $S_i$ ($m^2$) | Required $S_o$ ($m^2$) | Installed $S_i$ ($m^2$) | Installed $S_o$ ($m^2$) |
|---|---|---|---|---|
| A | 1.39 | 0.97 | 14.00 | 8.00 |
| B | **0.84** | **2.23** | 0.00 | 0.00 |
| C | 2.41 | **1.16** | 6.48 | 0.36 |

* Inadequate areas of inlet and outlet openings are highlighted in bold.

Adequate inlet and outlet openings are installed only in milking parlour A, so there is no problem with relative humidity. Other milking parlours have inadequate inlet and/or outlet openings and in these milking parlours the measured relative humidity was higher than allowed. To fix the problem with relative humidity in these milking parlours, it is necessary to make adequate inlet and outlet openings (or using forced ventilation installed in parlour B).

The lower temperature than the optimum during the measurement indicates inadequate heating in milking parlours. To set up adequate heating power, it is necessary to count the heat balance of a milking parlour (Kic et al., 2007; Zajicek & Kic, 2014). According to Czech standard CSN 73 0543–2, the heat balance is determined by following equation:

$$\dot{Q}_c + \dot{Q}_t - \dot{Q}_v - \dot{Q}_p = 0 \tag{10}$$

where: $\dot{Q}_c$ – apparent production of sensible heat (W); $\dot{Q}_t$ – adequate heating power (W); $\dot{Q}_v$ – ventilation heat loss (W); $\dot{Q}_p$ – building's heat loss (W).

Adequate heating power calculated according the equation (10) together with installed heating power is shown in Table 4.

**Table 4.** Adequate and installed heating power and adequate heating power using heat recovery system with 50% efficiency in milking parlours A–C in the winter period

| Parlour | Adequate $\dot{Q}_t$ (W) | Installed $\dot{Q}_t$ (W) | Adequate $\dot{Q}_t$ using heat recovery system with 50% efficiency (W) |
|---|---|---|---|
| A | **11,246** | 9,600 | –748 |
| B | 9,954 | 24,000 | –2,317 |
| C | **8,931** | 8,000 | –4,704 |

* Inadequate heating power is highlighted in bold.

According to the equation (10) and results in Table 4, it is obvious that heating power in milking parlour A and C is inadequate (the heating power in milking parlour B is adequate, but not used). The problem with heating power could be solved using forced ventilation with heat recovery system. When using forced ventilation with heat recovery system with 50% efficiency, the heating power calculated according to equation (10) is more than sufficient (see table 4).

## CONCLUSIONS

The results of measurement show that the indoor environment of milking parlours is influenced by thermal condition (operational temperature and relative humidity). From the results of measurements of selected milking parlours it is obvious that heating and ventilation is insufficient.

In the summer period, the operational temperature in the milking parlour corresponds to external temperature in days with high external temperature (around 30 °C). Internal relative humidity is below the critical limit of 85%; however, it is higher than external relative humidity. According to THI, combination of high temperature and relative humidity is stressful for dairy cows. Improving of the internal conditions could be ensured by installation of overpressure forced ventilation, which increases the air velocity in the milking parlour. The milking parlour for 24 dairy cows constructed from light-weight material (milking parlour B) needs a flow of fresh air with the volume of about 12,000 $m^3 h^{-1}$. The milking parlours constructed from medium-weight material (milking parlours A and C) need a flow of fresh air with the volume of about 10,500 $m^3 h^{-1}$.

Internal relative humidity over 85% indicates inadequate ventilation. In the winter period, natural ventilation is sufficient. Natural ventilation requires adequate inlet and outlet openings. Problem of low operational temperature is caused by inadequate installed heating power. One of the options for solving this problem is to increase the heating power by installation of additional radiant heating panels. Another solution can be using forced ventilation with heat recovery system instead of natural ventilation.

ACKNOWLEDGEMENTS. Supported by Internal grant agency of Faculty of Engineering, Czech University of Life Sciences in Prague no: 2015:31170/1312/3114.

## REFERENCES

Armstrong, D.V. 1994. Heat stress interaction with shade and cooling. *Journal of Dairy science* **77**, 2044–2050.

CSN 73 0543–2. 1998. *Internal environment in buildings for animals. Part 2: Ventilation and heating*. CNI, Praha, 36 pp. (in Czech)

Chloupek, J. & Suchy, P. 2008. *Microclimatic measurements in animal houses*. VFU, Brno, 229 pp. (in Czech)

Chysky, J., Hemzal, K., Drkal, F., Kubicek, L. & Novy, R. 1993. *Ventilation and Air Conditioning*. BOLIT, Brno, 560 pp. (in Czech)

Kabele, K & Veverkova, Z. 2003. Modelling of operational temperature. *Heating Ventilation Installation*. **12**, 33–37. (in Czech)

Kic, P. & Broz, V. 1995. *Creation of Stable Environment*. IVV MZe CR, Praha, 47 pp. (in Czech)

Kic, P. & Gurdil, GAK. 1999. Trends in ventilation and air conditioning of animal houses. *Conference Proceedings - International Conference on Trends in Agricultural Engineering.* CZU, Praha, CZ, pp. 389–393

Kic, P., Kalvoda, T., & Zavadil, V. 2007. Energy savings by heat recovery in ventilation. *Conference Proceedings - 3rd International Conference on Trends in Agricultural Engineering.* CZU, Praha, CZ, pp. 215–218

Koznarova, V. & Klabzuba, J. 2008. *Microclimate of Stables*. CZU, Praha, 29 pp. (in Czech)

Kunc, P., Knizkova, I., Prikryl, M., Maloun, J. & Novak, P. 2007. *Technical, Animalistic and Humane Aspects of Milking*. CZU, Praha, 60 pp. (in Czech)

Novy, R., Broz, K., Drkal, F., Hemzal, J. & Hemerka, J. 2006. *Environmental Engineering*. CVUT, Praha, 267 pp. (in Czech)

Papez, J. & Kic, P. 2013. Wood Moisture of Rural Timber Constructions. *Agronomy Research* **11**, 505–512.

Pavelek, M. & Stetina, J. 2007. *Experimental Methods in Environmental Engineering*. CERM, Brno, 215 pp. (in Czech)

Zejdova, P., Chladek, G. & Falta, D. 2014. *Influence of stable environment on behaviour and milk production of dairy cows*. Mendel University, Brno, 26 pp. (in Czech)

Zajicek, M. & Kic, P. 2014. Heating of large agricultural and industrial buildings. *Agronomy Research* **12**, 237–244.

*Agronomy Research* **13**(1), 253–260, 2015

# Producing the vacuum in modern drawn milking systems

M. Prikryl[1,*], P. Vaculik[1], A. Smejtkova[1], J. Hart[1] and P. Nemec[2]

[1]Czech University of Life Sciences Prague, Faculty of Engineering, Department of Technological Equipment of Buildings, Kamýcká 129, 165 21 Prague 6-Suchdol, Czech Republic; [*]Correspondence: prikryl@tf.czu.cz
[2]PREDA CZ, s.r.o., U popovic 618, 393 01 Pelhřimov, Czech Republic

**Abstract.** This paper deals with the measurement of the modern method of producing and regulating the vacuum in milking equipment which is currently in use. Individual measurements are primarily focused on evaluating the latest knowledge in the design, management and stabilization of the vacuum in modern milking systems. In the evaluation, emphasis was placed on economic efficiency with regard to energy consumption, environmental friendliness, high performance, operational reliability and ease of operation in the creation and control of the vacuum. The basic element of every milking system is the vacuum pump. This feature of the machine provides a vacuum for milking, milk transportation and for the activities of other devices whose task is, e.g., scanning the milking equipment or controlling movable barriers at milking parlours.
In this paper, a frequency converter was used, which is, used in milking technology for regulating and controlling the vacuum through changing the rotational speed of the vacuum pumps which do not require the use of centrifugal force to seal the working space to create a vacuum. The aim of the measurements using the above-mentioned inverter was to check the performance of the pump at different speeds and different vacuum levels to determine the actual air flow need over the milking cycle.

**Key words:** milking system, milking unit, vacuum system, vacuum regulation, vacuum air pump, frequency converter.

## INTRODUCTION

The aim of this paper is to present the results of measurements and a modern method of acquisition and regulation of the under-pressure in milking equipment. As an essential machinery element of milking equipment, the vacuum pump provides under-pressure for milking, transport of milk and for the activities of other devices (scanning of the milking equipment, controlling movable barriers at milking parlours, etc.) (Walstra et al., 1999; Laurs & Priekulis, 2008). The drive of the vacuum pump is usually mediated by an electric motor and thus forms a machine set whose accessories include an air receiver, control valve, a vacuum gauge and a portion of an exhaust pipe that discharges the air sucked out by the vacuum pump (Pittermann, 2008; Pavelka & Zděnek, 2010). An oil separator is mounted at the end of the exhaust pipe at the bladed vacuum pumps, which also acts as a muffler. For vacuum pumps that do not have oil lubrication, a muffler is mounted at the end of the exhaust pipe. Standard ČSN ISO 3918 defines the terms used in the construction, manufacturing and use of milking machines for dairy cows.

Some milking equipment manufacturers have also recently begun utilizing for milking machines a vacuum pump for milking with two identical rotors with a sponge-shaped cross section, known as a Roots blower. The pistons are coupled by a pair of precisely-manufactured gears so that they have opposite direction of rotation. During rotation, spaces are created between the walls of the cylinder and the rotors connected either via a suction or discharge port; however, with regard to leakage losses, there may never be simultaneous connection to the suction and discharge. With increasing pressure ratio of $p_2\ p_1^{-1}$ leakage losses also increase, and thus a pressure ratio is selected up to a maximum of 1.8. Air vacuum pumps are widely used also thanks to substantial volume flows that can reach up to 9,000 l min$^{-1}$ (the Roots blower with two-lobed rotors). In these vacuum pumps, the effect of leaks can also be corrected using high peripheral speeds (up to 100 m s$^{-1}$).

## MATERIALS AND METHODS

Performance of vacuum pump – the amount of air sucked out by the vacuum pump at working temperature, specific rotations and under-pressure level at the input. It is expressed by the quantity of free air per minute (Fig. 1) (ČSN ISO 3918).

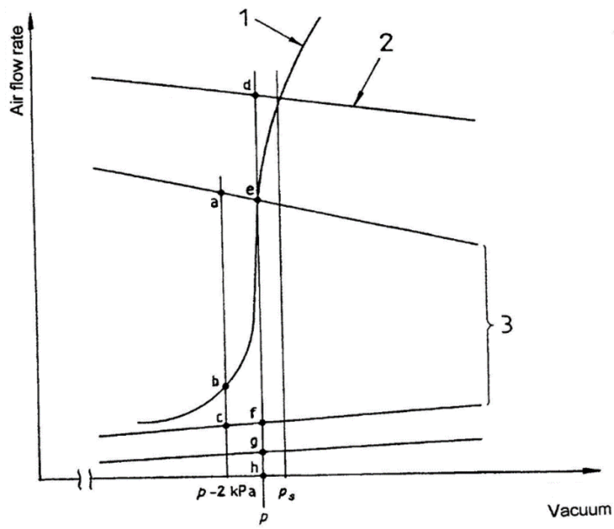


**Figure 1.** Relationship between pump capacity, air used by components, effective reserve, manual reserve and regulation characteristics (ČSN ISO 3918): 1 – regulation characteristic; 2 – vacuum pump capacity characteristic; 3 – air flow through regulator (spare capacity); *ab* – effective reserve; *ac* – manual reserve; *bc* – regulation loss; *dh* – vacuum pump capacity at working vacuum; *de* – air used by milking units; *fg* – air consumption of continuously operated components; *gh* – system leakage; *p* – working vacuum with all units operating; $p_s$ – working vacuum with no unit operating.

According to ČSN ISO 5707, the vacuum pump must be able to ensure the operating requirements (milking and cleaning) of the milking equipment, including other equipment that is active continuously or intermittently during milking, which requires under-pressure for its activities and consume air. In order to ensure operating requirements, the vacuum pump should have sufficient performance so that the decrease in under-pressure in or near a collection container does not exceed 2 kPa during normal milking, including insertion and removal of cups, air leakage in teat sleeves, or if the milking equipment falls. Performance must be measured in accordance with ISO 6690.

Performance must be measured in accordance with ČSN ISO 6690. If more than one vacuum pump is installed, it must be possible to disconnect the vacuum pumps not being used.

The performance of a vacuum pump during a nominal atmospheric pressure of 100 kPa will be acquired by multiplying the measured performance of the vacuum pump by the $K_1$ (1) (Table 1) coefficient, which we calculate as follows:

$$K_1 = \frac{p_{\max} - p_{nom} \cdot \dfrac{p_a}{p_{an}}}{p_{\max} - p} \tag{1}$$

where: $p_a$ – surrounding atmospheric pressure during measuring (kPa); $p_{an}$ – nominal atmospheric pressure (kPa); $p_{max}$ – maximum level of under-pressure with a fully-closed suction port of the vacuum pump during measuring (kPa); $p$ – level of under-pressure in the suction port of vacuum pump (kPa); $p_{nom}$ – nominal under-pressure level in the suction port of the vacuum pump (kPa).

**Table 1.** Correction coefficient $K_1$ for different atmospheric pressures (ČSN ISO 6690)

| Surrounding atmospheric pressure during measuring $p_a$ (kPa) | Correction coefficient $K_1$ for the vacuum level at the vacuum pump 50 kPa |
|---|---|
| 100 | 1.00 |
| 95 | 1.07 |
| 90 | 1.16 |
| 85 | 1.28 |
| 80 | 1.45 |

The performance of vacuum pump during a nominal atmospheric pressure for a given elevation will be acquired by multiplying the measured performance of the vacuum pump by the $K_2$ (2) (Table 2) coefficient:

$$K_2 = \frac{p_{\max} - p \cdot \dfrac{p_a}{p_s}}{p_{\max} - p} \tag{2}$$

where: $p_a$ – surrounding atmospheric pressure during measuring (kPa); $p_s$ – normal atmospheric pressure for the elevation (kPa); $p_{max}$ – maximum under-pressure level with a fully-closed suction port of vacuum pump during measuring (kPa); *p* – under-pressure level in the suction port of the vacuum pump (kPa).

**Table 2.** Correction coefficient $K_2$ for different atmospheric pressures (ČSN ISO 6690)

| Surrounding atmospheric pressure during measuring $p_a$ (kPa) | Correction coefficient $K_2$ Vacuum level at the vacuum pump (kPa) | | |
|---|---|---|---|
| | 40 | 45 | 50 |
| 109 | 0.94 | 0.92 | 0.91 |
| 106 | 0.96 | 0.95 | 0.93 |
| 103 | 0.98 | 0.97 | 0.96 |
| 100 | 1.00 | 1.00 | 1.00 |
| 97 | 1.03 | 1.03 | 1.04 |
| 94 | 1.05 | 1.07 | 1.09 |
| 91 | 1.09 | 1.11 | 1.14 |

Regulation of under-pressure via a change of vacuum pump rotations using a frequency converter – this method of regulation can be used in an under-pressure system with an air vacuum pump in which efficacy is not changed by changing the rotations, as it does not require the use of centrifugal force to seal the working parts. This regulation provides a way to reduce energy consumption and related costs. Most dairy farms use vacuum pumps with constant operation that continuously produce more under-pressure than is actually needed for the operation and cleaning of the milking system. Normally, one or two vacuum pumps are installed in a milking parlour in order to achieve a constant air flow of 170 l min$^{-1}$ by one milking unit. The amount of air that is actually consumed for 'balanced' milking – when all of the milking units are deployed and there is no leakage, is approx. 30–60 l min$^{-1}$ per one milking unit. Even the most advanced cleaning of a milking system requires only 60–70 l min$^{-1}$ of air per one milking unit, if the CIP (Sanitation/cleaning station) system is well designed and balanced.

However, during milking there occur moments where an additional air flow is required due to excessive clinging, such as during the attaching the milking machine, if the teat cup does not rest against it, or if the teat cup slips from the teat of the cow.

During cleaning using the CIP method, this may, for example, occur when the air injector is in the phase of in-taking air into the piping.

The vacuum pump does not need to be operated with constant rotations in order to achieve maximum air flow, which is only required in short time intervals during milking and cleaning. Instead, it is possible to save significant amounts of electricity by equipping the vacuum pumps with a rotation regulator. Such a regulator can speed up or slow down the vacuum pump so that it produces the amount of air that is necessary for any phase of the milking or cleaning. A vacuum pump equipped with a regulator works only at approx. half of the rotations, as opposed to not being equipped with such equipment. If the vacuum pump operates at lower rotations, then it will be quieter. Due to the fact that steady milking does not require excessive air flow, a vacuum pump equipped with a regulator will operate at relatively low rotations most of the time during milking and cleaning. This will significantly contribute to reducing the noise of the vacuum pump. Running a vacuum pump at lower rotations has a positive effect on the bearings and other internal components of the vacuum pump, which contributes to prolonging its lifespan. This is one more reason why a vacuum pump should be equipped with a regulator.

In view of the above facts, a parallel milking parlour of the most commonly used size in the Czech Republic, 2 x 8, was selected for further evaluation.

Own measuring – measuring was carried out for a 2 x 8 parallel milking parlour (Table 3) with the following objectives:

1) To verify the performance of the vacuum pump declared by the manufacturer at various rotations of the vacuum pump (Tables 4, 5), and at various under-pressure levels;

2) To determine the current air flow requirement during the course of the entire milking cycle, and to ascertain the electricity demands for creating the necessary amount of under-pressure using a frequency convertor as an under-pressure regulator (Fig. 2) and without using a convertor, wherein a control valve regulates the under-pressure; compare the measured values and determine the percentage of electricity savings during individual milking phases.

**Table 3.** Basic parameters of measured milking parlour

| Parameter | Value | Unit |
|---|---|---|
| Type of milking parlour | parallel with rapid withdrawal | - |
| Size of milking parlour | 2 x 8 | - |
| Performance of milking parlour specified by the manufacturer | 80 | Dairy cows $h^{-1}$ |
| Working under-pressure | 42 | kPa |

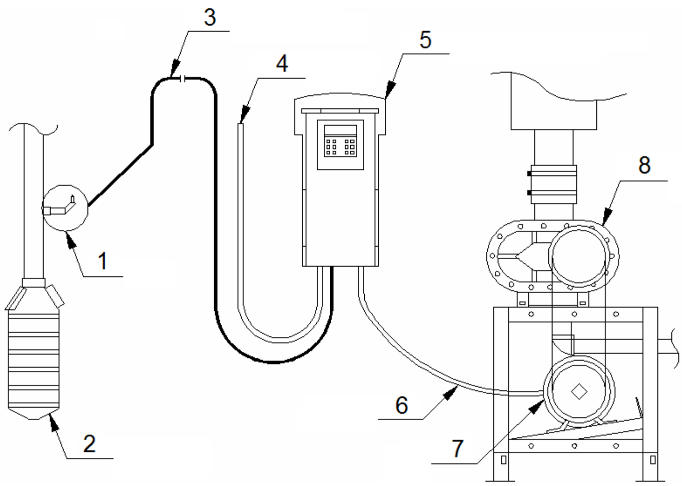


**Figure 2.** Connection diagram of frequency convertor (ACS 550-01-08A8-4) to the motor of the vacuum pump: 1 – sensor; 2 – separator; 3 – shielded cable; 4 – CYKY cable; 5 – frequency convertor; 6 – CYKY cable; 7 – motor; 8 – vacuum pump.

**Table 4.** Basic parameters of measured vacuum pump

| Parameter | | |
|---|---|---|
| Type | Bou-Matic AIR-STAR BP 140 | |
| Model | GACHDPA 0040 | |
| | Value | Unit |
| Minimal rotations | 1,000 | rotations minute$^{-1}$ |
| Maximum rotations | 3,000 | rotations minute$^{-1}$ |
| Nominal rotations | 2,920 | rotations minute$^{-1}$ |
| Nominal performance at 50 kPa | 1,960 | L min$^{-1}$ |
| Reduction ratio (vacuum pump/motor) | 1.277 | - |

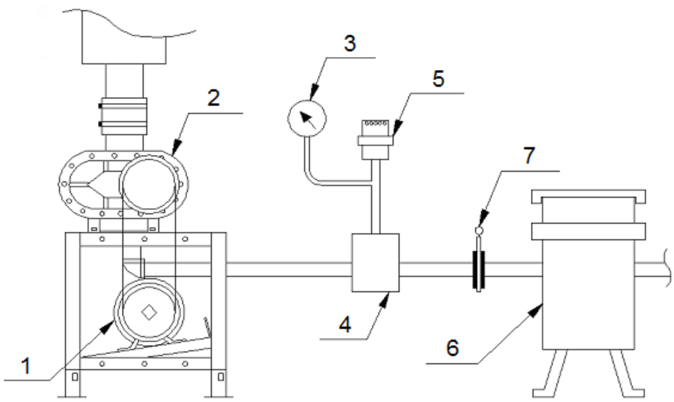


**Figure 3.** Diagram of the measurement of the performance of the vacuum pump: 1 – motor; 2 – vacuum pump; 3 – vacuum gauge; 4 – valve; 5 – flow meter; 6 – filter; 7 – slide.

**Table 5.** Basic parameters of vacuum pump motor

| Parameter | Value | Unit |
|---|---|---|
| Nominal rotations | 1,800 | rotations minute$^{-1}$ |
| Nominal performance | 7.5 | kW |

## RESULTS AND DISCUSSION

The performance of the vacuum pump was measured using a frequency convertor by which the rotations of the motor were set from 800 rotations minute$^{-1}$ intermittently by 100 rotations, up to the maximum permitted number of rotations of the motor, i.e. 2,820 rotations minute$^{-1}$.

Using a set for measuring the performance of a vacuum pump that contains a flow meter and vacuum gauge, the performance of the vacuum pump was measured at an under-pressure of 50 kPa, and at a working under-pressure of 42 kPa (Table 6). During this measurement, the under-pressure piping was closed using a slide in front of the air filter of the vacuum pump (Fig. 3). The values are specified in Graph 1.

**Table 6.** Values from measuring the performance of the vacuum pump

| Rotations of motor | Rotations of vacuum pump | Frequency | Performance | Performance 42 kPa | Frequency | Performance | Performance 50 kPa |
|---|---|---|---|---|---|---|---|
| rotations minute$^{-1}$ | rotations minute$^{-1}$ | Hz | kW | l min$^{-1}$ | Hz | kW | l min$^{-1}$ |
| 800 | 1,021 | 27.2 | 1.8 | 760 | 27.3 | 2.1 | 550 |
| 900 | 1,149 | 30.5 | 1.9 | 910 | 30.6 | 2.2 | 680 |
| 1,000 | 1,277 | 33.8 | 2.1 | 1,050 | 33.9 | 2.5 | 780 |
| 1,100 | 1,404 | 37.2 | 2.4 | 1,210 | 37.3 | 2.7 | 900 |
| 1,200 | 1,532 | 40.5 | 2.6 | 1,290 | 40.6 | 3.0 | 960 |
| 1,300 | 1,660 | 43.8 | 2.8 | 1,420 | 43.9 | 3.2 | 1,060 |
| 1,400 | 1,787 | 47.2 | 3.1 | 1,560 | 47.2 | 3.5 | 1,180 |
| 1,500 | 1,915 | 50.5 | 3.3 | 1,705 | 50.6 | 3.8 | 1,310 |
| 1,600 | 2,043 | 54.0 | 3.5 | 1,830 | 54.1 | 4.0 | 1,405 |
| 1,700 | 2,170 | 57.4 | 3.8 | 1,950 | 57.5 | 4.3 | 1,510 |
| 1,800 | 2,298 | 60.8 | 4.1 | 2,050 | 60.9 | 4.7 | 1,590 |
| 1,900 | 2,426 | 64.2 | 4.4 | 2,160 | 64.4 | 5.0 | 1,700 |
| 2,000 | 2,553 | 67.7 | 4.7 | 2,270 | 67.9 | 5.3 | 1,780 |
| 2,100 | 2,681 | 71.3 | 5.1 | 2,350 | 71.5 | 5.7 | 1,880 |
| 2,200 | 2,809 | 74.8 | 5.5 | 2,460 | 75.1 | 6.2 | 1,940 |
| 2,300 | 2,936 | 78.4 | 5.8 | 2,550 | 78.6 | 6.5 | 2,035 |
| 2,400 | 3,064 | 81.9 | 6.2 | 2,650 | 82.3 | 7.0 | 2,110 |
| 2,500 | 3,192 | 85.6 | 6.5 | 2,750 | 86.4 | 7.5 | 2,170 |
| 2,600 | 3,319 | 89.4 | 7.1 | 2,840 | 86.7 | 7.6 | 2,170 |
| 2,700 | 3,447 | 90.5 | 7.3 | 2,840 | 86.9 | 7.7 | 2,170 |
| 2,800 | 3,574 | 90.5 | 7.3 | 2,840 | 86.9 | 7.7 | 2,170 |

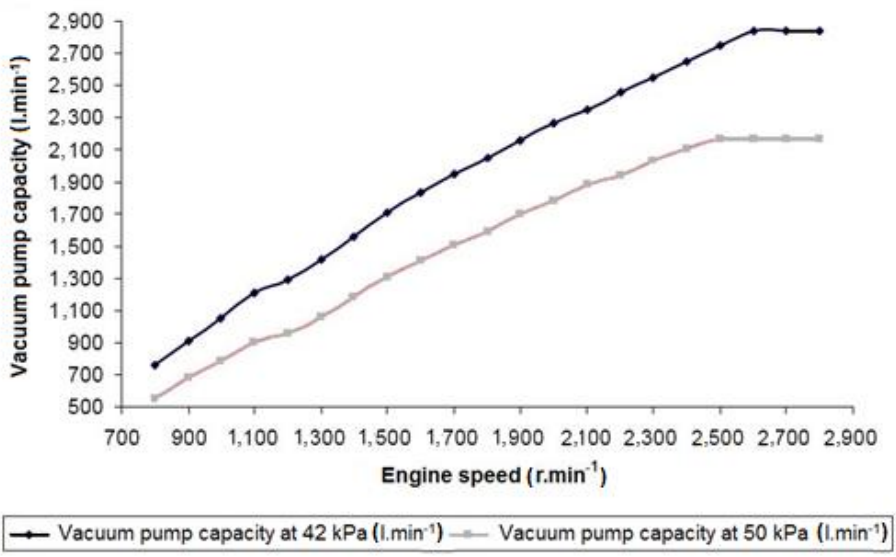


**Graph 1.** Graphical representation of measuring the performance of the vacuum pump.

The measured values show that the vacuum pump fulfils the performance declared by the manufacturer, as the actual measured performance during vacuum pump rotations of 2,920 rotations minute$^{-1}$ is 2,020 l min$^{-1}$ (this value is drawn from Graph 1).

The measured values also show that at a working under pressure of 42 kPa, there is no need to configure the frequency convertor so as to achieve the maximum permitted rotations of the motor of 2,800 rotations minute$^{-1}$, as the maximum performance of the vacuum pump is already achieved at 2,600 motor rotations minute$^{-1}$. The issue of energy savings when milking is very timely (Ahokas et al., 2013; Gaworski & Leola, 2014).

## CONCLUSIONS

The measured values show that during the entire course of the milking cycle, it was never necessary to have more air than 2,050 l min$^{-1}$. This maximum was only necessary during rinsing; during own milking the maximum air consumption was 1,570 l min$^{-1}$.

In addition, the required performance to produce under-pressure did not exceed 4.2 kW. These values are drawn from measuring when a frequency convertor is connected. For the alternatives without a frequency convertor, the motor rotations are constant (nominal speed of 1,800 rotations minute$^{-1}$). At these speeds the vacuum pump performs at 2,050 l min$^{-1}$. The measurements showed that the average speed during milking regulated by a frequency convertor is 807 rotations minute$^{-1}$, which corresponds to an air flow of 770 l min$^{-1}$.

This means that during milking without a frequency convertor but using a control valve, the average of additionally-sucked air is 1,280 l min$^{-1}$.

## REFERENCES

Ahokas, J. Mikkola, H., Jokiniemi, T., Rajaniemi, M., Schäfer, W., Rossner, H., Poikalainen, V., Praks, J., Veermäe, I., Frorip, J. & Kokin, E. 2013. ENPOS – Energy positive farm. *Agronomy Research* **11**(2), 523–527.

ČSN ISO 3918. 1999. Milking machine installations – Vocabulary. Prague: Český normalizační institut, 37 pp. (in Czech).

ČSN ISO 5707. 1999. Milking machine installations – Construction and performance. Prague: Český normalizační institut, 38 pp. (in Czech).

ČSN ISO 6690. 1999. Milking machine installations – Mechanical tests. Prague: Český normalizační institut, 29 pp. (in Czech).

Gaworski, M. & Leola, A. 2014. Effect of technical and biological potential on dairy production development. *Agronomy Research* **12**(1), 215–222.

Laurs, A. & Priekulis, J. 2008. Robotic milking of dairy cows. *Agronomy Research* **6**, 241–247.

Pavelka, J. & Zděnek, J. 2010. Elektrické pohony a jejich řízení. 1st Edition. Praha: České vysoké učení technické, 241 pp. ISBN 978-80-01-04642-5 (in Czech).

Pittermann, M. 2008. Elektrické pohony: základy. 1st Edition. Plzeň: Západočeská univerzita, 98 pp. ISBN 978-80-7043-729-2 (in Czech).

Walstra, P. Geurts, T.J., Noomen, A., Boekel, A. & Jellema, A. 1999. Dairy technology: principles of milk properties and processes. New York: Marcel Dekker, 727 pp. ISBN 0-8247-0228-X.

*Agronomy Research* **13**(1), 261–268, 2015

# Direct energy consumption and saving possibilities in milk production

M. Rajaniemi, M. Turunen and J. Ahokas*

University of Helsinki, Faculty of Agriculture and Forestry, Department of Agricultural Sciences, PL 28 (Koetilantie 5), 00014 Helsingin yliopisto, Finland;
*Correspondence: jukka.ahokas@helsinki.fi

**Abstract.** Direct energy consumption in milk production varies largely because of machinery, production systems, working habits and maintenance. There are good possibilities to save energy in milk production. The magnitude of energy savings are in the order of tens of percent, which means that energy saving potential is quite high. Energy saving can be achieved with efficient system and machinery choices. Also adjustments and maintenance have an effect on energy consumption. To save energy the farmers should have means to measure energy and follow energy consumption. There should also be more information of energy saving possibilities and machinery energy consumptions.

**Key words:** energy, milk production, ventilation, lighting, milking, milk cooling.

## INTRODUCTION

Energy consumption in milk production can be divided into two categories, direct and indirect. Direct energy is bought directly to the production, for instance electricity, gas and diesel oil. Indirect energy is used outside the main production, for instance feed material production needs energy but this energy is used mainly in field operations. In this study we concentrate on the direct energy used in the cattle house.

Fig. 1 shows energy consumption and its variation in milk production (Ludington & Johnson, 2003; Eerola, 2006; Vergicht et al., 2007; Hörndahl, 2008; Neuman, 2008). The variation in consumption is high depending on the machinery, production system and also working habits and maintenance. The four largest direct energy consumption will be handled in this study: lighting, milking and milk cooling, ventilation and feeding. In cowhouses the trend has been to move towards cold or semi-cold buildings with natural ventilation and with no or light heat insulation. This means that the cowhouse do not need heating. Only milking parlour, offices and dressing rooms need heating but this is minor consumption, normally less than 20 Wh $kg^{-1}$ milk (Turunen 2013).

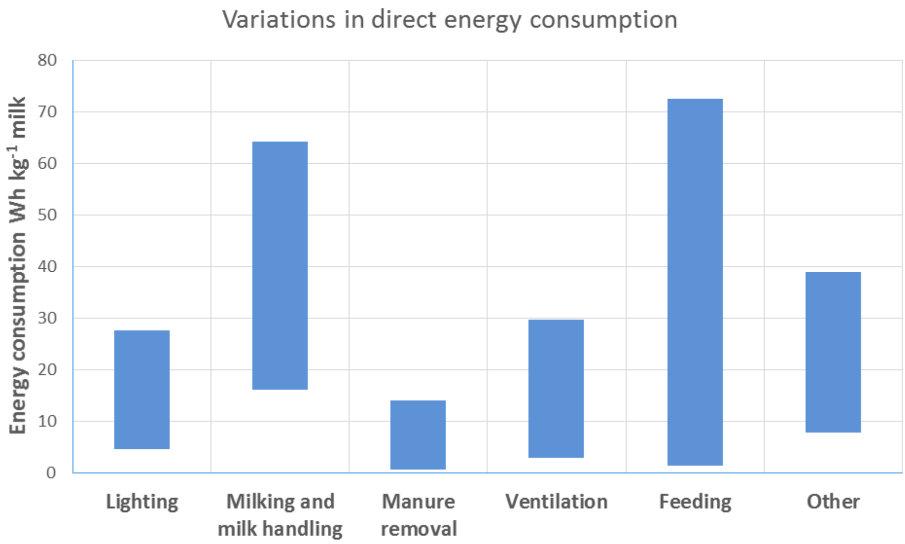


**Figure 1.** Direct energy consumption variation in milk production.

## MATERIALS AND METHODS

### Ventilation

The main purpose of building is to offer shelter to the cows and also to humans working in the building. For a good microclimate ventilation is needed to remove the harmful emissions and bring fresh air into the building. Water is used for washing and as drinking water, and part of this is also vaporized and needs to be removed from the building. Also cows produce moisture. Ventilation criteria changes mainly according to the ambient temperature. During warm and hot periods ventilation is needed to cool the cowhouse. During cold periods heat removal is not needed and then moisture and gas (mainly $CO_2$) dictate the ventilation rate.

The energy needed to run forced ventilation can be calculated from Equation (1).

$$E_v = \frac{q_v \cdot \Delta p}{\eta} \cdot t \,. \tag{1}$$

where: $q_v$ is the air volume flow; $\Delta$p the pressure difference between the fan inlet and outlet; $\eta$ the combined efficiency of the fan and motor running the fan and t is the time the ventilation is running.

For animal welfare and energy use it is important that the ventilation rate is according to need. Instead of forced ventilation, natural ventilation can be used. It is used typically in cold or semi-cold cowhouses and the ventilation rate is controlled with the adjustment of the openings and outlets. The micro climate in these buildings is, in most cases, good because of a sufficient ventilation rate and the energy consumption is minimal.

**Lighting**

Lighting is an animal welfare question but also proper lighting is needed for human workers. When animals are kept in building lighting is needed but also appropriate period is needed for rest without artificial lighting. Illumination affects safety, animal growth, fertility and production. Proper lighting can increase milk yield 5–16% (Crill et al., 2002). The light intensity (lx) recommendations depend on the operation of the room. In table 1 are typical recommendations for cattle houses.

**Table 1.** Recommended illumination intensities in cattle houses (MMM-RMO C3)

| Room | Recommended intensity lx |
|---|---|
| General illumination | 60–100 |
| Milking parlour | 200–250 |
| Offices | 150–300 |

Energy consumption in lighting depends on e.g. lamp type, distance and angle of light source from the illuminated surface and the time the lights are used.

**Milking**

In milking most of the energy is used in running the vacuum pump and in washing the milking machine. The energy used in vacuum pump can be calculated with Equation (2).

$$E_m = \frac{q_v \cdot \Delta p}{\eta} \cdot t \tag{2}$$

where: $E_m$ is the energy consumption; $q_\mathrm{v}$ is the air flow; $\Delta p$ is the vacuum; t is running time and $\eta$ is efficiency.

To reduce energy consumption the air flow should be according to the needs and the vacuum pump running time should be low.

**Milk cooling**

Milk temperature after milking is 35–38 °C and this has to be cooled to 3–4 °C temperature. The energy released in cooling can be calculated with Equation (3).

$$E_{mc} = m \cdot c_m \cdot \Delta T \tag{3}$$

where: $E_{mc}$ is the released energy; m is the mass of the milk; $c_\mathrm{m}$ is the specific heat capacity of milk (≈ 4 kJ $kg^{-1}$ $K^{-1}$ and $\Delta T$ is the temperature change in cooling (≈ 33 K). Milk cooling is done with refrigeration systems which normally have an energy efficiency ratios of about 3.

## RESULTS

### Ventilation

According to Equation (1) ventilation energy consumption depends on airflow, pressure drop in air ducts, ventilation running time and efficiency of fan and motor. The dependence is linear, change in one of this causes a corresponding energy consumption change. Energy consumption can be reduced by optimizing these items. Ventilation rate in forced ventilation should be adjusted according to the need of good microclimate. Ventilation control changes depending on temperatures, number of animals and animal weight; the control system should be able to function with changing criteria. Ventilation control should also be able to stop ventilation if natural ventilation is sufficient.

Air ducts should produce a low pressure drop. This is achieved with good design and cleaning and maintenance of the ducts. Annual cleaning of air ducts and fans can reduce energy consumption 10% (Hinge, 2001; Ludington et al., 2004).

There are differences in fan and motor efficiencies. Unfortunately it is not easy to get reliable information of the fans. EU has introduced efficiency demands for fans (EU 327/2011). The efficiency depends on power, fan type and assembly type. For instance for 1 kW axial fans the efficiency demand is between 30–50% depending on the assembly type. ASAE EP566 (2012) standard specify efficiency with $m^3\ h^{-1}\ W^{-1}$ figure when the pressure drop is 250 Pa. Small fans should produce 16 $m^3\ h^{-1}$ airflow for one watt motor power and large fans 30 $m^3 \cdot h^{-1}$ airflow for one watt motor power.

When natural ventilation is used, energy demand is low, only the control system consumes small amount of energy. In cold climate it is important to avoid freezing of drinking water or manure. During the winter time it is essential not to have too effective ventilation, which could lower the temperature under freezing point.

### Lighting

In lighting the trend is to replace incandescent light bulbs with more energy efficient lamps. Luminous efficacy of the bulb can be calculated by dividing the bulb lumen value by the electric power consumption of the bulb. The higher this value, the more energy efficient the bulb is. Incandescent lightbulbs' efficacy is 10–15 lm $W^{-1}$, energy saving lamps have 50–70 lm $W^{-1}$ efficacy (Tetri et al., 2011). LED lights can have higher efficacies. For instance LED light bulb efficacies varied in tests from 57 to 110 lm $W^{-1}$ (PremiumLight 2015).

Although the energy demand of a single bulb is low, the number of them in cow houses is high and they can be on continuously making the energy use high. For instance in milk production, lights can consume 10–30% of the total electricity used (Ludington & Johnson 2003; Hörndahl 2008). To save energy the lights should be used only when needed and with special lighting programs. In addition places which are seldom used could have automatic light switching systems.

Good natural lighting can be achieved with 10–15% transparent roof area (DairyCo, 2012). Depending on the time of the year the length of daylight period varies and especially in northern and southern parts of the hemisphere artificial lights are needed during the dark periods of the year.

In cattle houses the lights are covered with dust and dirt reducing the light power. Dunn et al. (2010) noticed that during two year period the light intensity was reduced by

30% because of dirt. Gooch & Ludington (2003) recommend that the lights should be cleaned in 6 months periods.

With dimming energy consumption can be also reduced. This can be utilised when natural light does not have sufficient luminosity or the cows have a rest time. For dimming the lamps must be dimmable type and there should be an automatic control system.

**Milking**

At the teats the vacuum should be constant and it should remain constant even if some of the clusters are kicked off. Washing operation needs a higher air flow than milking. This means that air flows in milking pumps are much higher than what is needed only for milking. Most of the vacuum pumps are working all the time with full capacity using a valve which regulates the vacuum by passing air to the system. Energy can be saved using variable speed motors, which change their speed according to the need. This saves energy up to 40–50% (Dunn et al., 2010).

Also the running time of the vacuum pump could be reduced by good arrangement of milking work. The shorter the vacuum pump running time is the less energy is used in milking.

**Milk cooling**

The energy released in milk cooling could be utilised. The easiest way to do this is to direct the warm air of the condenser to heating of the building. The warm air should be moved out from the refrigerator room. Otherwise the room is warmed up and the energy efficiency ratio of the system is decreased. This means an increase in electricity consumption.

The temperature of the milk can be reduced with precooling the milk before it flows into tank. This can be done with heat exchanger, where milk is cooled with cold water. When the water flow was equivalent to milk flow Karlsson et al. (2012) measured that milk temperature was cooled to 17 °C. According to Equation (3) this means about 50% saving in the cooling of the milk in the milk tank. The warmed water could be utilised in hot water production or heating.

A heat recovery system can be used in milk cooling, which utilises the heat of the cooling media. These systems can utilize two thirds of the cooling media energy (Karlsson et al., 2012).

One problem with heat recovery systems is that milking is only on milking robots rather continuous. In milking parlours milking is done twice or three time a day and heat can be recovered only during the milking times. There should be during milking an equivalent heat demand or adequate hot water boiler, where the heat could be stored, otherwise the excess heat cannot be utilised.

**Feeding**

Energy consumption in feeding consist normally from four different operations: transportation from the storage, feed material handling (milling, chopping), mixing and distribution. There are many different ways in arranging the feeding and it also depends how much grass and concentrates are used. Energy consumption in feeding can be quite high according to Fig. 1. Energy consumption in feeding also varies in large extends,

Table 2. Hörndahl (2008) measured energy consumptions on five farms and the feeding energy consumption was from 160 to 652 kWh cow$^{-1}$ a$^{-1}$.

**Table 1.** Energy consumption in feeding

| Operation | Energy consumption | Machine type | Reference |
|---|---|---|---|
| Loading and mixing of silage | 118–645 kWh cow$^{-1}$ a$^{-1}$ | Tractor front loader/wheel loader and tractor mixer | Hörndahl, 2008 |
| Silage distribution | 5.7 kWh cow$^{-1}$ a$^{-1}$ | Rail feed wagon | Hörndahl ,2008 |
| | 12.7 kWh cow$^{-1}$ a$^{-1}$ | Belt feeder | Hörndahl, 2008 |
| Bale shredder | 10–20 kWh cow$^{-1}$ a$^{-1}$ | Straw, hammer mill | Jakop & Jakop, 1976 |
| Bale shredder | 140–320 kWh cow$^{-1}$ a$^{-1}$ | Fast speed silage bale shredder | O'Kiely et al., 1999 |
| Bale shredder | 20 kWh cow$^{-1}$ a$^{-1}$ | Slow speed silage bale shredder | Turunen & Malvisto, 2011 |
| Diet mixer | 168 kWh cow$^{-1}$ a$^{-1}$ | Electrical motor driven mixer | Hörndahl, 2008 |
| | 163 kWh cow$^{-1}$ a$^{-1}$ | Tractor driven mixer | Hörndahl, 2008 |
| Grinding | 3–9 kWh t$^{-1}$ | Roller mill | Hörndahl, 2008; Pedersen & Hinge, 2002 |
| Grinding | 10–20 kWh t$^{-1}$ | Hammer mill | Hörndahl 2008; Pedersen & Hinge, 2002; Voss, 1974 |
| Grinding | 9–12 kWh t$^{-1}$ | Plate mill | Pedersen & Hinge, 2002; Voss, 1974 |
| Transport of concentrates | 1 kWh t$^{-1}$ | Spiral conveyor | Pedersen & Hinge, 2002 |
| Transport of concentrates | 0.2–0.4 kWh t$^{-1}$ | Horizontal screw conveyor | Pedersen & Hinge, 2002; Ringel et al., 1987 |
| Transport of concentrates | 0.5–3 kWh t$^{-1}$ | Pneumatic conveyor | Pedersen & Hinge, 2002; Ringel et al., 1987 |

Feeding consist of several parts and it can be arranged in different ways. Energy consumption figures should be available when feeding strategy and systems are designed and purchased. Unfortunately this kind of information is seldom available.

In feeding machines proper maintenance is required. It is known from hay making machines that dull knives can increase energy consumption 15–20% and very dull knives can almost double it (Sauter & Dùrr 2005; Kùper, 2012).

Straw length has an effect on shredder energy consumption. Jones (2009) found that short straw consumed only half of the energy compared to long straw. In this way energy consumption is related to field work machinery.

## CONCLUSIONS

Direct energy consumptions in milk production can vary in large extent. There are possibilities to save energy but there is not much information available how to save energy and when investments are profitable. The magnitude of energy savings are in the order of tens of percent, which means that energy saving potential is quite high. Energy saving can be achieved with efficient system and machinery choices. It must also be remembered that adjustments and maintenance have an effect on energy consumption. This could be solved with good advice work.

It would help the farmers if the electric driven devices had power and energy meters. With these it would be easy for the operator to see how different adjustments effect on energy consumption.

ACKNOWLEDGEMENTS. The project 'Rural Energy Academy' was financed by the European Agricultural Fund for Rural Development.

## REFERENCES

ASAE EP566. 2012. *Guidelines for Selection of Energy Efficient Agricultural Ventilation.* American Society of Agricultural and Biological Engineers. St. Joseph USA.

Crill, R., Hanchar, J., Gooch, C. & Richards, S. 2002. *Net present value economic analysis model for adoption of photoperiod manipulation in lactating cow barns*. Cornell University, Department of Animal Science, 2002, available at http://www.ansci.cornell.edu/pdfs/photoperiod.pdf (accessed July 2013).

DairyCo: *Dairy housing – a best practice guide*. 2012. DairyCo, a division of the Agriculture and Horticulture Development Board, Warwickshire, UK, available at http://www.dairyco.org.uk/resources-library/technical-information/buildings/dairy-housing-a-best-practice-guide/ (accessed July 2013).

Dunn, P., Butler, G., Bilsborrow, P., Brough, D. & Quinn, P. 2010. *Energy + efficiency, renewable energy and energy efficiency options for UK dairy farms*. Newcastle University, 2010, available at http://www.morrisons.co.uk/Global/0_FarmingPage/Energy%20Efficiency%20Options%20for%20UK%20Dairy%20Farms.pdf (accessed 12.1.2015).

Eerola, K. 2006. *Seosrehuruokinta ja siinä käytettävät yleisimmät koneketjut Suomessa*. (In Finnish, Mixed feeding and frequently used machine chains in Finland) Opinnäytetyö. Hamk. 46 s.

EU327/2011. *COMMISSION REGULATION (EU) No 327/2011 implementing Directive 2009/125/EC of the European Parliament and of the Council with regard to ecodesign requirements for fans driven by motors with an electric input power between 125 W and 500 kW.* COMMISSION REGULATION (EU) No 327/2011 of 30 March 2011, 13 p.

Gooch, C.A. & Ludington, D.C. 2003. *Lighting Design Considerations for Employment of Photoperiod Management in Freestall and Tiestall Dairy Barns*. In *Fifth International Dairy Housing Proceedings of the 29–31 January 2003*. Fort Worth, Texas USA. pp. 95–104.

Hinge, J. 2001. *Mekanisk ventilation – ligetryksanlæg*. (In Danish, Mechanical ventilation – equal pressure system) https://www.landbrugsinfo.dk/Energi/Spar-energi/Sider/Mekanisk_ventilation_ligetryksanlaeg.aspx. (accessed September 2013).

Hörndahl, L. 2008. *Energy use in farm buildings – a study of 16 farms with different enterprises*. Report 2008:8. Alnarp Sweden: University of Agricultural Sciences, Faculty of Landscape Planning, Horticulture and Agricultural Science. 69 p.

Jakop, P. & Jakop, R. 1976. *Aufbereitung und Eigenschaften von Einstreu in der Tierhaltung*. FAT–Blätter fur Landtechnik, 112. Forchungsanstalt für Betriebswirtshaft und landtechnik, Tänikon Switzerland. 5 p.

Jones, S.Q. 2009. *The effect of alfalfa and cornstalk round bale processing type on animal performance, wastage, preference, and mixing characteristics*. Kansas State University, Department of Animal Sciences and Industry College of Agriculture. 53 p. http://krex.k-state.edu/dspace/handle/2097/1418. (accessed January 2015)

Karlsson, E., Hörndahl, T., Pettersson, O. & Nordman, R. 2012. *Energiåtervinning från mjölkkylning* (In Swedish, Energy recover from milk cooling). Rapport 401, Landtbruk & Industri, JTI – Institutet för Jordbruks- och Miljö Teknik, Uppsala, Sweden, 54 p.

Küper, J-M. 2012. *Top Agrar systemvergleich: Scharfe Messer schneiden besser*. Top Agrar 5, 116–119.

Ludington, D. & Johnson, E. *Dairy farm energy audit summary report*. New York State Energy Research and Development Authority 2003. Available at https://www.nyserda.ny.gov/-/media/Files/Publications/Research/Energy-Audit-Reports/dairy-farm-energy.pdf (accessed January 2015), 30 p.

Ludington, D., Johnson, E., Kowalski, J.A., & Mage, A.L. 2004. *Dairy Farm Energy Management Guide.* Southern California Edison, An Edison International Company. http://www.mnproject.org/resourcecenter/Dairy%20Farm%20Energy%20Management%20Guide.pdf (accessed January 2015), 169 p.

MMM-RMO C3. *Kotieläinrakennusten valaistus* (In Finnish, Illumination in Cattle Houses). Maa- ja metsätalousministeriön rakentamismääräykset ja ohjeet.

http://www.mmm.fi/attachments/maaseutu/rakentaminen/5g7GzUkF9/L11-rmoC3-01.pdf. (accessed January 2015), 2 p.

Neuman, L. 2009. *Kartläggning av energianvändning på lantbruket 2008.* (In Swedish, Survey of energy consumption in agriculture). Stockholm Sweden: LRF Konsultat AB. http://www.bioenergiportalen.se/attachments/42/451.pdf , (accessed January 2015).

O'Kiely. P, Forristal, D. & Lenehan, J.J. 1999. *Baled Silage - Development Of Reliable Baled Silage Systems*. *End of project report*. Beef Production Series No., 11. Teagasc, Oak Park, Carlow USA. http://www.teagasc.ie/research/reports/beef/4284/eopr-4284.asp , (accessed January 2015).

Pedersen, J. & Hinge, J. (toim.). *Energisparekatalog i landbruget*. Landbrugets Rådgivningscenter. Århus. _Saatavissa: www.energisparekatalog.dk. (accessed January 2007), 141 p.

PremiumLight 2015. http://www.premiumlight.eu/. (accessed January 2015).

Ringel, R. Estler, M. & Ratschow, J.P. 1987.*Mühlen zum Zerkleinergn von Feuchtgetreide und Maiskorn-Spindel-Gemisch (Corn-Cob-Mix).* KTBL Arbeitzblatt 1076. Kuratorium für Technik und Bauweisen in der Land wirtschaft.

Sauter, J. & Dürr, L. 2005. *Einfluss der Messerschärfe auf den Leistungsbedarf von Mähwerken und Ballenpressen.* FAT-Berichte Nr. 6292005. Agroscope FAT Tänikon Switzerland. 4 p.

Tetri, E., Raunio, J. & Halonen, L. 2011. *Lamppuopas* (In Finnish, Lamp Info). Aalto-yliopisto, Sähkötekniikan korkeakoulu, Valaistusyksikkö, Espoo. http://www.lightinglab.fi/ekovalo/News/lamppuopas.pdf (accessed January 2015), 12 p.

Turunen, M. 2013. Energian käyttö ja säästö maidontuotannossa (In Finnish, Energy consumption and savings in milk production). In Ahokas, J. (ed.): *Energian kulutus ja säästö karjataloudessa*. Department of Agricultural Sciences Publication 27, University of Helsinki, pp. 49–99.

Turunen, M. & Malvisto A-M. 2011. *Pyöröpaalien vetomattoruokinta* (In Finnish, Round bales in belt feeding). http://hinkalo.fi/wpcontent/uploads/Kilpailukykya_Maidontuotantoon/Lypsylehmat/Ruokinta_juonti/Pyoropaalien_vetomattoruokinta.pdf (accessed July 2013).

Vergricht, J. Milacek, P. Ambroz, P. Machalek. 2007. *Parametric analysis of the properties of selected mixing feeding wagons.* Research in Agricultural Engineering **53(**3), 85–93.

Voss, U. 1974. *Schrotmühlen und Futtermischer*. Landtechnik **8**, 349–351.

## INSTRUCTIONS TO AUTHORS

Papers must be in English (British spelling). English will be revised by a proofreader, but authors are strongly urged to have their manuscripts reviewed linguistically prior to submission. Contributions should be sent electronically. Papers are considered by referees before acceptance. The manuscript should follow the instructions below.

**Structure:** Title, Authors (initials & surname; an asterisk indicates the corresponding author), Authors' affiliation with postal address (each on a separate line) and e-mail of the corresponding author, Abstract (up to 250 words), Key words (not repeating words in the title), Introduction, Materials and methods, Results and discussion, Conclusions, Acknowledgements (optional), References.

**Layout, page size and font**

- Use preferably the latest version of **Microsoft Word**, doc., docx. format.
- Set page size to **B5 Envelope or ISO B5 (17.6 x 25 cm)**, all margins at 2 cm.
- Use single line spacing and justify the text. Do not use page numbering. Use indent 0.8 cm (do not use tab or spaces instead).
- Use font Times New Roman, point size for the title of article **14 (Bold)**, author's names 12, core text 11; Abstract, Key words, Acknowledgements, References, tables and figure captions 10.
- Use *italics* for Latin biological names, mathematical variables and statistical terms.
- Use single ('…') instead of double quotation marks ("…").

**Tables**

- All tables must be referred to in the text (Table 1; Tables 1, 3; Tables 2–3).
- Use font Times New Roman, regular, 10 pt. Insert tables by Word's 'Insert' menu.
- Do not use vertical lines as dividers; only horizontal lines (1/2 pt) are allowed. Primary column and row headings should start with an initial capital.

**Figures**

- All figures must be referred to in the text (Fig. 1; Fig. 1 A; Figs 1, 3; Figs 1–3). Use only black and white or greyscale for figures. Avoid 3D charts, background shading, gridlines and excessive symbols. Use font **Arial** within the figures. Make sure that thickness of the lines is greater than 0.3 pt.
- Do not put caption in the frame of the figure.
- The preferred graphic format is EPS; for half-tones please use TIFF. MS Office files are also acceptable. Please include these files in your submission.
- Check and double-check spelling in figures and graphs. Proof-readers may not be able to change mistakes in a different program.

**References**

- **Within the text**

In case of two authors, use '&', if more than two authors, provide first author 'et al.':

Smith & Jones (1996); (Smith & Jones, 1996);
Brown et al. (1997); (Brown et al., 1997)

When referring to more than one publication, arrange them by following keys: 1. year of publication (ascending), 2. alphabetical order for the same year of publication:

(Smith & Jones, 1996; Brown et al., 1997; Adams, 1998; Smith, 1998)

- **For whole books**

Name(s) and initials of the author(s). Year of publication. *Title of the book* (*in italics*). Publisher, place of publication, number of pages.

Shiyatov, S.G. 1986. *Dendrochronology of the upper timberline in the Urals*. Nauka, Moscow, 350 pp. (in Russian).

- **For articles in a journal**

Name(s) and initials of the author(s). Year of publication. Title of the article. *Abbreviated journal title* (*in italic*) volume (in bold), page numbers.

Titles of papers published in languages other than English, German, French, Italian, Spanish, and Portuguese should be replaced by an English translation, with an explanatory note at the end, e.g., (in Russian, English abstr.).

Karube, I. & Tamiyra, M.Y. 1987. Biosensors for environmental control. *Pure Appl. Chem.* **59**, 545–554.

Frey, R. 1958. Zur Kenntnis der Diptera brachycera p.p. der Kapverdischen Inseln. *Commentat.Biol.* **18**(4), 1–61.

Danielyan, S.G. & Nabaldiyan, K.M. 1971. The causal agents of meloids in bees. *Veterinariya* **8**, 64–65 (in Russian).

- **For articles in collections:**

Name(s) and initials of the author(s). Year of publication. Title of the article. Name(s) and initials of the editor(s) (preceded by In:) *Title of the collection (in italics)*, publisher, place of publication, page numbers.

Yurtsev, B.A., Tolmachev, A.I. & Rebristaya, O.V. 1978. The floristic delimitation and subdivisions of the Arctic. In: Yurtsev, B. A. (ed.) *The Arctic Floristic Region*. Nauka, Leningrad, pp. 9–104 (in Russian).

- **For conference proceedings:**

Name(s) and initials of the author(s). Year of publication. Name(s) and initials of the editor(s) (preceded by In:) *Proceedings name (in italics)*, publisher, place of publishing, page numbers.

Ritchie, M.E. & Olff, H. 1999. Herbivore diversity and plant dynamics: compensatory and additive effects. In: Olff, H., Brown, V.K. & Drent R.H. (eds) *Herbivores between plants and predators. Proc. Int. Conf. The 38$^{th}$ Symposium of the British Ecological Society*, Blackwell Science, Oxford, UK, pp. 175–204.

.........................................................................................................………

**Please note**

- Use ‘.’ ( not ‘,’) for decimal point: 0.6 ± 0.2; Use ‘,’ for thousands – 1,230.4;
- Use ‘–’ (not ‘-’) and without space: pp. 27–36, 1998–2000, 4–6 min, 3–5 kg
- With spaces: 5 h, 5 kg, 5 m, 5°C, C : D = 0.6 ± 0.2; $p$ < 0.001
- Without space: 55°, 5% (not 55 °, 5 %)
- Use ‘kg ha$^{-1}$’ (not ‘kg/ha’);
- Use degree sign ‘ ° ’ : 5 °C (not 5 $^{O}$ C).